

The contribution of extrachloroplastic factors and plastid gene expression to chloroplast development and abiotic stress tolerance

Dissertation

Zur Erlangung des Doktorgrades
der Naturwissenschaften
(Dr. rer. nat.)



an der Fakultät für Biologie
der Ludwig-Maximilians-Universität München
vorgelegt von

Duorong Xu

Munich, 2020

Gutachter:

1. PD Dr. Tatjana Kleine

2. Prof. Dr. Peter Geigenberger

Datum der Abgabe: 23.04.2020

Datum der mündlichen Prüfung: 16.07.2020

Eidesstattliche Erklärung

Ich versichere hiermit an Eides statt, dass die vorgelegte Dissertation von mir selbstständig und ohne unerlaubte Hilfe angefertigt wurde. Des Weiteren erkläre ich, dass ich nicht anderweitig ohne Erfolg versucht habe, eine Dissertation einzureichen oder mich der Doktorprüfung zu unterziehen. Die folgende Dissertation liegt weder ganz, noch in wesentlichen Teilen einer anderen Prüfungskommission vor.

München, 23. April 2020

Duorong Xu

Statutory declaration

I declare that I have authored this thesis independently, that I have not used other than the declared (re)sources. As well I declare, that I have not submitted a dissertation without success and not passed the oral exam. The present dissertation (neither the entire dissertation nor parts) has not been presented to another examination board.

Munich, 23. April 2020

Duorong Xu

Contents

Statutory declaration.....	III
Contents	IV
Abbreviations	VI
Declaration of contribution as a co-author	VIII
Summary	IX
Zusammenfassung	XI
1. Introduction	1
1.1 Photosynthesis.....	1
1.2 Origin, structure and biogenesis of chloroplasts.....	2
1.2.1 Chloroplast biogenesis	6
1.2.2 Thylakoid complexes	7
1.3 Retrograde signaling.....	10
1.3.1 Tetrapyrrole signaling and <i>gun</i> mutants.....	11
1.3.2 Plastid gene expression	13
1.4 Abiotic stress and chloroplasts	14
2. Aim of the thesis.....	16
3. Results.....	18
3.1 Chapter 1	
Extrachloroplastic PP7L functions in chloroplast development and abiotic stress tolerance	18
3.2 Chapter 2	
VENOSA4, a human dNTPase SAMHD1 homolog, contributes to chloroplast development and abiotic stress tolerance.....	38
3.3 Chapter 3	
<i>Arabidopsis thaliana</i> mTERF10 and mTERF11, but not mTERF12, are involved in the response to salt stress	48
3.4 Chapter 4	
Cellulose defects in the Arabidopsis secondary cell wall promote early chloroplast development	67
4. Discussion.....	83
4.1 The role of PP7L in chloroplast development.....	83

4.2 VEN4 participates in regulating dNTP metabolism	84
4.3 Perturbed OGE lead to altered salt stress responses in plant.....	85
4.4 Cell wall integrity modulates nuclear gene expression in Arabidopsis seedling	86
References	88
Supplemental information	98
Supplemental information – Chapter 1	98
Supplemental information – Chapter 2	104
Supplemental information – Chapter 3	111
Supplemental information – Chapter 4	114
Acknowledgement.....	119
Curriculum vitae.....	120

Abbreviations

ABA	Absciscic acid
ADP	Adenosine diphosphate
ATP	Adenosine triphosphate
Ces	Cellulose synthase
Chl	Chlorophyll
Col-0	Arabidopsis ecotype Columbia
DNA	Deoxyribonucleic acid
dNTP	Deoxynucleoside triphosphate
EMS	Ethyl methane sulfonate
ETC	Electron transport chain
FNR	Ferredoxin-NADP ⁺ reductase
Fv/Fm	Maximum quantum yield of PSII
GFP	Green fluorescent protein
GLK	GOLDEN 2-LIKE (GLK) transcription factors
<i>gun</i>	<i>genomes uncoupled</i> mutant
Gya	Billion years ago
kbp	Kilo-base pair
LHC	Light harvesting complex
LHCB	Light-harvesting complex II
LIN	Lincomycin
MS	Murashige and Skoog medium
mTERF	Mitochondrial transcription termination factor
NADH	Nicotinamide adenine dinucleotide
NEP	Nuclear-encoded RNA polymerase
NF	Norflurazon
OEC	Oxygen-evolving complex
P680	Photosystem II primary donor
P700	Primary electron donor
PC	Plastocyanin
PEP	Plastid-encoded RNA polymerase
PGE	Plastid gene expression
PhANGs	Photosynthesis-associated nuclear-encoded genes
PPR	Pentatricopeptide repeat
PQH ₂	Plastoquinone
PSI	Photosystem I
PSII	Photosystem II
PTM	Plant homeodomain (PHD) transcription factor

RC	Reaction center
RNA	Ribonucleic acid
ROS	Reactive oxygen species
Sig	Sigma

Declaration of contribution as a co-author

Chapter 1:

Duorong Xu, Giada Marino, Andreas Klingl, Beatrix Enderle, Elena Monte, Joachim Kurth, Andreas Hiltbrunner, Dario Leister, Tatjana Kleine (2019). Extrachloroplastic PP7L functions in chloroplast development and abiotic stress tolerance. *Plant Physiol* **180**: 323–341

Research was designed by T.K. and D.X.; the *pp7l:En-1* mutant was confirmed by J.K.; most of the experiments were performed by D.X.; G.M. realized the shot-gun proteomics experiment; A.K. provided TEM pictures; B.E. performed phyB western-blot analysis; T.K., D. X., G.M., D.L., A.H., and E.M. analyzed the data; T.K. wrote the manuscript with input primarily from D.L., A.H., and E.M., and then all authors; the whole study was supervised by T.K.; all authors read and approved the article.

Chapter 2:

Duorong Xu, Dario Leister, Tatjana Kleine (2020). VENOSA4, a human dNTPase SAMHD1 homolog, contributes to chloroplast development and abiotic stress tolerance. *Plant Physiol* **182**: 721–729

Research was designed by T.K. and D.X. Most of the experiments were performed by D.X. D.X. and T.K. analyzed the data. T.K. wrote the manuscript with input from D.L. and D.X. The whole study was supervised by T.K. All authors read and approved the article.

Chapter 3:

Duorong Xu, Dario Leister and Tatjana Kleine (2017). *Arabidopsis thaliana* mTERF10 and mTERF11, but not mTERF12, are involved in the response to salt stress. *Front Plant Sci* **8**: 1213

Research was designed by TK. Research was performed by DX and TK. The manuscript was prepared by DX, DL, and TK.

Chapter 4:

Duorong Xu, Ravi Dhiman, Adriana Garibay, Hans-Peter Mock, Dario Leister, Tatjana Kleine (2020). Cellulose defects in the Arabidopsis secondary cell wall promote early chloroplast development. *Plant J* **101**: 156–170

Conceptualization: T.K., D.X.; Experiments: D.X., R.D., A.G., H.-P. M., T.K.; Writing original draft: T.K.; Writing- review and editing: D.L., D.X., R.D., A.G., H.-P.M., T.K.; Supervision: T.K.

Summary

Photosynthesis is a fundamental and vital physiological process in plants that occurs in the chloroplast. Chloroplast biogenesis is complex and is determined by nuclear, cytosolic, and chloroplastic activities. PP7L is a PP7-like protein that primarily resides in the nucleus. In the absence of PP7L, chloroplast development in cotyledons and young leaves is delayed. Sigma factor and light signaling mutants have been used to explore a potential relationship with *pp7l*. But molecular biology and phenotypic analyses of *pp7l* mutants indicate that PP7L operates via a novel pathway. Without PP7L, plants are defective in photosynthesis due to the inability of *pp7l* to promote chloroplast ribosomal RNA (rRNA) maturation and chloroplast protein translation. Furthermore, we identified a nuclear protein VENOSA4 (VEN4) in *Arabidopsis*, which plays a crucial role in chloroplast biogenesis. In plants, imbalances of the deoxynucleoside triphosphate (dNTP) pool can be caused by mutated ribonucleotide reductase, which is responsible for the de novo synthesis of dNTPs. However, the molecular mechanism of dNTP degradation, which contributes to the control of the intracellular dNTP pool in plants, is not understood well. This study provides evidence that VEN4 is homologous to a human sterile alpha motif and HD-domain containing protein 1 (SAMHD1), which is involved in dNTP catabolism. With respect to *ven4*, the synthesis processes of chloroplast proteins are affected, thereby decreasing the optimal quantum efficiency of photosystem II. We further found that treatment of germinated seeds with exogenous dCTP or a pool of dNTPs resulted in the rescue of photosynthesis-deficient phenotypes of *ven4* seedlings. This suggests that VEN4 maintains the homeostatic balance of dNTPs and is functional in the chloroplast development process of plants.

Coordinated subcellular exchange of signals is a basic feature of eukaryotic organisms. Plastid gene expression may elicit a retrograde signal during plant development and for acclimation to various environmental stress conditions. The mitochondrial transcription termination factor (mTERF) family binds to nucleic acids. In *Arabidopsis*, mTERF10, mTERF11, and mTERF12 belong to the “chloroplast-associated” group that has previously been described. Here we show that mTERF10, mTERF11, and mTERF12 are localized in chloroplast nucleoids. Abiotic stress

conditions set the approach to obtain more information about the physiological effects of PGE, as the investigation of *mterf10* and *mterf11* mutants and overexpression lines showed that mTERF-PGE is related to salt stress responses. Another strategy was based on the identification of currently unknown factors that are involved in PGE-retrograde signaling via forward-genetic screens. This strategy led to the identification of new mutants with *genomes uncoupled* (*gun*) like phenotypes that express nuclear-encoded *Lhcb* and *RbcS* transcripts in the presence of lincomycin, an inhibitor of plastid translation. The *holi6* mutant was among the identified mutants that displayed chlorophyll autofluorescence and a *gun* like phenotype when grown on MS plates supplemented with lincomycin. Surprisingly, in the *holi6* mutant, the mutation resided in the gene that encodes cellulose synthase, which is required for the synthesis of secondary cell walls. Thus, this study proposes and expands on new perspectives regarding how cell walls can affect chloroplast biogenesis.

Zusammenfassung

Die Photosynthese ist ein grundlegender und lebenswichtiger physiologischer Prozess in Pflanzen, der im Chloroplasten stattfindet. Die Chloroplasten-Biogenese wiederum ist sehr komplex und wird durch nukleäre, cytosolische und chloroplastische Aktivitäten bestimmt. PP7L ist ein PP7-ähnliches Protein, das sich hauptsächlich im Kern befindet. In Abwesenheit von PP7L ist die Chloroplasten-Entwicklung in Keimblättern und jungen Blättern verzögert. Sigmafaktor- und Lichtsignal-Mutanten wurden verwendet, um eine mögliche Beziehung zu *pp7l* zu untersuchen. Molekularbiologie und phänotypische Analysen von *pp7l*-Mutanten zeigen jedoch, dass PP7L über einen neuen Weg arbeitet. Ohne PP7L sind Pflanzen in der Photosynthese defekt, da PP7L ein positiver Faktor in der Reifung der ribosomalen Chloroplasten-RNA (rRNA) und der Translation der Chloroplastenproteine ist. Darüber hinaus haben wir in Arabidopsis ein Kernprotein VENOSA4 (VEN4) identifiziert, das eine entscheidende Rolle bei der Biogenese von Chloroplasten spielt. In Pflanzen können Ungleichgewichte des Desoxynukleosidtriphosphat (dNTP) -Pools durch mutierte Ribonukleotidreduktase verursacht werden, die für die De-novo-Synthese von dNTPs verantwortlich ist. Der molekulare Mechanismus des dNTP-Abbaus, der zur Kontrolle des intrazellulären dNTP-Pools in Pflanzen beiträgt, ist jedoch nicht gut verstanden. Diese Studie liefert Hinweise darauf, dass VEN4 homolog zu einem humanen sterilen Alpha-Motiv und HD-Domänen-Protein (SAMHD1) ist, das am dNTP-Katabolismus beteiligt ist. In der *ven4* Mutante werden die Synthesevorgänge von Chloroplastenproteinen beeinflusst, wodurch die optimale Quanteneffizienz des Photosystems II verringert wird. Wir fanden ferner heraus, dass die Behandlung von gekeimten Samen mit exogenem dCTP oder einem Pool von dNTPs zur Rettung von Photosynthesemangel-Phänotypen von *ven4*-Keimlingen führte. Dies legt nahe, dass VEN4 das homöostatische Gleichgewicht von dNTPs aufrechterhält und im Chloroplastenentwicklungsprozess von Pflanzen funktionsfähig ist.

Ein koordinierter subzellulärer Signalaustausch ist ein grundlegendes Merkmal eukaryotischer Organismen. Die Plastiden-Genexpression kann während der Pflanzenentwicklung und zur Anpassung an verschiedene

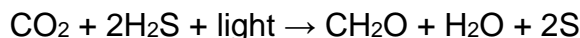
Umweltstressbedingungen ein retrogrades Signal auslösen. Die Familie der mitochondrialen Transkriptionsterminationsfaktoren (mTERF) bindet an Nukleinsäuren. In Arabidopsis gehören mTERF10, mTERF11 und mTERF12 zu der zuvor beschriebenen "Chloroplasten-assoziierten" Gruppe. Hier zeigen wir, dass mTERF10, mTERF11 und mTERF12 in Chloroplasten-Nukleoiden lokalisiert sind. Abiotische Stressbedingungen können dazu beitragen, die physiologischen Wirkung von PGE noch besser zu verstehen. Die Untersuchung von *mterf10*- und *mterf11*-Mutanten und Überexpressionslinien zeigte einen Zusammenhang zwischen mTERF-PGE und der Salzstressreaktion. Eine andere Strategie, Faktoren der PGE-retrograden Signaltransduktion zu identifizieren, basierte auf der Identifizierung derzeit unbekannter Faktoren durch vorwärtsgenetische Screenings. Diese Strategie führte zur Identifizierung neuer Mutanten mit *genomes uncoupled* (*gun*) Phänotypen, die kernkodierte *Lhcb*- und *RbcS*-Transkripte in Gegenwart von Lincomycin, einem Inhibitor der Plastidentranslation, exprimieren. Die *holi6*-Mutante gehörte zu den identifizierten Mutanten, die eine Chlorophyll-Autofluoreszenz und einen *gun* wie Phänotyp zeigten, wenn sie auf mit Lincomycin supplementierten MS-Platten angezogen wurden. Überraschenderweise befand sich die Mutation in der *holi6*-Mutante in dem Gen, das für eine Cellulosesynthase kodiert, die für die Synthese der sekundären Zellwände erforderlich ist. In dieser Studie werden daher neue Perspektiven vorgeschlagen und erweitert, wie Zellwände die Biogenese von Chloroplasten beeinflussen können.

1. Introduction

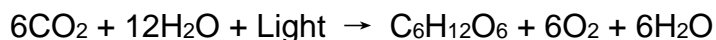
1.1 Photosynthesis

Photosynthesis is the most fundamental physiological process on Earth. The sun, as the ultimate power source, fuels energy for life forms. Photosynthesis is the only known process of biology that converts the kinetic energy of photons into the free energy required for living organisms. In addition, the ancient biomass in coal, petroleum, and natural gas was stored by fossils and accumulated over millions of years. It is generally believed that there are two types of photosynthetic processes: anoxygenic versus oxygenic photosynthesis.

Several lines of evidence suggest that anoxygenic photosynthesis emerged more than 3.4 billion years ago (Gya) (Tice and Lowe, 2004, 2006). Energy from light is used to convert CO₂ into more complex molecules but does not generate oxygen (Xiong and Bauer, 2002). The reactions are represented as follows:



All known processes of anoxygenic photosynthesis evolved among bacteria (Butterfield, 2015), including green sulfur bacteria, green and red filamentous anoxygenic phototrophs, purple bacteria, acidobacteria, and heliobacteria (Bryant and Frigaard, 2006; Bryant et al., 2007). Two types of reaction center complexes (RCs), which are termed type I and type II RCs, are present in green sulfur bacteria and purple bacteria, respectively (Blankenship, 2002). While both type I and type II RCs are found in cyanobacteria, which perform oxygenic photosynthesis (Blankenship, 2010), accumulated evidence suggests that oxygenic photosynthesis began later than anoxygenic photosynthesis, and potentially emerged before 2.4 Gya (Buick, 2008). Oxygenic photosynthesis is represented as follows:



During oxygenic photosynthesis, six molecules of carbon dioxide (CO₂) combine with 12 molecules of water (H₂O) using light energy to produce a single

carbohydrate molecule ($C_6H_{12}O_6$) and subsequently six molecular each of oxygen (O_2) and water are liberated as byproducts. The origin of oxygenic photosynthesis is one of the most important biological events that coincides with the appearance of the Great Oxidation Event (2.32–2.4 Gya) in Earth's history (Schirrmeister et al., 2013). Oxygen production by cyanobacteria changed Earth's primitive anoxygenic atmosphere to an oxic atmosphere and permitted the development of aerobic metabolism and advanced life forms (Blankenship, 1992). With near certainty, oxygenic photosynthesis evolved in ancestors of the present cyanobacteria and was then transferred to the eukaryotes through endosymbiosis (Meyer, 1883; Schimper, 1883; Mereschkowsky, 1905). This process ultimately produced the diversity of algae and plants found on our planet today.

1.2 Origin, structure and biogenesis of chloroplasts

In eukaryotes, photosynthesis occurs at thylakoid membranes in chloroplasts, which are the organelles derived from an endosymbiotic cyanobacterium (Schimper, 1883; Mereschkowsky, 1905). With the aid of molecular biology and electron microscopy (Figure 1), the symbiogenetic organelle concept is now widely accepted and established. The chloroplast genome originates from a branch of the genome of cyanobacteria, as supported by phylogenetic analyses (Palmer, 2000; McFadden and van Dooren, 2004; Keeling, 2010; Ochoa de Alda et al., 2014). However, the sizes of chloroplast genomes range between 80-200 kbp, which is just 5-11% of the genome of present-day cyanobacteria (Martin et al., 2002; Sato, 2002; Price et al., 2012). In contrast with genome size, chloroplasts harbor thousand proteins. Based on data from comparative studies on cyanobacteria and *Arabidopsis thaliana* nuclear genomes, 18% (~4,500 in 24,990) of nuclear genes in the higher-level plants were descended from cyanobacteria (Martin et al., 2002), which suggests that genes from the cyanobacterial ancestor of plastids were transferred to the host nucleus. Over time, less than half of these genes acquired a target peptide that enabled retargeting back to the chloroplast, but the rest of the gene products are targeted to other cell compartments to contribute to the plastid-independent subcellular processes

(Martin et al., 2002; Kleine et al., 2009b; Archibald, 2015). Therefore, three groups of gene products have established the chloroplast organelle: 1) a core set of chloroplast genes that are required for the light reactions of photosynthesis or functions related to transcription, RNA processing and maturation, and translation; 2) cyanobacterial genes that are transferred to the host nucleus; 3) host genes that were recruited for chloroplast duty with the addition of targeting sequences. Moreover, biochemical evidence suggests that cyanobacteria were closely related to the ancestors of chloroplasts (Weeden, 1981). For example, comparisons of chloroplast enzymes, the composition of light-harvesting complexes and their structural RNA components, and the protein import/targeting machinery with cyanobacterial counterparts suggest that cyanobacteria and chloroplasts share an ancient ancestral relationship (Wicke et al., 2011). Structural comparisons of the ultrastructure of cyanobacteria and chloroplasts reveal that they contain three major membrane systems: the outer membrane, plasma membrane, and an internal system of thylakoid membranes (Figure 1), with little to no change in topology or function. The chloroplast inner envelope membrane and the thylakoid membrane evolved directly from the plasma membrane and thylakoid membrane, respectively, of the cyanobacterium (Delwiche and Palmer, 1997; Gray, 1999; Cavalier-Smith, 2000; Cavalier-Smith, 2008). However, the origin of the chloroplast outer envelope membrane remains undetermined (Douce and Joyard, 1990; Reumann et al., 2005; Inoue, 2007).

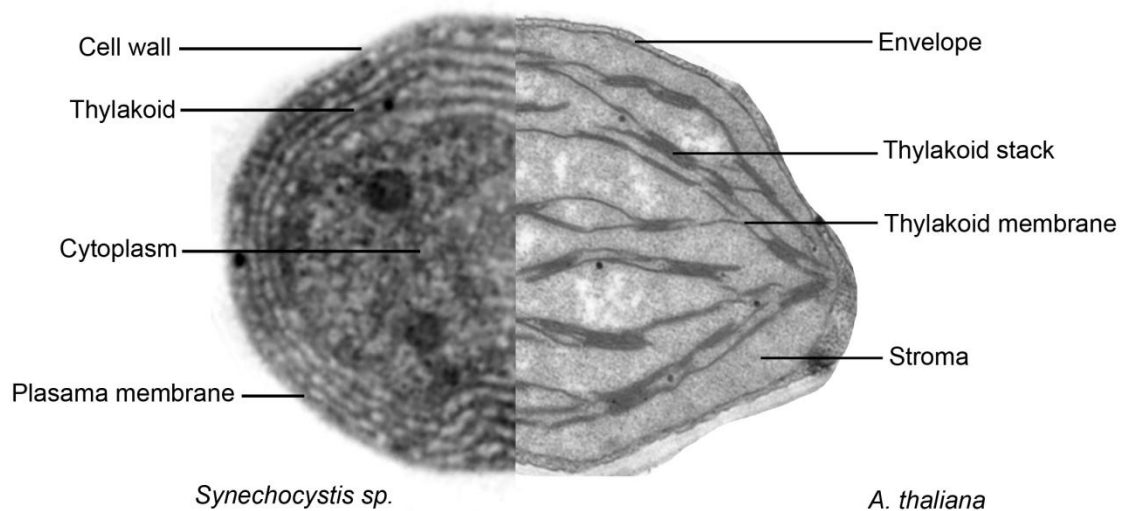


Figure 1. Ultrastructure of the cyanobacterium *Synechocystis sp.* (left) and *Arabidopsis thaliana* (right). A similar structure within the cyanobacterial cell and chloroplast is shown by transmission electron microscopy. *Synechocystis sp.* (left) image adapted from Westphal et al.(2003).

Chloroplasts are surrounded by outer and inner envelope membranes, which form a protective barrier that helps retain relative independence and promotes the exchange of proteins or metabolites in the stroma and cytosol (Neuhaus and Wagner, 2000; Reumann et al., 2005; Voithknecht and Soll, 2005). In addition to these membranes, chloroplasts have a well-defined third internal membrane, termed the thylakoid membrane system, which performs oxygenic photosynthesis. The thylakoids comprise a bilayer of unique lipids that form an elaborate interconnected network and enclose a single lumenal space (Liberton et al., 2011; Pribil et al., 2014; Mareš et al., 2019). Thus, chloroplasts demonstrate three different membrane structures and three aqueous compartments, which are the inter membrane space, the stroma, and the thylakoid lumen (Figure 2).

In higher-level plants, thylakoids have three regions: the grana lamellae, the stroma lamellae, and the marginal regions. The thylakoid membranes contain many protein complexes that are either embedded or peripherally attached. Four major multiprotein complexes are found in the thylakoid membranes, namely the photosystem II (PSII) and photosystem I (PSI) complexes with the photosynthetic antennae, cytochrome *b₆f* (Cyt *b₆f*) complex, and ATP synthase (Sakamoto et al., 2008). PSII is localized in the grana lamellae (Figure 2), while PSI and ATP

synthase are mostly localized in the stroma lamellae and the outer layers of the grana. Cyt *b₆f* is uniformly distributed throughout the grana and stroma lamellae (Figure 2) (Jensen and Leister, 2014). Disparate locations of PSII and PSI in the thylakoid membranes lead to mobile electron carriers that are required to shuttle electrons. Plastoquinone and plastocyanin are electron carriers that shuttle electrons from PSII to Cyt *b₆f* and carry electrons from Cyt *b₆f* to PSI (Figure 3), respectively. The Z-scheme electron transport chains (ETC) mediates electron transport from H₂O to NADPH with the generation of ATP and O₂.

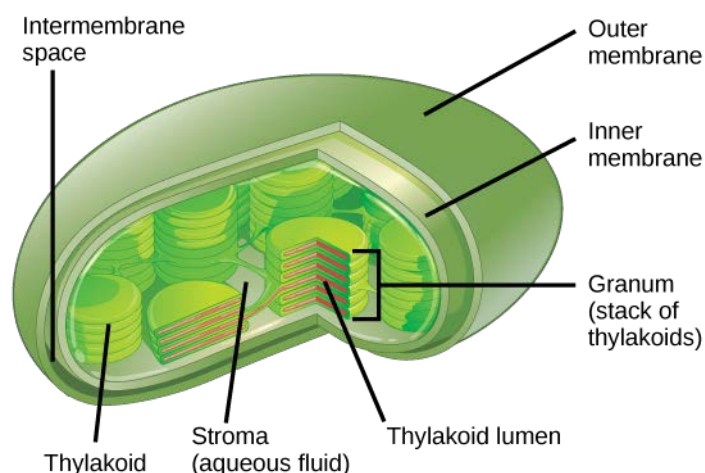


Figure 2. Structure of a chloroplast. The chloroplast is surrounded by an inner and outer envelope. A large amount of photosystems embedded in thylakoid membranes. Stroma contains water-soluble components. This figure was derived from Principles of Biology: Biology 211, 212, and 213.

The stroma contains nucleoid and plastid transcriptionally active chromosome (pTAC) involved in plastid transcription, DNA replication, RNA maturation, and translation. The stroma is also the location of the dark reactions— known as the Calvin cycle. The light-independent reactions of the Calvin cycle can be divided into three basic stages: carbon fixation, reduction, and regeneration. During the carbon fixation process, energy from NADPH and ATP molecules, as generated by the light reactions, drives the enzyme RuBisCO to incorporate carbon dioxide (CO₂) to build a three-carbon sugar termed glyceraldehyde 3-phosphate (G3P). G3P molecules are then sent to the cytoplasm to contribute to the formation of a wide variety of other sugars (such as glucose) and organic molecules, while others remain in the cycle to regenerate the RuBP acceptor.

1.2.1 Chloroplast biogenesis

In seed plants, chloroplasts develop from proplastids in the dark-grown cotyledon during a light-dependent differentiation process and from undifferentiated proplastids in the shoot apical meristem (SAM) and primordia of leaves during leaf morphogenesis (Adam et al., 2011; Pogson et al., 2015). Non-photosynthetic proplastids contain vesicles but no internal membrane systems. The chloroplast biogenesis and development process differs between cotyledons and true leaves (Pogson and Albrecht, 2011). In developed leaves, chloroplasts are further propagated by a division process that is similar to that of prokaryotes (Miyagishima, 2011). Nevertheless, the development of chloroplasts in seedlings after germination is complicated. Firstly, proplastid formation of an etioplast that contains a lattice-like membranous structure, termed the large prolamellar body (PLB), occurs. The PLB contains a few metabolites and proteins that are required for photosynthesis. Eventually, the lattice-like structured prothylakoids emanate into the chloroplast stroma, and the PLB disassembles and then reforms into thylakoids upon illumination (Solymosi and Schoefs, 2010).

Chloroplast biogenesis requires not only the transcription and translation of its own genes, but also nuclear-encoded protein import and assembly. However, as a semi-autonomous organelle, it remains only ~100 genes and the transcription and translation of these genes are strongly dependent on nuclear genomes. Thus, chloroplast biogenesis requires the coordinated expression of genes in the nucleus and chloroplast. Such coordination requires an exchange of information between the two cellular compartments (Kleine and Leister, 2016). Meanwhile, light cytosolic processes/extrachloroplastic and environmental factors also influence chloroplast biogenesis and development (Fitter et al., 2002; Albrecht et al., 2010; Leivar and Monte, 2014). In angiosperms, light is a key environmental signal that regulates the expression of genes that are involved in the assembly of chloroplast components, including multipartite light-responsive elements, and thus photoreceptors are important for the initiation of chloroplast biogenesis (Waters and Langdale, 2009). The perception of light by phytochromes (PHYs)

and cryptochromes (CYRs) is responsible for photomorphogenesis. The photomorphogenic pathways promote the expression of a number of genes including photosynthesis-associated nuclear-encoded genes (PhANGs) and genes encoding proteins involved in chlorophyll biosynthesis, and protein degradation. In *Arabidopsis*, PHYs are encoded by five genes: *PHYA* to *PHYE*. In the cytosol, the inactive Pr form is activated by light and converted into the active Pfr form, which subsequently moves into the nucleus to initiate light-mediated transcription (Quail, 2002). Cryptochromes are flavoproteins that are represented by three proteins CRY1, CRY2, and CRY3 (Kleine et al., 2003). Cryptochromes can modulate the transcription of chloroplast genes, which is achieved by mediating accumulation/localization of COP1 and HY5 during the photomorphogenesis phase (von Arnim and Deng, 1994; Thum et al., 2001; Lee et al., 2007; Facella et al., 2017). The other important factors that are necessary for chloroplast development are phytochrome-interacting factors (PIFs), HEMERA (HMR)/pTAC12, regulators of chloroplast biogenesis (RCBs), Golden2-like proteins (GLKs), and plastid sigma factors of the light signaling pathways (Møller et al., 2003; Leivar et al., 2008; Nakamura et al., 2009; Shin et al., 2009; Leivar and Quail, 2011; Ochoa de Alda et al., 2014; Chi et al., 2015; Belbin et al., 2017; Lupi et al., 2019; Yoo et al., 2019). Additionally, cytosolic components, such as the peroxisomes and cytoskeleton, also influence chloroplast development. A classic example is the SCO3 protein, which is located in peroxisomes and is required for chloroplast biogenesis in seedlings (Albrecht et al., 2010). Interestingly, PP7L (AT5G10900) and VENOSA4 (AT5G40270), as with SCO3, are also extrachloroplastic factors that play a role in chloroplast development. Details on these two proteins are described in the “Results” section.

1.2.2 Thylakoid complexes

The biogenesis and assembly of photosynthetic multiprotein complexes in the thylakoid membrane are critical for chloroplast biogenesis (Adam et al., 2011). The PSII complex typically exists as a core monomer, which contains nearly 25-30 protein subunits along with electron carriers, chlorophylls, and other cofactors.

The major core protein subunits of the PSII complex include the reaction center (RC) proteins D1 (PsbA) and D2 (PsbD) and the inner antenna proteins CP43 (PsbC) and CP47 (PsbB) (Figure 3). The RC binds to all of the redox-active cofactors, such as P680, α -Chlorophyll, pheophytin (Phe), Mn_4CaO_5 cluster, β -carotenes, and plastoquinone (PQ) (Figure 3). The RC is flanked by CP43 and CP47, which play a role in the energy transfer from the proximal antennae complexes to the PSII RC complex. The OEC (oxygen-evolving complex) contains PsbO, PsbP, and PsbQ proteins that are bound to the luminal surface of the RC complex. In addition, several low-molecular mass (LMM) subunits are associated with the PSII complex, including PsbE, PsbF, PsbH, PsbI, PsbJ, PsbK, PsbL, PsbM, PsbTc, PsbX, PsbY, PsbZ, and Ycf12 (Shi and Schröder, 2004). As such, the formation of functional PSII complexes requires coordinated expression of nuclear and plastid-encoded subunits, sequential assembly of the protein subunits, and a ligation of various cofactors during the assembly process (Rokka et al., 2005).

The Cyt *b₆f* complexes comprise the membrane-spanning multiprotein complex, which is composed of two monomers. The monomer unit consists of four major subunits (cyt *f*, cyt *b₆*, Rieske iron–sulfur protein, and subunit IV) and four minor subunits (PetG, PetL, PetM, and PetN) (Malone et al., 2019). The three major redox-active polypeptides, which are cyt *f* (PetA, c-type heme), cyt *b₆* (PetB, b-type hemes bL and bH; c-type heme c), and Fe_2S_2 Rieske protein (PetC), bind the redox-active prosthetic groups of the complex. Further, four small subunits of a picket fence-like structure may provide structural support (Cramer et al., 2004). The Cyt *b₆f* complex drives the proton-motive Q-cycle that translocates protons (H^+) via plastoquinol (PQH_2) from the stroma to the lumen, and the electrons proceed from PSII to the Cyt *b₆f* complex, which is mediated by PQH_2 (Rich, 1984; Joliot and Joliot, 1994). Between Cyt *b₆f* and PSI, the electrons are transported via Fe_2S_2 Rieske to cyt *f* and then via plastocyanin (PC) to PSI within the thylakoid lumen (Berry et al., 2000; Cooley et al., 2004). The Cyt *b₆f* complexes interconnect the two photosystems and catalyze transmembrane proton-coupled electron transfer for energy storage.

PSI is ferredoxin oxidoreductase, which is composed of 19 subunits in higher-level plants (Jordan et al., 2001; Croce, 2012). The core of PSI is formed by the heterodimeric PsaA-PsaB proteins, which cultivate intrinsic cofactors of the electron transport chain (Chl, two phylloquinones, and one of three [4Fe–4S] clusters) and bind to the antenna chlorophylls (Chl a/Chl a), as an electron acceptor and primary electron donor (P700), respectively. The antenna system of PSI is associated with the light-harvesting complex I (LHCI), thereby forming the PSI–LHCI super complex that is composed of 4 LHCI proteins (Lhca1–4), transmembrane subunits, extrinsic subunits, β -carotenes, 3 (Fe₄–S₄) clusters, and 2 phylloquinones (Mazor et al., 2015; Qin et al., 2015; Mazor et al., 2017). Light energy is collected by the antenna systems, transferred to the PSI core, and then the P700 and the electron acceptors convert excitation energy into redox energy. PSI is involved in the linear electron transfer process, by which PSI transfers single electrons to FNR and then two electrons transfer via FNR to both NADP⁺ and H⁺ to produce NADPH (Nelson and Junge, 2015; Suga et al., 2016). In addition, PSI also has a role in cyclic electron flow (CEF) to produce extra ATP without the accumulation of NADPH (Nelson and Yocum, 2006). The first step in PSI assembly is PsaB being synthesized and integrated into the thylakoid membrane, which is an anchor for the translation and integration of PsaA. Subsequently, PsaC assembles with the PsaA-PsaB heterodimer, and with PsaD and PsaE, integrates to the stromal side (Wostrikoff et al., 2004). Later, remaining subunits bind to the PSI core complex. Thus, PSI assembly occurs in a quick and orderly process.

ATP synthase is a multimeric protein complex that catalyzes the phosphorylation of ADP to ATP using the proton gradient that is generated by photosynthesis across the thylakoid membrane. ATP synthase has two sectors: the F₁ catalytic sector and the F₀ proton-translocating sector (Pedersen and Amzel, 1993; Pedersen et al., 2000; Rühle and Leister, 2015). F₁, as the soluble component, consists of five subunits ($\alpha\beta\gamma\delta\epsilon$), which form three catalytic nucleotides and one phosphate binding site that are involved in oxidative phosphorylation. The hydrophobic membrane-integrated F₀ is formed by the simplest subunit structure

(a1, b2, and c10-15 subunits) that is involved in proton transport across the membrane. F1 is projected into the stroma, whereas F0 is located within the thylakoid membrane. The assembly of the chloroplast ATP synthase is a complicated process that involves the coordinated association of nucleus- and chloroplast-encoded subunits. For example, the γ (atpC) and δ (atpD) subunits of the ATP synthase are encoded in the nuclear genome, while the α (atpA), β (atpB), and ϵ (atpE) subunits of CF1 are encoded by chloroplast genes (Alt et al., 1983; Bird et al., 1985; Westhoff et al., 1985; Hennig and Herrmann, 1986).

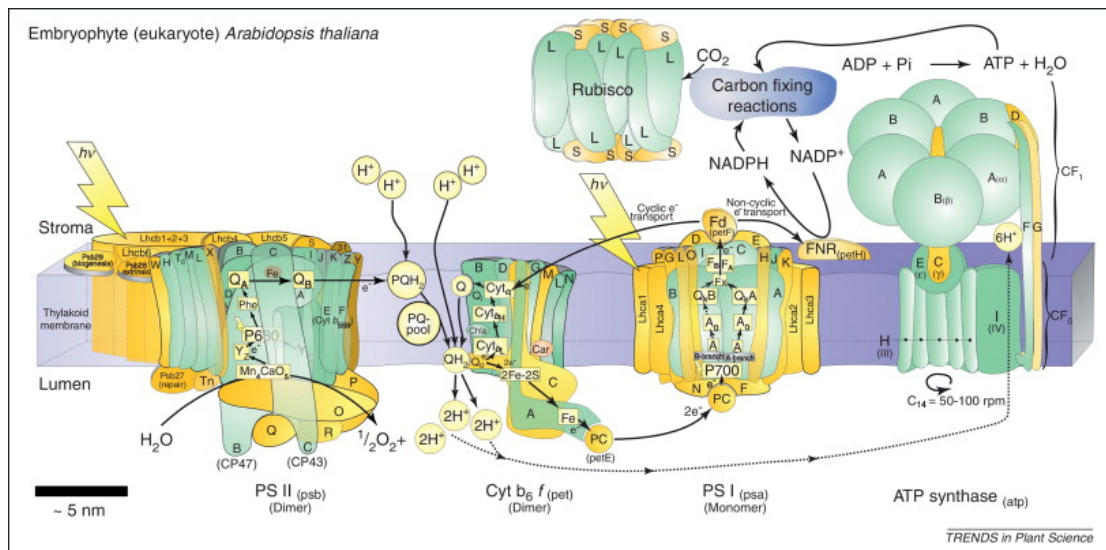


Figure 3. Major proteins and protein complexes of the chloroplast photosynthetic apparatus of a higher-level plant, as exemplified by *Arabidopsis thaliana*. Photosystem II (PSII); cytochrome b_6/f complex (Cyt b_6/f); photosystem I (PSI); ATP synthase. Polypeptide subunits encoded in the chloroplast are colored green; polypeptide subunits encoded in the nucleus are colored yellow. Figure from Allen et al., (2011).

1.3 Retrograde signaling

As previously mentioned, a majority of chloroplast protein complexes depend on being encoded in the nuclear genome and thus must be both translated in and imported from the cytosol. Therefore, chloroplast development and function are regulated by nuclear factors, and this control is referred to as anterograde control or signaling. Apart from this direct signaling pathway, chloroplasts can meet the metabolic and developmental state of the cell to allow the organelle to send retrograde signals, as part of plastid retrograde signaling, to the nucleus to regulate gene expression. These signaling processes between chloroplasts and

the nucleo-cytosol combine with the direct effects of environmental cues, such as nutrient levels and stressors, to coordinate nuclear and plastid gene expression, which is essential for chloroplast biogenesis and maintenance as well as to sustain photosynthesis (Sun et al., 2011). Accordingly, the dissection of the molecular mechanisms of plastid signaling is the prerequisite to develop knowledge-based approaches to manipulate and improve photosynthesis. More than 40 years later, as first described with plastids (Bradbeer et al., 1979), the process of retrograde signaling remains poorly understood, as previous studies mainly center on the sources of signals in chloroplasts. With respect to the downstream steps in plastid signaling, it was repeatedly attempted to dissect these signaling mechanisms by analyzing the pattern of plastid signaling molecules in the cytosol or nucleus. However, most signaling molecule candidates did not display the anticipated specificity and stability requirements for plastid signaling to occur (Kleine et al., 2009a) or are currently awaiting their confirmation by independent experiments (Leister, 2012). Overall, the mechanisms that mediate signal transduction through the cytosol remain elusive, and it is largely unclear how the target genes in the nucleus are regulated.

1.3.1 Tetrapyrrole signaling and *gun* mutants

In recent years, important breakthroughs have been made towards understanding the mechanisms of *A. thaliana* regarding *GUN* (genomes uncoupled) genes that are involved in retrograde signaling. Mutants with the *gun phenotype* exhibit elevated LHCB mRNA transcript levels when chloroplast development had been blocked by norflurazon (NF), an inhibitor of carotenoid biosynthesis. The *GUN1* gene encodes a pentatricopeptide repeat (PPR) protein that was postulated to integrate several signals within the plastid and act as a master switch of multiple plastid-to-nucleus signals (Chi et al., 2013). In contrast, all other *gun* mutations (*gun2*, *3*, *4*, and *5*) affect steps in the biosynthetic pathway of tetrapyrroles (chlorophylls and haem) (Vinti et al., 2000; Mochizuki et al., 2001; Surpin et al., 2002). *GUN2* and *GUN3* encode heme oxygenase and phytychromobilin synthase, respectively, and their mutants are defective in heme catabolism, which

leads to the accumulation of heme (Mochizuki et al., 2001). Further, GUN4 and GUN5 are involved in the Mg-chelation of protoporphyrin IX to produce Mg-protoporphyrin IX (Mg-proto), which is the first dedicated step of chlorophyll biosynthesis (Fe-chelation by ferrochelatases produces heme). Accumulated Mg-proto in photodamaged seedlings has been proposed to mediate the repression of photosynthetic genes. The revised search identified *GUN6* as a gene that encodes ferrochelatase 1 (FC1), which produces a specific heme pool that promotes photosynthetic gene expression (Woodson et al., 2011). It has been argued that most observations to date can be explained by the existence of two signals: a primary heme signal with biogenic function, based on the ability of plastids to incorporate and accommodate photosynthetic gene products, and a later repressive stress signal that may occur when thylakoids assembly stalls, which results from the short-lived presence of Mg-proto and singlet oxygen ($^1\text{O}_2$). This model provides an explanation for the phenotype of all the tetrapyrrole-related *gun* mutants of the tetrapyrrole pathway. One hypothesis is that GUN1 plays a role in limiting the production of the heme signal, which is supported by Shimizu et al. (Shimizu et al., 2019). Their work demonstrates that GUN1 directly binds to heme and other porphyrins and regulates the flow through the tetrapyrrole biosynthesis pathway (Shimizu et al., 2019). Moreover, several latest report anticipated that chloroplast RNA editing and chloroplast protein homeostasis could connect retrograde signaling via GUN1 (Tadini et al., 2016; Marino et al., 2019; Tadini et al., 2019; Wu et al., 2019; Zhao et al., 2019). In addition, the *cryptochrome 1* and *hy5* mutants and *GLK1/GLK2-overexpressing* lines exhibit the typical *gun* phenotype, which implicates that the light signaling pathways and transcription factors are involved in retrograde signaling (Ruckle et al., 2007; Leister and Kleine, 2016). One interesting signaling component was the chloroplast envelope-bound PTM protein (Sun et al., 2011). The *ptm* mutant is a *gun* mutant, which is similar to *gun1* and *abi4* (Sun et al., 2011). However, the results of recently published research suggest that *ptm* and *abi4* lack the *gun* phenotype in the presence of norflurazon and lincomycin (Page et al., 2017; Kacprzak et al., 2019). Thus, ABI4 and PTM may not be the signaling components

of the retrograde pathway.

1.3.2 Plastid gene expression

Plastid gene expression (PGE) in the level of appropriate precision is essential for the proper function of chloroplasts. In higher plants, nuclear-encoded RNA polymerase (NEP) and plastid-encoded RNA polymerase (PEP) that combine with PPRs and sigma factor proteins are involved in the regulation of plastid transcription (Chi et al., 2015; Kleine and Leister, 2016). The translation of plastid proteins is initiated in the chloroplast ribosomes, which are bacterial-type 70S ribosomes (Danon, 1997). Plastid gene expression has been implicated in retrograde signaling and regulates gene expression in response to chloroplast development and environmental stressors (Leister et al., 2017). Among the *Arabidopsis gun* mutants, *gun1* affects the PGE pathway of biogenic signals and was discovered using lincomycin, according to previous research (Woodson and Chory, 2008). Lincomycin differs from norflurazon in blocking chloroplast biogenesis, as it specifically inhibits plastid translation (Gray, 1995). A recent study suggests mTERF4 (mitochondrial Transcription termination factor 4) may cooperate with GUN1 in PEG and retrograde signaling (Sun et al., 2015). These data correspond to the proposed function of GUN1 as a mediator of PGE. Beyond biogenic signals, operation signals of retrograde signaling also play important functions in regulating the expression of nuclear genes that are responsible for the induction of plant responses to stress (Chan et al., 2016; Robles and Quesada, 2019). The chloroplast and mitochondrial prolyl-tRNA synthetase 1 (PRORS1) have been proposed to play a role during later plant developmental stages by repressing nuclear genes upon impairment of translation in plastids (Pesaresi et al., 2006).

The expression and regulation of PGE necessitate the participation of nucleic acid binding proteins, such as mTERFs, which contain multiple mTERF motifs. The mTERF motif contains 30 amino acids that form a helical repeat architecture (Rubinson and Eichman, 2012). Plants were found to possess 35-48 mTERF proteins, which were mostly located in mitochondria and/or chloroplasts (Kleine,

2012). In *Arabidopsis*, mTERF proteins are divided into five groups following co-expression analysis (Kleine, 2012). The largest mTERF group is the “chloroplast” group, which consists of nine chloroplast-localized proteins (mTERF1-9). The distinctive feature of the chloroplast-associated set is a discrete group, as members of the group (mTERF10-12) are not classified as the “chloroplast” group, but are targeted to the chloroplast. mTERF13–19 are mitochondria-localized proteins that belong to the “mitochondrial” group. mTERF20-22 and mTERF23-26 are placed in the mitochondrion-associated group and others, respectively. Increasing evidence suggests that PGE regulation via mTERFs is vital for plant development and tolerance to environmental stressors (Robles et al., 2012; Kleine and Leister, 2015; Robles et al., 2015; Quesada, 2016; Robles et al., 2018; Núñez-Delegido et al., 2019).

Overall, signals that are produced by plastid gene expression are considered to induce retrograde signaling from chloroplasts not only in developing chloroplasts, but also in mature chloroplasts.

1.4 Abiotic stress and chloroplasts

As sessile organisms, plants do not possess the ability to move when facing environmental stressors. Thus, plants must adjust their physiology and development to adapt to environmental changes. In fact, plants have developed an amazing capacity to sense and respond to unfavorable environmental conditions, which are categorized by biotic stress (damage from living organisms, such as bacteria, viruses, fungi, and parasites) and abiotic stress (including salinity, intense light, osmotic stress, drought, cold, and heat). Perception and conduction of stress are important for stress signaling, which controls the stress response, defense system, and metabolism to survive stressful conditions. The chloroplast is not only the sensor of stress, but also the source of various secondary messengers (Li et al., 2009; Sun and Guo, 2016; Zhu, 2016). PSI and PSII and Rubisco of the chloroplast serve as the primary sites for sensing various environmental stimuli, and then, via several signal transduction pathways, transduces them using secondary messengers to downstream signaling networks

(Biswal et al., 2008; Biswal et al., 2011). For instance, the plastid metabolite methylerythritol cyclodiphosphate (MEcPP), SAL1-PAP (phosphonucleotide 3'-phosphoadenosine 5'-phosphate), tetrapyrroles, PGE, mTERFs, reactive oxygen species (ROS), carotenoids, and plastid proteome remodeling act as the messengers that are activated by the chloroplasts under various environmental stressors (Wagner et al., 2004; Estavillo et al., 2011; Ramel et al., 2012; Xiao et al., 2012; Ling and Jarvis, 2015; Mignolet-Spruyt et al., 2016; Watson et al., 2018). These messengers, which are generated in chloroplasts, protect plants from abiotic stressors, including excess light, high temperature, drought, and salt (Figure 4). Further, a well-developed chloroplast is necessary to respond to abiotic stressors, as discussed in Chapters 1 and 2.

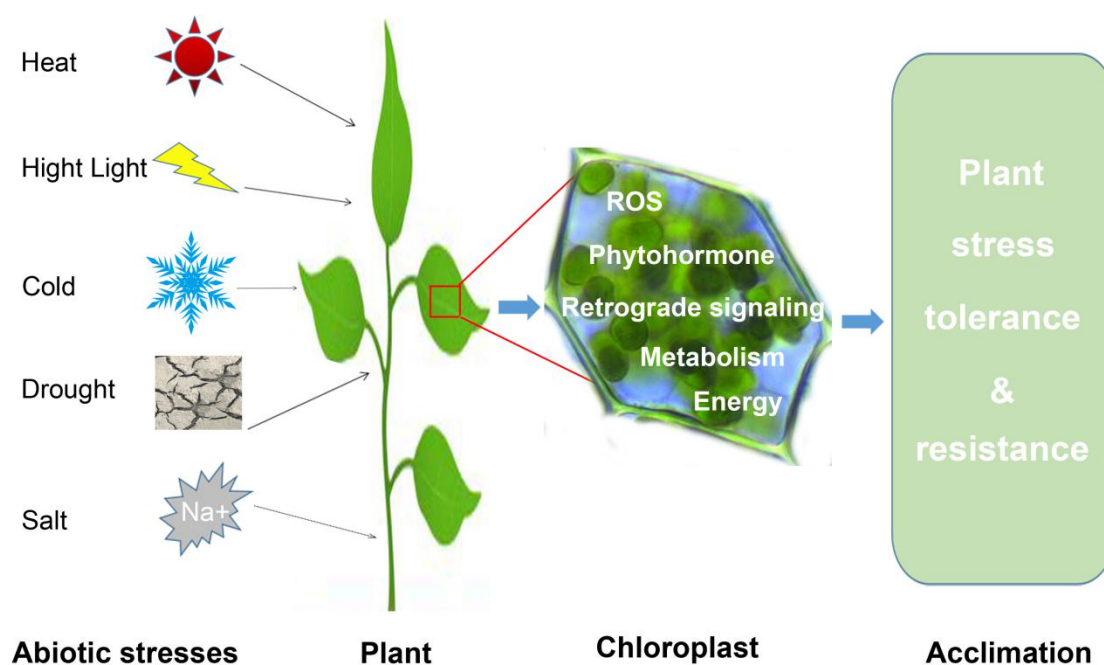


Figure 4. A scheme is shown that depicts a green leaf as the major target of environmental stressors. Chloroplasts in plant cells perceive external stresses and then signals are released and transduced into downstream components to the regulation of plant defensive responses. ROS, reactive oxygen species.

2. Aim of the thesis

The main aim of this thesis was to investigate the role and mechanism of nuclear-factors and chloroplast-factors in chloroplast biogenesis and abiotic stress responses in Arabidopsis.

The first aim was to investigate the localization and functional characterization of PP7L and VEN4, which was shown to be involved in chloroplast biogenesis. The PROTEIN PHOSPHATASE 7-LIKE (PP7L) is now known to be classified into plant protein phosphatase 7 (PP7s) family based on its catalytic subunits (Farkas et al., 2007). VENOSA4 (VEN4) shares amino acid sequence similarity with human SAMHD1, a major regulator of DNA precursor pools in mammalian cells. To understand the functions of PP7L and VEN4, *pp7l* and *ven4* T-DNA lines were analyzed. All the T-DNA lines exhibit delayed chloroplast development in cotyledons and leaves. Further, PP7L-GFP and VEN4-GFP are nuclear-encoded proteins that are localized in the nucleus/cytosol, which was demonstrated expression of GFP fusion protein in protoplasts. To determine how the molecular function of PP7L and VEN4 plays a role in chloroplast development, an in vivo pulse-labeling experiment was performed to confirm that the translation of thylakoid membrane proteins was affected in *pp7l* and *ven4*. In fact, transcriptional networks of *pp7l* indicated a role of phytochrome-interacting factors and CONSTITUTIVE PHOTOMORPHOGENIC9 (COP9) signalosome (CSN), and subsequently corresponding mutants have been identified by imaging PAM. However, quite unexpectedly, none shared the *pp7l* photosynthesis phenotype. Moreover, we found that maturation of chloroplast rRNA and accumulation of chloroplast ribosomal proteins that require the functional PP7L protein. The results of these investigations are shown in **Chapter 1**. VEN4 is homologous to human SAMHD1, which assists in regulating the number of available dNTPs to meet cellular needs and control viral infections (Lahouassa et al., 2012; Hollenbaugh et al., 2013). The aim of **Chapter 2** was to reveal the relevance of VEN4 and dNTP homeostasis for chloroplast biogenesis in cotyledons.

The second aim was to identify the role of PGE in the response, tolerance, and

acclimation to different abiotic stressors using knock-down or overexpression lines of mTERF10, mTERF11, or mTERF12, which are targeted to nucleoids of chloroplasts and are associated with PGE. Our results show a remarkable effect of PGE on salt stress, which indicates a potential role of PGE in ABA signaling. The results of this part are shown in **Chapter 3**.

The third aim was to identify novel candidates that are involved in retrograde signaling pathways via forward-genetic screening. An ethyl methanesulfonate (EMS)-mutagenized population was screened under lincomycin treatment. We have identified *happy* on lincomycin (*holi*) mutants and. Several *holi* mutants were isolated that showed de-repression of *LHCB1.2* expression and chlorophyll synthesis in the presence of LIN. After analysis of whole-genome sequencing, we found that various mutated genes of *holi* and *happy* on norflurazon (*hon*) mutants encoded proteins involved in the flavonoid pathway. Therefore, metabolite analysis and the *gun* phenotype test were performed. This study allowed an understanding of the correlation between *genome uncoupled* (*gun*) signaling and anthocyanin biosynthesis. Moreover, as a link between cell wall integrity and early chloroplast development was revealed. The results are presented in **Chapter 4**.

3. Results

3.1 Chapter 1

Extrachloroplastic PP7L functions in chloroplast development and abiotic stress tolerance

Extrachloroplastic PP7L Functions in Chloroplast Development and Abiotic Stress Tolerance¹[OPEN]

Duorong Xu,^a Giada Marino,^a Andreas Klingl,^b Beatrix Enderle,^c Elena Monte,^d Joachim Kurth,^b Andreas Hiltbrunner,^{c,e} Dario Leister,^a and Tatjana Kleine^{a,2,3}

^aPlant Molecular Biology (Botany), Department Biology I, Ludwig-Maximilians-Universität München, 82152 Planegg-Martinsried, Germany

^bPlant Development, Department Biology I, Ludwig-Maximilians-Universität München, 82152 Planegg-Martinsried, Germany

^cInstitute of Biology II, Faculty of Biology, University of Freiburg, 79104, Freiburg, Germany

^dPlant Development and Signal Transduction Program, Center for Research in Agricultural Genomics Consejo Superior de Investigaciones Científicas-Institute of Agrifood Research and Technology-Universidad Autónoma de Barcelona-Universidad de Barcelona, 08193 Barcelona, Spain

^eCentre for Biological Signalling Studies (BIOSS), University of Freiburg, 79104 Freiburg, Germany

ORCID IDs: 0000-0002-1525-4244 (G.M.); 0000-0002-7340-9355 (E.M.); 0000-0003-0438-5297 (A.H.); 0000-0003-1897-8421 (D.L.); 0000-0001-6455-3470 (T.K.).

Chloroplast biogenesis is indispensable for proper plant development and environmental acclimation. In a screen for mutants affected in photosynthesis, we identified the *protein phosphatase7-like* (*pp7l*) mutant, which displayed delayed chloroplast development in cotyledons and young leaves. PP7L, PP7, and PP7-long constitute a subfamily of phosphoprotein phosphatases. PP7 is thought to transduce a blue-light signal perceived by *crys* and *phy a* that induces expression of SIGMA FACTOR5 (SIG5). We observed that, like PP7, PP7L was predominantly localized to the nucleus in *Arabidopsis* (*Arabidopsis thaliana*), and the *pp7l* phenotype was similar to that of the *sig6* mutant. However, *SIG6* expression was unaltered in *pp7l* mutants. Instead, loss of PP7L compromised translation and ribosomal RNA (rRNA) maturation in chloroplasts, pointing to a distinct mechanism influencing chloroplast development. Promoters of genes deregulated in *pp7l-1* were enriched in PHYTOCHROME-INTERACTING FACTOR (PIF)-binding motifs and the transcriptome of *pp7l-1* resembled those of *pif* and CONSTITUTIVE PHOTOMORPHOGENESIS1 (COP1) signalosome complex (*csn*) mutants. However, *pif* and *csn* mutants, as well as *cop1*, *cryptochromes* (*cry*)1 *cry2*, and *phytochromes* (*phy*)A *phyB* mutants, do not share the *pp7l* photosynthesis phenotype. PhyB protein levels were elevated in *pp7l* mutants, but *phyB* overexpression plants did not resemble *pp7l*. These results indicate that PP7L operates through a different pathway and that the control of greening and photosystem biogenesis can be separated. The lack of PP7L increased susceptibility to salt and high-light stress, whereas PP7L overexpression conferred resistance to high-light stress. Strikingly, PP7L was specifically recruited to Brassicales for the regulation of chloroplast development. This study adds another player involved in chloroplast biogenesis.

¹This work was supported by the Deutsche Forschungsgemeinschaft (project C01 no. KL 2362/1-1 to T.K. and project C05 no. TRR175 to D.L.).

²Author for contact: tatjana.kleine@lmu.de.

³Senior author.

The author responsible for distribution of materials integral to the findings presented in this article in accordance with the policy described in the Instructions for Authors (www.plantphysiol.org) is: Tatjana Kleine (tatjana.kleine@lmu.de).

Research was designed by T.K. and D.X.; the *pp7l:En-1* mutant was confirmed by J.K.; most of the experiments were performed by D.X.; G.M. realized the shot-gun proteomics experiment; A.K. provided TEM pictures; B.E. performed *phyB* western-blot analysis; T.K., D. X., G.M., D.L., A.H., and E.M. analyzed the data; T.K. wrote the manuscript with input primarily from D.L., A.H., and E.M., and then all authors; the whole study was supervised by T.K.; all authors read and approved the article.

[OPEN] Articles can be viewed without a subscription.

www.plantphysiol.org/cgi/doi/10.1104/pp.19.00070

Chloroplasts are the site of photosynthesis and are essential for plant growth and development. They are the prototypes of a diverse family of organelles, the plastids, which are found in plants and various algae (Keeling, 2010). As descendants of cyanobacteria-like progenitors, plastids of higher plants are semiautonomous organelles that have retained a reduced genome of ~100 genes (Kleine et al., 2009). However, they also contain ~2,000–3,000 nuclear-encoded proteins (Abdallah et al., 2000; Yu et al., 2008). Consequently, chloroplast multiprotein complexes, such as the photosynthetic apparatus and the chloroplast gene expression machinery, comprise a mixture of proteins encoded by chloroplast and nuclear genes, and chloroplast function therefore requires stringent coordination of the expression of the two genomes (Woodson and Chory, 2008). This is achieved by bidirectional exchange of information between the organelles. During retrograde signaling, chloroplasts send out signals that

inform the nucleus about their developmental and physiological status so that nuclear gene expression can be adjusted accordingly (Bobik and Burch-Smith, 2015; Chan et al., 2016; Kleine and Leister, 2016). Because most chloroplast proteins are encoded in the nucleus, the nucleus exercises anterograde control over the plastids by regulating various functions, in particular chloroplast gene expression (Tiller and Bock, 2014; Schmitz-Linneweber et al., 2015; Shikanai, 2015).

In true leaves, chloroplasts develop from meristematic proplastids when the leaf primordia emerge; in cotyledons, chloroplasts develop from proplastids/eoplasts or etioplasts present in mesophyll tissue within the embryo (Waters and Langdale, 2009; Liebers et al., 2017). These precursors are rapidly converted into chloroplasts upon exposure to light. Thus, the development of photosynthetically competent chloroplasts in angiosperm seedlings is strictly dependent on exposure to light (Pogson and Albrecht, 2011) and involves the so-called chloroplast biogenic signaling pathway, which triggers massive changes in the nuclear transcriptome, with at least 20% of the genome showing light-regulated differential expression during seedling development (Jiao et al., 2007; Jarvis and López-Juez, 2013). Light is perceived mainly by two families of photoreceptors—the phytochromes (phys) and the cryptochromes (crys)—which are sensitive to red/far-red and UVA/blue light, respectively, and undergo conformational changes upon light perception that enable them to interact with downstream signaling partners (Jiao et al., 2007). The latter include PHYTOCHROME-INTERACTING FACTOR (PIF)-like transcription factors of the basic helix-loop-helix (bHLH) family and basic Leu zipper (bZIP) transcription factors, such as ELONGATED HYPOCOTYL5 (HY5) and HY5-like HYH (Jiao et al., 2007; Leivar and Monte, 2014). PIFs mainly repress photomorphogenesis genes in the dark, whereas HY5 and HYH activate those same genes upon illumination. Hence, PIFs and HY5/HYH have antagonistic functions in the regulation of e.g. protochlorophyllide production and reactive oxygen species (ROS)-responsive genes during the dark-to-light transition (Chen et al., 2013). In the dark, HY5 is targeted for degradation by the ubiquitin ligase CONSTITUTIVE PHOTOMORPHOGENESIS1 (COP1) in the nucleus (Osterlund et al., 2000). Therefore, COP1 suppresses photomorphogenic development when translocated to the nucleus (Yi and Deng, 2005) and its nuclear localization is regulated by a component of the COP9 signalosome complex (CSN; Wang et al., 2009). Conversely, upon light exposure, phys trigger PIF degradation and COP1 inactivation (Gommers and Monte, 2018). Strikingly, the HEMERA (HMR)/transcriptionally active chromosome protein 12 (pTAC12) not only contributes to phy signaling in the nucleus, but also forms part of the chloroplast's pTAC and is involved in plastid gene expression (Chen et al., 2010).

In higher plants, transcription of plastid DNA is carried out by a nuclear-encoded phage-type RNA polymerase and a plastid-encoded prokaryotic-like

RNA polymerase (PEP; Pfannschmidt et al., 2015). For its function, the multisubunit enzyme PEP requires a set of polymerase-associated proteins and sigma factors (SIGs), all of which are encoded in the nucleus (Chi et al., 2015; Pfannschmidt et al., 2015). In *Arabidopsis thaliana*, there are six different SIGs, designated as SIG1–SIG6. Depending on their promoter selectivity, SIGs may have overlapping functions as well as specialized roles (Chi et al., 2015). SIG5, for example, effectively mediates blue-light signaling by activating transcription from the “blue-light-responsive” *psbD* promoter (Nagashima et al., 2004), as its own expression is strictly dependent on blue light. The response to blue-light signals in the nucleus is assumed to involve the perception of blue light by crys and phyA, and transduction of the signal by the nucleus-localized protein phosphatase PP7, which in turn leads to the induction of SIG5 expression (Møller et al., 2003; Chi et al., 2015). PP7 is a member of the family of Ser/Thr-specific phosphoprotein phosphatases (PPPs; Farkas et al., 2007). The *Arabidopsis* PPP family comprises 26 members, which can be assigned to seven subfamilies. PPPs have roles in abscisic acid, auxin, and brassinosteroid signaling, phototropism, regulating the target of rapamycin pathway, cell stress responses, and flowering time (Uhrig et al., 2013; Lillo et al., 2014). For example, phy-associated Ser/Thr protein phosphatase, which belongs to the type-6 subfamily, dephosphorylates phyA in vitro and delays flowering (Kim et al., 2002). Members of the PPP family are present in all eukaryotes. However, the type-7 subfamily is unique to plants. In *Arabidopsis*, this subfamily contains three members—PP7, “long PP7,” and “inactive PP7” (Farkas et al., 2007; Uhrig et al., 2013). Only PP7 has been characterized in detail, and shown to regulate blue-light (Møller et al., 2003) as well as red/far-red light signaling (Genoud et al., 2008). Long PP7 is also designated “MAINTENANCE OF MERISTEMS-LIKE3” and encodes a protein bearing a putative aminotransferase domain in addition to the PP7 domain. The phenotype of *mail3-2*, in which a transfer-DNA (T-DNA) is inserted in the PP7 domain, is indistinguishable from that of wild-type plants (Ühlken et al., 2014).

Here, we characterize PP7-like (*pp7l*) mutants, the first of which was identified in a screen for mutants defective in photosynthesis. The *PP7L* gene encodes the PP7 homolog PP7L (previously designated as “inactive PP7”; Farkas et al., 2007). PP7L is localized to the nucleus, and is a positive regulator of protein synthesis in the developing chloroplast. However, it does not act by modulating SIG factor gene expression like PP7. Instead, the *pp7l* mutant is shown here to be defective in chloroplast ribosomal RNA (rRNA) maturation, and consequently in mRNA translation. Promoter analysis of genes deregulated in the *pp7l-1* mutant and database analysis of conditions or mutations associated with gene expression changes similar to those seen in *pp7l-1* suggested a tentative association of PP7L with PIFs and other light signaling components, but neither *pif*, *csn*, *cop1*, *cry1* *cry2*, or *phyA* *phyB* mutants display a

photosynthesis phenotype. Moreover, although phyB levels are enhanced in *pp7l* mutants, overexpression of phyB does not induce a photosynthesis phenotype. Seed germination of *pp7l* mutants was reduced by exposure to salt and high light, whereas overexpression of *PP7L* rendered 4-week-old plants more tolerant to high light.

RESULTS

Identification and Phenotypic Analysis of Mutants for the *PP7L* Locus

Screening of an Arabidopsis mutant collection carrying insertions of the maize transposable element *En-1* (Wisman et al., 1998) for lines that show alterations in the effective quantum yield of PSII, designated F_{II} , resulted in the recovery of a set of mutants with defects in photosynthesis (Varotto et al., 2000). In one of these (ZIGIA line V2-880), the effective (F_{II}) and maximum (F_v/F_m) quantum yields of PSII were significantly reduced in emerging leaves of 3-week-old plants compared to the wild type (Col-0), implying a defect in energy transfer within PSII. Isolation of the genomic sequence flanking the *En-1* transposon enabled identification of the insertion site in the second exon of the gene *AT5G10900* (Supplemental Fig. S1A). *AT5G10900* is listed in the UniProtKB database (<http://www.uniprot.org/uniprot/Q9LEV0>) as “Ser/Thr-protein phosphatase 7 (PP7) inactive homolog.” Thus, *AT5G10900* was designated “PP7L” and the mutant was named “*pp7l:En-1*.” Because the *pp7l:En-1* mutant germinated poorly, further mutant lines were identified with the SIGnAL T-DNA Express Arabidopsis Gene Mapping Tool (<http://signal.salk.edu/cgi-bin/tdnaexpress>). In these lines, named “*pp7l-1*” (SALK_018295), “*pp7l-2*” (SALK_033071), and “*pp7l-3*” (SALK_022053), the pROK2 T-DNA was inserted in exon 4, intron 5, and exon 7 of *PP7L* at positions 651, 1951, and 2251 relative to the start codon, respectively (Supplemental Fig. S1, A and B). In all identified *pp7l* mutants, both overall growth rates and F_v/F_m values were reduced in emerging leaves of 3-week-old soil-grown plants compared to the wild type (Supplemental Fig. S1A).

According to The Arabidopsis Information Resource genome annotation 10, *AT5G10900* is a single-copy gene with three predicted transcript splice forms *AT5G10900.1*, *AT5G10900.2*, and *AT5G10900.3*, which differ only at their 3' ends (Supplemental Fig. S1B). To confirm that the altered expression of *PP7L* was responsible for the mutant phenotype, reverse transcription quantitative PCR (RT-qPCR) was conducted. We found that the *PP7L* transcript was barely detectable in the *pp7l-2* mutant and undetectable in *pp7l-3*, but its level was elevated in *pp7l-1* (Supplemental Fig. S1C). The overexpression of the 39 segment of *PP7L* in the

pp7l-1 allele can be explained by the orientation of the T-DNA integration in the pROK2 vector in the 5'RB (right border)–T-DNA–left border 3' direction, because this vector contains the 35S promoter on the left border site (Baulcombe et al., 1986) and can potentially activate flanking genomic sequences (Ulker et al., 2008). However, because of these differences in *PP7L* transcript accumulation, all *pp7l* mutant lines were transformed with a genomic DNA fragment comprising the coding sequence from the start to the stop codon of *AT5G10900* fused upstream of the enhanced green fluorescence protein (eGFP) reporter gene, which was placed under the control of the Cauliflower Mosaic Virus 35S promoter. Independent transgenic lines for all three mutants were obtained (overexpression of *PP7L* [*oe-PP7L*] *pp7l-1* to -3) and their phenotypic and chlorophyll (Chl) fluorescence analyses showed that the wild-type function had been restored in all *oe-PP7L* lines (Supplemental Fig. S2A). This shows that the *pp7l* phenotype is indeed caused by the insertions within the *AT5G10900* gene. The striking dark-green coloration of *pp7l* leaves (Fig. 1A) was found not to be caused by a higher overall Chl content. In fact, both (Chl *a+b*) and the Chl *a/b* ratio were slightly, but not significantly,

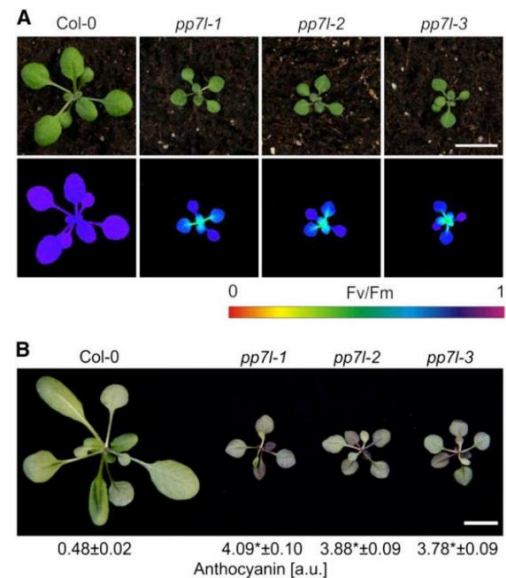


Figure 1. Phenotypic characterization of *pp7l* T-DNA insertion mutants. A, Phenotypes of 3-week-old wild-type (Col-0) and the different *pp7l* mutant plants grown in LD (16-h light/8-h dark) conditions. The maximum quantum yield of PSII (F_v/F_m) was measured with an imaging Chl fluorometer (Imaging PAM). Scale bar = 1 cm. B, The abaxial surface of leaves of plants grown in LD conditions reveals enhanced anthocyanin accumulation in *pp7l* plants. Anthocyanins were extracted and quantified photometrically, and amounts are reported in arbitrary units (a.u.). Data are shown as mean values \pm SD from three different plant pools. Each pool contained >20 plants. Significant differences between the data pairs were identified by Tukey's test, and significant differences ($P < 0.05$) with respect to Col-0 are indicated by asterisks.

reduced compared to the wild type (Supplemental Fig. S2B). Instead, the darker color of *pp7l* leaves, which is most prominent on the abaxial side, can be attributed to the approximately eightfold-higher content of anthocyanins (compared to wild-type levels) found in these mutants (Fig. 1B).

PP7L Is Localized to the Nucleus and the Cytosol

The *pp7l* mutants show a photosynthesis phenotype, which at first sight suggests chloroplast localization of the PP7L protein. However, computational prediction of the subcellular localization of PP7L by the algorithms implemented in SUBA4 (Hooper et al., 2017; <http://suba.plantenergy.uwa.edu.au>) did not result in a chloroplast localization, although various predictors assigned PP7L either to the nucleus, cytosol, or mitochondria, and the SUBAcon algorithm predicted a nuclear localization for PP7L. A putative nuclear localization signal (NLS) was indeed found by the cNLS mapper (Kosugi et al., 2009; http://nls-mapper.iab.keio.ac.jp/cgi-bin/NLS_Mapper_form.cgi), which predicts a bipartite NLS (ISKRVLDSKLEACKFAFLKL-SAVKTTRMK) spanning the region from amino acids 6 to 34. To experimentally examine the subcellular localization of PP7L, protoplasts were transformed with the 35S:PP7L-eGFP construct that had been used for complementation of the *pp7l* alleles. Visualizing eGFP fluorescence in the protoplasts confirmed that PP7L-eGFP was targeted to the nucleus (Fig. 2). Moreover, several protoplasts displayed eGFP fluorescence in the cytosol, indicating a dual (nuclear and cytosolic) localization of PP7L.

PP7L Is a Positive Regulator of Photosynthesis at Young Developmental Stages

In addition to the drop in F_v/F_m seen in emerging leaves of *pp7l* mutants, reduced photosynthetic activity

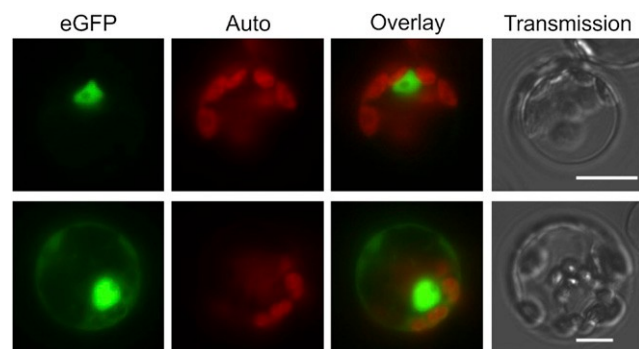


Figure 2. PP7L is localized to the nucleus and the cytosol. Fluorescence microscopy of Arabidopsis protoplasts transiently expressing PP7L fused to eGFP. The eGFP fluorescence (green) and chloroplast autofluorescence (red) are shown together in the overlay picture. Scale bars = 10 μ m.

was observed during seedling development. In 4-, 5-, 6-, and 7-d-old seedlings, F_v/F_m was significantly depressed in all *pp7l* mutants to 0.41, 0.54, 0.62, and 0.71, respectively, compared to the respective wild-type values of 0.75, 0.78, 0.79, and 0.80 (Fig. 3A), and this depressed F_v/F_m recovered completely after 10 d (Fig. 3B). Interestingly, this phenotype is reminiscent of those of *sig2* and *sig6* seedlings (Fig. 3B) and of young leaves of the *sig6* mutant (Fig. 3C). It was previously shown that *sig2* and *sig6* mutant seedlings are pale green and accumulate fewer plastid- and nuclear-encoded transcripts for photosynthesis proteins, whereas *sig1*, *sig3*, *sig4*, and *sig5* seedlings appear more like wild type (Woodson et al., 2013); for the *sig5* mutant, see Figure 3C. Because PP7 has been implicated in the induction of *SIG5* expression (reviewed in Chi et al., 2015), we asked whether PP7L might similarly act through SIG-mediated gene expression changes. Because *sig2* and *sig6* seedlings show a transient photosynthesis phenotype that resembles the *pp7l* phenotype, *SIG2* and *SIG6* mRNA levels were studied in 4- and 5-d-old wild-type and *pp7l-1* seedlings by RNA gel-blot analysis. In fact, we found that levels of *SIG2* and *SIG6* transcripts were increased and not decreased in *pp7l-1* (Fig. 3D).

To obtain an overall insight into the RNA expression pattern of nuclear- and organelle-encoded genes when PP7L function is compromised, RNAs isolated from 4-d-old wild-type and *pp7l-1* mutant seedlings grown in long-day (LD; 16-h light/8-h dark) conditions were subjected to long non-coding (lnc)RNA sequencing. With this method, the elevated levels of *SIG2* (1.8-fold) and *SIG6* (1.7-fold) mRNA were confirmed. Also, *SIG1*, *SIG3*, and *SIG4* transcripts were slightly increased, whereas *SIG5* mRNA levels were almost unchanged (0.9-fold) in *pp7l-1* (Fig. 3E; Supplemental Table S2). Moreover, comparison of whole genome transcriptome changes in *pp7l-1* with previously published mRNA-sequencing (Seq) data for *sig6* showed that *pp7l-1* and *sig6* mutants do not provoke similar gene expression changes (Fig. 3F).

In summary, PP7L does not positively regulate SIG gene expression. Therefore, PP7L likely acts through a mechanism that is different from that of PP7.

PP7L Is Involved in the Regulation of Chloroplast Gene Expression

The lncRNA-Seq analysis revealed substantial changes in gene expression in 4-d-old *pp7l-1* seedlings, specifically 1,198 and 1,004 genes whose mRNA levels were significantly (more than twofold) reduced or elevated, respectively (Supplemental Table S2). Genes encoding enzymes of the phenylpropanoid pathway leading to anthocyanin like DIHYDROFLAVONOL4-REDUCTASE (TRANSPARENT TESTA3), ANTHOCYANIDIN SYNTHASE, and the key enzyme CHALCONE SYNTHASE were upregulated 14-, seven-, and fourfold, respectively, a finding that is consistent with higher anthocyanin

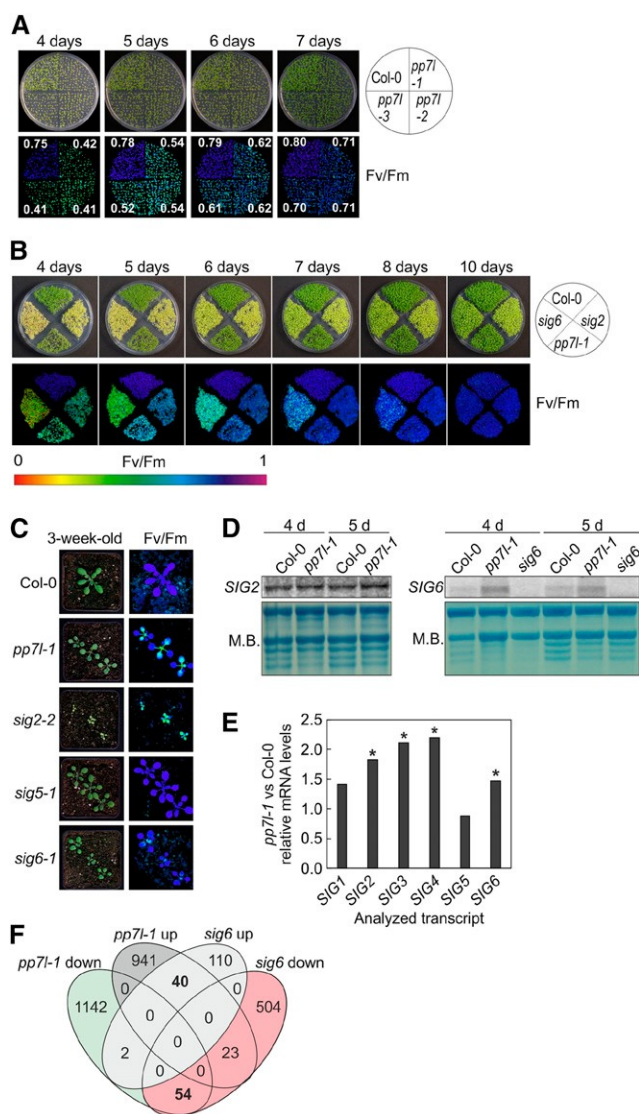


Figure 3. Comparative analysis of *pp7l-1* and *sig* (*sig2* and *sig6*) mutants. A, Phenotypes of 4- to 7-d-old Col-0 and the different *pp7l* mutant seedlings together with Imaging PAM pictures showing maximum quantum yields of PSII (F_v/F_m). SDs are provided in Supplemental Table S1. B, Phenotypes and Imaging PAM images representing the F_v/F_m activity of 4- to 10-d-old Col-0, *pp7l-1* and *sig2* and *sig6* mutant seedlings. C, Phenotypes of 3-week-old Col-0, *pp7l-1*, and *sig* mutant plants and Imaging PAM pictures showing maximum quantum yields of PSII (F_v/F_m). Scale bars = 1 cm. D, Northern-blot analysis of *SIG2* and *SIG6* transcripts in 4- and 5-d-old Col-0 and *pp7l-1* plants. For the detection of *SIG6* mRNA levels, the *sig6* mutant was included as a control, because several unspecific bands were detected with the *SIG6* probe. Total RNAs were fractionated in a formaldehyde-containing denaturing gel, transferred onto a nylon membrane, and probed with (α - ^{32}P) dCTP-labeled cDNA fragments specific for the different *SIG* transcripts. The rRNA was visualized by staining the membrane with methylene blue (M.B.) and served as a loading control. E, Graph representing the changes (relative to Col-0 values) in *SIG* mRNA levels in *pp7l-1*, as determined by lncRNA-Seq analysis. Significant differences (DESeq2 analysis running with the fit type set to "parametric"; adjusted $P < 0.05$) with respect to Col-0 are denoted by asterisks. The SD was not calculated, because differentially expressed genes were identified with

accumulation in *pp7l* mutants (see Fig. 1B). Although photosynthetic activity is reduced in *pp7l* mutants (see Figs. 1A and 3A), no enrichment for genes related to photosynthesis or the chloroplast could be identified among those downregulated in *pp7l-1* mutant seedlings with the gene ontology (GO) analysis tool DAVID (Huang et al., 2009; Fig. 4A). Instead, under the categories "cellular component," "biological process," and "molecular function," DAVID detected an enrichment of genes encoding proteins for the "RNA polymerase II transcription factor complex," "response to sucrose starvation," and "glutaredoxin activity," respectively (Fig. 4A). These groups encompass genes encoding bHLH transcription factors, or extracellular proteins like protease inhibitor/seed storage/lipid transfer family proteins, xyloglucan endotransglucosylase/hydrolase proteins, and peroxidase superfamily proteins.

However, among the elevated transcripts within the "cellular component" category, most component categories were associated with the chloroplast, in particular "nucleoid," "plastid chromosome," "chloroplast stroma," "envelope," and "thylakoid" (Fig. 4B). In the category "biological process," the GOs "chloroplast rRNA processing" and "chlorophyll biosynthesis" were the most highly enriched (Fig. 4B). In particular, the rise in transcripts for proteins involved in chloroplast RNA metabolism has already been noted in mutants and conditions that impair protein synthesis in the chloroplast (Leister and Kleine, 2016).

Investigation of plastid-encoded transcripts in the lncRNA-Seq data showed that transcripts of only five genes were reduced by more than twofold. These encode subunit 8 of the cytochrome *b₆f* complex, several PSII proteins (D1, PsbK, PsbI), and the PSI protein Psaj (Supplemental Table S2). Conversely, expression levels of 44 plastid genes rose by more than twofold. Among these are genes encoding tRNAs, ribosomal proteins, subunits of RNA polymerase and ATP synthase, and the PSII proteins CP47, D2, and PsbT.

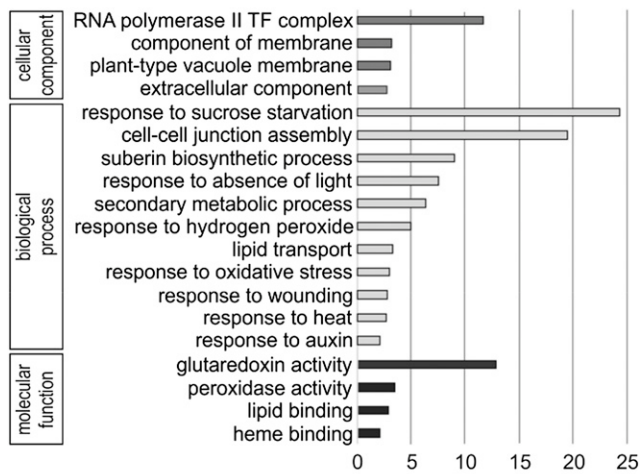
Taken together, these transcriptome changes point to a role for PP7L in posttranscriptional processes in the chloroplast.

Lack of PP7L Impairs Chloroplast Translation and Development

To investigate whether the defect in photosynthetic activity found in the *pp7l* mutants was a consequence of reduced accumulation of photosynthetic proteins, shot-gun proteomics was performed on total protein extracts from 4-d-old wild-type and *pp7l-1* seedlings grown under LD conditions. In the *pp7l-1* mutant,

"parametric" and not "mean" fit settings in DESeq2. F, Venn diagrams depicting the degree of overlap between the sets of genes whose expression levels were altered by at least twofold (up or down) in the *pp7l-1* mutant compared with the *sig6* mutant.

A *pp7l-1* vs Col-0 down



B *pp7l-1* vs Col-0 up

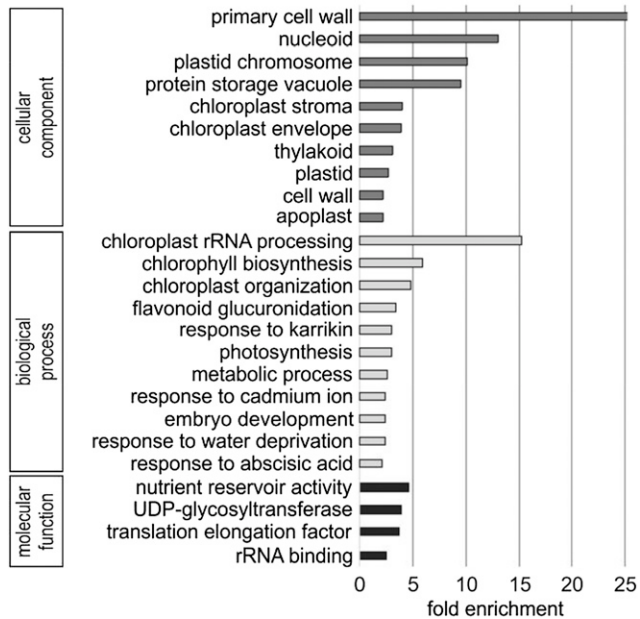


Figure 4. GO analysis of genes whose expression is reduced (A) or elevated (B) in *pp7l-1* seedlings compared to Col-0 grown for 4 d in LD conditions. GO annotations for the cellular component, biological process, and molecular function categories were extracted from DAVID (Huang et al., 2009). GO terms with a ≥ 2 -fold change and a Benjamini corrected value of <0.05 are shown. TF, transcription factor.

chloroplast-encoded subunits of PSI and PSII, the chloroplast ATP synthase, the cytochrome *b₆f* complex, the large subunit of Rubisco, and also ribosomal proteins accumulated to lower levels than that in wild type (Fig. 5, A and B; Supplemental Table S3). Western-blot analyses confirmed this for representative subunits of the different photosynthesis complexes (Fig. 5C), and also confirmed that protein levels were restored in *oe-PP7L pp7l-1* and -2 lines. In contrast, lncRNA-Seq indicated that most of the corresponding transcripts—except *psbA*—accumulated to higher levels than those

seen for the protein levels in the *pp7l-1* mutant (Fig. 5, A and B; Supplemental Table S2), which was confirmed by RNA gel-blot analysis for representative instances (Fig. 5D). A scatter plot demonstrates that the relative changes in protein amounts are negatively correlated with those in the levels of the corresponding mRNAs (Fig. 5B). For example, *psbD* mRNA was nearly at wild-type levels (protein: $\sim 10\%$ of wild type) and *rbcl* transcripts were only slightly reduced if at all (RNA-Seq data: 100% wild type; RNA gel blot: 75% wild type) but amounts of the corresponding proteins were drastically reduced ($\sim 15\%$ of wild type; Fig. 5, C and D). Thus, the reduced amounts of chloroplast-encoded proteins in the *pp7l-1* mutant cannot be explained by a relative dearth of their transcripts. Closer inspection of Figs. 3D and 5D revealed, however, that amounts of chloroplast rRNAs were abnormally low in *pp7l-1* seedlings, as indicated by methylene-blue staining of membranes. In the chloroplasts of land plants, the rRNAs are encoded in the rRNA operon, which contains the genes for tRNAs for Ile, Ala, and Arg, and for 16S, 23S, 4.5S, and 5S rRNAs (Supplemental Fig. S3A). This gene cluster is transcribed as a single molecule and processed via endonucleolytic cleavage and exonucleolytic trimming events (Strittmatter and Kössel, 1984). Indeed, RNA gel-blot analyses showed that in all *pp7l* alleles, levels of mature 23S rRNA were lower than in the wild type, whereas unprocessed precursors overaccumulated and 16S rRNA was unaffected (Supplemental Fig. S3B). This, together with the fact that amounts of chloroplast ribosomal proteins were reduced in *pp7l-1* (Fig. 5A), suggests that *pp7l* mutants might experience a general reduction in chloroplast translation capacity—an inference that is compatible with the overall analysis of lncRNA-Seq data. To assess this possibility, the effects of the *pp7l-1* mutation on the translational efficiency of chloroplast transcripts were further examined by analyzing the association of *psbD* and *rbcl* mRNAs with polysomes. Seedling extracts were fractionated in Suc gradients under conditions that preserve polysome integrity, and mRNAs were identified by hybridization with specific probes. In general, efficiently translated RNAs migrate deep into the gradient because almost all are associated with ribosomes. Methylene blue staining of rRNAs in wild type and *pp7l-1* polysome gradients showed similar, though not identical distributions, indicating that there was no general difference in ribosome distribution between mutant and wild-type plants. However, *psbD* and *rbcl* mRNA were shifted toward nonpolysomal fractions in *pp7l-1* as compared to the wild type (Fig. 5E), indicating that these mRNAs were less likely to be associated with polysomes in the *pp7l-1* mutant and that at least some of the mRNAs in *pp7l-1* chloroplasts are less engaged in translation.

The effects of the *pp7l-1* mutation on the translation of chloroplast transcripts were further investigated by in vivo labeling, which allows one to quantify de novo protein synthesis. To this end, synthesis of plastid-encoded thylakoid membrane proteins was monitored by pulse labeling of wild-type, *pp7l-1* mutant, and

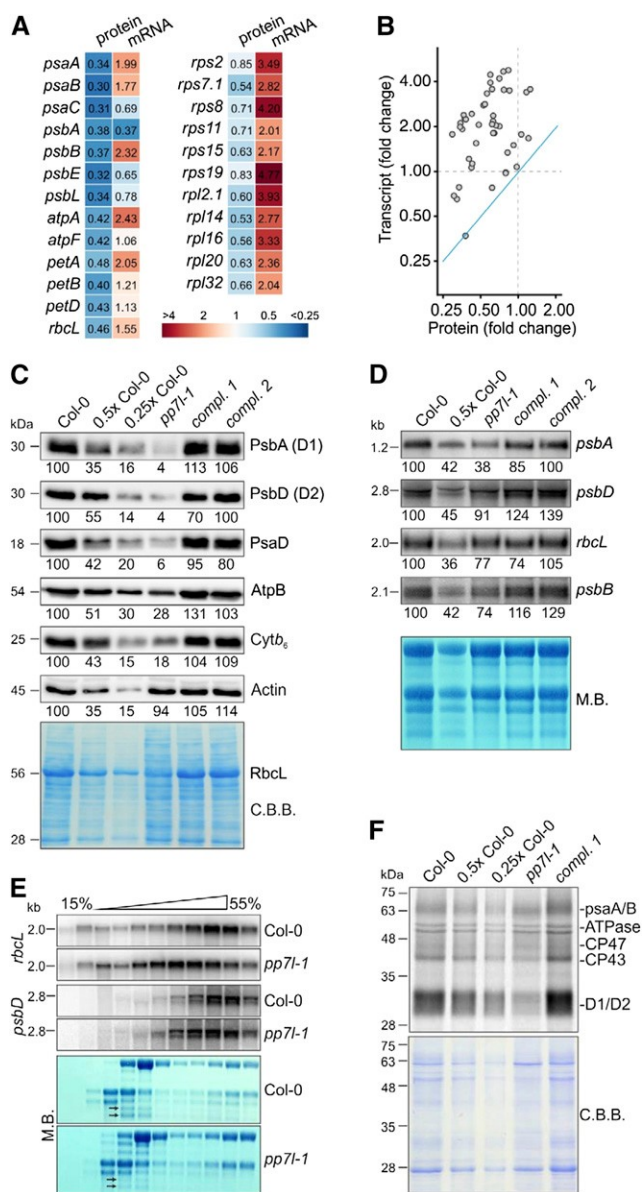


Figure 5. Accumulation of chloroplast-encoded proteins is perturbed at steps downstream of chloroplast transcription in *pp7l-1*. **A**, Heat-map showing relative protein (determined by shot-gun proteomics) and transcript levels (determined by lncRNA-Seq) in 4-d-old *pp7l-1* seedlings compared to Col-0 grown in LD conditions. Only a selection of all data are shown. **B**, Scatter plot showing the anticorrelation between changes in the levels of mRNAs and their protein products. The blue line indicates the theoretical 1:1 correlation. **C**, Immunoblot analysis of representative thylakoid proteins. Total protein extracts from 4-d-old wild-type (Col-0), *pp7l-1*, and *oe-PP7L pp7l* complemented (compl.) seedlings were fractionated by SDS-PAGE, and blots were probed with antibodies raised against individual subunits of photosynthetic complexes. Decreasing levels of wild-type proteins were loaded in the lanes marked Col-0, 0.5x Col-0, and 0.25x Col-0 (1x Col = 5 μ g). Actin and the Coomassie Brilliant Blue (C.B.B.)-stained membrane served as loading controls. Please note that RbcL protein levels are decreased in *pp7l-1* seedlings. Thus they are also reduced on the C.B.B.-stained membrane. **D**, Steady-state levels of transcripts of photosynthetic genes. Total RNA was isolated from 4-d-old Col-0, *pp7l-1*, and *oe-PP7L pp7l*

oe-PP7L pp7l-1 seedlings in the presence of cycloheximide, which inhibits the translation of nuclear-encoded proteins. After pulse labeling for 30 min, de novo synthesis of the D1 and D2 proteins was found to be strongly reduced in *pp7l-1* relative to the wild type (Fig. 5F)—although *psbD* (encoding the D2 protein) transcript levels were notably high (Fig. 5D; Supplemental Table S2).

To further investigate the role of PP7L in chloroplast development, the ultrastructure of *pp7l* chloroplasts was investigated. Cotyledons from 4-d-old wild-type and *pp7l-1* seedlings were fixed, embedded, sectioned, and examined for the morphology of chloroplasts by transmission electron microscopy (TEM). Thin sections of wild-type cotyledons revealed normally developed chloroplasts with their internal structures intact. Because the plant material was directly fixed after 8 h in the dark, wild-type chloroplasts did not show any starch granules and, moreover, the stroma and grana thylakoids were well structured (Fig. 6). The chloroplasts of the *pp7l-1* mutant contained large starch granules and an elevated number of plastoglobuli. Moreover, the thylakoids in these chloroplasts were less well ordered, indicating a delay in chloroplast development in the *pp7l-1* mutant.

Together, these findings suggest that chloroplast transcription is not primarily affected in *pp7l*, but hint at a disturbance of subsequent processes in chloroplast gene expression that would account for the reduction in synthesis of chloroplast proteins and the delay in chloroplast development in the *pp7l* mutants.

Photosynthesis Is Not Affected in Photomorphogenesis and Light Signaling Mutants

In addition to driving photosynthesis, light is a major factor in controlling the expression of photosynthesis genes (Berry et al., 2013). The most prominent light-sensing proteins that mediate light-responsive gene

(compl.) seedlings, and aliquots (7 and 3.5 μ g from Col-0; 7 μ g from all other lines) were fractionated in a formaldehyde-containing denaturing gel, transferred onto a nylon membrane, and probed with (α -³²P)dCTP-labeled cDNA fragments specific for transcripts encoding individual subunits of PSII (*psbA*, *psbB*, *psbD*) and *rbcL*. rRNA was visualized by staining the membrane with methylene blue (M.B.) and served as a loading control. **E**, Chloroplast mRNAs accumulate in nonpolysomal fractions in *pp7l-1* plants. Whole-cell extracts from Col-0 and *pp7l-1* plants were fractionated in linear 0.44–1.6 M (15% to 55%) Suc gradients by ultracentrifugation. Gradients were divided into 11 fractions, and RNA was isolated from equal volumes. RNA blots were hybridized with [α -³²P]dCTP-labeled cDNA fragments specific for *psbD* and *rbcL*. Ribosomal RNAs were stained with M.B. Arrows indicate the difference in 23S rRNA accumulation. **F**, In vivo pulse-labeling of thylakoid membrane proteins with [³⁵S]Met in the presence of cycloheximide indicates that translation occurs at reduced rates in *pp7l-1* chloroplasts. Proteins were resolved by SDS-PAGE after pulse-labeling for 30 min, and visualized by autoradiography. The C.B.B.-stained membrane served as a loading control.

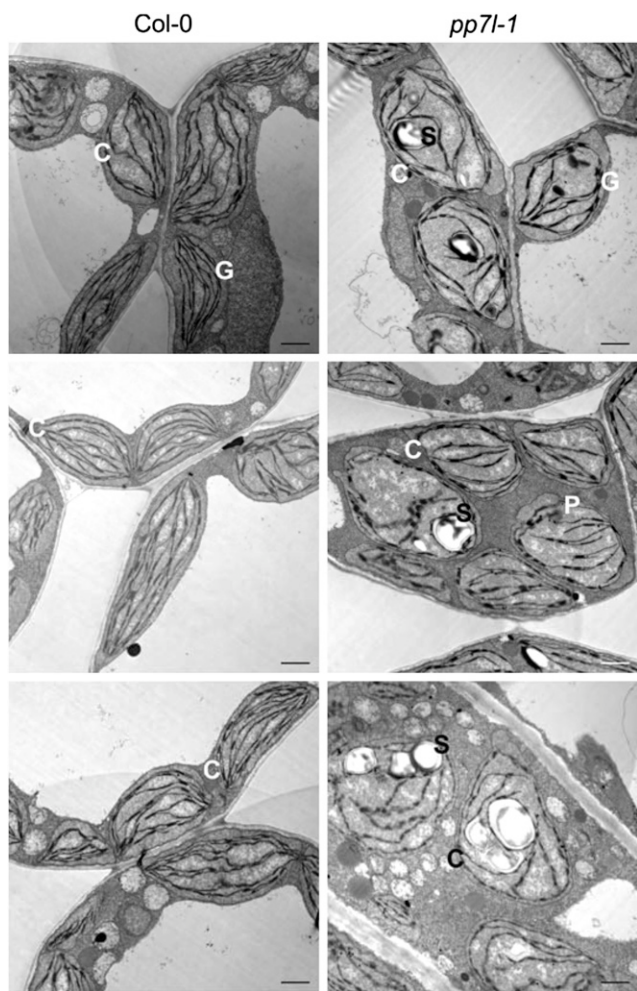


Figure 6. Chloroplast development is disturbed in the *pp7l-1* mutant. TEM images of ultrathin sections of 4-d-old wild-type and *pp7l-1* cotyledons. The wild type shows chloroplasts with a well-developed thylakoid system and grana stacks. Chloroplasts in the *pp7l-1* mutant contain large starch grains, although the seedlings were stored in darkness before the cotyledons were thin-sectioned. Moreover, *pp7l-1* chloroplasts contain more plastoglobuli and the thylakoid system is less developed. Bar = 1 μ m. C, chloroplast; G, grana; P, plastoglobule; S, starch grain.

expression are *phys* and *cry1* and *cry2*. Crys mediate blue-light induction of nuclear genes that encode chloroplast photosynthesis proteins or components of the chloroplast transcriptional apparatus (reviewed in Yu et al., 2010). Diverse developmental and physiological processes are controlled by *phyA* and *phyB*, including Chl synthesis (McCormac and Terry, 2002). In fact, 4-d-old *pp7l* seedlings contain less Chl than do wild-type seedlings (Fig. 7A). Moreover, photoactivated crys (Yu et al., 2010) and *phys* (Li et al., 2011) repress the COP1-dependent degradation of transcription factors that control the expression of light-responsive genes, and Chl content is reduced in *cop1-4* seedlings just as in *pp7l-1* seedlings (Fig. 7A). F_v/F_m measurements are a simple read-out for PSII function.

However, to our knowledge, these measurements have not been extensively performed on *cry*, *phy*, and *cop1* mutants grown under normal light conditions, and F_v/F_m values can only be extracted from the controls used in stress studies of adult plants (Kleine et al., 2007; Rusaczonok et al., 2015). Thus, we determined F_v/F_m values in 4-week-old wild-type, *cop1-4*, *cry1-304 cry2-1*, *phyA-211 phyB-9*, and—as a control—*pp7l-1* mutant plants grown under LD conditions. As expected, F_v/F_m was reduced in the younger leaves of *pp7l-1* plants, but none of the other mutants showed any decrease in the maximum quantum yield of PSII (Supplemental Fig. S4).

Promoters of Genes Deregulated in *pp7l-1* Contain PIF-Related Cis-Acting Elements

To study the transcriptional networks activated by lack of PP7L, the lncRNA-Seq data were investigated in more detail. Cis-acting elements that are overrepresented in promoters of differentially regulated genes in the *pp7l-1* mutant were identified by scanning 1,000-basepair (bp) promoter sequences for 8-bp cis-elements with the expectation-maximization-based program Amadeus (Linhart et al., 2008). Because a very large set of genes is differentially regulated in the *pp7l-1* mutant, we focused on genes with more than 4-fold up- or downregulation (363 down; 188 up). The putative cis-elements thus identified were used to search the JASPAR plant database (<http://jaspar.genereg.net/>; Khan et al., 2018) for Arabidopsis transcription factors known to bind to similar sequences. The highest similarity between queried motifs is defined by the lowest E-value. The motifs with the lowest E-value found by JASPAR for both the promoters of up- and downregulated gene sets contained the G-box motif CACGTG (Fig. 7B). The G-box motif is highly conserved and is bound by bHLH and bZIP transcription factors in organisms ranging from yeasts to humans. In plants, these two transcription factor families have expanded massively; e.g. in Arabidopsis, >100 bHLH transcription factors have been described (Carretero-Paulet et al., 2010). Sequences flanking the G-boxes define the specificity of protein binding (Williams et al., 1992) and enable one to predict the in vitro binding of bZIP homodimers (Ezer et al., 2017). In addition, a number of studies have experimentally determined the binding motifs of several transcription factors (Becker et al., 2017). In fact, among the downregulated gene set, binding sites for the phytochrome-interacting factors PIF4 and PIF5, as well as the bHLH transcription factor MYC3, were identified by JASPAR, whereas interaction sites for PIF1, PIF3, and the abscisic-acid response element binding factor 1 were found in the upregulated gene set (Fig. 7B).

To obtain more information on the putative function of PP7L, the list of genes that are differentially expressed in the *pp7l-1* mutant was submitted to the

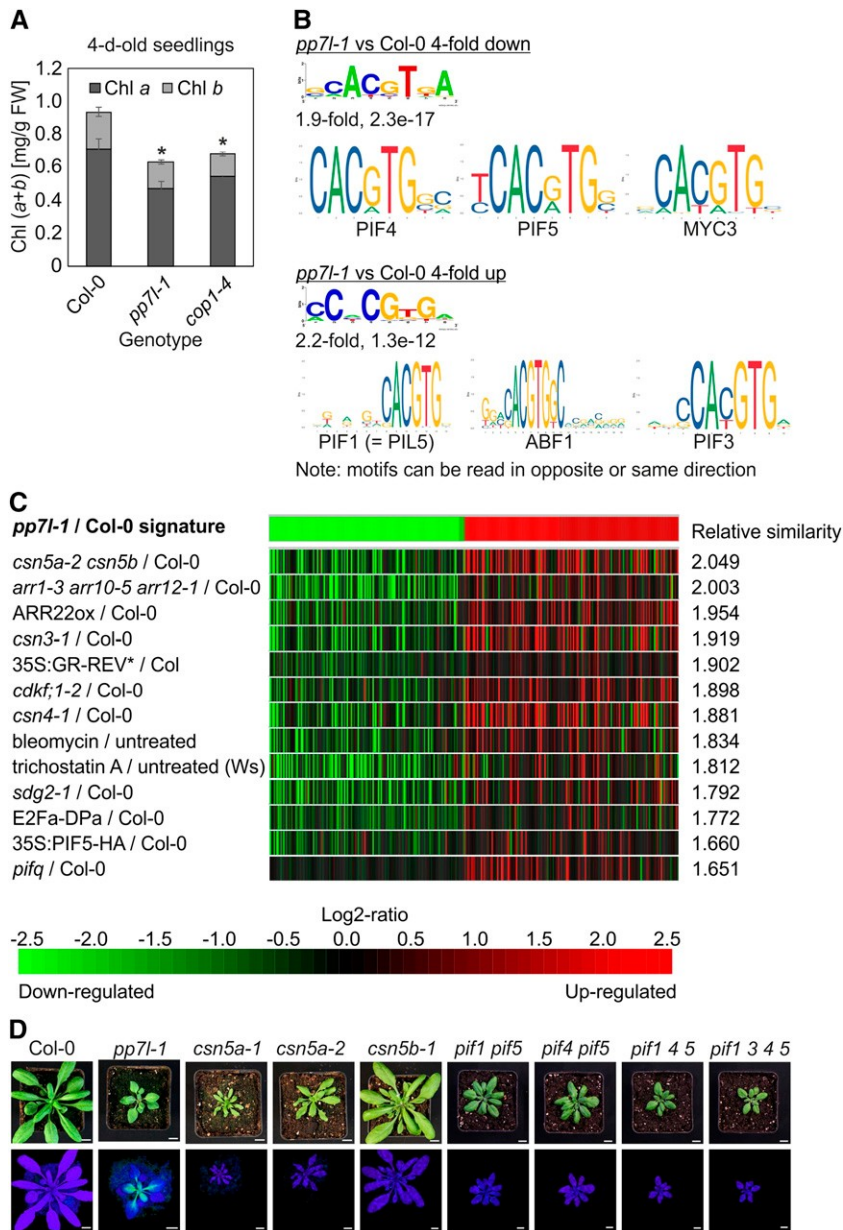


Figure 7. Chl content of 4-d-old *pp7l-1* and *cop1-4* seedlings, and identification of cis-elements in *pp7l-1* deregulated genes and conditions that have a similar effect on the transcriptome to those seen in the *pp7l-1* mutant. A, Determination of total Chl (Chl a + b) content. Note that Chl is significantly reduced in 4-d-old *pp7l-1* seedlings, in contrast to its essentially wild-type content in 4-week-old *pp7l-1* plants (see Supplemental Fig. S2B). Pigments were acetone-extracted, measured spectrophotometrically, and concentrations were determined as described in Jeffrey and Humphrey (1975). Data are shown as mean values \pm sd from three different plant pools. Each pool contained >20 plants. The significant difference (Tukey's test; $P < 0.05$) between the mutants and Col-0 was identified by Tukey's test, and is denoted by an asterisk. B, Sequence logos of the most significantly identified cis-elements of genes whose expression was reduced or elevated in the *pp7l-1* mutant compared to Col-0. The names of the putative transcription factors binding to the identified cis-elements, together with their respective logos, are also shown. C, Identification of perturbations that induce similar changes in gene expression to those identified in the *pp7l-1* mutant. The gene expression changes of the 200 most strongly up- or downregulated genes in 4-d-old *pp7l-1* seedlings were submitted to the Genevestigator Signature Tool (Hruz et al., 2008). Mutants or conditions that triggered the most similar gene expression profiles were identified by Pearson distance clustering. Note that the higher the relative similarity parameter, the higher the similarity to the *pp7l-1* signature. D, Phenotypes of 4-week-old Col-0, *pp7l-1*, and the various *csn* and *pif* mutant plants. In the bottom row, Imaging PAM pictures depict the maximum quantum yields of PSII (F_v/F_m). Scale bars = 1 cm.

Genevestigator database (Hruz et al., 2008; <https://www.genevestigator.com/gv/>) to identify mutants and conditions associated with similar transcriptomic profiles. The most similar transcriptomic responses were found in the *csn5a-2 csn5b* mutant (Dohmann et al., 2008), in which the function of the CSN multi-protein complex is compromised, and the *pif1 pif3 pif4 pif5* quadruple mutant (Leivar et al., 2008; Fig. 7C). These results prompted us to test whether the F_v/F_m was reduced in the emerging leaves of 4-week-old *csn5a-1*, *csn5a-2*, *csn5b-1*, *pif1 pif5*, *pif4 pif5*, *pif1 pif4 pif5*, and *pif1 pif3 pif4 pif5* quadruple mutants, as it is in the *pp7l* mutants. The *csn5a csn5b* double mutant was not included, because it ceases growing at earlier stages of development (Dohmann et al., 2005). However, although all mutants—with the exception of the *csn5b-1*

mutant—displayed a growth phenotype similar to that of *pp7l-1*, none of them exhibited any change (relative to that in the wild type) in the F_v/F_m value (Fig. 7D).

phyB mRNA and Protein Levels Are Elevated in *pp7l-1*

Inspection of the lncRNA-Seq data revealed that transcripts coding for several phy/PIF signaling-associated proteins like pTAC12 (Chen et al., 2010), GOLDEN2-LIKE1 (Martín et al., 2016), and NUCLEOSIDE DIPHOSPHATE KINASE2 (Shen et al., 2005; Supplemental Table S2) accumulate to higher levels in *pp7l-1* mutants. Moreover, *PHYB* mRNA levels were twofold-increased (Supplemental Table S2), a finding that was confirmed for all three *pp7l* alleles by RT-qPCR

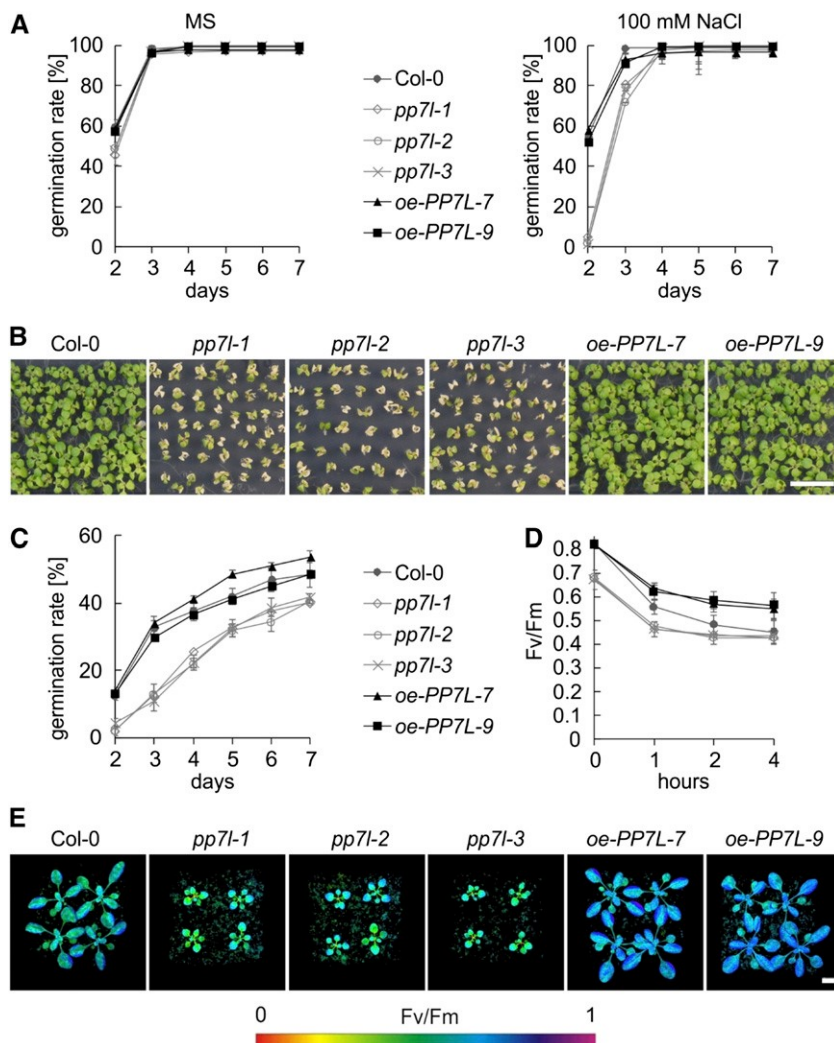
(Supplemental Fig. S5A). To test whether the elevated *PHYB* mRNA levels were reflected in corresponding changes in phyB protein levels, immunoblot analysis using antiphyB antibodies was performed on total protein extracts isolated from 4-d-old seedlings grown under LD conditions. Indeed, in three independent experiments, the phyB protein level was found to be ~2.5-fold elevated in the *pp7l-1* mutant, but was similar to that in wild type in *oe-PP7L pp7l-1* (Supplemental Fig. S5B). Therefore, we asked whether the *pp7l* F_v/F_m phenotype might be a consequence of the overexpression of phyB. For this purpose, a line was used in which phyB was overexpressed under the control of the 35S promoter in the No-0 background (designated “ABO”; Wagner et al., 1991). However, the maximum quantum yield of PSII was not reduced in 3- and 4-d-old ABO seedlings (Supplemental Fig. S5C).

We therefore conclude that the reduced photosynthetic capacity of the *pp7l* mutants is not caused (solely) by their abnormally high levels of phyB.

PP7L Is Involved in the Tolerance to Salt and High-Light Stress

Perturbations of organellar gene expression frequently result in the alteration of acclimation and tolerance responses to adverse growth conditions (Leister et al., 2017), which include the tolerance to salt (Lee et al., 2014) and high-light stress (Coll et al., 2009). To investigate whether PP7L might play a role in the response to the aforementioned stresses, seeds of wild type, *pp7l* mutants, and *PP7L* overexpression lines (*oe-PP7L*; Supplemental Fig. S6) were germinated on Murashige and Skoog (MS) medium supplemented with 100 mM NaCl and on MS medium without supplement as control (Fig. 8A). Additionally, seeds were germinated under high light (1,000 $\mu\text{mol photons m}^{-2} \text{s}^{-1}$; Fig. 8C), and germination rates were followed from d 2 to d 7. After 2 d on control MS medium under growth light, 60% of wild-type and *oe-PP7L* line seeds germinated (Fig. 8A). Germination rates of *pp7l* mutants (48%) were slightly delayed, but after 3 d all lines displayed an 100% germination rate. The delay in

Figure 8. PP7L affects salt and high-light tolerance. A, Seed germination of wild type (Col-0), *pp7l* mutants and *oe-PP7L* lines on MS medium without NaCl (“MS”), and on MS supplemented with 100-mM NaCl. The data represent mean values \pm SD of three independent experiments, each performed with 100 seeds per treatment and genotype. B, Phenotypes of wild type (Col-0), *pp7l* mutants, and *oe-PP7L* lines grown for 2 weeks on MS supplemented with 100 mM NaCl. Scale bar = 1 cm. C, Germination of wild-type (Col-0), *pp7l* mutants, and *oe-PP7L* line seeds grown under high light (1,000 $\mu\text{mol m}^{-2} \text{s}^{-1}$). The data represent mean values \pm SD of three independent experiments, each performed with 100 seeds per treatment and genotype. D, Graph displaying F_v/F_m values of 4-week-old (Col-0), *pp7l* mutants, and *oe-PP7L* lines treated for the indicated time with high light (1,000 $\mu\text{mol m}^{-2} \text{s}^{-1}$). The data represent mean values \pm SD of three independent experiments. E, Imaging PAM pictures showing the maximum quantum yields of PSII (F_v/F_m) of 4-week-old plants subjected to 1 h of high light (1,000 $\mu\text{mol m}^{-2} \text{s}^{-1}$). Scale bar = 1 cm.



germination of *pp7l* mutants was pronounced when seeds were challenged with 100 mM NaCl. Only 2% to 5% of *pp7l* mutants germinated after 2 d, whereas *oe-PP7L* lines and wild type displayed ~55% germination (Fig. 8A). Although after 4 d all lines displayed nearly 100% germination, the enhanced sensitivity of the *pp7l* mutants to NaCl was manifested after 2 weeks; the growth of *pp7l* seedlings was substantially delayed and cotyledons appeared bleached (Fig. 8B).

When seeds were germinated under high light, the germination rates of *pp7l* mutants were lower than those of the wild-type and the *oe-PP7L* lines during the whole time course (Fig. 8C). The *oe-PP7L-7* line germinated even slightly faster than the wild type. To investigate the high-light phenotype in adult plants, 4-week-old plants were shifted to high light and the maximum quantum yield of PSII was measured after 1, 2, and 4 h (Fig. 8, D and E). In the wild type, highlight caused a drop of the F_v/F_m value from 0.81 to 0.56, 0.48, and 0.45 after 1, 2, and 4 h of treatment, respectively. The *pp7l* mutant displayed photoinhibition that was slightly enhanced compared to that in the wild type. However, at 0.67, the F_v/F_m value of the *pp7l* mutants was already significantly lower in normal growth conditions (Fig. 8, D and E). Importantly, overexpression of PP7L rendered plants more high-light-tolerant with higher F_v/F_m values under high-light treatment compared to that of the wild type.

These results show that PP7L plays a positive role in seed germination especially under adverse growth conditions and that overexpression of PP7L renders plants more high-light-tolerant.

PP7L Evolved 43–92 Million Years Ago in the Lineage Leading to Brassicales

The type-7 subfamily of PPPs is specific to plants (Farkas et al., 2007; Uhrig et al., 2013). The increasing number of plant genomes sequenced in recent years (see for example: <http://plants.ensembl.org>) allowed us to refine the analysis of the evolution of the type-7 subfamily. To this end, type-7 members were identified by BLAST searches in the PLAZA database (<https://bioinformatics.psb.ugent.be/plaza/>; Van Bel et al., 2018) and PP7 was found to be ubiquitously present in the plant families included in the database. PP7L and long PP7, however, were only present in *Arabidopsis lyrata*, *Arabidopsis*, *Brassica oleracea*, *Brassica rapa*, *Capsella rubella*, *Schrenkiella parvula*, and *Tarenaya hassleriana* (Fig. 9). These plant species are members of the Brassicaceae or Cleomaceae (*T. hassleriana*) families, which are grouped in the order Brassicales. To expand this analysis to more Brassicales species and to species beyond the Brassicales, the NCBI Blastp suite (<https://blast.ncbi.nlm.nih.gov/Blast.cgi?PAGE=Proteins>) was used to identify further sequences homologous to the PP7L protein sequence. In fact, PP7L was also detected in *Camelina sativa* and *Aethionema arabicum*, both of which belong to the Brassicaceae, but not in *Carica*

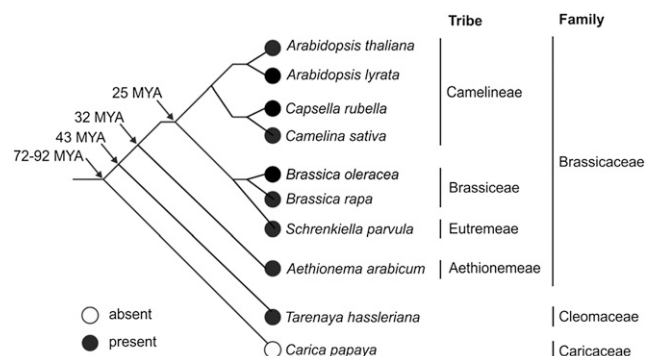


Figure 9. Presence of PP7L in Brassicales. The phylogenetic tree for a part of the Brassicales species is based on the information from Wikström et al. (2001) and Edger et al. (2018). Arrows indicate estimated dates of divergence (in MYA) at different nodes; open circle, PP7L absent; black circle, PP7L present.

papaya, which belongs to the Caricaceae family. The Brassicaceae and Caricaceae diverged from a common ancestor ~72–92 million years ago (MYA; Wikström et al., 2001; Edger et al., 2018). In light of the absence of PP7L in *C. papaya*, and its presence in *T. hassleriana*, it can be concluded that PP7L evolved after the divergence of Caricaceae from the other Brassicales families, but before the separation of Cleomaceae from Brassicaceae, i.e. between 43 and 92 MYA. Therefore, regulation of chloroplast and plant development in Brassicales differs, at least with respect to the elements that are dependent on PP7L, from that in species descended from other plant orders.

DISCUSSION

Lack of PP7L leads to pleiotropic phenotypic effects, which include a small rosette size, increased anthocyanin levels (Fig. 1), susceptibility to salt and high-light stress (Fig. 8) and perturbed chloroplast development (Fig. 6), accompanied by a general reduction in the expression of proteins synthesized in the chloroplast (Fig. 5). Using the maximum quantum yield of PSII (F_v/F_m) as a proxy for chloroplast development, we have shown that chloroplast development is disturbed in cotyledons (Fig. 3), as well as in emerging true leaves (Fig. 1) in *pp7l* mutants, a finding that was further corroborated by ultrastructural analysis of cotyledons of 4-d-old seedlings (Fig. 6).

PP7L Acts as a Positive Regulator of Chloroplast Development in Seedlings and in Emerging True Leaves

The different cytological origins of chloroplasts in cotyledons and leaves (Waters and Langdale, 2009; Jarvis and López-Juez, 2013; Van Dingenen et al., 2016), together with differences between the programs of gene expression triggered by light in the cotyledons and the shoot apex (López-Juez et al., 2008), suggest that

chloroplasts in cotyledons develop through mechanisms that are at least partly distinct from those in leaves. Moreover, various mutants have been isolated in which the greening of cotyledons and leaves are differentially affected (Waters and Langdale, 2009). Thus, chloroplast development mutants have been described that exhibit variegated phenotypes in true leaves, but develop normal green cotyledons. Among these, the best-characterized chloroplast biogenesis mutants are those designated as *immutans* mutants and *variegated* (*var*; Putarjunan et al., 2013). The genes *IMMUTANS* and *VAR* code for the plastid terminal oxidase and the AtFtsH2 subunit of the thylakoid FtsH metalloprotease complex, respectively. The FtsH complex is mainly involved in turnover of the PSII reaction-center D1 protein. Conversely, the three *snowy cotyledon* (*sco*) mutants, namely *sco1* (Albrecht et al., 2006), *sco2/cyo1* (Shimada et al., 2007; Albrecht et al., 2008), and *sco3* (Albrecht et al., 2010), have white or pale green cotyledons but green leaves. The *SCO* class appears not to have a common specific function that causes the cotyledon-specific mutant phenotypes, because its members include proteins involved in different processes, such as plastid protein translation (*SCO1*; Albrecht et al., 2006), folding of Cys-rich thylakoid proteins (*SCO2/CYO1*; Shimada et al., 2007), or association with microtubules and the peroxisome (*SCO3*; Albrecht et al., 2010). Seeds of many oilseed plants like *Arabidopsis* are green due to the presence of photosynthetically active chloroplasts during embryogenesis, which dedifferentiate into nonphotosynthetic eoplasts during the desiccation phase (Lieberers et al., 2017). Immature green *sco* embryos dissected from siliques are green (Ruppel and Hangarter, 2007; Albrecht et al., 2008, 2010), and precocious germination of *sco2* and *sco3* mutants rescues their *sco* cotyledon phenotype (Albrecht et al., 2008, 2010). Thus, it was suggested that the defects are specific to the development of chloroplasts from proplastids/eoplasts in cotyledons, and *SCO* proteins were assumed to be cotyledon-specific factors (Waters and Langdale, 2009). However, under short-day conditions, smaller and pale-green true leaves can be observed in *sco2* mutants, and disruption of *SCO2* in *Lotus japonicus* results not only in paler cotyledons but also in variegated true leaves (Zagari et al., 2017).

Two of the six nuclear-encoded SIGs that interact with PEP have also been proposed to have a specific function in the development of cotyledon chloroplasts (Privat et al., 2003; Ishizaki et al., 2005). Although the cotyledons of *SIG2* antisense plants are Chl-deficient, the true leaves are green (Privat et al., 2003); similarly, *sig6-1* null mutants exhibit delayed greening of cotyledons, but the true leaves were described as normal (Ishizaki et al., 2005). Under our growth conditions, the true leaves of *sig6-1* also appeared normal in color, but a more detailed analysis of photosynthesis by Imaging pulse amplitude modulation (PAM) revealed that chloroplast development was perturbed (Fig. 3C). In consequence, some proteins that were previously

classified as being specific for chloroplast development in cotyledons or true leaves are less specific than was once thought. More sensitive phenotyping methods like Imaging PAM analysis (this study) or the application of diverse growth conditions (as in the case of *sco2*; Zagari et al., 2017) will be instrumental in the future analysis of mutants that appear to be specifically affected at certain developmental stages.

The Role of PP7L in Chloroplast Development Is Not Mediated by the Principal Photomorphogenesis Pathways

It has been noted before that light and chloroplast signaling pathways converge at some point (Ruckle et al., 2007; Leister et al., 2014; Martín et al., 2016). In agreement with this, we have identified PIF-related cis-elements in the promoters of *pp7l*-deregulated genes (Fig. 7B), and the *pp7l* gene expression signature resembles the changes in gene expression induced by *csn* and *pif* mutations (Fig. 7C). Moreover, in *pp7l*, transcripts coding for several phy/PIF signaling-associated proteins (Supplemental Table S2) accumulate to a greater extent than that in wild type, and phyB expression is itself elevated at the transcript (Supplemental Fig. S5A; Supplemental Table S2) and protein level (Supplemental Fig. S5B). In seedlings, chloroplasts develop from etio-plasts that develop from proplastids/eoplasts in darkness (Pribil et al., 2014). Upon exposure to light, photoactivated phy inhibit PIFs and the proteasome, thus inducing transcriptional reprogramming, which in turn promotes photomorphogenesis, including greening (Xu et al., 2015). Consequently, Chl content is reduced in *phyB* and *phyA phyB* seedlings (Neff and Chory, 1998), and Chl content is also reduced in *cop1-4* seedlings and *pp7l-1* seedlings (Fig. 7A). Therefore, we tested the possibility that PP7L acts through the phy/PIF or proteasome pathway. However, none of the tested mutants lacking the main PIFs, photoreceptors, or the COP and CSN proteins associated with photomorphogenesis show any change in F_v/F_m (Supplemental Fig. S4). In addition, overexpression of phyB does not result in a reduction of photosynthesis (Supplemental Fig. S5). This indicates that (1) PP7L operates through a different pathway to regulate chloroplast development, and (2) that greening and photosystem biogenesis are controlled by separate systems.

Photosynthetic activity in *pp7l* mutants during seedling development is most strongly affected in young seedlings (Fig. 3A; Supplemental Table S1), recovers gradually during subsequent seedling development, and is essentially normal after 10 d (Fig. 3B). Recently, the linear developmental program of thylakoid biogenesis in cotyledons was documented by TEM, RNA-Seq, and photosynthesis protein level analysis (Liang et al., 2018). When seeds are germinated under continuous light, thylakoid biogenesis begins between 24 and 36 h after imbibition (HAI), and PSII complexes are first inserted into the thylakoid

membrane at 36 HAI, when polysomes attach to the flattening thylakoids (Liang et al., 2018). Cotranslational insertion of PSII by thylakoid-membrane-bound polysomes further enriches PSII-light-harvesting complex II at 60 HAI (2.5 d; Liang et al., 2018). Protein subunits of the PSI complex are detected only after 84 HAI, suggesting that PSI assembly is initiated at ~84 HAI, corresponding to 3.5 d and thus matching our results in which full photosynthetic activity is reached between days 3 and 4. Importantly, the results of Liang et al. (2018) suggest that thylakoid-bound polysomes mediate critical stages of chloroplast biogenesis. Indeed, this is supported by the fact that a disturbance in chloroplast ribosome assembly in the *rh3-4* mutant, in which the DEAD-box RNA helicase RH3 is defective (Asakura et al., 2012), causes a delay in thylakoid development (Liang et al., 2018). In *pp7l*, fewer mature chloroplast 23S rRNA molecules (Figs. 3D and 5D; Supplemental Fig. S3) and smaller amounts of ribosomal proteins accumulate (Fig. 5A; Supplemental Table S3). Thus, we hypothesize that the delay in thylakoid development in the *pp7l* mutant (Fig. 6) is caused by a perturbation of rRNA maturation and accumulation of chloroplast ribosomal proteins, which results in a reduction in the numbers of functional ribosomes and a decrease in protein synthesis in the chloroplast (Fig. 5, E and F).

PP7L Contributes to the Tolerance to Abiotic Stresses

Plants as sessile organisms are constantly exposed to environmental changes and stresses, and they consequently evolved mechanisms to cope with different stresses. Because (1) *pp7l* mutants are more susceptible to salt and high-light treatment and (2) overexpression of PP7L enhances the capacity of plants to tolerate high light intensities (see Fig. 8), PP7L is clearly involved in salt and high-light tolerance. The reasons for the multiple stress susceptibility of *pp7l* mutants is not plainly evident, but one plausible explanation is that it can be ascribed at least in part to the perturbations of chloroplast gene expression observed in *pp7l* mutants (see Fig. 5). In fact, it was already noted before that changes in chloroplast gene expression can trigger alterations in tolerance responses, presumably via retrograde signaling (Leister et al., 2017). Interestingly, an impairment in chloroplast gene expression results not automatically in stress susceptibility, but can render plants even more resistant to stresses. This is exemplified by the “happy on norflurazon” mutants *hon5* and *hon23* affected in the ClpR4 subunit of the chloroplast-localized Clp protease complex, and a protein with homology to prokaryotic translation initiation factor2, cpIF2, respectively; they display a constitutive stress response that enhances resistance against a combined low-temperature/high-light stress (Saini et al., 2011). Moreover, lack of the major chloroplast FtsH complex component FtsH2 in the *var2* mutant leads to a reduced capacity to acclimate to high-light stress (Miura et al., 2007). When a

mutation in *FUG1*, which encodes a chloroplast protein with homology to cpIF2, is introduced into *var2*, the high-light sensitivity of *var2* is suppressed—pointing to an importance of the balance between chloroplast protein synthesis and degradation in stress acclimation (Miura et al., 2007).

How Does the Nucleocytosolic Compartment Influence Chloroplast Development?

Chloroplast proteins are synthesized both in the nucleocytosolic compartment and the organelle, which necessitates coordination of the expression of nuclear and chloroplast genomes. Additionally, gene expression in the chloroplast itself is a complex process that depends on the supply of a plethora of nuclear-encoded proteins. Primary transcripts are produced by PEP and nuclear-encoded phage-type RNA polymerase (Liere et al., 2011). Subsequently, these RNAs undergo processing, splicing, editing, turnover, and maturation (Stern et al., 2010; Stoppel and Meurer, 2012) before they are translated (Tiller and Bock, 2014). Lack of nuclear-encoded proteins at early stages of chloroplast development impacts on phenotypes in various degrees, ranging from no visible phenotype to pale green cotyledons and rosette leaves to seedling- and embryo-lethality (Barkan and Small, 2014; Kleine and Leister, 2015). In screens for mutants with altered chloroplast biology at this stage, most studies have identified chloroplast-localized proteins involved in chloroplast development and showing a photosynthesis phenotype. Exceptions include PALE GREEN1 (Hsieh et al., 2017) and SCO3 (Albrecht et al., 2010), which are localized to mitochondria and peroxisomes, respectively. Interestingly, the cytoskeleton is altered in *sco3-1*, and microtubule inhibitors have similar effects on chloroplast biogenesis to *sco3-1* (Albrecht et al., 2010), suggesting a role for the cytoskeleton and peroxisomes in chloroplast biogenesis. Thus, it is increasingly clear that, in addition to the already known pathways, the development of chloroplasts requires a number of other processes.

The import of photosynthetic preproteins is mediated by translocon at the outer envelope membrane of chloroplasts (Toc)33 and Toc159 proteins. Accordingly, the *plastid protein import1* (*ppi1*; *toc33*) and *ppi2* (*toc159*) mutants are defective in chloroplast biogenesis (Bauer et al., 2000; Kubis et al., 2003). Moreover, not only the process of protein uptake by the chloroplast, but pre-import steps such as quality control by the cytosolic ubiquitin–proteasome system (Ling et al., 2012) and the establishment of the appropriate balance between chloroplast and cytosolic translation (Wang et al., 2018), affect chloroplast development.

Notably, alterations in chloroplast protein import in the *ppi2* and *translocon at the inner chloroplast envelope 56-1* mutants result in decreased accumulation of plastid ribosomal proteins (Köhler et al., 2016) as in the *pp7l-1* mutant (Fig. 5A; Supplemental Table S3). However,

reduced ribosomal protein accumulation is not a feature common to all *albino/pale green* (*apg*) mutants, because ribosomal subunits accumulate to wild-type levels in the *apg1*, *apg2*, and *apg3* mutants, which are defective in proteins that participate in diverse chloroplast functions (Motohashi et al., 2012). Because Toc159 is an import receptor for photosynthesis-related proteins, a straightforward explanation for the *ppi2* photosynthesis phenotype is that it is caused by a defect in the import of the photosynthesis proteins. However, the mechanism must be more complex, because in the *ppi2* mutant many nuclear-encoded photosynthesis proteins are downregulated at the transcript level, which points to the activation of retrograde signaling (Bischof et al., 2011). This is not the case at least for the vast majority of mRNAs for photosynthesis proteins in the *pp7l-1* mutant (Supplemental Table S2) nor in the *sco2/cyo1* mutant (Shimada et al., 2007). Why mutants with similar molecular chloroplast phenotypes do not trigger similar gene expression profiles in the nucleus remains elusive.

It is interesting to note that, although the mRNA levels of *PHYB*, *SIG2*, *SIG6*, *GLK1*, and *Chl* biosynthesis genes are upregulated in *pp7l*, greening in *pp7l* is defective (Fig. 7A), questioning whether the elevated cytosolic mRNA levels reflect functional protein levels. Among the elevated nuclear-encoded transcripts, the GO category “chloroplast rRNA processing” is, in addition to “chlorophyll biosynthesis,” the most highly enriched term (Fig. 4). Processing of 23S rRNA is defective in the *pp7l* mutant (Supplemental Fig. S3), which might be a secondary effect of reduced chloroplast protein translation. Because chloroplast rRNA maturation requires a plethora of nuclear-encoded proteins (Stoppel and Meurer, 2012), this finding could also support the concept of negative correlation of mRNA and protein levels. Indeed, an increasing number of observations indicate that mRNA transcript levels and protein synthesis are often correlated only to a limited degree (e.g. Oelze et al., 2014). Before a protein destined for the chloroplast reaches the quality-control and import stages, it must first undergo a series of complex processes. The expression level of its mRNA is itself determined by the relative rates of transcription and degradation (Roy and von Arnim, 2013), and the decoding of mRNA by the ribosome involves a plethora of initiation, elongation, and termination factors (Moore et al., 2016). Once the protein is finally made, it may also require posttranslational modification or be degraded by the proteasome (Arsova et al., 2018). This shows that many steps from primary transcript to protein translation and modification can account for a negative correlation between mRNA and protein abundance. The remaining key questions are which nucleo(cytosolic) process is exactly disturbed in the *pp7l* mutant provoking the delayed chloroplast development, and which transcript changes in *pp7l* are attributable to retrograde signaling activated by the delay in chloroplast development. Of note is the 8-fold-higher anthocyanin content in the *pp7l* mutant (Fig. 1B).

Anthocyanin accumulation is also induced by abiotic stresses like high light (Kleine et al., 2007), cold (Schulz et al., 2015), or specifically by Suc (Solfanelli et al., 2006). Photosynthesis-derived Suc is exported from chloroplasts to other cellular compartments or to non-photosynthetic sink tissues, and carbon supply can be sensed through sugar signaling (Wingler, 2018). Despite the obvious linkage of photosynthesis and energy metabolism and signaling, little is known about the connections between cytoplasmic and nucleus-localized key regulators of cellular metabolism like the SNF1-related protein kinase1 and organelles (Wurzing et al., 2018). Moreover, mRNA levels of many photosynthetic genes are dependent on SNF1-related protein kinase1 activity (Zhang et al., 2009). One possible PP7L function would be that PP7L is at the receiver site of sugar signaling in the nucleus. The perturbed starch mobilization (Fig. 6) and the small growth phenotypes of the *pp7l* mutant (Fig. 1) would be in accordance with sugar-signaling regulators playing a central role in the regulation of starch metabolism (Sakr et al., 2018; Wurzing et al., 2018). With its predicted function as an inactive Ser/Thr phosphatase, it is unlikely that it is a transcription factor and future studies will have to clarify the molecular function of PP7L.

The Brassicaceae *Arabidopsis* is a member of the order Brassicales, which is known for the production of mustard oil (glucosinolate) compounds (Cardinal-McTeague et al., 2016). This order contains, in addition to several model plants, many species that are of economical relevance, such as mustard (*Brassica juncea*), broccoli (*Brassica oleracea* var. *italica*), cabbage (*Brassica oleracea* var. *capitata*), kale (*Brassica oleracea* var. *sabellica*), rapeseed (*Brassica napus*), and caper (*Capparis spinosa*). Because PP7L evolved specifically in the order Brassicales (Fig. 9) and because of the prominent phenotype of the *pp7l* mutant, it appears that PP7L is specific for the regulation of chloroplast and plant development in Brassicales. Other plant orders might (1) have recruited a protein different from PP7L or (2) might differ in their chloroplast and plant development and therefore not require PP7L. Thus, further investigation of PP7L should help to elucidate the aspects of chloroplast and plant development specific to this order, which are of potential significance for the improvement of agronomically valuable crops.

MATERIALS AND METHODS

Plant Material and Growth Conditions

The *pp7l:En-1* mutant (ZIGIA line V2-880) was identified in the mutant collection of Wisman et al. (1998) based on alterations in the effective quantum yield of PSII (Fii). The mutants *pp7l-1* (SALK_018295), *pp7l-2* (SALK_033071), and *pp7l-3* (SALK_022053) were identified in the SIGnAL database (Alonso et al., 2003). The *sig2-2* (SALK_045706) mutant allele has been described previously (Kanamaru et al., 2001), as have the mutants *sig5-1* (SALK_049021; (Tsunoyama et al., 2004), *sig6-1* (SAIL_893_C09; Woodson et al., 2013), *cop1-4* (McNeill et al., 1994), *cry1-304 cry2-1* (Mockler et al., 1999), *csn5a-1*, *csn5a-2*, *csn5b-1* (Dohmann et al., 2005), *pif1pif5*, *pif4pif5*, *pif1pif4pif5*, *pif1pif3pif4pif5* (Pfeiffer et al., 2014), *phyB-9* and *phyA-211 phyB-9* (Su et al., 2015), and ABO

(Shinomura et al., 1998). All mutants except of ABO are in the Col-0 background.

Arabidopsis (*Arabidopsis thaliana*) plants were routinely grown on potting soil (Stender) under controlled greenhouse conditions and on a 16-/8-h light/ dark cycle (daylight was supplemented with illumination from HQI Powerstar 400W/NDL, providing a total fluence of $180 \text{ mmol photons m}^{-2} \text{ s}^{-1}$ on leaf surfaces). Wuxal Super fertilizer (8% N, 8% P_2O_5 , and 6% K_2O ; MANNA) was used according to the manufacturer's instructions. Where indicated, seedlings were grown on 0.8% (w/v) agar (Sigma-Aldrich) containing 1% (w/v) Suc at 22°C under $100 \text{ mmol photons m}^{-2} \text{ s}^{-1}$ provided by white fluorescent lamps.

Complementation of pp7L Mutants, Expression, and Intracellular Localization of eGFP Fusions

To complement the mutant phenotype, the sequence of PP7L (AT5G10900) without the stop codon was amplified from genomic DNA with the primers indicated in Supplemental Table S4. This PCR product was introduced into the donor vector pDONR207 by the BP clonase reaction (Invitrogen) as described in the Gateway manual. After sequence analysis of the recombinant DNA sequence, the attL recombination clonase reaction (Invitrogen) was performed to introduce the fusion construct into the destination vector pB7FWG2 (35S promoter, eGFP), generating 35S:PP7L-GFP. Subsequently, the construct was introduced into Col-0, *pp7L-1*, *pp7L-2*, and *pp7L-3* backgrounds. Transformed seedlings were selected with the herbicide Basta. For transformations into *pp7L* mutants, plants showing a wild-type phenotype were selected. Then expression of PP7L mRNA levels in different genotypes was analyzed by RT-PCR using an appropriate primer combination (Supplemental Table S4).

Subcellular localization analysis of fused proteins was conducted in protoplasts isolated from wild type. Protoplasts were imaged with a Fluorescence Axio Imager microscope (Zeiss) after transformation as described in Dovzhenko et al. (2003). Fluorescence was excited with the X-Cite Series 120 fluorescence lamp (EXFO) and images were collected at 500–550 nm (eGFP fluorescence) and 670–750 nm (Chl autofluorescence).

Chl a Fluorescence Measurements

Chl fluorescence parameters were measured using an imaging Chl fluorometer (Imaging PAM, M-Series; Walz). The method employed involved preprogrammed treatments of 30-min dark periods to determine F_0/F_m , for which F_0 was measured at a low frequency of pulse-modulated measuring light, whereas F_m was obtained at saturation pulses of $\sim 2,700 \text{ mmol photons m}^{-2} \text{ s}^{-1}$, for a duration of 0.8 s. The calculations and plotting of the parameters were performed using the ImagingWin software.

Chl Concentration Measurements

Chl content was measured according to Jeffrey and Humphrey (1975). Briefly, 100 mg of fresh tissue was ground in 1 mL of cold 80% (v/v) acetone and centrifuged at 12,000 g for 5 min at 4°C and the supernatant was saved. Another 1 mL of 80% (v/v) acetone was added, and the extract was centrifuged again. The procedure was repeated until the green color of the pellet was no longer discernible. Chl concentrations were calculated from spectroscopic absorbance measurements at 663, 646, and 710 nm.

Anthocyanin Measurement

Measurement of anthocyanin content was conducted according to Neff and Chory (1998). Briefly, 100-mg samples of seedlings of each genotype that had been exposed to diverse light treatments were incubated with 300 μL of 1% (v/v) HCl in methanol at 4°C overnight in the dark with shaking. Then 200 μL of distilled water and 500 μL of chloroform were added, vortexed, and briefly centrifuged to separate anthocyanins from Chls. The total anthocyanin content was determined by measuring A530 and A657 of the aqueous phase using a spectrophotometer (Amersham Biosciences). The equation $(A530 - 0.25 \times A657) \times TV / (FW \times 1000)$ was used to quantify the relative amount of anthocyanin, where TV = total volume of the extract (in milliliters) and FW = fresh weight of seedlings (in grams).

Polysome Analysis

Polysome isolation was performed according to Barkan (1993). Seedlings (200 mg) were ground in liquid N using a mortar and pestle. Subsequently, the microsomal membranes were extracted and solubilized with 0.5% (w/v) sodium deoxycholate. The solubilized material was then layered onto 15/55% (w/v) Suc step-gradients (corresponding to 0.44/1.6 M) and centrifuged at $250,000 \text{ g}$ for 65 min at 4°C. The step gradient was fractionated, and the mRNA associated with polysomes was extracted with phenol/chloroform/isoamyl alcohol (25:24:1), precipitated at room temperature with 95% (v/v) ethanol, and subjected to RNA gel-blot analysis.

In Vivo Labeling of Thylakoid Proteins

Four-day-old seedlings were preincubated in 1 mL of labeling solution containing 20 mg/mL cycloheximide, 10 mM ris(hydroxymethyl)aminomethane (TRIS), 5 mM MgCl_2 , 20 mM KCl (pH 6.8), and 0.1% (v/v) TWEEN 20 (a polyethylene glycol sorbitan monolaurate) under illumination at a fluence rate of $80 \text{ mmol photons m}^{-2} \text{ s}^{-1}$ for 30 min to block cytosolic translation. Then labeling was performed in the same solution containing 1 mCi mL^{-1} [^{35}S]Met under the same lighting conditions for 30 min. After labeling, the thylakoid membranes were isolated and the proteins were fractionated on 10% sodium dodecyl sulfate polyacrylamide gel electrophoresis (SDS-PAGE) and analyzed by fluorography (Variable Mode Imager Typhoon TRIO; Amersham Biosciences).

Protein Isolation and Western Blotting

Seedling samples (100 mg) were ground in liquid N and total proteins were solubilized in protein extraction buffer (0.125 M TRIS, 1% SDS, 10% [v/v] glycerol, 0.05 M sodium metabisulfite) containing 1 mM phenylmethylsulfonyl fluoride and protease inhibitor cocktail (Sigma-Aldrich). Cell debris was removed by centrifugation for 10 min and the supernatant was boiled with SDS loading buffer at 95°C for 10 min. Equal amounts of total proteins were fractionated on 10% SDS-PAGE gels and transferred to polyvinylidene fluoride membranes (Millipore) using a semidry method. The primary antibodies directed against PsbA (1:4,000), PsbD (1:5,000), RbcL (1:10,000), PsdA (1:1,000), AtpB (1:4,000), and cytb6 (1:10,000) used in this study were obtained from Agrisera. The B6-B3 monoclonal antibody specific for phyB is described in Hirschfeld et al. (1998). Signals were detected with the PierceECL Western Blotting Kit (Thermo Fisher Scientific) and quantified using the software ImageJ (National Institutes of Health).

Nucleic Acid Extraction

Leaf tissue (100 mg) was homogenized in extraction buffer containing 200 mM TRIS/HCl (pH 7.5), 25 mM NaCl, 25 mM ethylenediaminetetraacetic acid, and 0.5% (w/v) SDS. After centrifugation, DNA was precipitated from the supernatant by adding isopropyl alcohol. After washing with 70% (v/v) ethanol, the DNA was dissolved in distilled water.

For RNA isolation, frozen tissue was ground in liquid N. Total RNA was extracted by using TRIzol reagent (Invitrogen) according to the manufacturer's protocol. RNA samples were treated with DNase I (New England BioLabs) and quantified with a Nanodrop spectrophotometer (Thermo Fisher Scientific). Isolated RNA was stored at -80°C until further use.

RNA Gel-Blot Analysis

For northern blotting, total RNA was extracted using Trizol reagent (Invitrogen). Aliquots (7 μg) of each sample were electrophoresed on a 1.5% (w/v) agarose gel containing formaldehyde, and transferred to a nylon membrane (Hybond-N+; Amersham Biosciences). The membrane was hybridized overnight at 65°C with ^{32}P -labeled cDNA fragments probes. Primers used to amplify the probes are listed in Supplemental Table S4. Signals were quantified with a phosphorimager (Typhoon; Amersham Biosciences) using the program Image-Quant (GE Healthcare).

cDNA Synthesis and RT-qPCR Analysis

Total RNA was extracted with the Direct-zol RNA Kit (Zymo Research) according to the manufacturer's protocol, and 2 μg of the RNA was employed

to synthesize cDNA using the iScript cDNA Synthesis Kit (Bio-Rad). RT-qPCR analysis was performed on a Bio-Rad iQ5 real-time PCR instrument with the iQ SYBR Green Supermix (Bio-Rad). The gene-specific primers used for this assay are listed in Supplemental Table S4. Each sample was quantified in triplicate and normalized using *AT4G36800*, which codes for an RUB1-conjugating enzyme (*RCE1*) as an internal control.

Sample Preparation for Quantitative Proteomics

Total proteins were extracted from 4-d-old wild-type and *pp7l-1* seedlings (four biological replicates for each genotype) by grinding 200 mg of frozen plant material into a fine powder in liquid N. After suspending the powder in 1 mL of extraction buffer (100 mM N-2-hydroxyethylpiperazine-N'-2-ethanesulfonic acid, pH 7.5, 150 mM NaCl, 10 mM dithiothreitol, 1% [w/v] SDS, 1x Roche cComplete Protease Inhibitor Cocktail), cell debris was removed by centrifugation at 10,000 g for 30 min. Proteins were then precipitated with chloroform-methanol (Wessel and Flügge, 1984), pellets were solubilized in 6 M guanidine hydrochloride and protein concentration was determined by bicinchoninic assay (Pierce BCA Protein Assay Kit; Thermo Fisher Scientific). Proteome aliquots of 100 µg were reduced with 10 mM dithiothreitol (30 min, 37°C), alkylated with 50 mM iodoacetamide (30 min, room temperature, in the dark), and recovered by chloroform-methanol precipitation before digestion with trypsin (SERVA) at a proteome/enzyme ratio 100:1 (w/w). After overnight incubation at 37°C, stable-isotope dimethyl labeling was performed in solution according to Boersema et al. (2009). Briefly, the samples were labeled separately with 20 mM NaCH₃CN and either 40 mM CH₂O (wild type, "light formaldehyde") or 40 mM ¹³CD₂O (*pp7l-1*, "heavy formaldehyde") for 4 h at 37°C. Excess reagent was quenched by adding 100 mM of TRIS at pH 6.8 (1 h, 37°C). After acidification with 2% (v/v) formic acid, equal amounts of light and heavy labeled samples were combined to generate four duplex samples. Before liquid chromatography-tandem mass spectrometry (LC-MS/MS) analysis, all samples were desalted with home-made C18 stage tips (Rappsilber et al., 2007), eluates were vacuum-dried to near-dryness and stored at -80°C before LC-MS/MS analysis.

LC-MS/MS

LC-MS/MS was performed on a nano-LC-system (Ultimate 3000 RSLC; Thermo Fisher Scientific) coupled to an Impact II high resolution quadrupole time of flight (Bruker) using a CaptiveSpray nano electrospray ionization source (Bruker Daltonics). The nano-LC system was equipped with an Acclaim Pepmap nano-trap column (C18, 100 Å, 700 mm 3 2 cm; Thermo Fisher Scientific) and an Acclaim Pepmap RSLC analytical column (C18, 100 Å, 75 mm 3 50 cm; Thermo Fisher Scientific). The peptide mixture was fractionated by applying a linear gradient of 5% to 45% acetonitrile at a flow rate of 250 nL/min over a period of 150 min. MS1 spectra were acquired at 3 Hz with a mass range from *m/z* 200–2000, with the Top-18 most intense peaks selected for MS/MS analysis using an intensity-dependent spectra acquisition time between 4 and 16. The mass spectrometry proteomics data have been deposited to the ProteomeXchange Consortium via the PRIDE (Vizcaino et al., 2016) partner repository with the dataset identifier PXD012105.

MS Data Analysis

MS raw files were analyzed with MaxQuant software (version 1.6.0.13; <https://maxquant.org/>) and peak lists were searched against the Arabidopsis UniProt database (version February 2017) using the Andromeda search engine with default settings. Cys carbamidomethylation was set as a fixed modification, and acetylation of protein N-termini and Met oxidation were set as variable modifications. Lys and N-terminal demethylation (light formaldehyde +28.03 D; heavy formaldehyde +34.06 D) were set as labels, and "requantified" was enabled.

Statistical Analysis

All statistical and bioinformatics analysis were performed using the softwares Perseus (version 1.6.0.2) and Microsoft Office Excel. Two-tailed Student's *t*-test (*P* < 0.05) was used to define which protein groups are significantly changed and a Box-plot analysis of the ratio of the frequency of occurrence of each peptide in *pp7l-1* mutant versus wild-type samples was used to identify significant (*P* ≤ 0.05) outliers from the mean ratio of all peptides.

lncRNA-Seq and Data Analysis

Total RNA from plants was isolated using Trizol (Invitrogen) and purified using Direct-zol RNA MiniPrep Plus columns (Zymo Research) according to the manufacturer's instructions. RNA integrity and quality was assessed by a 2100 Bioanalyzer (Agilent). rRNA depletion, generation of RNA-Seq libraries, and 150-bp paired-end sequencing on an HiSeq 2500 system (Illumina) were conducted at Novogene Biotech with standard Illumina protocols. Three independent biological replicates were used per genotype.

RNA-Seq reads were analyzed on the Galaxy platform (<https://usegalaxy.org/>). After grooming FASTQ files, adaptors were removed with Trimmomatic (Bolger et al., 2014), and sequencing quality was accessed with FastQC (<http://www.bioinformatics.babraham.ac.uk/projects/fastqc/>). Reads were mapped to The Arabidopsis Information Resource genome annotation 10 with the gapped-read mapper TopHat 2.1.1 (Kim et al., 2013) set for Forward Read unstranded libraries and adjusting the maximum intron length to 5,000 bp. Reads were counted with featureCounts (Liao et al., 2014) with the help of the gene annotation in Araport11 (www.araport.org/data/araport11). Differentially expressed genes were obtained with DESeq2 (Love et al., 2014) running with the fit type set to "parametric," and applying a twofold change cutoff and an adjusted *P* value < 0.05.

Sequencing data have been deposited to Gene Expression Omnibus (Edgar et al., 2002) under the accession number GSE122495.

TEM

The plant material was directly fixed after 4-d-old seedlings had been kept for 8 h in darkness. Cotyledons were fixed using 75-mM cacodylate buffer containing 2.5% (v/v) glutaraldehyde. Postfixation was carried out using 1% (w/v) osmium tetroxide in water for 1 h followed by en-bloc staining with 1% (w/v) uranyl acetate. After dehydration in a graded acetone series, the sample material was gradually infiltrated with Spurr's Resin. After polymerization, the embedded samples were ultrathin-sectioned and poststained with lead citrate. TEM was carried out using a model no. EM912 (Zeiss) with an integrated OMEGA-filter in the zero-loss mode and with an acceleration voltage of 80 kV. For image acquisition, we used a Tröndle 2k x 2k slow-scan charge-coupled device camera together with the respective software package (Tröndle Restlichtverstärkersysteme).

Accession Numbers

Sequence data from this article can be found in the GenBank/EMBL data libraries under the accession numbers provided in Supplemental Table S4.

Supplemental Data

The following supplemental materials are available.

Supplemental Figure S1. Identification of *pp7l* T-DNA insertion mutants.

Supplemental Figure S2. Chl content and complementation of *pp7l* T-DNA insertion mutants.

Supplemental Figure S3. rRNA maturation in 4-d-old Col-0 and *pp7l* mutant seedlings.

Supplemental Figure S4. Phenotypes of 4-week-old Col-0, *pp7l-1*, *cop1-4*, and the different photoreceptor (*cry1-304 cry2-1* and *phyA-211 phyB-9*) mutant plants.

Supplemental Figure S5. PhyB levels are elevated in *pp7l* mutants, but overexpression of phyB does not result in a *pp7l* phenotype.

Supplemental Figure S6. Overexpression of *PP7L* in Col-0.

Supplemental Table S1. SDS of the *F_v/F_m* values measured in the different *pp7l* mutant seedlings presented in Figure 3A.

Supplemental Table S2. Genes whose transcript levels differed by more than twofold relative to Col-0 in 4-d-old LD-grown *pp7l-1* seedlings.

Supplemental Table S3. Relative protein accumulation in the *pp7l-1* mutant compared to Col-0 grown for 4 d in LD conditions as determined by shotgun proteomics.

Supplemental Table S4. Primers used in this study.

ACKNOWLEDGMENTS

We thank Claus Schwechheimer, Ute Höcker, Christian Schmitz-Linne-weber, Ferenc Nagy, and Eva Adam for providing the *csn*, *cop1*, *sig5*, and *P35S:PHYB-YFP phyB-9* seeds, respectively. We thank Paul Hardy for critical reading of the manuscript and Elisabeth Gerick for technical assistance.

Received January 17, 2019; accepted February 5, 2019; published February 13, 2019.

LITERATURE CITED

- Abdallah F, Salamini F, Leister D (2000) A prediction of the size and evolutionary origin of the proteome of chloroplasts of Arabidopsis. *Trends Plant Sci* 5: 141–142
- Albrecht V, Ingenfeld A, Apel K (2006) Characterization of the *snowy cotyledon 1* mutant of *Arabidopsis thaliana*: The impact of chloroplast elongation factor G on chloroplast development and plant vitality. *Plant Mol Biol* 60: 507–518
- Albrecht V, Ingenfeld A, Apel K (2008) Snowy cotyledon 2: The identification of a zinc finger domain protein essential for chloroplast development in cotyledons but not in true leaves. *Plant Mol Biol* 66: 599–608
- Albrecht V, Simková K, Carrie C, Delannoy E, Giraud E, Whelan J, Small ID, Apel K, Badger MR, Pogson BJ (2010) The cytoskeleton and the peroxisomal-targeted snowy cotyledon3 protein are required for chloroplast development in Arabidopsis. *Plant Cell* 22: 3423–3438
- Alonso JM, Stepanova AN, Leisse TJ, Kim CJ, Chen H, Shinn P, Stevenson DK, Zimmerman J, Barajas P, Cheuk R, et al (2003) Genome-wide insertional mutagenesis of *Arabidopsis thaliana*. *Science* 301: 653–657
- Arsova B, Watt M, Usadel B (2018) Monitoring of plant protein post-translational modifications using targeted proteomics. *Front Plant Sci* 9: 1168
- Asakura Y, Galarneau E, Watkins KP, Barkan A, van Wijk KJ (2012) Chloroplast RH3 DEAD box RNA helicases in maize and Arabidopsis function in splicing of specific group II introns and affect chloroplast ribosome biogenesis. *Plant Physiol* 159: 961–974
- Barkan A (1993) Nuclear mutants of maize with defects in chloroplast polysome assembly have altered chloroplast RNA metabolism. *Plant Cell* 5: 389–402
- Barkan A, Small I (2014) Pentatricopeptide repeat proteins in plants. *Annu Rev Plant Biol* 65: 415–442
- Bauer J, Chen K, Hiltbunner A, Wehrli E, Eugster M, Schnell D, Kessler F (2000) The major protein import receptor of plastids is essential for chloroplast biogenesis. *Nature* 403: 203–207
- Baulcombe DC, Saunders GR, Bevan MW, Mayo MA, Harrison BD (1986) Expression of biologically-active viral satellite RNA from the nuclear genome of transformed plants. *Nature* 321: 446–449
- Becker MG, Walker PL, Pulgar-Vidal NC, Belmonte MF (2017) SeqEnrich: A tool to predict transcription factor networks from co-expressed Arabidopsis and *Brassica napus* gene sets. *PLoS One* 12: e0178256
- Berry JO, Yerramsetty P, Zielinski AM, Mure CM (2013) Photosynthetic gene expression in higher plants. *Photosynth Res* 117: 91–120
- Bischof S, Baerenfaller K, Wildhaber T, Troesch R, Vidi PA, Roschitzki B, Hirsch-Hoffmann M, Hennig L, Kessler F, Gruissem W, et al (2011) Plastid proteome assembly without Toc159: Photosynthetic protein import and accumulation of N-acetylated plastid precursor proteins. *Plant Cell* 23: 3911–3928
- Bobik K, Burch-Smith TM (2015) Chloroplast signaling within, between and beyond cells. *Front Plant Sci* 6: 781
- Boersema PJ, Raijmakers R, Lemeer S, Mohammed S, Heck AJR (2009) Multiplex peptide stable isotope dimethyl labeling for quantitative proteomics. *Nat Protoc* 4: 484–494
- Bolger AM, Lohse M, Usadel B (2014) Trimmomatic: A flexible trimmer for Illumina sequence data. *Bioinformatics* 30: 2114–2120
- Cardinal-McTeague WM, Sytsma KJ, Hall JC (2016) Biogeography and diversification of Brassicales: A 103-million-year tale. *Mol Phylogenet Evol* 99: 204–224
- Carretero-Paulet L, Galstyan A, Roig-Villanova I, Martínez-García JF, Bilbao-Castro JR, Robertson DL (2010) Genome-wide classification and evolutionary analysis of the bHLH family of transcription factors in Arabidopsis, poplar, rice, moss, and algae. *Plant Physiol* 153: 1398–1412
- Chan KX, Phua SY, Crisp P, McQuinn R, Pogson BJ (2016) Learning the languages of the chloroplast: Retrograde signaling and beyond. *Annu Rev Plant Biol* 67: 25–53
- Chen D, Xu G, Tang W, Jing Y, Ji Q, Fei Z, Lin R (2013) Antagonistic basic helix-loop-helix/bZIP transcription factors form transcriptional modules that integrate light and reactive oxygen species signaling in Arabidopsis. *Plant Cell* 25: 1657–1673
- Chen M, Galvão RM, Li M, Burger B, Bugea J, Bolado J, Chory J (2010) Arabidopsis HEMERA/pTAC12 initiates photomorphogenesis by phytochromes. *Cell* 141: 1230–1240
- Chi W, He B, Mao J, Jiang J, Zhang L (2015) Plastid Sigma factors: Their individual functions and regulation in transcription. *Biochim Biophys Acta* 1847: 770–778
- Coll NS, Danon A, Meurer J, Cho WK, Apel K (2009) Characterization of *soldat8*, a suppressor of singlet oxygen-induced cell death in Arabidopsis seedlings. *Plant Cell Physiol* 50: 707–718
- Dohmann EM, Kuhnle C, Schwechheimer C (2005) Loss of the CONSTITUTIVE PHOTOMORPHOGENIC9 signalosome subunit 5 is sufficient to cause the cop/det/fus mutant phenotype in Arabidopsis. *Plant Cell* 17: 1967–1978
- Dohmann EM, Levesque MP, Isono E, Schmid M, Schwechheimer C (2008) Auxin responses in mutants of the Arabidopsis CONSTITUTIVE PHOTOMORPHOGENIC9 signalosome. *Plant Physiol* 147: 1369–1379
- Dovzhenko A, Dal Bosco C, Meurer J, Koop HU (2003) Efficient regeneration from cotyledon protoplasts in *Arabidopsis thaliana*. *Protoplasma* 222: 107–111
- Edgar R, Domrachev M, Lash AE (2002) Gene Expression Omnibus: NCBI gene expression and hybridization array data repository. *Nucleic Acids Res* 30: 207–210
- Edger PP, Hall JC, Harkess A, Tang M, Coombs J, Mohammadin S, Schranz ME, Xiong Z, Leebens-Mack J, Meyers BC, et al (2018) Brassicales phylogeny inferred from 72 plastid genes: A reanalysis of the phylogenetic localization of two paleopolyploid events and origin of novel chemical defenses. *Am J Bot* 105: 463–469
- Ezer D, Shepherd SJK, Brestovitsky A, Dickinson P, Cortijo S, Charoensawan V, Box MS, Biswas S, Jaeger KE, Wigge PA (2017) The G-box transcriptional regulatory code in Arabidopsis. *Plant Physiol* 175: 628–640
- Farkas I, Dombrádi V, Miskei M, Szabados L, Koncz C (2007) Arabidopsis PPP family of serine/threonine phosphatases. *Trends Plant Sci* 12: 169–176
- Genoud T, Santa Cruz MT, Kulisic T, Sparla F, Fankhauser C, Métraux JP (2008) The protein phosphatase 7 regulates phytochrome signaling in Arabidopsis. *PLoS One* 3: e2699
- Gommers CMM, Monte E (2018) Seedling establishment: A dimmer switch-regulated process between dark and light signaling. *Plant Physiol* 176: 1061–1074
- Hirschfeld M, Tepperman JM, Clack T, Quail PH, Sharrock RA (1998) Coordination of phytochrome levels in *phyB* mutants of Arabidopsis as revealed by apoprotein-specific monoclonal antibodies. *Genetics* 149: 523–535
- Hooper CM, Castleden IR, Tanz SK, Aryamanesh N, Millar AH (2017) SUBA4: The interactive data analysis centre for Arabidopsis subcellular protein locations. *Nucleic Acids Res* 45(D1): D1064–D1074
- Hruz T, Laule O, Szabo G, Wessendorp F, Bleuler S, Oertle L, Widmayer P, Gruissem W, Zimmermann P (2008) Genevestigator v3: A reference expression database for the meta-analysis of transcriptomes. *Adv Bioinforma* 2008: 420747
- Hsieh WY, Liao JC, Wang HT, Hung TH, Tseng CC, Chung TY, Hsieh MH (2017) The Arabidopsis thiamin-deficient mutant *pale green1* lacks thiamin monophosphate phosphatase of the vitamin B₁ biosynthesis pathway. *Plant J* 91: 145–157
- Huang W, Sherman BT, Lempicki RA (2009) Bioinformatics enrichment tools: Paths toward the comprehensive functional analysis of large gene lists. *Nucleic Acids Res* 37: 1–13
- Ishizaki Y, Tsunoyama Y, Hatano K, Ando K, Kato K, Shinmyo A, Kobori M, Takeba G, Nakahira Y, Shiina T (2005) A nuclear-encoded sigma factor, Arabidopsis SIG6, recognizes Sigma-70 type chloroplast promoters and regulates early chloroplast development in cotyledons. *Plant J* 42: 133–144
- Jarvis P, López-Juez E (2013) Biogenesis and homeostasis of chloroplasts and other plastids. *Nat Rev Mol Cell Biol* 14: 787–802

- Jeffrey SW, Humphrey GF (1975) New spectrophotometric equations for determining chlorophylls *a*, *b*, *c*1 and *c*2 in higher plants, algae and natural phytoplankton. *Biochem Physiol Pflanz* 167: 191–194
- Jiao Y, Lau OS, Deng XW (2007) Light-regulated transcriptional networks in higher plants. *Nat Rev Genet* 8: 217–230
- Kanamaru K, Nagashima A, Fujiwara M, Shimada H, Shirano Y, Nakabayashi K, Shibata D, Tanaka K, Takahashi H (2001) An Arabidopsis sigma factor (SIG2)-dependent expression of plastid-encoded tRNAs in chloroplasts. *Plant Cell Physiol* 42: 1034–1043
- Keeling PJ (2010) The endosymbiotic origin, diversification and fate of plastids. *Philos Trans R Soc Lond B Biol Sci* 365: 729–748
- Khan A, Fornes O, Stigliani A, Gheorghe M, Castro-Mondragon JA, van der Lee R, Bessy A, Chèneby J, Kulkarni SR, Tan G, et al (2018) JASPAR2018: Update of the open-access database of transcription factor binding profiles and its web framework. *Nucleic Acids Res* 46(D1): D260–D266
- Kim DH, Kang JG, Yang SS, Chung KS, Song PS, Park CM (2002) A phytochrome-associated protein phosphatase 2A modulates light signals in flowering time control in Arabidopsis. *Plant Cell* 14: 3043–3056
- Kim D, Perteu G, Trapnell C, Pimentel H, Kelley R, Salzberg SL (2013) TopHat2: Accurate alignment of transcriptomes in the presence of insertions, deletions and gene fusions. *Genome Biol* 14: R36
- Kleine T, Leister D (2015) Emerging functions of mammalian and plant mTERFs. *Biochim Biophys Acta* 1847: 786–797
- Kleine T, Leister D (2016) Retrograde signaling: Organelles go networking. *Biochim Biophys Acta* 1857: 1313–1325
- Kleine T, Kindgren P, Benedict C, Hendrickson L, Strand A (2007) Genome-wide gene expression analysis reveals a critical role for CRYPTOCHROME1 in the response of Arabidopsis to high irradiance. *Plant Physiol* 144: 1391–1406
- Kleine T, Maier UG, Leister D (2009) DNA transfer from organelles to the nucleus: The idiosyncratic genetics of endosymbiosis. *Annu Rev Plant Biol* 60: 115–138
- Köhler D, Helm S, Agne B, Baginsky S (2016) Importance of translocon subunit Tic56 for rRNA processing and chloroplast ribosome assembly. *Plant Physiol* 172: 2429–2444
- Kosugi S, Hasebe M, Tomita M, Yanagawa H (2009) Systematic identification of cell cycle-dependent yeast nucleocytoplasmic shuttling proteins by prediction of composite motifs. *Proc Natl Acad Sci USA* 106: 10171–10176
- Kubis S, Baldwin A, Patel R, Razzaq A, Dupree P, Lilley K, Kurth J, Leister D, Jarvis P (2003) The Arabidopsis *ppi1* mutant is specifically defective in the expression, chloroplast import, and accumulation of photosynthetic proteins. *Plant Cell* 15: 1859–1871
- Lee K, Lee HJ, Kim DH, Jeon Y, Pai HS, Kang H (2014) A nuclear-encoded chloroplast protein harboring a single CRM domain plays an important role in the Arabidopsis growth and stress response. *BMC Plant Biol* 14: 98
- Leister D, Kleine T (2016) Definition of a core module for the nuclear retrograde response to altered organellar gene expression identifies GLK overexpressors as *gun* mutants. *Physiol Plant* 157: 297–309
- Leister D, Romani I, Mittermayr L, Paiari F, Fenino E, Kleine T (2014) Identification of target genes and transcription factors implicated in translation-dependent retrograde signaling in Arabidopsis. *Mol Plant* 7: 1228–1247
- Leister D, Wang L, Kleine T (2017) Organellar gene expression and acclimation of plants to environmental stress. *Front Plant Sci* 8: 387
- Leivar P, Monte E (2014) PIFs: systems integrators in plant development. *Plant Cell* 26: 56–78
- Leivar P, Monte E, Oka Y, Liu T, Carle C, Castillon A, Huq E, Quail PH (2008) Multiple phytochrome-interacting bHLH transcription factors repress premature seedling photomorphogenesis in darkness. *Curr Biol* 18: 1815–1823
- Li J, Li G, Wang H, Wang Deng X (2011) Phytochrome signaling mechanisms. *Arabidopsis Book* 9: e0148
- Liang Z, Zhu N, Mai KK, Liu Z, Tzeng D, Osteryoung KW, Zhong S, Staehelin LA, Kang BH (2018) Thylakoid-bound polysomes and a dynamine-related protein, FZL, mediate critical stages of the linear chloroplast biogenesis program in greening Arabidopsis cotyledons. *Plant Cell* 30: 1476–1495
- Liao Y, Smyth GK, Shi W (2014) featureCounts: An efficient general purpose program for assigning sequence reads to genomic features. *Bioinformatics* 30: 923–930
- Liebers M, Grübler B, Chevalier F, Lerbs-Mache S, Merendino
- L, Blanvillain R, Pfannschmidt T (2017) Regulatory shifts in plastid transcription play a key role in morphological conversions of plastids during Plant development. *Front Plant Sci* 8: 23
- Liere K, Weihe A, Börner T (2011) The transcription machineries of plant mitochondria and chloroplasts: Composition, function, and regulation. *J Plant Physiol* 168: 1345–1360
- Lillo C, Kataya AR, Heidari B, Creighton MT, Nemie-Feyissa D, Ginbot Z, Jonassen EM (2014) Protein phosphatases PP2A, PP4 and PP6: Mediators and regulators in development and responses to environmental cues. *Plant Cell Environ* 37: 2631–2648
- Ling Q, Huang W, Baldwin A, Jarvis P (2012) Chloroplast biogenesis is regulated by direct action of the ubiquitin-proteasome system. *Science* 338: 655–659
- Linhart C, Halperin Y, Shamir R (2008) Transcription factor and micro-RNA motif discovery: The Amadeus platform and a compendium of metazoan target sets. *Genome Res* 18: 1180–1189
- López-Juez E, Dillon E, Magyar Z, Khan S, Hazeldine S, de Jager SM, Murray JA, Beemster GT, Bögre L, Shanahan H (2008) Distinct light-initiated gene expression and cell cycle programs in the shoot apex and cotyledons of Arabidopsis. *Plant Cell* 20: 947–968
- Love MI, Huber W, Anders S (2014) Moderated estimation of fold change and dispersion for RNA-seq data with DESeq2. *Genome Biol* 15: 550
- Martin G, Leivar P, Ludevid D, Tepperman JM, Quail PH, Monte E (2016) Phytochrome and retrograde signalling pathways converge to antagonistically regulate a light-induced transcriptional network. *Nat Commun* 7: 11431
- McCormac AC, Terry MJ (2002) Light-signalling pathways leading to the coordinated expression of HEMA1 and Lhcb during chloroplast development in *Arabidopsis thaliana*. *Plant J* 32: 549–559
- McNellis TW, von Arnim AG, Araki T, Komeda Y, Miséra S, Deng XW (1994) Genetic and molecular analysis of an allelic series of cop1 mutants suggests functional roles for the multiple protein domains. *Plant Cell* 6: 487–500
- Miura E, Kato Y, Matsushima R, Albrecht V, Laalami S, Sakamoto W (2007) The balance between protein synthesis and degradation in chloroplasts determines leaf variegation in Arabidopsis yellow variegated mutants. *Plant Cell* 19: 1313–1328
- Mockler TC, Guo H, Yang H, Duong H, Lin C (1999) Antagonistic actions of Arabidopsis cryptochromes and phytochrome B in the regulation of floral induction. *Development* 126: 2073–2082
- Møller SG, Kim YS, Kunkel T, Chua NH (2003) PP7 is a positive regulator of blue light signaling in Arabidopsis. *Plant Cell* 15: 1111–1119
- Moore M, Gossmann N, Dietz KJ (2016) Redox regulation of cytosolic translation in plants. *Trends Plant Sci* 21: 388–397
- Motohashi R, Rödiger A, Agne B, Baerenfaller K, Baginsky S (2012) Common and specific protein accumulation patterns in different albino/pale-green mutants reveals regulon organization at the proteome level. *Plant Physiol* 160: 2189–2201
- Nagashima A, Hanaoka M, Shikanai T, Fujiwara M, Kanamaru K, Takahashi H, Tanaka K (2004) The multiple-stress responsive plastid sigma factor, SIG5, directs activation of the psbD blue light-responsive promoter (BLRP) in *Arabidopsis thaliana*. *Plant Cell Physiol* 45: 357–368
- Neff MM, Chory J (1998) Genetic interactions between phytochrome A, phytochrome B, and cryptochrome 1 during Arabidopsis development. *Plant Physiol* 118: 27–35
- Oelze ML, Muthuramalingam M, Vogel MO, Dietz KJ (2014) The link between transcript regulation and de novo protein synthesis in the retrograde high light acclimation response of *Arabidopsis thaliana*. *BMC Genomics* 15: 320
- Osterlund MT, Hardtke CS, Wei N, Deng XW (2000) Targeted destabilization of HY5 during light-regulated development of Arabidopsis. *Nature* 405: 462–466
- Pfannschmidt T, Blanvillain R, Merendino L, Courtois F, Chevalier F, Liebers M, Grübler B, Hommel E, Lerbs-Mache S (2015) Plastid RNA polymerases: Orchestration of enzymes with different evolutionary origins controls chloroplast biogenesis during the plant life cycle. *J Exp Bot* 66: 6957–6973
- Pfeiffer A, Shi H, Tepperman JM, Zhang Y, Quail PH (2014) Combinatorial complexity in a transcriptionally centered signaling hub in Arabidopsis. *Mol Plant* 7: 1598–1618
- Pogson BJ, Albrecht V (2011) Genetic dissection of chloroplast biogenesis and development: An overview. *Plant Physiol* 155: 1545–1551

- Pribil M, Labs M, Leister D (2014) Structure and dynamics of thylakoids in land plants. *J Exp Bot* 65: 1955–1972
- Privat I, Hakimi MA, Buhot L, Favory JJ, Mache-Lerbs S (2003) Characterization of *Arabidopsis* plastid sigma-like transcription factors SIG1, SIG2 and SIG3. *Plant Mol Biol* 51: 385–399
- Putarjuna A, Liu X, Nolan T, Yu F, Rodermel S (2013) Understanding chloroplast biogenesis using second-site suppressors of *immutans* and *var2*. *Photosynth Res* 116: 437–453
- Rappsilber J, Mann M, Ishihama Y (2007) Protocol for micro-purification, enrichment, pre-fractionation and storage of peptides for proteomics using StageTips. *Nat Protoc* 2: 1896–1906
- Roy B, von Arnim AG (2013) Translational regulation of cytoplasmic mRNAs. *Arabidopsis Book* 11: e0165
- Ruckle ME, DeMarco SM, Larkin RM (2007) Plastid signals remodel light signaling networks and are essential for efficient chloroplast biogenesis in *Arabidopsis*. *Plant Cell* 19: 3944–3960
- Ruppel NJ, Hangarter RP (2007) Mutations in a plastid-localized elongation factor G alter early stages of plastid development in *Arabidopsis thaliana*. *BMC Plant Biol* 7: 37
- Rusaczek A, Czarnocka W, Kacprzak S, Witoń D, Ślesak I, Szechyńska-Hebda M, Gawroński P, Karpiński S (2015) Role of phytochromes A and B in the regulation of cell death and acclimatory responses to UV stress in *Arabidopsis thaliana*. *J Exp Bot* 66: 6679–6695
- Saini G, Meskauskiene R, Pijacka W, Roszak P, Sjögren LL, Clarke AK, Straus M, Apel K (2011) 'happy on norflurazon' (*hon*) mutations implicate perturbation of plastid homeostasis with activating stress acclimatization and changing nuclear gene expression in norflurazon-treated seedlings. *Plant J* 65: 690–702
- Sakr S, Wang M, Dédaldéchamp F, Perez-Garcia MD, Ogé L, Hamama L, Atanassova R (2018) The sugar-signaling hub: Overview of regulators and interaction with the hormonal and metabolic network. *Int J Mol Sci* 19: 2506
- Schmitz-Linneweber C, Lampe MK, Sultan LD, Ostersetzer-Biran O (2015) Organellar maturases: A window into the evolution of the spliceosome. *Biochim Biophys Acta* 1847: 798–808
- Schulz E, Tohge T, Zuther E, Fernie AR, Hinch DK (2015) Natural variation in flavonol and anthocyanin metabolism during cold acclimation in *Arabidopsis thaliana* accessions. *Plant Cell Environ* 38: 1658–1672
- Shen Y, Kim JI, Song PS (2005) NDPK2 as a signal transducer in the phytochrome-mediated light signaling. *J Biol Chem* 280: 5740–5749
- Shikanai T (2015) RNA editing in plants: Machinery and flexibility of site recognition. *Biochim Biophys Acta* 1847: 779–785
- Shimada H, Mochizuki M, Ogura K, Froehlich JE, Osteryoung KW, Shirano Y, Shibata D, Masuda S, Mori K, Takamiya K (2007) *Arabidopsis* cotyledon-specific chloroplast biogenesis factor CYO1 is a protein disulfide isomerase. *Plant Cell* 19: 3157–3169
- Shinomura T, Hanzawa H, Schäfer E, Furuya M (1998) Mode of phytochrome B action in the photoregulation of seed germination in *Arabidopsis thaliana*. *Plant J* 13: 583–590
- Solfanelli C, Poggi A, Loreti E, Alpi A, Perata P (2006) Sucrose-specific induction of the anthocyanin biosynthetic pathway in *Arabidopsis*. *Plant Physiol* 140: 637–646
- Stern DB, Goldschmidt-Clermont M, Hanson MR (2010) Chloroplast RNA metabolism. *Annu Rev Plant Biol* 61: 125–155
- Stoppel R, Meurer J (2012) The cutting crew - ribonucleases are key players in the control of plastid gene expression.
- Strittmatter G, Kössel H (1984) Cotranscription and processing of 23S, 4.5S and 5S rRNA in chloroplasts from *Zea mays*. *Nucleic Acids Res* 12: 7633–7647
- Su L, Hou P, Song M, Zheng X, Guo L, Xiao Y, Yan L, Li W, Yang J (2015) Synergistic and antagonistic action of phytochrome (Phy) A and PhyB during seedling de-etiolation in *Arabidopsis thaliana*. *Int J Mol Sci* 16: 12199–12212
- Tiller N, Bock R (2014) The translational apparatus of plastids and its role in plant development. *Mol Plant* 7: 1105–1120
- Tsunoyama Y, Ishizaki Y, Morikawa K, Kobori M, Nakahira Y, Takeba G, Toyoshima Y, Shiina T (2004) Blue light-induced transcription of plastid-encoded *psbD* gene is mediated by a nuclear-encoded transcription initiation factor, AtSig5. *Proc Natl Acad Sci USA* 101: 3304–3309
- Ühlken C, Horvath B, Stadler R, Sauer N, Weingartner M (2014) MAIN- LIKE1 is a crucial factor for correct cell division and differentiation in *Arabidopsis thaliana*. *Plant J* 78: 107–120
- Uhrig RG, Labandera AM, Moorhead GB (2013) *Arabidopsis* PPP family of serine/threonine protein phosphatases: Many targets but few enzymes. *Trends Plant Sci* 18: 505–513
- Ulker B, Peiter E, Dixon DP, Moffat C, Capper R, Bouché N, Edwards R, Sanders D, Knight H, Knight MR (2008) Getting the most out of publicly available T-DNA insertion lines. *Plant J* 56: 665–677
- Van Bel M, Diels T, Vancaester E, Kreft L, Botzki A, Van de Peer Y, Coppens F, Vandepoel K (2018) PLAZA 4.0: An integrative resource for functional, evolutionary and comparative plant genomics. *Nucleic Acids Res* 46(D1): D1190–D1196
- Van Dingenen J, Blomme J, Gonzalez N, Inzé D (2016) Plants grow with a little help from their organelle friends. *J Exp Bot* 67: 6267–6281
- Varotto C, Pesaresi P, Maiwald D, Kurth J, Salamini F, Leister D (2000) Identification of photosynthetic mutants of *Arabidopsis* by automatic screening for altered effective quantum yield of photosystem 2. *Photosynthetica* 38: 497–504
- Vizcaíno JA, Csordas A, Del-Toro N, Dienes JA, Griss J, Lavidas I, Mayer G, Perez-Riverol Y, Reisinger F, Tement T, et al (2016) 2016 update of the PRIDE database and its related tools. *Nucleic Acids Res* 44: 11033
- Wagner D, Tepperman JM, Quail PH (1991) Overexpression of phytochrome B induces a short hypocotyl phenotype in transgenic *Arabidopsis*. *Plant Cell* 3: 1275–1288
- Wang R, Zhao J, Jia M, Xu N, Liang S, Shao J, Qi Y, Liu X, An L, Yu F (2018) Balance between cytosolic and chloroplast translation affects leaf variegation. *Plant Physiol* 176: 804–818
- Wang X, Li W, Piqueras R, Cao K, Deng XW, Wei N (2009) Regulation of COP1 nuclear localization by the COP9 signalosome via direct interaction with CSN1. *Plant J* 58: 655–667
- Waters MT, Langdale JA (2009) The making of a chloroplast. *EMBO J* 28: 2861–2873
- Wessel D, Flüggé UI (1984) A method for the quantitative recovery of protein in dilute solution in the presence of detergents and lipids. *Anal Biochem* 138: 141–143
- Wikström M, Savolainen V, Chase MW (2001) Evolution of the angiosperms: Calibrating the family tree. *Proc Biol Sci* 268: 2211–2220
- Williams ME, Foster R, Chua NH (1992) Sequences flanking the hexameric G-box core CACGTG affect the specificity of protein binding. *Plant Cell* 4: 485–496
- Wingler A (2018) Transitioning to the next phase: The role of sugar signaling throughout the plant life cycle. *Plant Physiol* 176: 1075–1084
- Wisman E, Hartmann U, Sagasser M, Baumann E, Palme K, Hahlbrock K, Saedler H, Weissshaar B (1998) Knock-out mutants from an *En-1* mutagenized *Arabidopsis thaliana* population generate phenylpropanoid biosynthesis phenotypes. *Proc Natl Acad Sci USA* 95: 12432–12437
- Woodson JD, Chory J (2008) Coordination of gene expression between organellar and nuclear genomes. *Nat Rev Genet* 9: 383–395
- Woodson JD, Perez-Ruiz JM, Schmitz RJ, Ecker JR, Chory J (2013) Sigma factor-mediated plastid retrograde signals control nuclear gene expression. *Plant J* 73: 1–13
- Wurtinger B, Nukarinen E, Nägele T, Weckwerth W, Teige M (2018) The SnRK1 kinase as central mediator of energy signaling between different organelles. *Plant Physiol* 176: 1085–1094
- Xu X, Paik I, Zhu L, Huq E (2015) Illuminating progress in phytochrome-mediated light signaling pathways. *Trends Plant Sci* 20: 641–650
- Yi C, Deng XW (2005) COP1—From plant photomorphogenesis to mammalian tumorigenesis. *Trends Cell Biol* 15: 618–625
- Yu QB, Li G, Wang G, Sun JC, Wang PC, Wang C, Mi HL, Ma WM, Cui J, Cui YL, et al (2008) Construction of a chloroplast protein interaction network and functional mining of photosynthetic proteins in *Arabidopsis thaliana*. *Cell Res* 18: 1007–1019
- Yu X, Liu H, Klejnot J, Lin C (2010) The cryptochrome blue light receptors. *Arabidopsis Book* 8: e0135
- Zagari N, Sandoval-Ibañez O, Sandal N, Su J, Rodriguez-Concepcion M, Stougaard J, Pribil M, Leister D, Pulido P (2017) SNOWY COTYLE- DON 2 promotes chloroplast development and has a role in leaf variegation in both *Lotus japonicus* and *Arabidopsis thaliana*. *Mol Plant* 10: 721–734
- Zhang Y, Primavesi LF, Jhureea D, Andralojc PJ, Mitchell RA, Powers SJ, Schluepmann H, Delatte T, Wingler A, Paul MJ (2009) Inhibition of SNF1-related protein kinase1 activity and regulation of metabolic pathways by trehalose-6-phosphate. *Plant Physiol* 149: 1860–1871

3.2 Chapter 2

VENOSA4, a human dNTPase SAMHD1 homolog, contributes to chloroplast development and abiotic stress tolerance

Research Report

VENOSA4, a Human dNTPase SAMHD1 Homolog, Contributes to Chloroplast Development and Abiotic Stress Tolerance¹[OPEN]

Duarong Xu, Dario Leister, and Tatjana Kleine^{2,3}

Plant Molecular Biology (Botany), Department Biology I, Ludwig-Maximilians-Universität München, 82152 Planegg-Martinsried, Germany

ORCID IDs: 0000-0002-0566-3722 (D.X.); 0000-0003-1897-8421 (D.L.); 0000-0001-6455-3470 (T.K.).

Chloroplast biogenesis depends on an extensive interplay between the nucleus, cytosol, and chloroplasts, involving regulatory nucleus-encoded chloroplast proteins, as well as nucleocytoplasmic photoreceptors such as phytochromes (phys) and other extrachloroplastic factors. However, this whole process is only partially understood. Here, we describe the role of VENOSA4 (VEN4) in chloroplast development and acclimation to adverse growth conditions. A 35S:VEN4-eGFP fusion protein localizes to the nucleus in *Arabidopsis thaliana* protoplasts, and VEN4 homologs are present in a wide range of eukaryotes including humans, where the corresponding homolog (SAMHD1) cleaves dNTPs. Defective photosynthesis in *ven4* seedlings results from reduced accumulation of photosynthetic proteins and appears to be caused by a reduction in the translational capacity of chloroplasts. The negative effect of the *ven4* mutation on photosynthesis can be phenotypically suppressed by germinating seeds in the presence of excess dCTP or a pool of dNTPs, implying that VEN4, like human SAMHD1, is involved in dNTP catabolism. Moreover, VEN4 activity is also required for optimal responses to cold and salt stresses. In conclusion, our work emphasizes the importance of the nucleocytoplasmic compartment and the fine-tuning of dNTP levels for chloroplast translation and development.

Chloroplast biogenesis is indispensable for normal plant development and environmental acclimation in plants. This process is complicated by the fact that most of the several thousand chloroplast proteins are encoded by nuclear genes, whereas chloroplasts have retained a reduced genome of only ~100 genes (Kleine et al., 2009). Consequently, chloroplast formation requires tight coordination of the activities of the plastid and nuclear genomes, which is achieved by extensive exchange of information between the two organelle types (Pogson et al., 2015; Kleine and Leister, 2016). Furthermore, chloroplast biogenesis in angiosperms is dependent on light, and this dependence is mediated by a complex, and only partially understood, communication network that involves chloroplast-localized proteins,

nucleocytoplasmic light sensors including cryptochromes (crys) and phytochromes (phys), and other extrachloroplastic factors (Fitter et al., 2002; Albrecht et al., 2010; Leivar and Monte, 2014). PP7L is one of the extrachloroplastic proteins that promotes chloroplast development in seedlings and in emerging true leaves of *Arabidopsis thaliana*, as manifested by the reduced maximum quantum yield of PSII (F_v/F_m) observed in its absence (Xu et al., 2019). Another lately identified protein involved in chloroplast biogenesis is VENOSA4 (VEN4; Yoshida et al., 2018). Whereas PP7L was specifically recruited to regulate chloroplast development in Brassicales (Xu et al., 2019), VEN4 homologs are present in a wide range of eukaryotes including Chlorophyta and Viridiplantae (<https://bioinformatics.psb.ugent.be/plaza/>; Van Bel et al., 2018), zebrafish (*Danio rerio*), mouse (*Mus musculus*), and human (*Homo sapiens*; <https://www.ncbi.nlm.nih.gov/homologene/?term=5AT5G40270>). The human homolog of VEN4 is SAMHD1, a sterile alpha motif (SAM) and His-Asp (HD) domain-containing protein, which is a 2'-deoxynucleoside-5'-triphosphate (dNTP) triphosphohydrolase that cleaves physiological dNTPs into 2'-deoxynucleosides and inorganic triphosphate. SAMHD1 is required to restrict infection by viruses, such as HIV-1, because the dNTPase activity reduces cellular dNTP levels to such low levels that retroviral reverse transcription is limited (Laguet et al., 2011).

Interestingly, the VEN4 gene was first identified by a second-site mutation in the *phyB-9* mutant, and altered chlorophyll accumulation and reduced photosynthetic

¹This work was supported by the Deutsche Forschungsgemeinschaft (DFG) (KL 2362/1-1 and TRR175, projects C01 and C05 to D.L. and T.K.) and the Chinese Research Council (to D.X.).

²Author for contact: tatjana.kleine@lmu.de.

³Senior author.

The author responsible for distribution of materials integral to the findings presented in this article in accordance with the policy described in the Instructions for Authors (www.plantphysiol.org) is: Tatjana Kleine (tatjana.kleine@lmu.de).

D.X. and T.K. designed the research and analyzed the data; D.X. performed most of the experiments; T.K. wrote the manuscript with input from D.X. and D.L.; T.K. supervised the whole study; all authors read and approved the article.

performance in *phyB-9* is attributable to the lack of VEN4 and not PHYB (Yoshida et al., 2018). In *pp7l* mutants, levels of *PHYB* mRNA and its protein product are increased (Xu et al., 2019), raising the possibility that overexpression of PHYB might phenocopy the *pp7l* mutant. In experiments undertaken to test this assumption, our attention was drawn to VEN4, because both overexpression of PHYB (in the *phyB-9* background) and a lack thereof in the *phyB-9* mutant are associated with reduced photosynthetic performance, suggesting that a second mutation might be present in *phyB-9*. During our attempts to identify this putative second mutation, the VEN4 manuscript mentioned above (Yoshida et al., 2018) was published.

Here, we describe two further *ven4* mutants. We characterize these mutants, together with *pp7l-1*, a *phyB-9* line that still contains the original *ven4* mutation, and a *phyB-9* line in which that second mutation had been out-crossed, with respect to germination behavior and photosynthetic performance in both light-grown and etiolated seedlings. VEN4 is localized to the nucleus, and feeding experiments with a mixed dNTP pool and each single dNTP suggest that the protein is involved in dNTP metabolism. Additionally, VEN4, but not PHYB, is a positive regulator of chloroplast protein synthesis. Reduced photosynthetic performance was detected in both seedlings and older, but not emerging leaves. Seed germination in all investigated mutants was reduced by exposure to cold, and both *ven4* seedlings and mature plants displayed enhanced sensitivity to salt stress.

RESULTS AND DISCUSSION

PSII Activity Is Reduced in Seedlings and Older Leaves in *ven4* Mutants

Because in *pp7l* mutants, PHYB levels are increased (Xu et al., 2019), we set out to test whether the overexpression of PHYB in *pp7l* might be responsible for altered chloroplast development in the mutant. To this end, we initially used a *phyB-9* mutant line that overexpresses a PHYB-YFP fusion under the control of the 35S promoter (*oe-PHYB* [*phyB-9*]; Medzihradsky et al., 2013), and measured the F_v/F_m as an indicator of chloroplast development. Overexpression of PHYB was indeed accompanied by reduced F_v/F_m values in 3-d-old seedlings, although this effect was less pronounced than in the *pp7l-1* mutant (Supplemental Fig. S1A). Moreover, in 4-week-old plants, overexpression of PHYB phenocopied the *pp7l* phenotype with respect to both reduced F_v/F_m and reduced rosette size (Supplemental Fig. S1A). If overexpression of PHYB alone is sufficient to cause the photosynthesis phenotype of the *pp7l* mutant, then that phenotype should be corrected in the *pp7l phyB-9* mutant. However, the double mutant still exhibited reduced photosynthetic performance (Supplemental Fig. S1, A and B). In addition, when F_v/F_m values

were measured daily in 3- to 7-d-old seedlings (Supplemental Fig. S1B) and 4-week-old plants (Supplemental Fig. S1A), a reduction of F_v/F_m was also seen in the *phyB-9* mutant, although the *phyA phyB* double mutant displayed wild-type-like F_v/F_m values (Xu et al., 2019). The F_v/F_m values were reduced to a similar intermediate extent in *phyB-9* and *oe-PHYB* (*phyB-9*) seedlings. On the face of it, these findings imply either that a delicately adjusted level of PHYB accumulation is required for proper chloroplast development, or that overexpression of PHYB in the *phyB-9* line fails to complement the *phyB-9* photosynthesis phenotype, although it rescues the hypocotyl growth phenotype. Taken together, these data point to the presence of a second mutation in the *phyB-9* line. Indeed, during the process of double mutant selection, we had observed an unexpected segregation ratio, which supports the supposition that the *phyB-9* line might harbor a second mutation. During our attempts to identify this putative second mutation, a manuscript was published as a *Letter to the Editor* in *Plant Physiology* in which the second-site mutation was localized to the *VENOSA4* (*VEN4*; *AT5G40270*) gene (Yoshida et al., 2018). We confirmed that our *phyB-9* and *oe-PHYB* (*phyB-9*) lines also harbored the mutation in *VEN4* (Supplemental Fig. S2A). As already highlighted by Yoshida et al. (2018), *phyB* is one of the most extensively studied proteins in Arabidopsis, and the *phyB-9* mutant line was frequently used because of its Col-0 background and the EMS-induced premature stop codon (Reed et al., 1993). This line was also used in recent studies of chloroplast development and chloroplast-to-nucleus signaling (Ganguly et al., 2015; Lv et al., 2019). In an experiment designed to determine the roles of *phyA* and *phyB* in UV-C radiation stress, control *phyB-9* plants had lower F_v/F_m values compared with Col-0, whereas the *phyA-211 phyB-9* double mutant (which does not carry the *VEN4* mutation; Yoshida et al., 2018) displayed a higher F_v/F_m value (Rusaczek et al., 2015). Therefore, we wanted to gain more insight into the functional consequences on chloroplast development and photosynthetic performance caused by the second-site mutation in *VEN4*. For the sake of clarity, and in accordance with the nomenclature introduced by Yoshida et al. (2018), from here on we refer to the original *phyB-9* line bearing the *VEN4* mutation, a back-crossed line that carries only the *PHYB* mutation, and the line that harbors only the *VEN4* mutation as *phyB-9^{OG}*, *phyB-9^{BC}*, and *bnen*, respectively. It was noted before that F_v/F_m is not depressed in *phyB-9^{BC}*, but is reduced in first-node true leaves of 13-d-old *phyB-9^{OG}* and *bnen* seedlings (Yoshida et al., 2018). It was also shown that the reduction of F_v/F_m is less pronounced in emerging leaves of *phyB-9^{OG}* and *bnen*, which clearly contrasts with the fact that F_v/F_m is strongly reduced in emerging *pp7l-1* leaves and young seedlings (Fig. 1, A and F; Supplemental Fig. S1A; Xu et al., 2019). These results raise the question of whether VEN4's role in chloroplast development is restricted to mature stages, especially because chloroplast development in cotyledons and leaves might differ slightly (Waters and Langdale, 2009). To test this, and to

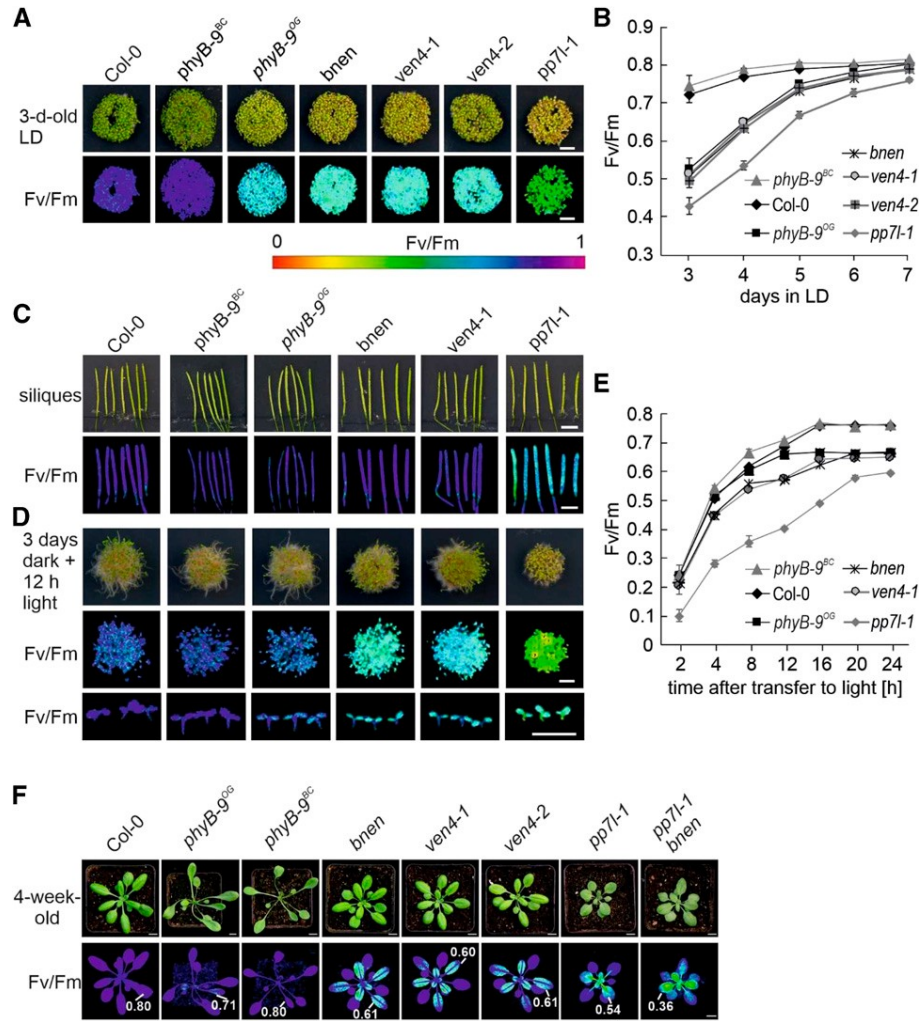


Figure 1. Phenotypic characterization of *phyB-9^{OG}*, *phyB-9^{BC}*, *bnen*, *ven4-1*, *ven4-2*, and *pp7l-1* seedlings. A, Phenotypes of 3-d-old wild-type (Col-0) and *phyB-9^{OG}* (the original *phyB-9* line that also carries the *VEN4* mutation), *phyB-9^{BC}* (a back-crossed line which harbors only the *PHYB* mutation), *bnen* (a back-crossed line which bears only the *VEN4* mutation), *ven4-1*, *ven4-2*, and *pp7l-1* seedlings grown under long-day (LD; 16-h light/8-h dark) conditions. The F_v/F_m was measured with an imaging Chl fluorometer (Imaging PAM). Scale bars = 1 cm. B, Graph displaying F_v/F_m values measured for 3- to 7-d-old Col-0 and mutant seedlings. The data represent mean values \pm SD of three independent experiments, each performed with at least 10 seedlings per genotype. C, Opened green siliques of Col-0 and mutant plants grown under LD (16-h light/8-h dark) conditions. Corresponding F_v/F_m pictures illustrate F_v/F_m . Scale bars = 0.5 cm. D, Phenotypes (top) and corresponding F_v/F_m pictures (two at bottom) of 3-d-old etiolated seedlings, which had been exposed to 12-h continuous light. Scale bars = 0.5 cm. E, Graph displaying F_v/F_m values measured for 3-d-old etiolated seedlings, which had been exposed to 2–24-h continuous light. The data represent mean values \pm SD of three independent experiments, each performed with at least 10 seedlings per genotype. F, Images of 4-week-old Col-0 and mutant plants grown under LD conditions ($\sim 120 \text{ mmol photons m}^{-2} \text{ s}^{-1}$ on leaf surfaces; 16-h light/8-h dark) together with their Imaging PAM profiles. F_v/F_m values are indicated for selected leaves of the same age. Scale bars = 1 cm.

determine whether *phyB* has an impact on chloroplast development in early stages of plant development, F_v/F_m values were measured daily in 3- to 7-d-old *phyB-9^{OG}*, *phyB-9^{BC}*, *bnen*, *ven4-1*, *ven4-2* (Fig. 1B), and, as controls, wild-type and *pp7l-1* seedlings. The F_v/F_m values for 3- to 5-d-old *phyB-9^{BC}* seedlings were slightly elevated compared to wild type (Fig. 1, A and B), indicating that lack of *PHYB* does not negatively affect photosynthesis in young seedlings and corroborating the observed

higher F_v/F_m value in the *phyA-211 phyB-9* double mutant (Rusaczon et al., 2015). Reductions in F_v/F_m were observed in the *phyB-9^{OG}*, *bnen*, *ven4-1*, and *ven4-2* mutant lines on days 3, 4, and 5 (Fig. 1, A and B). However, at 6 d, F_v/F_m values in these lines were comparable with wild type. Focusing on 3-d-old seedlings, we found that F_v/F_m was markedly reduced in the *pp7l-1* mutant (0.42) compared with wild type (0.72), whereas the effect was somewhat milder (at 0.50) in *phyB-9^{OG}*, *bnen*, *ven4-1*, and

ven4-2 (Fig. 1, A and B), indicating that inactivation of VEN4 does have an impact – albeit a weaker one than the absence of PP7L – on photosynthesis in seedlings. Because chloroplast development could be delayed by differences in germination rates, wild-type and mutant seedlings were germinated on Murashige and Skoog (MS) plates and germination rates were scored after 24, 36, 48, and 72 h. Indeed, germination efficiency of the *pp7l-1* mutant was delayed especially in the early time points, whereas 100% germination was achieved after 72 h (Supplemental Fig. S1C). Germination rates of mutants lacking PHYB were slightly, but not significantly, reduced, and those of mutants lacking VEN4 were wild type like (Supplemental Fig. S1C). Accordingly, *pp7l-1* was the only mutant with perturbed chloroplast development in developing seeds as demonstrated by the measurement of F_v/F_m values in opened green siliques (Fig. 1C). To exclude that a developmental delay caused by retarded germination – at least in *pp7l-1* – was responsible for impaired chloroplast development in young seedlings, we investigated etiolated seedlings and their photosynthetic performance after onset of light. To this end, wild-type and mutant seedlings were grown for 3 d in darkness and were then transferred for 24 h into continuous light. The maximum quantum yield of PSII was recorded in 2- or 4-h intervals after the onset of light exposure. Under these conditions, all mutant seedlings behaved comparable with seedlings directly germinated in light with respect to photosynthetic performance. Reductions in F_v/F_m were observed in the *phyB-9^{OG}*, *bnen*, *ven4-1*, and *pp7l-1* mutant lines during the whole time-course (Fig. 1, D and E), indicating again that whereas germination differences have an impact on photosynthetic development, a delay of such development occurs also when germination differences become irrelevant in young seedlings lacking either VEN4 or PP7L.

VEN4 Is a Nuclear Protein Involved in dNTP Metabolism

Notably, VEN4 is predicted to be localized to the nucleus and/or the cytosol (The Arabidopsis Information Resource; <https://www.arabidopsis.org/servlets/TairObject?id5134598&type5locus>; SUBA4; <http://suba.live/factsheet.html?id5AT5G40270.1>). To experimentally determine the subcellular localization of VEN4, Arabidopsis protoplasts were transformed with a 35S:VEN4-eGFP construct. Fluorescence imaging of eGFP in protoplasts confirmed that VEN4-eGFP, like PP7L-eGFP (Xu et al., 2019), was targeted to the nucleus (Fig. 2A). To test whether VEN4 and PP7L genetically interact, *pp7l-1 bnen* double mutants were selected from the F2 offspring of *pp7l-1 phyB-9^{OG}* crosses that no longer harbored the *phyB-9* mutation. In 4-week-old plants, F_v/F_m was reduced to 0.6 in all mutant alleles lacking VEN4 and to 0.54 in *pp7l-1* mutants compared with a wild-type value of 0.80 (Fig. 1F). A clearly additive phenotype was observed in *pp7l-1 bnen* leaves, which displayed a reduction of F_v/F_m to 0.36.

VEN4 is homologous to human SAMHD1, which is involved in dNTP catabolism (see the first section of this study). Interestingly, a mutation in the large subunit of ribonucleotide reductase (RNR) and therefore an altered dNTP pool in the Arabidopsis *crinkled leaves8* mutant results in defects in leaf development and chloroplast division (Garton et al., 2007). Therefore, disturbed chloroplast development in *ven4* mutants could also be a consequence of an imbalanced dNTP pool. To test this assumption, Col-0, *ven4-1*, and *ven4-2* seeds were germinated on MS control plates without supplement and on plates supplemented with either dATP, dCTP, dGTP, or dTTP, or an equally mixed pool of dNTPs, and maximum quantum yield of PSII was visualized after 3 d with an ImagingPAM fluorometer M-Series (Walz). As expected, reductions in F_v/F_m were observed in *ven4-1* and *ven4-2* mutants compared with the wild type under control conditions (Fig. 2B). Addition of either 2 mM dATP or 2 mM dGTP had deleterious effects: germination efficiencies of wild-type and *ven4* mutant lines were reduced and F_v/F_m values in all three genotypes were equally low. Addition of 2 mM dNTPs reduced germination efficiency, but had only a low impact on photosynthetic activity of the wild type. Intriguingly, under these conditions, photosynthetic activity of seedlings lacking VEN4 was recovered. Addition of either 2 mM dCTP or 2 mM dTTP to the medium did not alter wild-type properties with respect to germination and photosynthetic activity. However, *ven4* seedling behaved wild type-like in the presence of 2 mM dCTP, and performed worse, comparable with that under control conditions, in the presence of 2 mM dTTP. The positive effect of dCTP addition was specific for *ven4* and is not applicable to all mutants defective in chloroplast gene expression, because the *pp7l* photosynthesis phenotype did not recover by the addition of dCTP to the medium (Fig. 2C). These results suggest that Arabidopsis VEN4, like human SAMHD1, is indeed involved in dNTP catabolism, in ways that paradoxically lead to presumably a lower dCTP pool and higher dGTP, dTTP, and dATP pools in the absence of VEN4. Here, it has to be said that the maintenance of a balanced dNTP pool is complex. In the presence of all four dNTP substrates, the hydrolysis rates by SAMHD1 are in the order of $dGTP > dCTP > dTTP > dATP$, which is the opposite of that obtained in the single dNTP substrate experiments ($dATP > dTTP > dCTP > dGTP$; Ji et al., 2014). Excess dGTP on the other hand leads to a decrease of dCTP and dTTP, but increased dATP pools (Kunz, 1982). RNR is responsible for de novo dNTP synthesis, and this process is under allosteric regulation in which dATP is an inhibitor of RNR activity (Hofer et al., 2012).

Lack of VEN4 Impairs Chloroplast Translation

But why is photosynthetic activity reduced in *ven4* mutants? This is a consequence of reduced accumulation of photosynthetic proteins, because PsbD and PsbD

(D2), representative subunits of PSI and PSII, respectively, were less than half as abundant in *phyB-9^{OG}*, *bnen*, *ven4-1*, and *ven4-2* seedlings as in wild type (Fig. 3A). In addition, staining of Western blots with Coomassie Brilliant Blue indicated reduced amounts of RbcL. In contrast, levels of *psaD*, *psbD*, *rbcL*, and *psbB* transcripts were virtually unchanged or slightly elevated in *phyB-9^{OG}*, *bnen*, *ven4-1*, and *ven4-2* seedlings, as quantified on RNA gel blots and by reverse transcription quantitative PCR (RT-qPCR; Fig. 3, B and C). Although *psbA* (encoding D1) and *psaA* transcripts were less abundant in *ven4-1* and *ven4-2* (Fig. 3C), the reduced amounts of chloroplast-encoded proteins in the *ven4* mutants cannot be attributed solely to a relative deficiency of their transcripts. To evaluate whether perturbation of VEN4 function also reduces chloroplast translational capacity, as seen in the *pp7l-1* mutant (Xu et al., 2019), the synthesis of plastid-encoded thylakoid membrane proteins was studied by in vivo labeling. After pulse labeling for 30 min, de novo synthesis of the D1 (encoded by *psbA*) and D2 (encoded by *psbD*) proteins was found to be reduced to less than half of the wild-type levels in *phyB-9^{OG}*, *bnen*, *ven4-1*, and *ven4-2*

seedlings (Fig. 3D), although *psbD* (encoding the D2 protein) transcript levels were slightly elevated. These findings suggest that chloroplast transcription is not primarily affected in *ven4* seedlings, but hint at a perturbation of downstream processes in chloroplast gene expression, which would account for the reduction in synthesis of chloroplast proteins and the delay in chloroplast development in *ven4* seedlings. Notably, accumulation of chloroplast-encoded proteins and transcripts and the translation capacity of *phyB-9^{BC}* seedlings were either unchanged or enhanced compared to the wild type, again supporting the notion that a lack of *phyB* does not have a negative impact on chloroplast development (Fig. 3).

VEN4 and PP7L Are Required for Chloroplast Biogenesis under Various Stresses

Disturbances of organellar gene expression can result in altered stress responses. Examples include the reduced cold tolerance of plants lacking chloroplast ribonucleoprotein CP29A or CP31A (Kupsch et al., 2012),

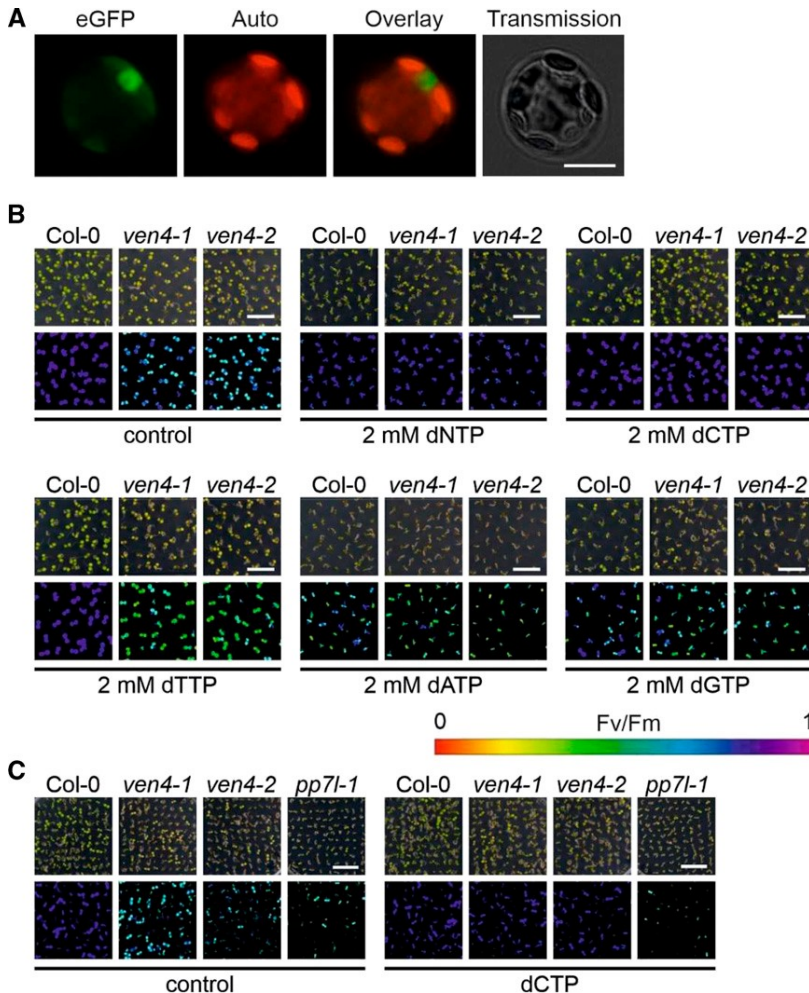


Figure 2. Lack of the nuclear VEN4 protein affects dNTP homeostasis. A, Fluorescence microscopy of Arabidopsis protoplasts transiently expressing VEN4 fused to eGFP. The eGFP fluorescence (eGFP; green) and chloroplast autofluorescence (Auto; red) are shown together in the overlay picture. Scale bars = 10 μ m. B, Images of Col-0, *ven4-1*, and *ven4-2* seedlings grown for 3 d on MS medium without supplement (control), and on MS supplemented with 2 mM dNTP, dCTP, dTTP, dATP, or dGTP, respectively. The Imaging PAM pictures show the F_v/F_m . Scale bar = 1 cm. C, Images of Col-0, *ven4-1*, *ven4-2*, and *pp7l-1* seedlings grown for 3 d on MS medium without supplement (control), and on MS supplemented with 2 mM dCTP. The Imaging PAM pictures show the F_v/F_m . Scale bar = 1 cm.

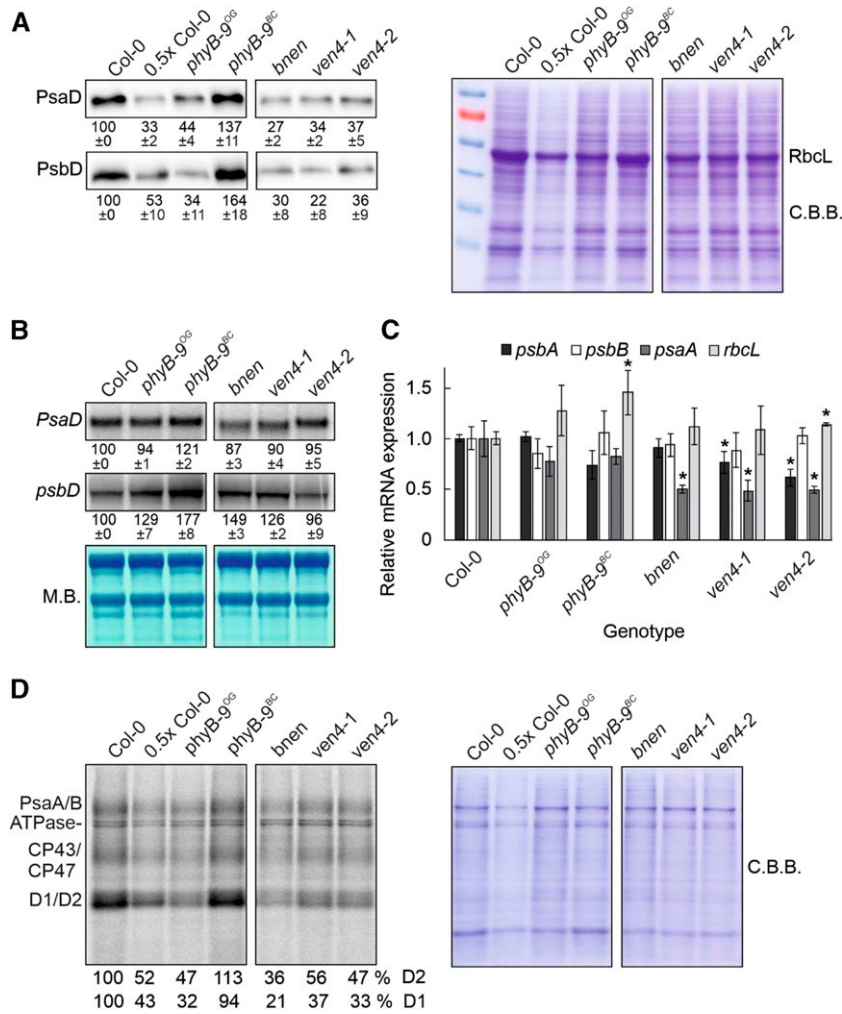


Figure 3. The nuclear VEN4 protein functions in chloroplast gene expression. **A**, Immunoblot analysis of representative thylakoid proteins. Total protein extracts from wild-type (Col-0), *phyB-9^{oc}*, *phyB-9^{bc}*, *bnen*, *ven4-1*, and *ven4-2* seedlings (78 h after imbibition) were fractionated by SDS-PAGE, and blots were probed with antibodies raised against PsaD and PsbD. Decreasing levels of wild-type proteins were loaded in the lanes marked Col-0 and 0.5x Col-0 (1x Col-0 = 5 μ g). The membrane stained with Coomassie Brilliant Blue (C.B.B.) served as a loading control. Please note that samples were run on the same gel, and RbcL protein levels are decreased in seedlings bearing the *ven4* mutation. The numbers represent mean values \pm SD from three different plant pools. The results were normalized to Col-0, which was set to 100. **B**, Steady-state levels of transcripts of photosynthetic genes. Total RNA was isolated from Col-0 and mutant seedlings (78 h after imbibition), and 7- μ g aliquots were fractionated in a formaldehyde-containing denaturing gel, transferred onto a nylon membrane, and probed with [α -³²P]dCTP-labeled complementary DNA fragments specific for *PsaD* and *psbD* transcripts. rRNA was visualized by staining the membrane with methylene blue (M.B.) and served as a loading control. **C**, RT-qPCR analysis of wild-type (Col-0) and mutant plants. RT-qPCR was performed with primers specific for the transcripts of interest and for *AT4G36800* (*RCE1*, encoding a RUB1-conjugating enzyme), which served as a control. Expression values are reported relative to the corresponding transcript levels in Col-0. The results were normalized with respect to the expression level of *RCE1*. Data are shown as mean values \pm SD from three independent experiments. Statistically significant differences (Tukey's test; $P < 0.05$) between wild-type and mutant samples are indicated by an asterisk. **D**, In vivo pulse-labeling of thylakoid membrane proteins with [³⁵S]Met in the presence of cycloheximide indicates that translation occurs at reduced rates in chloroplasts of lines lacking functional VEN4, but at normal (wild-type) rates in the *phyB-9* back-crossed line lacking functional phyB. Thylakoid proteins were loaded based on equivalent amounts of radioactivity (100,000 cpm) and were resolved by SDS-PAGE (SDS) after pulse-labeling for 30 min and visualized by autoradiography. Quantification of radioactivity was performed by ImageQuant with equal amounts of all samples loaded on a single gel. The radioactivity incorporated into D1/D2 proteins of Col-0 after the 30-min pulse was set to 100%. Note that the membrane stained with C.B.B. confirms that chloroplast protein levels are lower in the lines lacking functional VEN4 than in the wild type.

and the diminished tolerance to salt and high light intensities seen in plants lacking PP7L (Xu et al., 2019). Multiple lines of evidence support the notion that photoreceptors, especially phyB, are also involved in direct perception and/or modulation of stress responses to low and high temperatures (Kim et al., 2002; Franklin and Whitelam, 2007; Lee and Thomashow, 2012; Jung et al., 2016; Legris et al., 2016; Song et al., 2017). Although the *phyb-9* mutant was used in some of these experiments (Kim et al., 2002; Lee and Thomashow, 2012; Legris et al., 2016), the role of phyB in thermomorphogenesis (temperature dependence of hypocotyl length) is securely supported by the usage of further *phyB* alleles and modeling approaches (Legris et al., 2016). To clarify whether VEN4 and/or phyB are involved in cold- (4°C, not freezing), heat-, or salt-stress tolerance, and whether PP7L is involved also in cold and heat tolerance, *phyB-9^{OG}*, *phyB-9^{BC}*, *bnen*, *ven4-1*, *pp7l-1*, and wild-type seedlings were germinated and grown for 6 weeks under cold conditions (4°C). Additionally, 18-d-old plants were shifted for 12 d to 4°C and 32°C, respectively, and 14-d-old plants were watered for 7 d with NaCl. After 6 weeks under cold conditions, the majority of wild-type seedlings had well-developed green cotyledons and, accordingly, F_v/F_m was detectable in wild-type seedlings, indicating the formation of functional PSII complexes (Fig. 4A). On the contrary, *phyB-9^{OG}*, *phyB-9^{BC}*, *bnen*, *ven4-1*, and *pp7l-1* cotyledons accumulated anthocyanins, but did

not turn green, and some cotyledons of *phyB-9^{BC}* only started to turn green (Fig. 4A). When adult plants were shifted to cold conditions, F_v/F_m values of wild type and all mutants were reduced after 1 d compared with control conditions (Fig. 4B; Supplemental Fig. S3A). All mutants except of *phyB-9^{BC}* did not show a noticeable difference in the trend of their F_v/F_m values during the next 12 d when compared with the wild type; *phyB-9^{BC}*, indeed, was more sensitive to cold treatment corroborating the involvement of phyB in temperature responses. F_v/F_m values remained more or less constant in wild type and *phyB-9^{BC}* under heat conditions (Fig. 4B; Supplemental Fig. S3A). However, heat helped all other genotypes to recover photosynthetic activity, especially in plants lacking VEN4 that recovered to wild-type-like F_v/F_m values after 5 d (Supplemental Fig. S3A). When plants were watered with NaCl, growth of all plants was retarded, especially that of the *pp7l-1* mutant, and the reduction in F_v/F_m of plants lacking VEN4 was exacerbated (Fig. 4B). The enhanced sensitivity of *ven4* mutants to NaCl was reproducible when seeds were germinated in the presence of NaCl; the F_v/F_m phenotype of *bnen* and *ven4* seedlings became evident on salt-supplemented medium, but was not apparent under control conditions (Supplemental Fig. S3B). The enhanced sensitivity of the *pp7l-1* mutant to NaCl was manifested by the substantially retarded growth of *pp7l-1* seedlings (Supplemental Fig. S3B). This suggests that VEN4 and to a lesser extent PP7L are both necessary for optimal tolerance of salt stress.

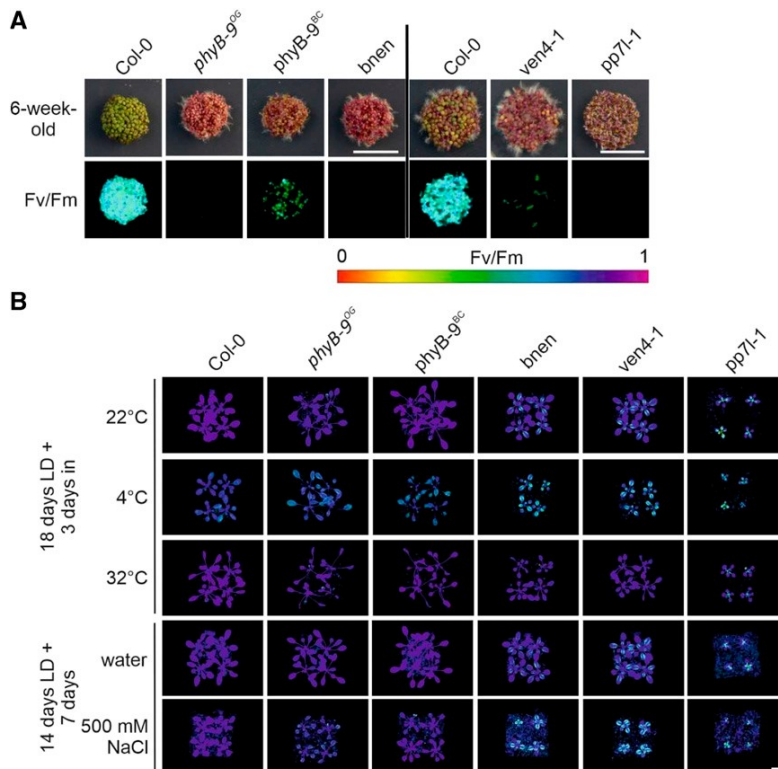


Figure 4. Lack of either VEN4, PHYB, or PP7L affects tolerance responses to varying degrees. A, Images of wild-type (Col-0), *phyB-9^{OG}*, *phyB-9^{BC}*, *bnen*, *ven4-1*, and *pp7l-1* seedlings grown for 6 weeks on MS under cold stress (4°C, 100 $\mu\text{mol photons m}^{-2} \text{s}^{-1}$). The Imaging PAM pictures show the F_v/F_m . Scale bar = 1 cm. B, Images of wild-type (Col-0), *phyB-9^{OG}*, *phyB-9^{BC}*, *bnen*, *ven4-1*, and *pp7l-1* plants grown for 18 d (cold and heat experiment) or 14 d (salt experiment) under long-day conditions (LD; $\sim 120 \mu\text{mol photons m}^{-2} \text{s}^{-1}$ on leaf surfaces; 16-h light/8-h dark). The plants have been subsequently shifted for the indicated time periods to cold (LD, 4°C and 35 $\mu\text{mol photons m}^{-2} \text{s}^{-1}$) or heat (continuous light, 32°C) conditions, respectively, or were watered with salt (500 mM NaCl). The Imaging PAM pictures show the F_v/F_m . Scale bar = 2 cm.

CONCLUSION

Overall, these data show that the nuclear proteins PP7L and VEN4 are independently required for physiologically optimal chloroplast development. PP7L acts mainly in cotyledons and emerging leaves, whereas VEN4 acts on chloroplast development in older leaves and has a weaker function in cotyledons. The negative impact on chloroplast development seen in *phyB-9^{OG}* seedlings is entirely attributable to the *bnen* mutation, as the lack of PHYB alone (in *phyB-9^{BC}*) can actually enhance chloroplast development in young seedlings. It has to be noted here that delayed chloroplast development in *bnen* or *ven4* mutants can be partially promoted by simultaneous loss of PHYB and VEN4 in *phyB-9^{OG}* plants (see Fig. 1; Supplemental Fig. S3), uncovering an epistatic relationship between *phyB* and *ven4*. In addition, biochemical activity of VEN4 is required for optimal responses to cold and salt stresses, because dNTP imbalances in *ven4* mutants render plants more sensitive to these stresses. Therefore, our results indicate that finely tuned dNTP levels are necessary for chloroplast development and acclimation to adverse environmental conditions.

MATERIALS AND METHODS

Plant Material and Growth Conditions

All *Arabidopsis thaliana* plants used in this study are in the Col-0 ecotype background. The transfer DNA insertion lines SALK_023714 (*ven4-1*) and SALK_077401 (*ven4-2*) were obtained from the Nottingham Arabidopsis Stock Centre (<http://arabidopsis.info/>); *phyB-9* (*phyB-9^{OG}*) and *pp7l-1* have been already described (Yoshida et al., 2018; Xu et al., 2019). Seeds of *P35S:PHYB-YFP phyB-9^{OG}* were kindly provided by Ferenc Nagy (Medzihradsky et al., 2013). To obtain *pp7l-1 bnen*, *pp7l-1* was crossed with *phyB-9^{OG}*. *phyB-9^{OG}* was crossed with Col-0 to obtain *phyB-9^{BC}* and *bnen*. Primer sequences are listed in Supplemental Table S1.

Unless specifically noted, wild-type and mutant seeds were sterilized with 20% (v/v) bleach and 0.01% (v/v) Triton X-100 and sown on half-strength MS medium, pH 5.8, containing 0.8% (w/v) agar (Sigma-Aldrich) and 1% (w/v) Suc, and placed in the dark at 4°C for 2 d to ensure synchronized germination. Plates were then placed under 100 $\mu\text{mol photons m}^{-2} \text{s}^{-1}$ and a 16/8-h day/night cycle at 22°C. For salt treatment, the surface sterile wild-type and mutant seeds were sown on half-strength MS medium as described containing different NaCl concentrations (0, 100, and 150 mM) in lots of 80–100 seeds. For dNTP supplementation experiments, wild-type and mutant seeds were sown on half-strength MS medium as described containing 2 mM of each dNTP as indicated in Figure 2B. For cold stress experiments, seeds were germinated and grown on half-strength MS plates for 6 weeks in a 4°C chamber (Percival Scientific LED 41HL2) equipped with white and red LEDs set at 18% intensity (equivalent to 100 $\mu\text{mol photons m}^{-2} \text{s}^{-1}$). Soil-grown plants were raised on potting soil (Stender) under controlled greenhouse conditions (daylight supplemented with illumination from HQI Powerstar 400W/D, providing a total fluence of $\sim 120 \mu\text{mol photons m}^{-2} \text{s}^{-1}$ on leaf surfaces; 16-h light/8-h dark cycle).

Chlorophyll Fluorescence Analysis

To measure chlorophyll fluorescence emission, the Imaging PAM (M-Series; Walz) was used according to the instructions provided by the manufacturer. Samples were dark adapted for 30 min before determination of PSII quantum efficiency (F_v/F_m) at room temperature. For cold tolerance experiments, dark acclimation was carried out at 4°C. The maximum yield of chlorophyll fluorescence in the dark-adapted state (F_m) was induced by an 0.8-s pulse of saturating white light ($2700 \mu\text{mol photon m}^{-2} \text{s}^{-1}$). Variable fluorescence F_v , which is defined as the difference of the maximum fluorescence (F_m) and the minimum

fluorescence in the dark-adapted state (F_0), was used to calculate the F_v/F_m . The calculations of the parameters were performed using the ImagingWin software (Walz).

Protein Extraction and Immunoblotting

For immunoblot analysis, 100 mg cotyledon tissues from seedlings at 78 h after imbibition (HAI) were dissected and homogenized in 400 μL of sample buffer of 0.125 M Tris, 1% (v/v) SDS, 10% (v/v) glycerol, 0.05 M sodium metabisulfite containing 1 mM phenylmethylsulfonyl fluoride and protease inhibitor cocktail (Sigma-Aldrich). The samples were cleared of insoluble debris by centrifugation at 16,000 g for 20 min at room temperature, and the supernatant was boiled with 5x loading dye [5% (w/v) β -mercaptoethanol, 0.02% (w/v) bromophenol blue, 30% (v/v) glycerol] at 95°C for 5 min. For each lane, equal amounts of total protein were resolved on a 10% (w/v) SDS-PAGE minigel and blotted 30 min onto a polyvinylidene difluoride membrane using the transblot turbo transfer system (Bio-Rad). After incubation with primary and secondary antibodies (Agrisera; catalog no. AS09 602), chemiluminescence was generated using the PierceECL western blotting kit (Thermo Scientific), and the blots were imaged with the Fusion FX7 system (Vilber Lourmat). Antibodies against PsdA (AS09 461, 1:1000) and PsbD (AS06 146, 1:5000) were purchased from Agrisera.

RNA Extraction and Northern Analysis

RNA extractions from 78-HAI-old seedlings (50–100 mg) using the Trizol RNA reagent (Invitrogen) and RNA gel blot analyses were performed as described by Xu et al. (2019). RT-PCR amplification products of *PsdA* and *PsbD* were used as probes for northern analyses. Primer sequences are listed in Supplemental Table S1.

Complementary DNA Synthesis and RT-qPCR Analysis

Total RNA was extracted from 78-HAI-old seedlings with the RNeasy Plant Mini Kit (Qiagen). Total RNA (1 μg) was reverse transcribed with the iScript cDNA Synthesis Kit (Bio-Rad). Real-time qPCR was performed using the iQ5 real-time PCR instrument with the iQ SYBR Green Supermix (Bio-Rad) with primers listed in Supplemental Table S1.

In Vivo Translation Assay of Thylakoid Proteins

Chloroplast proteins were labeled in vivo using 78-HAI-old seedlings. In brief, seedlings were vacuum-infiltrated in 1 mL of labeling buffer containing 20 $\mu\text{g/mL}$ cycloheximide; 10 mM Tris-HCl; 5 mM MgCl_2 ; 20 mM KCl, pH 6.8; and 0.1% (v/v) Tween 20, and incubated for 30 min to block cytosolic translation. [^{35}S]Met (1 mCi) was applied to the same solution, and the leaves were vacuum-infiltrated for 10 s. After a 30-min labeling pulse, thylakoid proteins were isolated with cold buffer: 300 mM Suc, 50 mM HEPES-KOH, pH 7.6, 5 mM MgCl_2 , 1 mM Na-EDTA, 1.25% bovine serum albumin (w/v), 22 mM ascorbate, and 10 mM NaF. Subsequently, thylakoid proteins were fractionated on 15% Tricine-SDS-PAGE gel. The gels were dried using a Geldryer (Bio-Rad) and exposed to an autoradiograph film.

Intracellular Localization of the VEN4-eGFP Fusion

The sequence of VEN4 (*AT5G40270*) without the stop codon was amplified from complementary DNA with primers listed in Supplemental Table S1. This amplified sequence was introduced into pDONR207 and subsequently into the destination vector pB7FWG2 (35S promoter, eGFP) by the BP and LR clonase reactions (Invitrogen), respectively, generating 35S:VEN4-eGFP. Subcellular localization analysis of the fused protein was conducted in protoplasts isolated from Col-0 as described (Xu et al., 2019).

Statistical Analyses

Statistical analyses were performed with the SPSS 17.0 Statistics software.

SUPPLEMENTAL DATA

The following supplemental materials are available.

Supplemental Figure S1. Phenotypic characterization of the original *phyB-9* and the *oe-PHYB* (*phyB-9*) lines.

Supplemental Figure S2. Identification of *phyB-9* and *ven4* mutants.

Supplemental Figure S3. VEN4 and PP7L function is required for salt tolerance.

ACKNOWLEDGMENTS

We thank Ferenc Nagy and Eva Adam for providing *P35S:PHYB-YFP phyB-9^{OG}* seeds. We thank Paul Hardy for critical reading of the manuscript and Elisabeth Gerick for technical assistance.

Received October 7, 2019; accepted November 12, 2019; published December 2, 2019.

LITERATURE CITED

- Albrecht V, Simková K, Carrie C, Delannoy E, Giraud E, Whelan J, Small ID, Apel K, Badger MR, Pogson BJ (2010) The cytoskeleton and the peroxisomal-targeted snowy cotyledon3 protein are required for chloroplast development in *Arabidopsis*. *Plant Cell* 22: 3423–3438
- Fitter DW, Martin DJ, Copley MJ, Scotland RW, Langdale JA (2002) GLK gene pairs regulate chloroplast development in diverse plant species. *Plant J* 31: 713–727
- Franklin KA, Whitelam GC (2007) Light-quality regulation of freezing tolerance in *Arabidopsis thaliana*. *Nat Genet* 39: 1410–1413
- Ganguly D, Crisp P, Harter K, Pogson BJ, Albrecht-Borth V (2015) Genetic suppression of plant development and chloroplast biogenesis via the Snowy Cotyledon 3 and Phytochrome B pathways. *Funct Plant Biol* 42: 676–686
- Garton S, Knight H, Warren GJ, Knight MR, Thorlby GJ (2007) *Crinkled leaves 8*—a mutation in the large subunit of ribonucleotide reductase—leads to defects in leaf development and chloroplast division in *Arabidopsis thaliana*. *Plant J* 50: 118–127
- Hofer A, Crona M, Logan DT, Sjöberg BM (2012) DNA building blocks: Keeping control of manufacture. *Crit Rev Biochem Mol Biol* 47: 50–63
- Ji X, Tang C, Zhao Q, Wang W, Xiong Y (2014) Structural basis of cellular dNTP regulation by SAMHD1. *Proc Natl Acad Sci USA* 111: E4305–E4314
- Jung JH, Domijan M, Klose C, Biswas S, Ezer D, Gao M, Khattak AK, Box MS, Charoensawan V, Cortijo S, et al (2016) Phytochromes function as thermosensors in *Arabidopsis*. *Science* 354: 886–889
- Kim HJ, Kim YK, Park JY, Kim J (2002) Light signalling mediated by phytochrome plays an important role in cold-induced gene expression through the C-repeat/dehydration responsive element (C/DRE) in *Arabidopsis thaliana*. *Plant J* 29: 693–704
- Kleine T, Leister D (2016) Retrograde signaling: Organelles go networking. *Biochim Biophys Acta* 1857: 1313–1325
- Kleine T, Maier UG, Leister D (2009) DNA transfer from organelles to the nucleus: The idiosyncratic genetics of endosymbiosis. *Annu Rev Plant Biol* 60: 115–138
- Kunz BA (1982) Genetic effects of deoxyribonucleotide pool imbalances. *Environ Mutagen* 4: 695–725
- Kupsch C, Ruwe H, Gusewski S, Tillich M, Small I, Schmitz-Linneweber C (2012) *Arabidopsis* chloroplast RNA binding proteins CP31A and CP29A associate with large transcript pools and confer cold stress tolerance by influencing multiple chloroplast RNA processing steps. *Plant Cell* 24: 4266–4280
- Laguette N, Sobhian B, Casartelli N, Ringgaard M, Chable-Bessia C, Ségéral E, Yatim A, Emiliani S, Schwartz O, Benkirane M (2011) SAMHD1 is the dendritic- and myeloid-cell-specific HIV-1 restriction factor counteracted by Vpx. *Nature* 474: 654–657
- Lee CM, Thomashow MF (2012) Photoperiodic regulation of the C-repeat binding factor (CBF) cold acclimation pathway and freezing tolerance in *Arabidopsis thaliana*. *Proc Natl Acad Sci USA* 109: 15054–15059
- Legris M, Klose C, Burgie ES, Rojas CC, Neme M, Hiltbrunner A, Wigge PA, Schäfer E, Vierstra RD, Casal JJ (2016) Phytochrome B integrates light and temperature signals in *Arabidopsis*. *Science* 354: 897–900
- Leivar P, Monte E (2014) PIFs: Systems integrators in plant development. *Plant Cell* 26: 56–78
- Lv R, Li Z, Li M, Dogra V, Lv S, Liu R, Lee KP, Kim C (2019) Uncoupled expression of nuclear and plastid photosynthesis-associated genes contributes to cell death in a lesion mimic mutant. *Plant Cell* 31: 210–230
- Medzihradsky M, Bindics J, Ádám É, Viczián A, Klement É, Lorrain S, Gyula P, Mérai Z, Fankhauser C, Medzihradsky KF, et al (2013) Phosphorylation of phytochrome B inhibits light-induced signaling via accelerated dark reversion in *Arabidopsis*. *Plant Cell* 25: 535–544
- Pogson BJ, Ganguly D, Albrecht-Borth V (2015) Insights into chloroplast biogenesis and development. *Biochim Biophys Acta* 1847: 1017–1024
- Reed JW, Nagpal P, Poole DS, Furuya M, Chory J (1993) Mutations in the gene for the red/far-red light receptor phytochrome B alter cell elongation and physiological responses throughout *Arabidopsis* development. *Plant Cell* 5: 147–157
- Rusaczonok A, Czarnocka W, Kacprzak S, Witoń D, Ślesak I, Szechyńska-Hebda M, Gawroński P, Karpiński S (2015) Role of phytochromes A and B in the regulation of cell death and acclimatory responses to UV stress in *Arabidopsis thaliana*. *J Exp Bot* 66: 6679–6695
- Song J, Liu Q, Hu B, Wu W (2017) Photoreceptor phyb involved in *Arabidopsis* temperature perception and heat-tolerance formation. *Int J Mol Sci* 18: 1194
- Van Bel M, Diels T, Vancaester E, Kreft L, Botzki A, Van de Peer Y, Coppens F, Vandepoele K (2018) PLAZA 4.0: An integrative resource for functional, evolutionary and comparative plant genomics. *Nucleic Acids Res* 46(D1): D1190–D1196
- Waters MT, Langdale JA (2009) The making of a chloroplast. *EMBO J* 28: 2861–2873
- Xu D, Marino G, Klingl A, Enderle B, Monte E, Kurth J, Hiltbrunner A, Leister D, Kleine T (2019) Extrachloroplastic PP7L functions in chloroplast development and abiotic stress tolerance. *Plant Physiol* 180: 323–341
- Yoshida Y, Sarmiento-Mañús R, Yamori W, Ponce MR, Micol JL, Tsukaya H (2018) The *Arabidopsis phyB-9* mutant has a second-site mutation in the *VENOSA4* gene that alters chloroplast size, photosynthetic traits, and leaf growth. *Plant Physiol* 178: 3–6

3.3 Chapter 3

Arabidopsis thaliana mTERF10 and mTERF11, but not mTERF12, are involved in the response to salt stress



Arabidopsis thaliana mTERF10 and mTERF11, but Not mTERF12, Are Involved in the Response to Salt Stress

Duorong Xu, Dario Leister and Tatjana Kleine *

Plant Molecular Biology, Department Biology I, Ludwig-Maximilians-Universität München, Planegg-Martinsried, Germany

OPEN ACCESS

Edited by:

Julian Eaton-Rye, University of Otago, New Zealand

Reviewed by:

Victor Quesada, Universidad Miguel Hernández de Elche, Spain
Ren Maozhi, Chongqing University, China

*Correspondence:

Tatjana Kleine
tatjana.kleine@lmu.de

Specialty section:

This article was submitted to Plant Cell Biology, a section of the journal Frontiers in Plant Science

Received: 20 March 2017

Accepted: 27 June 2017

Published: 14 July 2017

Citation:

Xu D, Leister D and Kleine T (2017) *Arabidopsis thaliana* mTERF10 and mTERF11, but Not mTERF12, Are Involved in the Response to Salt Stress. Front. Plant Sci. 8:1213. doi: 10.3389/fpls.2017.01213

Plastid gene expression (PGE) is crucial for plant development and acclimation to various environmental stress conditions. Members of the “mitochondrial transcription termination factor” (mTERF) family, which are present in both metazoans and plants, are involved in organellar gene expression. *Arabidopsis thaliana* contains 35 mTERF proteins, of which mTERF10, mTERF11, and mTERF12 were previously assigned to the “chloroplast-associated” group. Here, we show that all three are localized to chloroplast nucleoids, which are associated with PGE. Knock-down of *MTERF10*, *MTERF11*, or *MTERF12* has no overt phenotypic effect under normal growth conditions. However, in silico analysis of *MTERF10*, -11, and -12 expression levels points to a possible involvement of mTERF10 and mTERF11 in responses to abiotic stress. Exposing mutant lines for 7 days to moderate heat (30°C) or light stress (400 $\mu\text{mol photons m}^{-2} \text{s}^{-1}$) fails to induce a phenotype in *mterf* mutant lines. However, growth on MS medium supplemented with NaCl reveals that overexpression of *MTERF11* results in higher salt tolerance. Conversely, *mterf10* mutants are hypersensitive to salt stress, while plants that modestly overexpress *MTERF10* are markedly less susceptible. Furthermore, *MTERF10* overexpression leads to enhanced germination and growth on MS medium supplemented with ABA. These findings point to an involvement of mTERF10 in salt tolerance, possibly through an ABA-mediated mechanism. Thus, characterization of an increasing number of plant mTERF proteins reveals their roles in the response, tolerance and acclimation to different abiotic stresses.

Keywords: *Arabidopsis*, chloroplast, nucleoid, mTERF, acclimation, stress, salt

INTRODUCTION

Chloroplasts are of cyanobacterial origin (Raven and Allen, 2003) and harbor nowadays a reduced genome that mainly encodes proteins involved in photosynthesis and plastid gene expression (PGE). PGE is crucial for plant development and photosynthesis, but its regulation is only partially understood. This is largely because, although plastids still display characteristics of a prokaryotic-like structure of their genome, their gene expression machinery is much more elaborated compared to that of their cyanobacterial ancestor (reviewed in: Liere et al., 2011). Therefore, PGE requires plenty of proteins encoded in the nucleus that support transcription, splicing, trimming and editing of organellar RNAs, and regulate their translation (Schmitz-Linneweber and Small, 2008; Stern et al., 2010; Hammani et al., 2014; Tiller and Bock, 2014; Börner et al., 2015).

Also the nucleus-encoded proteins of the mitochondrial transcription termination factor (mTERF) family regulate mitochondrial and PGE at diverse levels (Kleine and Leister, 2015). The mTERF proteins have been identified in both plants and metazoans (Linder et al., 2005). Human mTERF1, which is the first characterized mTERF, is one of four mammalian mTERF proteins, and was identified nearly 30 years ago as a factor that acts on transcription termination in mitochondrial extracts (Kruse et al., 1989). Its presumptive function as a transcription terminator (of heavy-strand transcripts) gave the family its name. More recently however, models have been suggested in which mTERF1 acts chiefly as a terminator of antisense transcription (Terzioglu et al., 2013) or in polar replication fork arrest (Shi et al., 2016). The true molecular function of mouse mTERF2 also remains unclear, with some reports suggesting that it binds to the same mitochondrial DNA region as mTERF1 and mTERF3 (Wenz et al., 2009), while another contends that the DNA-binding activity of mTERF2 is not sequence-specific (Pellegrini et al., 2009). Knock-out of *Mterf3* in mice leads to embryonic lethality (Park et al., 2007), and conditional knockout of *Mterf3* in the heart has identified a novel role for its protein product in the biogenesis of metazoan mitochondrial ribosomes (Wredenberg et al., 2013). *Mterf4* knock-out mice are also embryonic lethal (Camara et al., 2011). Interestingly, human mTERF4 forms a complex with NSUN4, which is required for assembly of the small and large ribosomal subunits of the mitochondrial ribosome (Metodiev et al., 2014). Consequently, while the function for mTERF2 remains to be clarified, the remainder of the mammalian mTERFs do not support transcription termination, as it is suggested by their notation, but seem to take part in antisense transcription termination and ribosome biogenesis.

The number of mTERF family members has increased to approximately 30 throughout the evolution of land plants (Kleine, 2012), but information on their functions is only beginning to emerge. Most of the 35 *A. thaliana* mTERF proteins (mTERF1-mTERF35; Kleine, 2012) are localized to chloroplasts and/or mitochondria (Babychuk et al., 2011), and seven of them (mTERF1, -4, -5, -6, -9, -15, and -18) have been functionally investigated in more detail (reviewed in: Kleine and Leister, 2015; Quesada, 2016). Essential functions of mTERF proteins in plant development are revealed by the effects of complete inactivation of three *MTERF* genes: *A. thaliana* mutants devoid of SOLDAT10 (SINGLETON OXYGEN-LINKED DEATH ACTIVATOR10)/mTERF1 (Meskauskiene et al., 2009) or BSM (BELAYA SMERT)/RUG2 (RUGOSA2)/mTERF4 (Babychuk et al., 2011; Quesada et al., 2011) are arrested in embryo development, and knock-out *mterf6-2* plants are albino and stop growing after 2 weeks (Romani et al., 2015). Moreover, the dissection of *mterf* mutants supports an involvement of plant mTERFs in responses to abiotic stress (reviewed in: Kleine and Leister, 2015; Quesada, 2016). Indeed, SOLDAT10 (Meskauskiene et al., 2009) and SUPPRESSOR OF *hot1-4* 1 (SHOT1; Kim et al., 2012) were isolated in forward genetic screens for loci that influence responses to abiotic stress. The *hot1-4* mutant is a dominant-negative allele of the heat-shock protein gene *HSP101*. SHOT1/mTERF18 is a mitochondrial protein and the *shot1-1* missense mutant and

the *shot1-2* T-DNA insertion mutant each suppress the heat hypersensitivity of *hot1-4* plants. Moreover, other heat-sensitive mutant phenotypes are also suppressed by *shot1-2*, and *shot1-2* single mutants display a higher heat tolerance (Kim et al., 2012). SOLDAT10 is localized to chloroplasts, and plants homozygous for a weaker *soldat10* allele suffer from mild photo-oxidative stress already in low-light conditions; this results in turn in a stress acclimation response, which appears to confer improved hardiness against a combination of high-light and low-temperature stress (Meskauskiene et al., 2009). Other *mterf* mutants are also linked to stress responses. For example, *mda1* (*mterf5*), and *mterf9* seedlings are less susceptible to osmotic and salt treatments, which might be linked to their decreased sensibility to ABA (Robles et al., 2012, 2015). Furthermore, the *rug2-1* mutant is abnormally sensitive to temperature stress. At 26°C, *rug2-1* homozygotes undergo growth arrest, whereas at 16°C this growth phenotype is not expressed (Quesada et al., 2011).

A co-expression network for all *MTERF* genes (26 out of 35) which were present on the Affymetrix ATH1 genome array has been constructed (Kleine, 2012). The resulting clusters and information related to the subcellular locations of the proteins that are encoded by genes co-expressed with each *MTERF* gene were then used to assign the mTERFs into five groups, referred to as the “chloroplast,” “chloroplast-associated,” “mitochondrial,” “mitochondrion-associated,” and the “low expression” clusters.

In the present study, we characterized the members of the “chloroplast-associated” group, which comprises mTERF10 (AT2G34620), mTERF11 (AT3G18870), and mTERF12 (AT4G09620). The sub-chloroplast localization of mTERF10, -11, and -12 was defined by fluorescence microscopy of mTERF-GFP fusions and an RFP fusion protein (as a control for nucleoid localization). Lines with altered *MTERF10*, *MTERF11*, and *MTERF12* levels did not display phenotypes under normal growth conditions. *In silico* analyses with the eFP browser and Genevestigator were conducted, which pointed to an involvement of these three mTERFs in abiotic stress responses. To follow this up, the mutant lines were exposed to moderate heat (30°C), high light (400 µmol photons m⁻² s⁻¹), or salt (175 mM NaCl) stress, and subjected to ABA treatment. The *mterf10*, -11, and -12 mutant lines responded to heat and high light stress like the wild type (WT). However, lack of mTERF10 or mTERF11 led to enhanced or reduced sensitivity to salt, respectively, while overexpression of *MTERF10* rendered seedlings more tolerant than WT to both salt and ABA.

MATERIALS AND METHODS

Plant Material and Growth Conditions

The mutants *mterf10-1* (SAIL_12A03), *mterf10-2* (SALK_097699), *mterf11-1* (FLAG_357F09), *mterf11-2* (GABI_211D05), and *mterf12-1* (GABI_407E04) were identified in the SIGnAL database (Alonso et al., 2003), the *abi4-1* mutant was ordered from The European Arabidopsis Stock Centre (NASC; ID N8104). All mutants are in the Col-0 background except of *mterf11-1* which is a WS line.

Arabidopsis thaliana plants were grown in long-day conditions (16 h light/8 h dark) on potting soil (Stender). Plants were illuminated with HQI Powerstar 400 W/D lamps and a fluence rate of approximately 100 $\mu\text{mol photons m}^{-2} \text{s}^{-1}$. To accomplish salt and ABA stress experiments, seedlings were grown on plant agar (Sigma-Aldrich) containing half-strength MS medium and 1.5% (w/v) sucrose at 22°C under 100 $\mu\text{mol photons m}^{-2} \text{s}^{-1}$ provided by white fluorescent lamps under continuous light or long-day conditions. For salt stress experiments, MS medium was supplemented with 125 mM or 175 mM NaCl as indicated. For ABA experiments, MS medium was supplemented with 1 μM ABA.

Nucleic Acid Extraction

For DNA isolation, leaf tissue was homogenized in extraction buffer containing 200 mM Tris/HCl (pH 7.5), 25 mM NaCl, 25 mM EDTA, and 0.5% (w/v) SDS. After centrifugation, DNA was precipitated by adding isopropyl alcohol. After washing with 70% (v/v) ethanol, the DNA was dissolved in distilled water.

For RNA isolation, frozen tissue was ground in liquid nitrogen. Following the addition of TRIzol (Invitrogen) and chloroform according to the manufacturer's instructions, RNA was precipitated from the aqueous phase with isopropyl alcohol, then washed with 70% (v/v) ethanol, and dissolved in RNase-free water. Concentration and purity of RNA samples were determined spectroscopically in a GeneQuant pro RNA/DNA Calculator (GE Healthcare Europe GmbH). Isolated RNA was stored at -80°C until further use.

cDNA Synthesis and Real-Time PCR Analysis

cDNA synthesis and real-time PCR analysis were performed as outlined before (Voigt et al., 2010). All reactions were done in triplicate on three biological replicates. The target genes and the respective primers, are listed in **Supplementary Table S1**. The *RCE1* gene was used as an internal reference in other studies (Voigt et al., 2010; Romani et al., 2015). *RCE1* transcript levels are not changed upon diverse conditions, especially not under diverse stress conditions including lincomycin and norflurazon treatment which affect organellar gene expression.

RNAi, Overexpression and Intracellular Protein Localization

To reduce *MTERF12* mRNA levels by RNAi, a 145-bp fragment was amplified from genomic DNA with the primer pair AT4G09620-GST-attB1 and -attB2 (see **Supplementary Table S1**). The gel-purified PCR product was used for BP and LR Clonase reactions (GATEWAY Cloning; Invitrogen) which led to the final construct pB7GWIWG2/*MTERF12* (for pB7GWIWG2, see Karimi et al., 2002). For overexpression and localization studies of *mTERF10*, *mTERF11* and *mTERF12*, cDNAs encompassing the coding regions were amplified by PCR (see **Supplementary Table S1** for primer information). Notably, in our Col-0 strain,

MTERF11 has an additional triplet (CAT; coding for histidine) inserted after nucleotide 27 (relative to the start codon) compared with the coding sequence from The Arabidopsis Information Resource (TAIR; www.arabidopsis.org). *MTERF10*, *MTERF11*, and *MTERF12* were cloned by GATEWAY technology (see above) into pB7FWG2 to generate fusions with enhanced GFP (eGFP), expression of which is controlled by the *Cauliflower mosaic virus* 35S promoter. For RAP-RFP fusions, the pENTR/RAP plasmid (Prof. Jörg Nickelsen, LMU Munich) was introduced into p2GWR7 by GATEWAY cloning. For overexpression of *mTERF10*, *MTERF10* was introduced by classical cloning with the NcoI restriction enzyme into pCambia1302. For RNAi experiments with *MTERF12* and overexpression of *mTERF10* and *mTERF11*, the plasmids pB7GWIWG2/*MTERF12*, pCambia1302/*MTERF10*, and pB7FWG2/*MTERF11* were independently transferred into *Agrobacterium tumefaciens*, and *A. thaliana* (ecotype Col-0 for *MTERF10* overexpression and *MTERF12* RNAi; ecotype WS for *MTERF11* overexpression) plants were transformed by the floral-dip method (Clough and Bent, 1998). After seed set, transgenic plants were selected on the basis of their resistance to BASTA (pB7GWIWG2/*MTERF12* and pB7FWG2/*MTERF11*) or hygromycin (pCambia1302/*MTERF10*), respectively.

For fluorescence visualization, leaves of 3-week-old Col-0 plants grown on MS medium were cut into small pieces and incubated for 16 h at 24°C in the dark in a protoplasting solution (10 mM MES, 20 mM CaCl_2 , 0.5 M mannitol (pH 5.8), 0.1 g ml^{-1} macerozyme (Duchefa), 0.1 g ml^{-1} cellulase (Duchefa). After isolation and transformation of protoplasts as described (Dovzhenko et al., 2003), preparations were examined with a Fluorescence Axio Imager microscope (Zeiss). Fluorescence was excited with the X-Cite Series 120 fluorescence lamp (EXFO) and images were collected at 500–550 nm (eGFP fluorescence), 570–640 nm (RFP fluorescence) and 670–750 nm (chlorophyll autofluorescence).

Chlorophyll a Fluorescence Measurements

In vivo chlorophyll a fluorescence of whole plants was recorded using an imaging chlorophyll fluorometer (ImagingPAM, Walz GmbH, Effeltrich, Germany). Plants were dark adapted for 15 min and then exposed to a pulsed, blue measuring light (1 Hz, intensity 4) and a saturating light flash (intensity 5) to determine the maximum fluorescence F_m and the ratio $(F_m - F_0)/F_m = F_v/F_m$.

Computational Analyses

Protein sequences were retrieved from the National Center for Biotechnology Information (NCBI; <http://www.ncbi.nlm.nih.gov/>) and The Arabidopsis Information Resource (TAIR; <http://www.arabidopsis.org>). Amino acid sequences were aligned using the ClustalW program (<http://www.ebi.ac.uk/clustalw>; Chenna et al., 2003). The unrooted tree was constructed with the PhyML server Mobyle at the Pasteur Institute (<http://mobyle.pasteur.fr/cgi-bin/portal.py#welcome>).

RESULTS

All Members of the Chloroplast-Associated mTERF Cluster Are Localized to Nucleoids

The localizations of almost all *A. thaliana* mTERF proteins have been investigated by fluorescence microscopy of mTERF-GFP fusions transiently expressed in isolated protoplasts, and in guard cells of transgenic plants (Babychuk et al.,

2011). These data indicated that mTERF10, -11, and -12 are targeted to chloroplasts. To confirm these results and if possible define the precise locations of the proteins within the chloroplast, the eGFP fluorescence of mTERF10-, mTERF11-, or mTERF12-eGFP fusions, transiently overexpressed in Col-0 protoplasts, was monitored. Localization of all three fusion proteins to chloroplasts was confirmed (**Figure 1A**). However, the fluorescence signals were not uniformly distributed, but

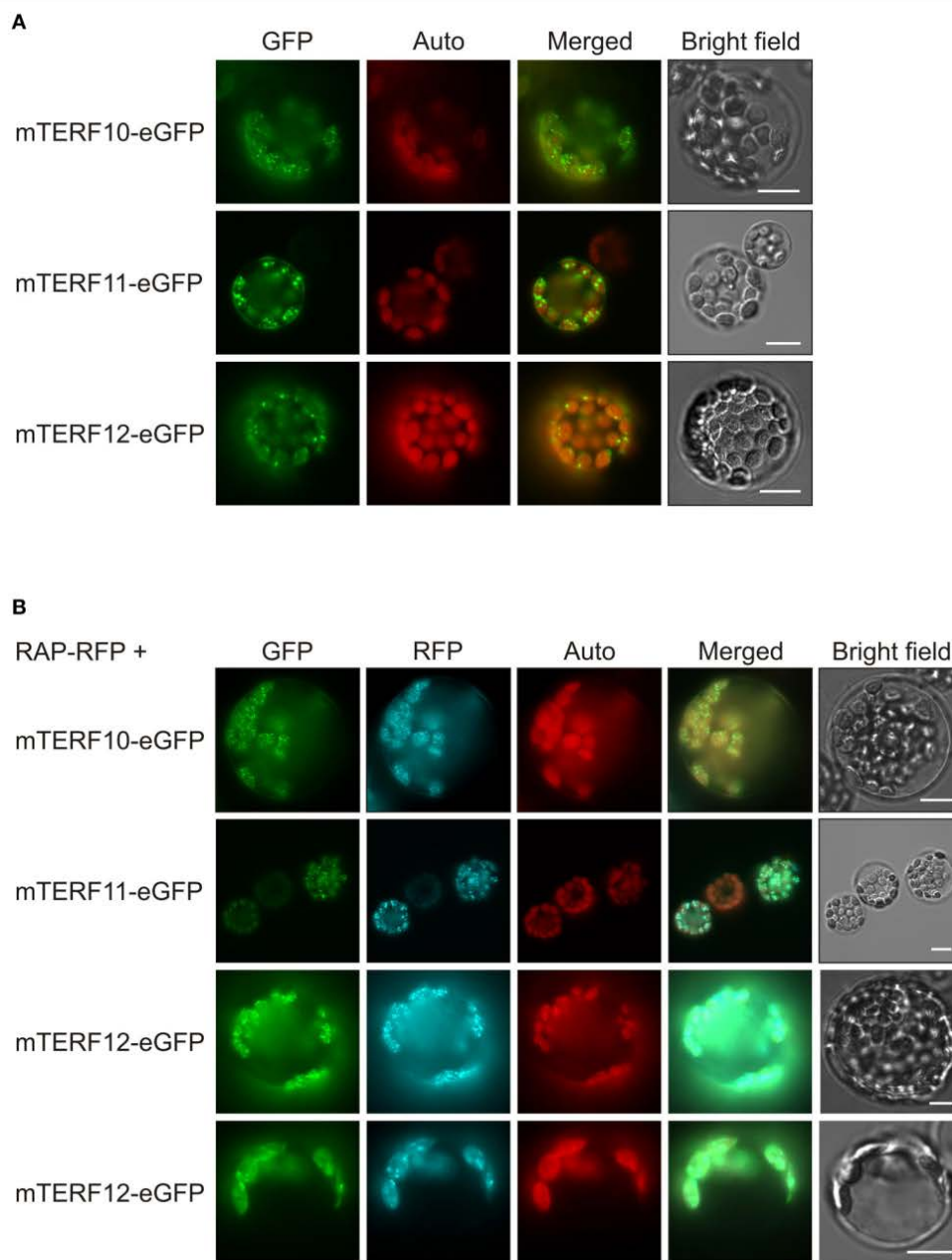


FIGURE 1 | Localization of mTERF10, mTERF11 and mTERF12. **(A)** Fluorescence microscopy of *A. thaliana* protoplasts transiently expressing mTERF10, mTERF11 or mTERF12 fused to eGFP (mTERF10-eGFP, mTERF11-eGFP and mTERF12-eGFP). **(B)** To visualize nucleoids, protoplasts were co-transformed with a RAP-RFP fusion in combination with mTERF10-eGFP, mTERF11-eGFP, or mTERF12-eGFP. The eGFP fluorescence is shown in green (GFP), RFP fluorescence in cyan (RFP), autofluorescence of chloroplasts in red (Auto). The scale bars correspond to 10 μ m.

appeared as small dots in the chloroplasts. The size and distribution of these dots were suggestive of nucleoids, which are associated with PGE (Majeran et al., 2012). Localization of the *A. thaliana* RNA-binding protein RAP to nucleoids was previously established using a transiently expressed RAP-eGFP fusion (Kleinknecht et al., 2014). Therefore, Col-0 protoplasts were co-transformed with a RAP-RFP fusion in combination with mTERF10-eGFP, mTERF11-eGFP, or mTERF12-eGFP. Indeed, for each mTERF-eGFP construct, signals were found in dots together with the RFP signal. Merging of both signals confirmed colocalization of the mTERF10, -11, and -12 fusions with RAP, and therefore localization of all three mTERFs to nucleoids (**Figure 1B**). It is noteworthy, that especially mTERF12—and a minor fraction of RAP—tend to be localized in the chloroplast stroma when both mTERF12-eGFP and RAP-RFP are expressed together in protoplasts.

Identification and Phenotypic Analysis of Mutants for the *MTERF10*, *MTERF11*, *MTERF12* Loci

To obtain insight into the physiological functions of mTERFs 10, 11, and 12, T-DNA insertion lines were identified in the SIGnAL database (Alonso et al., 2003). The insertions were confirmed by PCR (**Figure 2A**) and homozygous lines were selected. In the mutants *mterf10-1* (SAIL_12A03) and *mterf10-2* (SALK_097699) the T-DNAs are inserted in the 5' UTR and the second exon, respectively (**Figure 2B**). The *mterf11-1* (FLAG_357F09) and *mterf11-2* (GABI_211D05) mutants both have their T-DNA insertion in the gene's single exon. For *MTERF12*, only one insertion line could be identified (*mterf12-1*, GABI_407E04), which contains a T-DNA in the promoter region (**Figure 2B**). To repress the *MTERF12* gene by RNAi, Col-0 lines were generated that contained constructs with an inverted repeat of a fragment spanning the first exon and a part of exon 2 of *MTERF12* (**Figure 2A**) which was under control of the constitutive *Cauliflower mosaic virus* 35S promoter.

Figure 2C shows the numbers and distributions of mTERF domains in the mTERF10, -11, and -12 proteins. In mTERF10 and mTERF11, six and five mTERF motifs are predicted by the Simple Modular Architecture Research Tool SMART (<http://smart.embl-heidelberg.de/>). One mTERF motif has been predicted for mTERF12 (our previous results, and see also Supporting Information of Babiychuk et al., 2011), but this domain is not annotated anymore with confidence by the SMART tool (http://smart.embl-heidelberg.de/smart/show_motifs.pl?ID=Q93ZZ2_ARATH). Thus, the classification of mTERF12 as an mTERF protein must be regarded as uncertain.

All mutants are in the Col-0 background except of *mterf11-1* which is a WS line. Hence, in all following experiments, *mterf11-1* was compared with WS, while Col-0 was used as the WT standard for the other lines. Real-time PCR analysis was employed to determine the extent of repression of *MTERF* transcripts in the different mutant lines (**Figure 3A**). In 3-week-old *mterf10-1* and *mterf10-2* plants, *MTERF10* transcript

levels were reduced to 29 and 4% of WT, respectively. To determine *MTERF11* transcript levels, primer pair A was chosen to detect transcripts initiated 5' of the T-DNA insertions (**Figure 2A**). Using this set-up, *MTERF11* transcript levels were found to be unchanged (*mterf11-1*) and nearly 6-fold induced (*mterf11-2*) relative to their WT (**Figure 3A**). In the *mterf11-1* allele (which is FLAG_357F09), the T-DNA of the pGKB5 vector integrated in the 5'LB-T-DNA-RB3' direction. It is of note here that the pGKB5 vector used to generate the FLAGdb T-DNA insertion line collection contains the 35S promoter on the LB side (Samson et al., 2002). The 35S promoter drives the expression of *PHOSPHINOTRICIN ACETYL TRANSFERASE* (*PAT*) used to select transgenic plants, and the *PAT* transcripts are terminated by the G7 terminator. It was already shown with two independent FLAG lines as an example that the G7 terminator can be an inefficient terminator in the context of the pGKB5 vector, allowing transcription to continue through and beyond the terminator sequence (Ulker et al., 2008). However, real-time PCR carried out with a primer pair covering the region 3' of the T-DNA insertion detected greatly reduced *MTERF11* transcript levels in the *mterf11* mutants: 0.09% of WT in *mterf11-1* and 0.01% in *mterf11-2* (**Figure 3A**). *MTERF12* transcript levels were not affected in the *mterf12-1* mutant (**Figure 3A**). Therefore, *MTERF12* RNAi lines were tested for their ability to repress *MTERF12* gene expression. Six independent lines were screened, but the most effectively repressed lines, *mterf12i-1* and *mterf12i-2*, still retained 32% and 59% of WT (Col-0) amounts of *MTERF12* transcripts, respectively (**Figure 3A**). Under normal growth conditions, all identified mutant lines were phenotypically indistinguishable from WT (**Figure 3B**). To look for subtle photosynthetic phenotypes, the maximum quantum yield of photosystem II (F_v/F_m) was measured in Col-0, WS and all *mterf* mutants (**Figure 3B**), but no deviations in this parameter were detected in the mutants.

To summarize, the expression of all mTERF motifs should be strongly reduced in the *mterf10* mutants (particularly *mterf10-2*), while the *mterf11* mutants produce truncated transcripts. Assuming the latter are translated, the protein products would lack the last two mTERF domains (*mterf11-1*) or mTERF domain 5 only (*mterf11-2*) (**Figure 2C**). In the *mterf12i* lines, transcripts including the single putative mTERF domain were—at best—reduced to one-third of Col-0 levels. At all events, none of the *mterf* mutant lines display any obvious phenotype under normal growth conditions.

Phylogenetic Position of the mTERF10, -11, and -12 Proteins

Because the *mterf10*, -11, and -12 mutant lines lacked a clear phenotype under normal growth conditions (**Figure 3**), we asked whether this might be attributable to functional redundancy within the mTERF family. Several *MTERF* genes have undergone tandem duplications (on chromosome 1) and one block duplication (*AT4G19650* and *AT5G45113*; Kleine, 2012). But neither *MTERF12* nor *MTERF10* or *MTERF11* originated from a duplication event, so we can exclude the possibility of

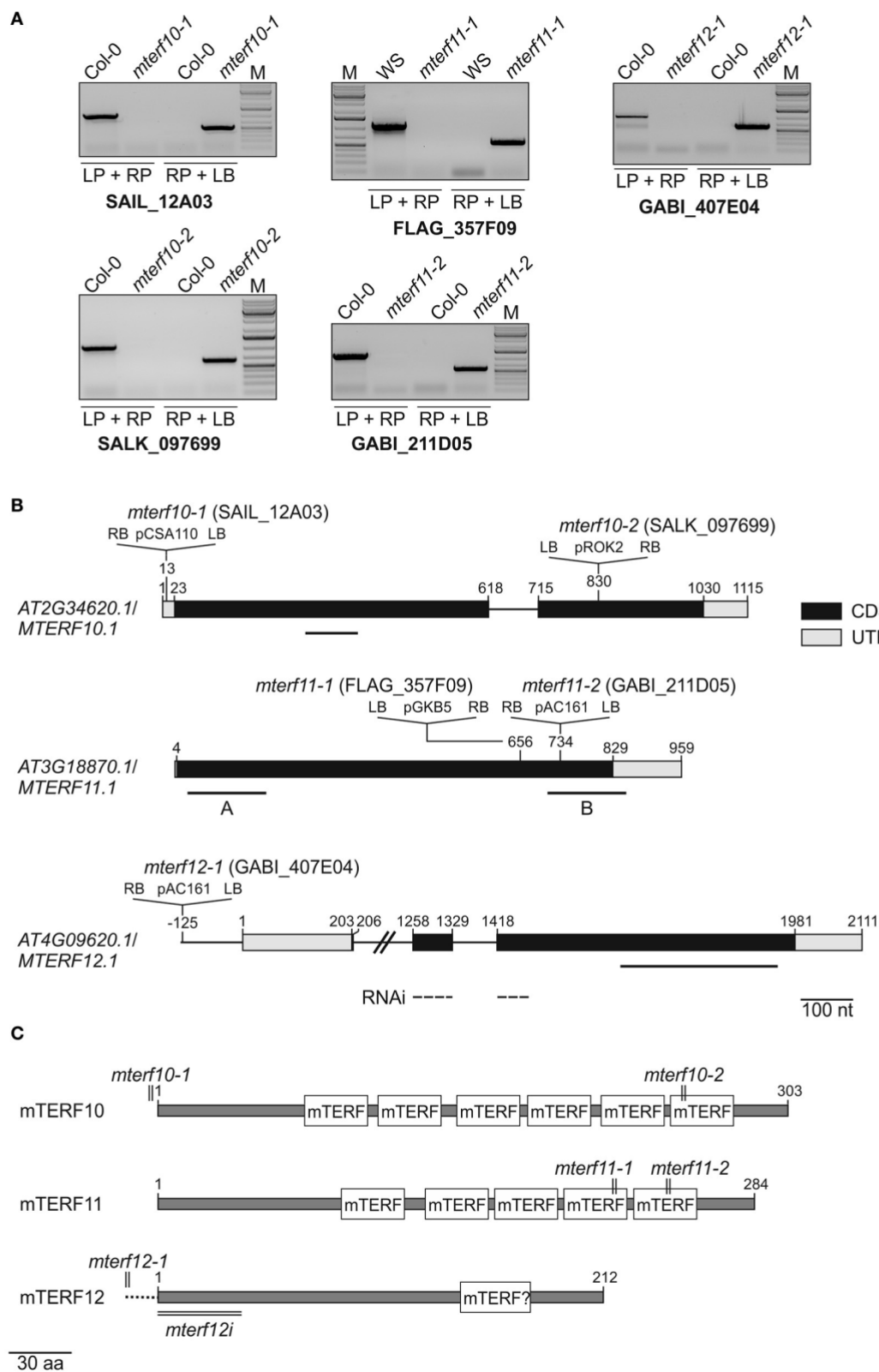


FIGURE 2 | Identification of *mterf10*, *mterf11* and *mterf12* T-DNA insertion mutants, and generation of *MTERF12* RNAi lines. **(A)** Confirmation and identification of homozygous T-DNA insertions in the different *mterf* mutant lines. The combination of the gene-specific left and right primers (LP and RP) was used for amplification of

(Continued)

FIGURE 2 | Continued

sequences around the T-DNA insertion. The combination of RP and T-DNA left border primer (LB) was used for the verification of the T-DNA insertion. **(B)** Schematic representation and T-DNA tagging of the *MTERF10* (AT2G34620), *MTERF11* (AT3G18870), and *MTERF12* (AT4G09620) loci. Exons (black boxes), introns (black lines) and the 5' and 3'UTRs (gray boxes) are shown. Numbers are given relative to the transcription start site of the gene loci. Locations and orientation of T-DNA insertions are indicated, as deduced from RP + LB PCR products shown in **(A)** which were subsequently sequenced. Note that the insertions are not drawn to scale. Furthermore, the location of the *MTERF12* RNAi-directed sequence is indicated as a dashed line. **(C)** Schematic representation of mTERF10, mTERF11, and mTERF12 proteins. The numbers and locations of mTERF domains are shown as white boxes. The relative positions of T-DNA and RNAi tagging are indicated.

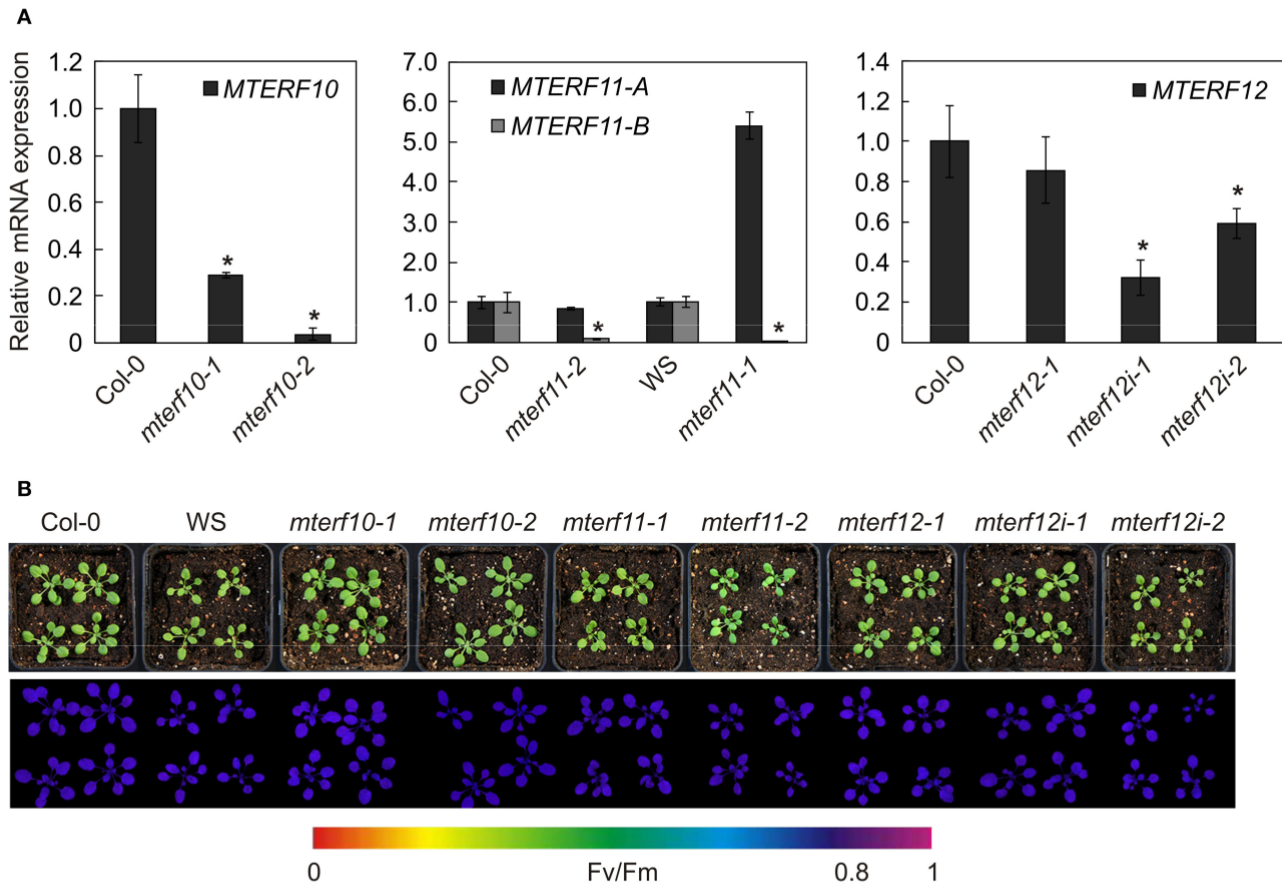
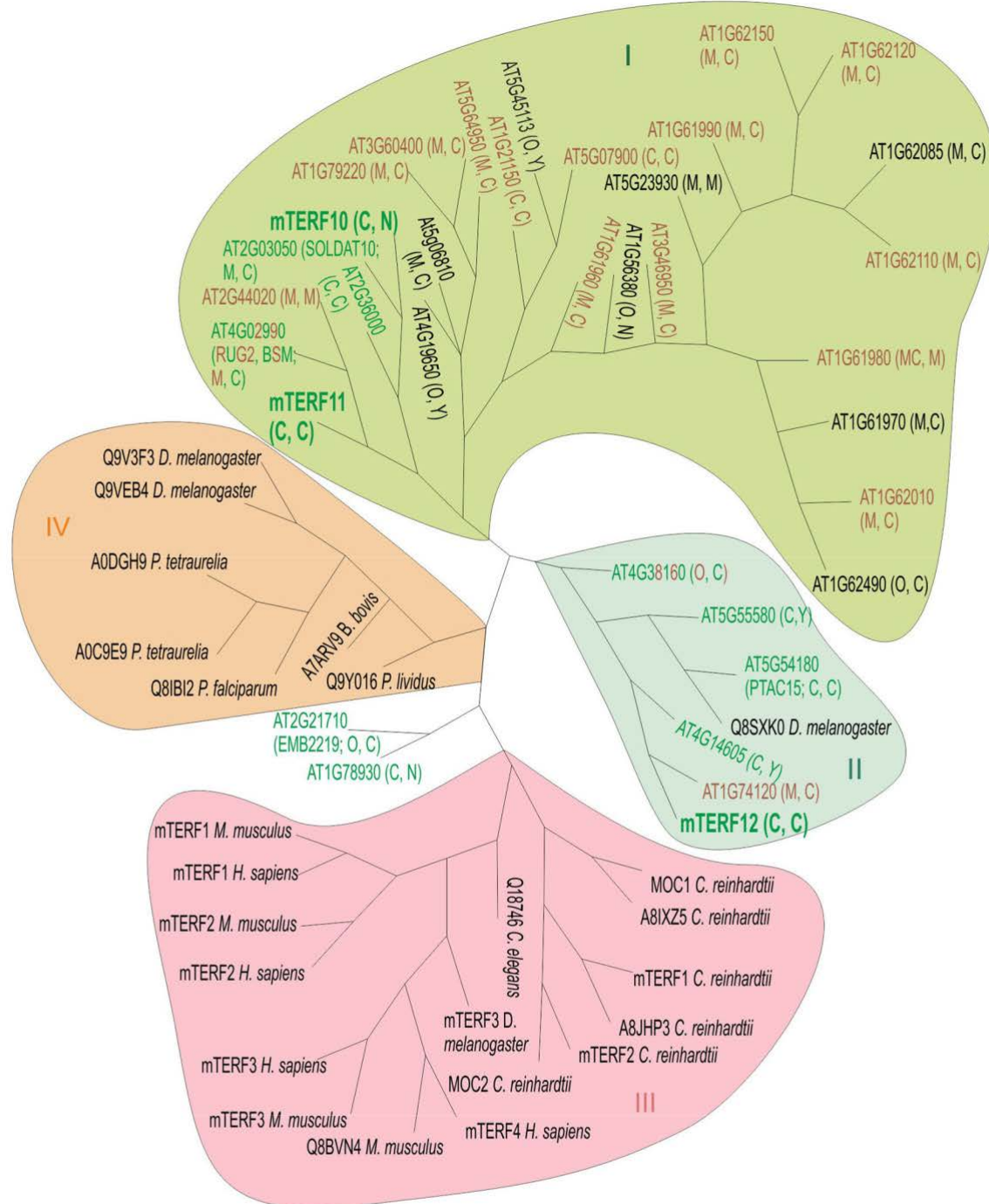


FIGURE 3 | Characterization of *mterf10*, *mterf11*, *mterf12* T-DNA insertion and *MTERF12* RNAi (*mterf12i*) lines. **(A)** Real-time PCR analysis of *MTERF10*, *MTERF11*, and *MTERF12* mRNA levels. Real-time PCR was performed with primers specific for fragments indicated by horizontal black lines below the corresponding gene in **Figure 2B**. Expression values are reported relative to the corresponding transcript levels in Col-0. The results were normalized with respect to the expression level of At4g36800, which codes for a RUB1-conjugating enzyme (*RCE1*). Bars indicate standard deviations. Statistically significant differences (t-test; $p < 0.05$) between wild-type and mutant samples are indicated by an asterisk. **(B)** Phenotypes of 3-week-old wild-type (WS for *mterf11-1-1* and Col-0 for the remaining mutant lines) and mutant plants grown under long-day (16/8 h) light conditions. The maximum quantum yield of PSII (F_v/F_m) was measured with an ImagingPAM fluorometer.

protein redundancy arising from gene duplication. To obtain an impression of the overall degree of sequence similarity within the mTERF protein family, we constructed a phylogenetic tree which included in addition to *A. thaliana* mTERFs, mTERF members from the green alga *Chlamydomonas reinhardtii*, *Homo sapiens*, *Mus musculus*, *Drosophila melanogaster*, and other organisms (**Figure 4**). The tree reveals four main clades. The mTERF members of *C. reinhardtii*, *H. sapiens* and *M. musculus* are all in the same clade. The majority of *A. thaliana* mTERFs form clade I which includes mTERF10 and -11, while mTERF12 along with five other *A. thaliana* mTERFs and one *D. melanogaster* mTERF

constitute clade II. The mTERF10, -11, and -12 proteins are most closely related to mTERF1/SOLDAT10 (Meskauskiene et al., 2009), mTERF4/BSM/RUG (Babiyshuk et al., 2011; Quesada et al., 2011) and mTERF15 (Hsu et al., 2014) proteins. Mutants for each of these three display phenotypes under normal growth conditions and have been shown to be involved in PGE or mitochondrial gene expression. Moreover, levels of sequence identity/similarity between mTERF10 and mTERF1 (38/68% over a stretch of 240 amino acids), mTERF11 and mTERF4 (26/41% over a stretch of 222 amino acids) and mTERF12 and mTERF15 (29/53% over a stretch of 77 amino acids), respectively, are



(Continued)

FIGURE 4 | Continued

of four main clades (I–IV). Clade I encompasses proteins encoded by a tandem gene cluster on *A. thaliana* chromosome 1 and several other *A. thaliana* mTERF proteins. In clade III, *C. reinhardtii* mTERFs are grouped together with animal mTERF proteins. Clade IV comprises mTERF proteins from diverse species including paramecium, sea urchin (*P. lividus*), parasites (*P. falciparum* and *B. bovis*) together with mTERFs from *Drosophila*. The mTERF proteins mTERF10 and -11 (highlighted in large, bold letters) form clade I together with 25 other mTERF proteins, while mTERF12 (also highlighted in big, bold letters) is assigned to clade II, together with five other *A. thaliana* mTERFs and one *Drosophila* mTERF. C, chloroplast; M, mitochondrion; N, nucleus; Y, cytosol; O, other.

noteworthy for the mTERF10/mTERF1 pair, but negligible for the other two.

Changes in *MTERF* Transcript Levels in Response to Abiotic Stresses

To gain deeper insights into the functions of mTERF10, -11, and -12, their mRNA expression patterns were analyzed. Co-expression analysis of 26 *MTERF* genes and their corresponding gene ontology annotations have already been reported (Kleine, 2012). However, that study was designed to provide a global classification. Hence subsequent Genevestigator analyses only dealt with the numbers of conditions/treatments that altered *MTERF* gene expression. In the present study, we extracted *MTERF* transcript levels from the Arabidopsis eFP browser (<http://bar.utoronto.ca/efp/cgi-bin/efpWeb.cgi>) with “Abiotic Stress” as a data source (Winter et al., 2007). In these experiments, 18-day-old plants were subjected to different stresses, and samples were taken over a time course of 24 h from stress-treated and control plants. We calculated the relative changes in *MTERF10*, -11, and -12 transcript levels from plants exposed to drought, high salt, heat, or cold compared to control conditions (Figure 5A). Because *mda1* (*mterf5*) and *mterf9* mutants are known to exhibit altered stress responses (Robles et al., 2012, 2015), *MTERF5* and -9 were included for reference. Under drought and heat stress, transcript levels of all investigated *MTERF* genes were only moderately changed (Figure 5A). With a 3-fold rise after 1 h of heat stress (*MTERF10*) and an approximately 0.3-fold change (*MTERF5* and 9), those transcripts were the most responsive. Under salt and cold treatment, *MTERF* transcript levels tended to be reduced. Under both salt and cold stress, *MTERF10* and *MTERF11* levels were most responsive, and especially after 24 h of cold treatment *MTERF5*, 10, 11, and 12 transcript levels were reduced (Figure 5A). To confirm these data and to find other conditions under which the *MTERFs* of interest might be regulated, the Genevestigator Perturbations Tool (<https://genevestigator.com/gv>; Hruz et al., 2008) was employed on all deposited *A. thaliana* ATH1 arrays together with a 2-fold change filter and a *p*-value of < 0.05. An overview of all changes in *MTERF10*, *MTERF11*, and *MTERF12* mRNA levels in response to perturbations (relative to untreated controls) can be found in Supplementary Figures S1–S3. In Figure 5B selected conditions are shown which are associated with changes in temperature and light, and with salt and drought stress conditions. Levels of *MTERF10* mRNA were most susceptible to perturbation, being induced by light, raised after germination, and strongly reduced under drought conditions and various cold and high-light regimes, and on exposure to salt or ABA (Figure 5B).

Knockdown of *MTERF10* or *MTERF11* Alters Sensitivity to Salt Stress

To experimentally probe the involvement of mTERFs in stress responses, 3-week-old WT and *mterf10*, -11, and -12 mutant plants grown under standard conditions (22°C at 100 $\mu\text{mol photons m}^{-2} \text{ s}^{-1}$) were exposed for 7 days to moderate temperature stress (30°C, at a fluence rate of 100 $\mu\text{mol photons m}^{-2} \text{ s}^{-1}$) or moderate light stress (400 $\mu\text{mol photons m}^{-2} \text{ s}^{-1}$ at a temperature of 22°C). After 7 days of moderate temperature stress, the leaf petioles of WT and all *mterf* mutants were shortened, but otherwise all plants looked healthy (Figure 6A). After 3 days, F_v/F_m was slightly reduced in all *mterf11* and *mterf12* mutant lines, but was restored to normal levels after 7 days (Figures 6A, B). Also after 7 days of moderate light stress, the leaf petioles of WT and all *mterf* mutants were shortened—albeit to a lesser extent. Furthermore, the edges of older leaves in all lines began to show signs of necrosis (Supplementary Figure S4A). After 1 h of moderate light stress, F_v/F_m was slightly reduced in all lines (Supplementary Figure S4B). This reduction continued in the *mterf11-1* mutant after 2 and 4 h, but all lines recovered to the initial F_v/F_m values after 96 h (Supplementary Figure S4B).

After 3 and 24 h of salt stress, *MTERF5* and *MTERF9* transcript levels were reduced to half of those in control conditions (Figure 5A), and indeed, *mda1* (*mterf5*) and *mterf9* seedlings are less sensitive to salt and osmotic stresses (Robles et al., 2012, 2015). Because *MTERF10* and *MTERF11* transcripts were reduced to an even larger extent than *MTERF5* and *MTERF9* RNAs following exposure to salt stress for 6 and 24 h (Figure 5A), we asked whether inactivation of *MTERF10* or *MTERF11* might enable the mutant plants to better tolerate salt stress. To this end, WT and *mterf* mutant lines were germinated on MS medium (control) and MS medium supplemented with 125 mM or 175 mM NaCl, and germination rates were scored after different time points (Figure 7A). All lines germinated to nearly 100% on the control MS medium. Germination rates of all lines with a Col-0 background grown for 48 h on MS medium supplemented with 125 mM NaCl or for 72 h on medium supplemented with 175 mM NaCl were very similar (Figure 7A). In the aforementioned conditions, germination rates of Col-0 seeds were approximately 60% (Figure 7A). The germination rates of *mterf10-1* and -2, *mterf11-2* and all *mterf12* seeds were all lower (ranging from 26 to 47%) than those of Col-0 seeds. However, after 96 h on MS medium supplemented with 175 mM NaCl the germination rates of *mterf12* seeds (76 to 87%) were comparable to that of Col-0 seeds (84%). Interestingly, *mterf10-1*, *mterf10-2*, and *mterf11-2* still displayed enhanced sensitivity to salt inhibition, with germination rates of 54, 55, and 61%, respectively (Figure 7A). WS seeds were

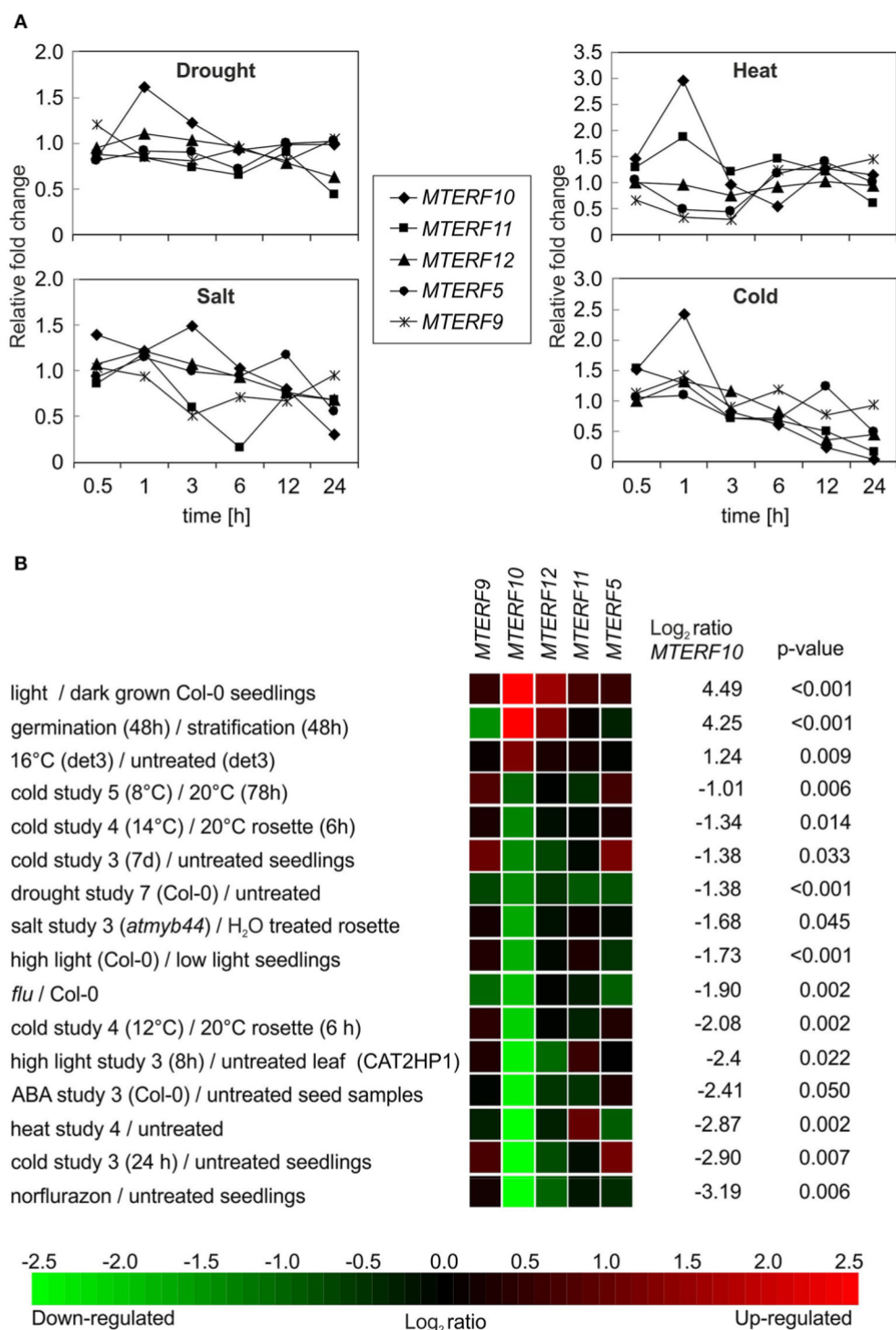
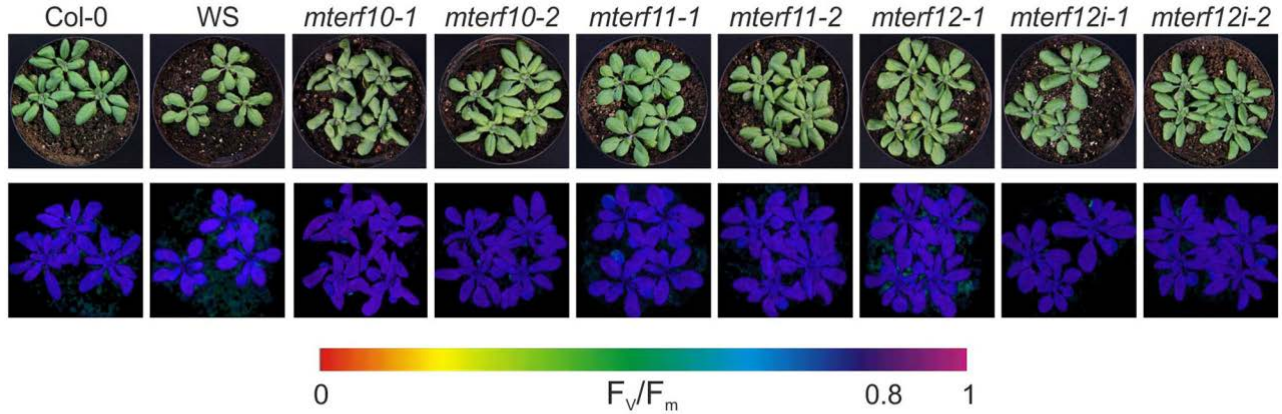


FIGURE 5 | In silico analyses of changes in levels of MTERF transcripts in response to abiotic stresses. **(A)** MTERF transcript levels were extracted from the Arabidopsis eFP Browser (<http://bar.utoronto.ca/efp/cgi-bin/efpWeb.cgi>) with “Abiotic Stress” as a data source (Winter et al., 2007). Plant material from stress-treated and control plants was analyzed over a time course of 24 h. Here, the expression values are reported relative to the corresponding transcript levels in control conditions. **(B)** The Genevestigator Perturbations Tool (<https://genevestigator.com/gv/>; Hruz et al., 2008) was applied to all available *A.thaliana* microarrays in combination with the 2-fold change filter and a *p*-value of < 0.05. Shown here is a selection of conditions related to abiotic stresses. Conditions were ordered according to the magnitude of the relative change in MTERF10 mRNA (from high to low). An overview of all transcriptional responses of MTERF10, MTERF11, and MTERF12 to perturbations can be found in **Supplementary Figures S1–S3**.

A

7 days 30°C



B

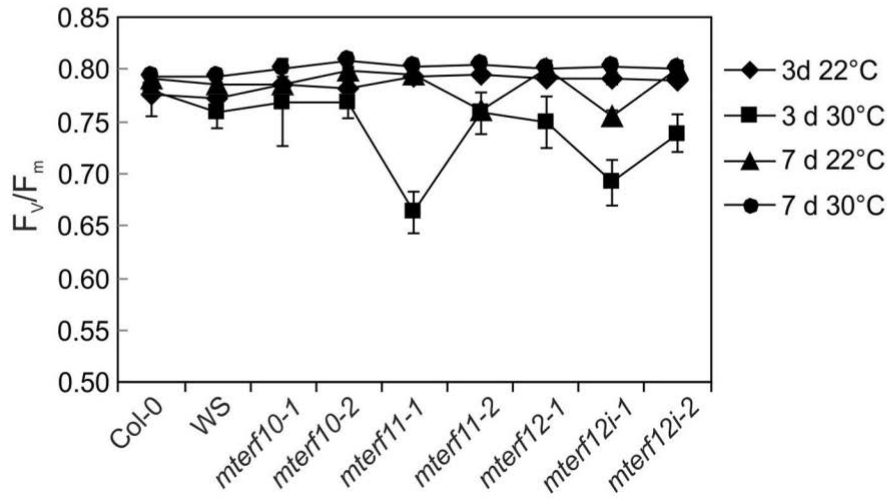


FIGURE 6 | Behavior of wild-type (Col-0) and *mterf10*, -11 and -12 mutant plants under moderate heat stress of 30°C. **(A)** To score the phenotypes under moderate heat stress, plants were first grown for 3 weeks under normal growth conditions (100 $\mu\text{mol photons m}^{-2}\text{s}^{-1}$, 22°C) and then exposed to 30°C for 7 days. **(B)** The maximum quantum yield of PSII (F_v/F_m) of Col-0 and *mterf* mutant plants was determined after 3 and 7 days (d) in 30°C. The data are shown as mean values \pm SD from 8 to 10 different leaves.

very susceptible to salt stress and failed to germinate under the conditions used to investigate the Col-0 descendant lines. For this reason, a milder salt stress treatment was applied to all lines with a WS background. Still, after 72 h growth on MS medium supplemented with 125 mM, the germination rate of WS was only 7% and raised to 48% after 96 h (**Figure 7A**). Although the *mterf11-2* mutant was more sensitive to salt stress compared to Col-0, the germination rates of *mterf11-1* seeds were comparable to their corresponding WT (WS; **Figure 7A**).

To ascertain whether the altered activity of *MTERF10* was indeed responsible for the salt-stress phenotypes and whether overexpression of *MTERF11* might lead to enhanced salt-stress tolerance, 35S:*MTERF10*:MGFP5 and 35S:*MTERF11*:EGFP constructs were introduced into Col-0 and WS, respectively, to generate oe-mTERF10 and oe-mTERF11 lines. Although

MTERF10 mRNA levels were only approximately 2.3-fold higher in oe-mTERF10-1 and oe-mTERF10-2 lines than in Col-0 (**Figure 8A**), these lines—with germination rates of approximately 85 and 95%, respectively, after 48 h on MS medium with 125 mM NaCl and 72 h on MS medium with 175 mM NaCl—were nevertheless resistant to the deleterious effect of salt (**Figure 7A**). This confirms that the salt sensitivity of *mterf10-1* and *mterf10-2* mutants is indeed caused by knockdown of the *MTERF10* gene. Moreover, we identified three oe-mTERF11 lines that displayed a high diversity of *MTERF11* transcript over accumulation which ranged from 12- to 117-fold (**Figure 8B**). Two of these lines were challenged with salt stress, and actually displayed much higher germination rates than WS and therefore, enhanced salt stress tolerance (**Figure 7A**).

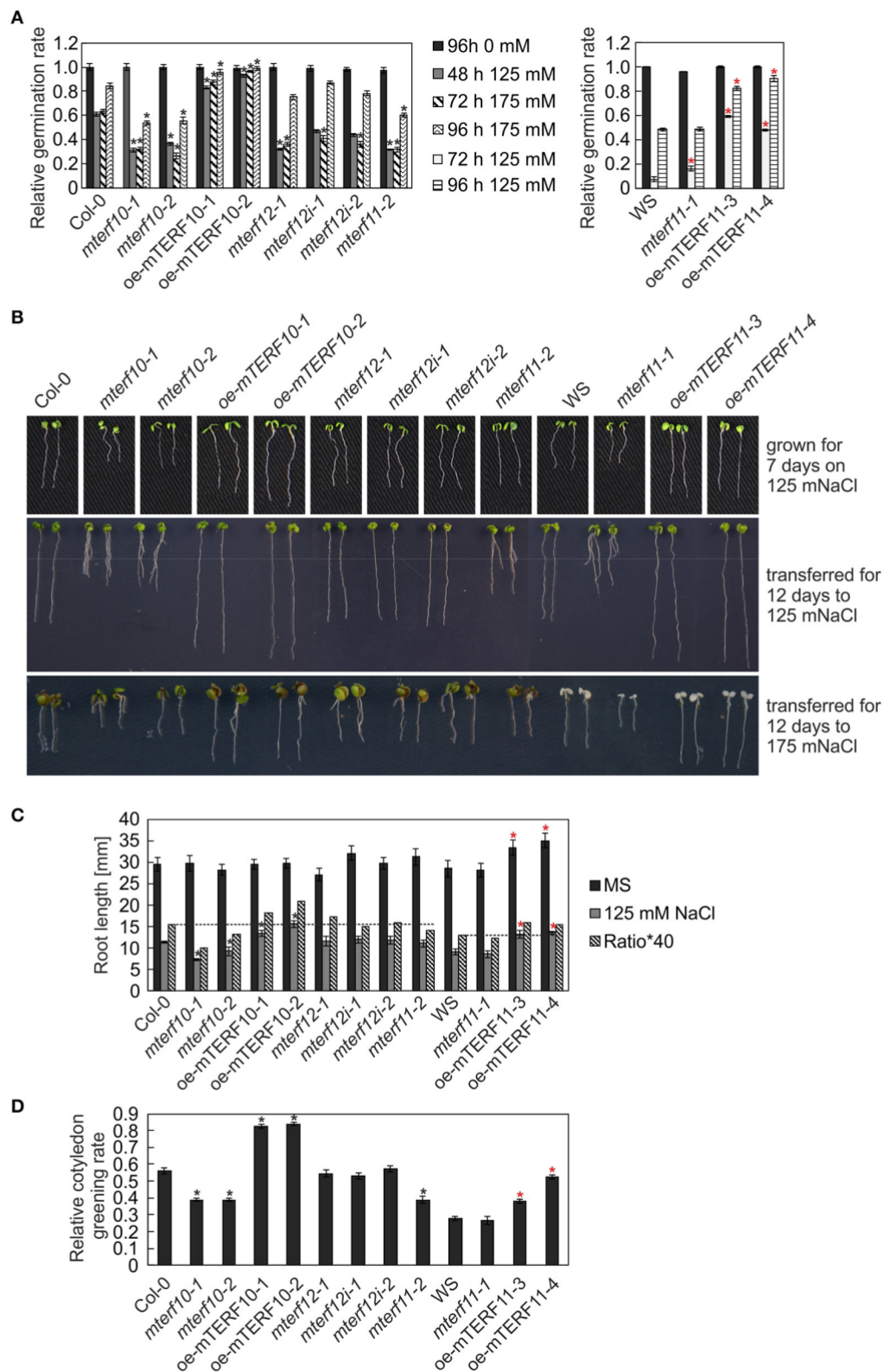


FIGURE 7 | Responses of WT seedlings (WS for *mterf11-1* and *oe-mTERF11* lines, and Col-0 for the remaining mutant lines), T-DNA (*mterf10-1* and *-2*, *mterf11-1* and *-2*, and *mterf12-1*), RNAi (*mterf12i-1* and *-2*) and overexpression lines (*oe-mTERF10* and *oe-mTERF11*) to salt stress treatment under long-day conditions. **(A)**

(Continued)

FIGURE 7 | Continued

Seed germination was investigated on MS medium in the absence and presence of 125 and 175 mM NaCl. Radicle emergence was scored after indicated time points. Germination rates were calculated relative to the number of total seeds. **(B)** Phenotypes of 7-day-old WT and mutant seedlings were germinated on either MS medium supplemented with 125 mM NaCl (grown for 7 days on 125 mM NaCl), or on MS medium and transferred directly after radicle emergence for 12 days to MS medium supplemented with 125 mM NaCl (transferred for 12 days to 125 mM NaCl) or 175 mM NaCl (transferred for 12 days to 175 mM NaCl), respectively. The root lengths **(C)** and cotyledon greening rates of seedlings grown on 125 mM NaCl—displayed as the ratio of the number of green cotyledons to the total number of cotyledons **(D)** were determined after 7 and 5 days, respectively. The data in **(A,C,D)** represent mean values \pm SD of three independent experiments, each performed with at least 100 seeds per treatment and genotype. Statistically significant differences (t-test; $p < 0.05$) between WT (Col-0 or WS) and corresponding mutant lines are indicated by an asterisk (black for Col-0; red for WS).

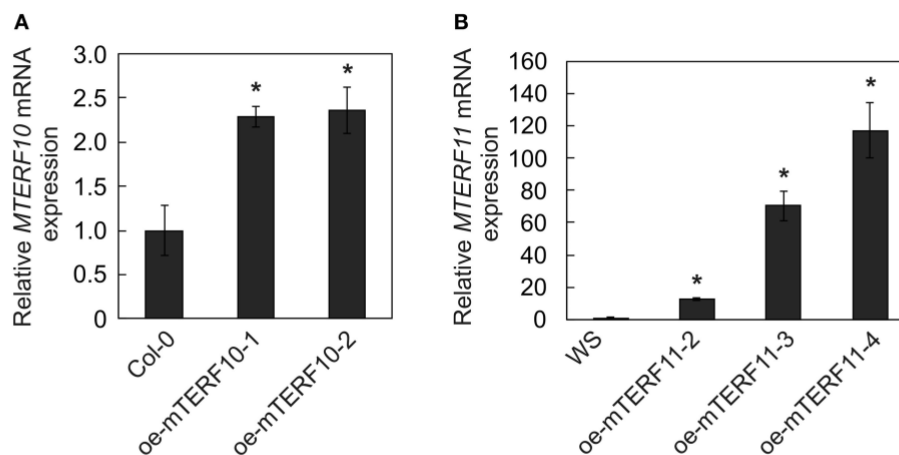


FIGURE 8 | *MTERF10* **(A)** and *MTERF11* **(B)** transcript levels in Col-0 lines overexpressing *MTERF10* (oe-mTERF10) and WS lines overexpressing *MTERF11* (oe-mTERF11), respectively. Transcript levels were determined by real-time PCR analysis. Expression values are reported relative to the corresponding transcript levels in Col-0. The results were normalized with respect to the expression level of *At4g36800* (*RCE1*). Bars indicate standard deviations. Statistically significant differences (t-test; $p < 0.05$) between Col-0 and oe-mTERF10 lines and WS and oe-mTERF11 lines, respectively, are indicated by an asterisk.

To investigate this further, the performance of *mterf* mutants and mTERF overexpression lines was investigated during post-germination development. As shown in **Figures 7B,C**, the root lengths of *mterf10-1* and -2 seedlings challenged with 125 mM NaCl were significantly shorter compared to Col-0, while the root lengths of oe-mTERF10 seedlings were longer (**Figure 7C**). Moreover, compared to WS, overexpression of *MTERF11* results in longer root lengths, reflecting findings of the germination rates (**Figure 7A**). In addition, cotyledon greening—displayed as the ratio of the number of green cotyledons to the total number of cotyledons—of *mterf10-1* and -2 seedlings was delayed by salt stress, while in contrast, overexpression of *MTERF10* or *MTERF11* enabled seedlings to display higher cotyledon greening rates than their corresponding wild types (**Figure 7D**).

ABA operates as a signal during developmental processes including seed germination, and moreover, in response to abiotic stresses including salt stress (Christmann et al., 2006). Furthermore, *A. thaliana* mutants in which the *ABI4* (*ABSCISIC ACID INSENSITIVE4*) gene has been inactivated are more salt tolerant than WT (Quesada et al., 2000; Shkolnik-Inbar et al., 2013). To investigate whether reduced *MTERF* transcript levels in the *mterf10*, -11, and -12 mutant lines or overexpression of mTERF10 or mTERF11 alter ABA sensitivity, wild-type, *mterf*, oe-mTERF10, oe-mTERF11 and as a control *abi4-1* mutant seedlings were grown on MS supplemented with 1

μ M ABA, and germination rates were scored after 96 h (lines with a Col-0 background) and 120 h (lines with a WS background). With a 69% germination rate, the control line *abi4-1* germinated better than Col-0 (49%; **Figure 9A**). All *mterf12* lines displayed a slightly, but not significantly, higher germination rate than Col-0, but *mterf10* and *mterf11* lines were as sensitive as Col-0 to ABA stress. Importantly, especially oe-mTERF10 lines were also less susceptible to ABA stress (**Figure 9A**), like they were to salt stress (**Figure 7A**). After 120 h on 1 μ M ABA, WS germinated to 32%, and both *mterf11-1* and oe-mTERF11 lines displayed even lower germination rates (**Figure 9A**).

To follow this up, the phenotypes of seedlings grown on 1 μ M ABA were examined after 7 days. Col-0 and WS seedlings displayed short roots and cotyledons had only started to emerge (**Figure 9B**). In contrast, *abi4-1* seedlings had longer roots and fully expanded cotyledons. All mutant lines with reduced *MTERF10*, -11, or -12 transcript levels showed the same behavior as the wild types. However, the cotyledon phenotype of the oe-mTERF10 lines was comparable to that of the *abi4-1* mutant (**Figure 9B**). This was also manifested in the higher relative cotyledon greening rate of oe-mTERF10 lines (25 and 30%) compared to Col-0 (**Figure 9C**).

It appears that challenging Arabidopsis seedlings with ABA or salt stress under continuous light reduces germination efficiencies or cotyledon greening of Col-0 to a greater extent

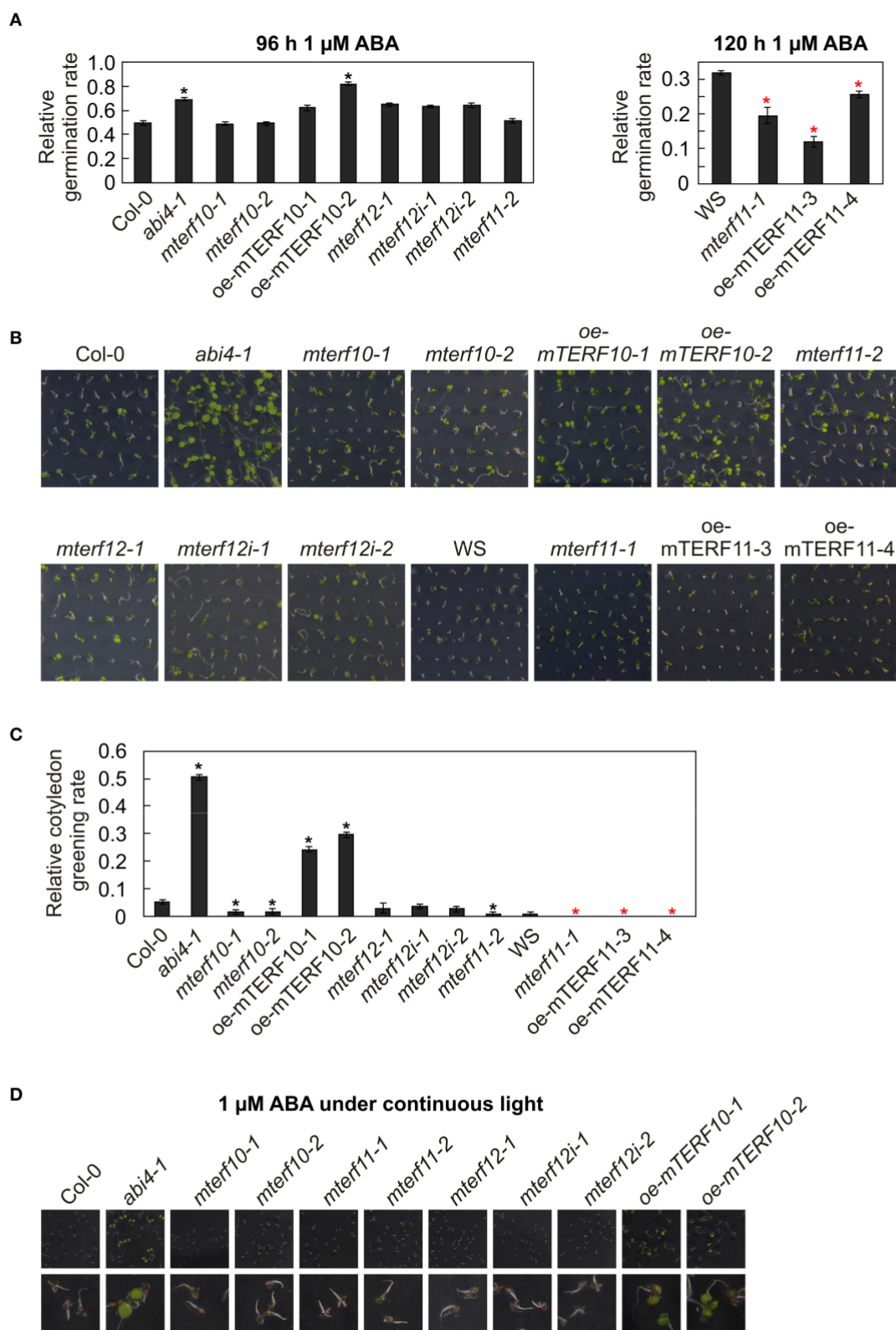


FIGURE 9 | Responses of WT seedlings (WS for *mterf11-1* and *oe-mTERF11* lines, and Col-0 for the remaining mutant lines), T-DNA (*mterf10-1* and -2, *mterf11-1* and -2, and *mterf12-1*), RNAi (*mterf12i-1* and -2) and overexpression lines (*oe-mTERF10* and *oe-mTERF11*) and—as control—the *abi4-1* mutant to ABA treatment

(Continued)

FIGURE 9 | Continued

under long-day conditions **(A–C)** and under continuous light **(D)**. **(A)** Seed germination was investigated on MS medium in the absence and presence of 1 μ M ABA. Radicle emergence was scored after indicated time points. **(B)** Phenotypes of 7-day-old seedlings grown on MS medium in the presence of 1 μ M ABA. **(C)** The ratio of cotyledon greening was determined after 6 days. **(D)** Phenotypes of 7-day-old seedlings grown on MS medium in the presence of 1 μ M ABA under continuous light. The pictures of the lower row are magnifications of the pictures above them. The data in **(A,C)** represent mean values \pm SD of three independent experiments, each performed with at least 100 seeds per treatment and genotype. Statistically significant differences (t-test; $p < 0.05$) between WT (Col-0 or WS) and corresponding mutant lines are indicated by an asterisk (black for Col-0; red for WS).

(Reyes and Chua, 2007; Chen et al., 2008; Hwang et al., 2015) compared to long-day conditions (**Figure 7**; Hu et al., 2013). To tackle the oe-mTERF10 ABA phenotype, we grew Col-0, *mterf* mutant lines and oe-mTERF10 lines in continuous light and a temperature of 20°C on MS medium (control) and MS medium supplemented with 1 μ M ABA, and the phenotypes were scored after 7 days (**Figure 9D**). Because lines with a WS background were already very sensitive to ABA in long-day conditions, these lines were omitted. Indeed, Col-0 and *mterf* mutant seedlings displayed even shorter roots compared to long-day conditions and the cotyledons that had started to emerge did not turn green to this time point (**Figure 9D**). In contrast, *abi4-1* seedlings had longer roots and fully expanded green cotyledons. All mutant lines with reduced *MTERF10*, -11, or -12 transcript levels showed the same behavior as Col-0. However, also in continuous light the phenotype of oe-mTERF10 lines was comparable to that of the *abi4-1* mutant, with longer roots and expanded green cotyledons (**Figure 9D**).

In sum, these results indicate that lower or higher *MTERF11* levels result both in increased ABA sensitivity. But, strikingly, higher *MTERF10* levels are associated with decreased sensitivity to ABA, which might in turn be linked to the higher salt tolerance of oe-mTERF10 lines.

DISCUSSION

Arabidopsis thaliana contains 35 mTERF proteins, of which seven have been investigated in more detail (reviewed in: (Kleine and Leister, 2015; Quesada, 2016)). Twenty-six of the 35 mTERFs have been sorted into groups based on their expression profiles and co-expression behavior (Kleine, 2012). The mTERF proteins that have been investigated in more detail are members of the “chloroplast” cluster (mTERF1, -4, -5, -6, and -9; the cluster itself contains 9 members) and the “mitochondrial” cluster (mTERF15 and -18; this cluster contains 7 members). In this study, we added to the inventory of characterized mTERFs and investigated all members of the “chloroplast-associated” cluster (mTERF10, -11, and -12).

In a fluorescence microscopy study of mTERF-GFP fusion proteins, 16 mTERFs were shown to be targeted to mitochondria, 11 to chloroplasts and one to the nucleus/cytosol (Babiychuk et al., 2011). That study revealed localization of mTERF4 to chloroplasts and mTERF6 to mitochondria. Later studies demonstrated that mTERF4 (Quesada et al., 2011) and mTERF6 (Romani et al., 2015) are in fact found in both mitochondria and chloroplasts. The mTERF proteins in the chloroplast-associated group were also assigned to the chloroplasts in the large-scale study cited above (Babiychuk et al., 2011). However, to

confirm or extend these data, and also to define the sub-chloroplast localization of mTERF10, -11, and -12, we transiently transformed *A. thaliana* protoplasts with GFP fusion proteins. By co-transformation with a RAP-RFP fusion protein, which is a marker for the chloroplast nucleoid (Kleinknecht et al., 2014), we show that all members of the chloroplast-associated cluster are localized to chloroplast nucleoids (see **Figure 1**). Also the maize homologs of Arabidopsis mTERFs-2, -3, -4, -5, -7, -9, -16, and -27 were identified in enriched maize nucleoids (Majeran et al., 2012) and Arabidopsis mTERF8 was found in preparations of the plastid transcriptionally active chromosome (pTAC; Pfalz et al., 2006) which is related to the nucleoid (Pfalz and Pfannschmidt, 2013). The nucleoid houses proteins that are associated with DNA organization, replication and repair, and furthermore, are involved in transcription, and processing, splicing and editing of transcripts, suggesting that mTERFs participate in PGE (Majeran et al., 2012). In fact, the three plant mTERF proteins whose molecular functions are known do participate in PGE: mTERF4 is involved in chloroplast group II intron splicing (Babiychuk et al., 2011; Hammani and Barkan, 2014), mTERF6 promotes maturation of a chloroplast tRNA (Romani et al., 2015) and in *mterf15* mutants intron splicing of mitochondrial *nad2* transcripts is perturbed (Hsu et al., 2014). Because levels of 16 and 23S rRNAs, and thus chloroplast protein synthesis, are reduced in the *soldat10* mutant (Meskauskiene et al., 2009), it can be assumed that the mTERF1/SOLDAT10 protein is likewise involved in PGE.

Most of the previously characterized *mterf* mutants show phenotypes under normal growth conditions. Inactivation of mTERF1 (Meskauskiene et al., 2009) or mTERF4 (Babiychuk et al., 2011) is embryo lethal, the *mterf6* and *mterf15* knockout mutants are seedling lethal (Romani et al., 2015) and retarded in growth and development (Hsu et al., 2014), respectively, and *mda1* (*mterf5*) and *mterf9* mutants are small and pale (Robles et al., 2012, 2015). We were unable to discern any phenotypic alterations in *MTERF12* RNAi lines, either under normal or challenging growth conditions. In fact, mTERF12 might not be a bona fide mTERF protein, because an analysis with the SMART tool fails to identify any mTERF domain in mTERF12 (see above). On the other hand, *MTERF12* is expressed at moderate to high levels in many developmental stages and organs (Kleine, 2012), and the mTERF12-eGFP fusion protein is localized to nucleoids (see **Figure 1B**). Therefore, while mTERF12 might not belong to the eponymous family, it may nevertheless be involved in PGE. Moreover, the residual amount of *MTERF12* (32% of WT transcript levels) present in *mterf12i-1* (see **Figure 3A**) may suffice to maintain a WT-like phenotype under all the conditions examined here, or alternatively we may not have hit

upon the conditions required to provoke an abnormal phenotype in *mterf12i* lines. The latter possibility appears to be the more likely. For *MTERF12* mRNA levels are highest in pollen (Wang et al., 2008; Kleine, 2012) and the most pronounced change in *MTERF12* transcript level occurs in response to supplementation with nitrate (see **Supplementary Figure S3**), an intervention to which *mterf12i* lines were not subjected. Moreover, functional redundancy cannot be completely ruled out, although none of the three genes of interest originated from a duplication event (Kleine, 2012) and our phylogenetic tree (see **Figure 4**) and protein sequence comparisons (see above) do not strongly support this idea.

In addition to their pale color and growth restricted phenotype, the *mda1* (*mterf5*) and *mterf9* mutants are less susceptible to salt and osmotic stresses, perhaps caused by reduced sensitivity to ABA (Robles et al., 2012, 2015). Notably, acclimation outputs are also altered by impairments in several other mTERF proteins (Meskauskienė et al., 2009; Quesada et al., 2011; Kim et al., 2012). Indeed, the emerging role of *A. thaliana* and maize mTERFs in acclimation and stress responses has already been noted and discussed (Zhao et al., 2014; Kleine and Leister, 2015; Quesada, 2016). This notion is especially of importance for crop plants, because plant development and growth is reduced in challenging growth conditions, leading finally to reduced yield. For this reason, several strategies have been tried to produce abiotic stress tolerance crop plants (Sah et al., 2016). With the aim to find a starting point to investigate stress tolerance in cotton, the response of cotton to abiotic stress treatments was studied with a cDNA library derived from samples treated with different stress conditions. Indeed, many transcripts for known stress-related genes, transcription factors and also mTERFs were enriched in this library (Zhou et al., 2016). Moreover, investigation of transcript level changes of six maize *MTERF* genes (maize *MTERF2*, -5, -11, -12, -13, and -28) in response to salt, ABA and NAA treatments showed an upregulation of *MTERF28* transcripts in all tested stress conditions, while *MTERF12* transcript levels were induced nearly 2-fold after salt stress treatment. This suggests that of these tested mTERFs, maize mTERF28 is the strongest candidate participating in all tested stress responses, while mTERF12 might be especially involved in salt stress responses (Zhao et al., 2014). Our results show that in contrast to the strong *mterf* mutant phenotypes which point to essential functions of several mTERFs (Meskauskienė et al., 2009; Babychuk et al., 2011; Romani et al., 2015), lines with altered *MTERF10* or *MTERF11* levels show only conditional phenotypes, which become manifest under adverse growth conditions (see **Figures 7, 9**). Strikingly, under continuous light, lower *MTERF10* levels are associated with reductions in salt tolerance, while oe-mTERF10 lines are more tolerant of salt and ABA than wild-type plants. The altered responsiveness to ABA of *oge* and also plastid signaling mutants has been noted before. For example, the “mitochondrial PPR protein PENTATRICOPEPTIDE REPEAT PROTEIN FOR GERMINATION ON NaCl” (PGN; Laluk et al., 2011), the tetrapyrrole biosynthesis proteins GUN4 and GUN5 (Voigt et al., 2010) and the plastid-targeted PPR protein GUN1 (Cottage et al., 2010) alter responses to ABA. Notably, *gun1* mutants show only subtle growth phenotypes, but GUN1 is an important integrator of plastid signals (Koussevitzky et al., 2007). Like

mTERF proteins, PPR proteins are typically targeted to chloroplasts or mitochondria, and alter expression of transcripts by influencing editing, turnover, processing or translation (Barkan and Small, 2014). With more than 400 members, the PPR protein family is one of the largest in land plants (Barkan and Small, 2014) and far exceeds the mTERF family in size. The enlargement of the plant PPR family has been linked to the evolution of a complex organellar gene expression system that is characteristic for plant organelles (Barkan and Small, 2014), and this is likely to be true of the mTERF protein family also (Kleine, 2012). Moreover, and in contrast to animals, plants are sessile organisms that are exposed to environmental changes and stresses. During evolution, the expansion and functional diversification of protein families has helped plants to successfully adapt to or tolerate different environmental stresses (Quesada, 2016). The mTERF family is a good case study for this phenomenon. With the characterization of an increasing number of plant mTERF proteins, it is becoming evident that they play a wide range of roles in mediating tolerance and acclimation to different abiotic stresses.

AUTHOR CONTRIBUTORS

Research was designed by TK. Research was performed by DX and TK. The manuscript was prepared by DX, DL, and TK.

FUNDING

This work was supported by the Deutsche Forschungsgemeinschaft [KL 2362/1-1 to TK, and TRR175 to DL (project C05) and TK (project C01)].

ACKNOWLEDGMENTS

We thank Elisabeth Gerick for technical assistance and Jörg Nickelsen for providing the RAP construct.

SUPPLEMENTARY MATERIAL

The Supplementary Material for this article can be found online at: <http://journal.frontiersin.org/article/10.3389/fpls.2017.01213/full#supplementary-material>

Supplementary Figure S1 | Quantification of changes in *MTERF10* mRNA expression in response to perturbations as determined with the Genevestigator Perturbations Tool. The tool was employed on all deposited *A. thaliana* ATH1 arrays together with a 2-fold change filter and a p-value of < 0.05.

Supplementary Figure S2 | Quantification of changes in *MTERF11* mRNA expression in response to perturbations as determined with the Genevestigator Perturbations Tool. The tool was employed on all deposited *A. thaliana* ATH1 arrays together with a 2-fold change filter and a p-value of < 0.05.

Supplementary Figure S3 | Quantification of changes in *MTERF12* mRNA expression in response to perturbations as determined with the Genevestigator Perturbations Tool. The tool was employed on all deposited *A. thaliana* ATH1 arrays together with a 2-fold change filter and a p-value of < 0.05.

Supplementary Figure S4 | Behavior of wild-type (Col-0) and *mterf10*, -11 and -12 mutant plants under moderate light stress of 400 μ mol photons

$\text{m}^{-2} \text{s}^{-1}$. **(A)** To score the phenotypes under moderate heat stress, plants were first grown for 3 weeks under normal growth conditions ($100 \mu\text{mol photons m}^{-2} \text{s}^{-1}$, 22°C) and then exposed to $400 \mu\text{mol photons m}^{-2} \text{s}^{-1}$ for 7 days. **(B)** The maximum quantum yield of PSII (F_v/F_m) of Col-0 and

mtorf mutant plants was determined after the indicated periods of exposure to a fluence of $400 \mu\text{mol photons m}^{-2} \text{s}^{-1}$. The data are shown as mean values \pm SD from 8 to 10 different leaves.

Supplementary Table S1 | Primers used in this study.

REFERENCES

- Alonso, J. M., Stepanova, A. N., Leisse, T. J., Kim, C. J., Chen, H., Shinn, P., et al. (2003). Genome-wide insertional mutagenesis of *Arabidopsis thaliana*. *Science* 301, 653–657. doi: 10.1126/science.1086391301/5633/653[pil]
- Babiychuk, E., Vandepoele, K., Wissing, J., Garcia-Diaz, M., De Rycke, R., Akbari, H., et al. (2011). Plastid gene expression and plant development require a plastidic protein of the mitochondrial transcription termination factor family. *Proc. Natl. Acad. Sci. U.S.A.* 108, 6674–6679. doi: 10.1073/pnas.1103442108
- Barkan, A., and Small, I. (2014). Pentatricopeptide repeat proteins in plants. *Annu. Rev. Plant Biol.* 65, 415–442. doi: 10.1146/annurev-arplant-050213-040159
- Börner, T., Aleynikova, A. Y., Zubo, Y. O., and Kusnetsov, V. V. (2015). Chloroplast RNA polymerases: role in chloroplast biogenesis. *Biochim. Biophys. Acta* 1847, 761–769. doi: 10.1016/j.bbabo.2015.02.004
- Camara, Y., Asin-Cayuela, J., Park, C. B., Metodiev, M. D., Shi, Y., Ruzzenente, B., et al. (2011). MTERF4 regulates translation by targeting the methyltransferase NSUN4 to the mammalian mitochondrial ribosome. *Cell Metab.* 13, 527–539. doi: 10.1016/j.cmet.2011.04.002
- Chen, H., Zhang, J., Neff, M. M., Hong, S. W., Zhang, H., Deng, X. W., et al. (2008). Integration of light and abscisic acid signaling during seed germination and early seedling development. *Proc. Natl. Acad. Sci. U.S.A.* 105, 4495–4500. doi: 10.1073/pnas.0710778105
- Chenna, R., Sugawara, H., Koike, T., Lopez, R., Gibson, T. J., Higgins, D. G., et al. (2003). Multiple sequence alignment with the Clustal series of programs. *Nucleic Acids Res.* 31, 3497–3500. doi: 10.1093/nar/gkg500
- Christmann, A., Moes, D., Himmelbach, A., Yang, Y., Tang, Y., and Grill, E. (2006). Integration of abscisic acid signalling into plant responses. *Plant Biol. (Stuttg)* 8, 314–325. doi: 10.1055/s-2006-924120
- Clough, S. J., and Bent, A. F. (1998). Floral dip: a simplified method for *Agrobacterium*-mediated transformation of *Arabidopsis thaliana*. *Plant J.* 16, 735–743. doi: 10.1046/j.1365-313x.1998.00343.x
- Cottage, A., Mott, E. K., Kempster, J. A., and Gray, J. C. (2010). The *Arabidopsis* plastid-signalling mutant gun1 (genomes uncoupled1) shows altered sensitivity to sucrose and abscisic acid and alterations in early seedling development. *J. Exp. Bot.* 61, 3773–3786. doi: 10.1093/jxb/erq186
- Dovzhenko, A., Dal Bosco, C., Meurer, J., and Koop, H. U. (2003). Efficient regeneration from cotyledon protoplasts in *Arabidopsis thaliana*. *Protoplasma* 222, 107–111. doi: 10.1007/s00709-003-0011-9
- Hammani, K., and Barkan, A. (2014). An mTERF domain protein functions in group II intron splicing in maize chloroplasts. *Nucleic Acids Res.* 42, 5033–5042. doi: 10.1093/nar/gku112
- Hammani, K., Bonnard, G., Bouchoucha, A., Gobert, A., Pinker, F., Salinas, T., et al. (2014). Helical repeats modular proteins are major players for organelle gene expression. *Biochimie* 100, 141–150. doi: 10.1016/j.biochi.2013.08.031
- Hruz, T., Laule, O., Szabo, G., Wessendorp, F., Bleuler, S., Oertle, L., et al. (2008). Genevestigator v3: a reference expression database for the meta-analysis of transcriptomes. *Adv. Bioinformatics* 2008:420747. doi: 10.1155/2008/420747
- Hsu, Y. W., Wang, H. J., Hsieh, M. H., Hsieh, H. L., and Jauh, G. Y. (2014). *Arabidopsis* mTERF15 is required for mitochondrial nad2 intron 3 splicing and functional complex I activity. *PLoS ONE* 9:e112360. doi: 10.1371/journal.pone.0112360
- Hu, Y., Chen, L., Wang, H., Zhang, L., Wang, F., and Yu, D. (2013). *Arabidopsis* transcription factor WRKY8 functions antagonistically with its interacting partner VQ9 to modulate salinity stress tolerance. *Plant J.* 74, 730–745. doi: 10.1111/tpj.12159
- Hwang, J. H., Seo, D. H., Kang, B. G., Kwak, J. M., and Kim, W. T. (2015). Suppression of *Arabidopsis* AtPUB30 resulted in increased tolerance to salt stress during germination. *Plant Cell Rep.* 34, 277–289. doi: 10.1007/s00299-014-1706-4
- Karimi, M., Inze, D., and Depicker, A. (2002). GATEWAY vectors for *Agrobacterium*-mediated plant transformation. *Trends Plant Sci.* 7, 193–195. doi: 10.1016/S1360-1385(02)02251-3
- Kim, M., Lee, U., Small, I., des Francs-Small, C. C., and Vierling, E. (2012). Mutations in an *Arabidopsis* mitochondrial transcription termination factor-related protein enhance thermotolerance in the absence of the major molecular chaperone HSP101. *Plant Cell* 24, 3349–3365. doi: 10.1105/tpc.112.101006
- Kleine, T. (2012). *Arabidopsis thaliana* mTERF proteins: evolution and functional classification. *Front. Plant Sci.* 3:233. doi: 10.3389/fpls.2012.00233
- Kleine, T., and Leister, D. (2015). Emerging functions of mammalian and plant mTERFs. *Biochim. Biophys. Acta* 1847, 786–797. doi: 10.1016/j.bbabo.2014.12.009
- Kleinknecht, L., Wang, F., Stube, R., Philippar, K., Nickelsen, J., and Bohne, A. V. (2014). RAP, the sole octatricopeptide repeat protein in *Arabidopsis*, is required for chloroplast 16S rRNA maturation. *Plant Cell* 26, 777–787. doi: 10.1105/tpc.114.122853
- Koussevitzky, S., Nott, A., Mockler, T. C., Hong, F., Sachetto-Martins, G., Surpin, M., et al. (2007). Signals from chloroplasts converge to regulate nuclear gene expression. *Science* 316, 715–719. doi: 10.1126/science.1140516
- Kruse, B., Narasimhan, N., and Attardi, G. (1989). Termination of transcription in human mitochondria: identification and purification of a DNA binding protein factor that promotes termination. *Cell* 58, 391–397. doi: 10.1016/0092-8674(89)90853-2
- Laluk, K., Abuqamar, S., and Mengiste, T. (2011). The *Arabidopsis* mitochondria-localized pentatricopeptide repeat protein PGN functions in defense against necrotrophic fungi and abiotic stress tolerance. *Plant Physiol.* 156, 2053–2068. doi: 10.1104/pp.111.177501
- Liere, K., Weihe, A., and Börner, T. (2011). The transcription machineries of plant mitochondria and chloroplasts: composition, function, and regulation. *J. Plant Physiol.* 168, 1345–1360. doi: 10.1016/j.jplph.2011.01.005
- Linder, T., Park, C. B., Asin-Cayuela, J., Pellegrini, M., Larsson, N. G., Falkenberg, M., et al. (2005). A family of putative transcription termination factors shared amongst metazoans and plants. *Curr. Genet.* 48, 265–269. doi: 10.1007/s00294-005-0022-5
- Majeran, W., Friso, G., Asakura, Y., Qu, X., Huang, M., Ponnala, L., et al. (2012). Nucleoid-enriched proteomes in developing plastids and chloroplasts from maize leaves: a new conceptual framework for nucleoid functions. *Plant Physiol.* 158, 156–189. doi: 10.1104/pp.111.188474
- Meskauskiene, R., Wursch, M., Laloi, C., Vidi, P. A., Coll, N. S., Kessler, F., et al. (2009). A mutation in the *Arabidopsis* mTERF-related plastid protein SOLDAT10 activates retrograde signaling and suppresses $^1\text{O}_2$ -induced cell death. *Plant J.* 60, 399–410. doi: 10.1111/j.1365-313X.2009.03965.x
- Metodiev, M. D., Spahr, H., Loguerio Polosa, P., Meharg, C., Becker, C., Altmueller, J., et al. (2014). NSUN4 is a dual function mitochondrial protein required for both methylation of 12S rRNA and coordination of mitochondrial assembly. *PLoS Genet.* 10:e1004110. doi: 10.1371/journal.pgen.1004110
- Park, C. B., Asin-Cayuela, J., Camara, Y., Shi, Y., Pellegrini, M., Gaspari, M., et al. (2007). MTERF3 is a negative regulator of mammalian mtDNA transcription. *Cell* 130, 273–285. doi: 10.1016/j.cell.2007.05.046
- Pellegrini, M., Asin-Cayuela, J., Erdjument-Bromage, H., Tempst, P., Larsson, N. G., and Gustafsson, C. M. (2009). MTERF2 is a nucleoid component in mammalian mitochondria. *Biochim. Biophys. Acta* 1787, 296–302. doi: 10.1016/j.bbabo.2009.01.018
- Pfalz, J., Liere, K., Kandlbinder, A., Dietz, K. J., and Oelmüller, R. (2006). pTAC2, -6, and -12 are components of the transcriptionally active plastid chromosome that are required for plastid gene expression. *Plant Cell* 18, 176–197. doi: 10.1105/tpc.105.036392
- Pfalz, J., and Pfannschmidt, T. (2013). Essential nucleoid proteins in early chloroplast development. *Trends Plant Sci.* 18, 186–194. doi: 10.1016/j.tplants.2012.11.003

- Quesada, V. (2016). The roles of mitochondrial transcription termination factors (MTERFs) in plants. *Physiol. Plant.* 157, 389–399. doi: 10.1111/ppl.12416
- Quesada, V., Ponce, M. R., and Micol, J. L. (2000). Genetic analysis of salt-tolerant mutants in *Arabidopsis thaliana*. *Genetics* 154, 421–436.
- Quesada, V., Sarmiento-Manus, R., Gonzalez-Bayon, R., Hricova, A., Perez-Marcos, R., Gracia-Martinez, E., et al. (2011). Arabidopsis RUGOSA2 encodes an mTERF family member required for mitochondrion, chloroplast and leaf development. *Plant J.* 68, 738–753. doi: 10.1111/j.1365-3113X.2011.04726.x
- Raven, J. A., and Allen, J. F. (2003). Genomics and chloroplast evolution: what did cyanobacteria do for plants? *Genome Biol.* 4:209.
- Reyes, J. L., and Chua, N. H. (2007). ABA induction of miR159 controls transcript levels of two MYB factors during Arabidopsis seed germination. *Plant J.* 49, 592–606. doi: 10.1111/j.1365-3113X.2006.02980.x
- Robles, P., Micol, J. L., and Quesada, V. (2012). Arabidopsis MDA1, a nuclear-encoded protein, functions in chloroplast development and abiotic stress responses. *PLoS ONE* 7:e42924. doi: 10.1371/journal.pone.0042924
- Robles, P., Micol, J. L., and Quesada, V. (2015). Mutations in the plant-conserved MTERF9 alter chloroplast gene expression, development and tolerance to abiotic stress in *Arabidopsis thaliana*. *Physiol. Plant.* 154, 297–313. doi: 10.1111/ppl.12307
- Romani, I., Manavski, N., Morosetti, A., Tadini, L., Maier, S., Kuhn, K., et al. (2015). A member of the arabidopsis mitochondrial transcription termination factor family is required for maturation of chloroplast transfer RNA^{Leu}(GAU). *Plant Physiol.* 169, 627–646. doi: 10.1104/pp.15.00964
- Sah, S. K., Reddy, K. R., and Li, J. (2016). Abscisic acid and abiotic stress tolerance in crop plants. *Front. Plant Sci.* 7:571. doi: 10.3389/fpls.2016.00571
- Samson, F., Brunaud, V., Balzergue, S., Dubreucq, B., Lepiniec, L., Pelletier, G., et al. (2002). FLAGdb/FST: a database of mapped flanking insertion sites (FSTs) of *Arabidopsis thaliana* T-DNA transformants. *Nucleic Acids Res.* 30, 94–97. doi: 10.1093/nar/30.1.94
- Schmitz-Linneweber, C., and Small, I. (2008). Pentatricopeptide repeat proteins: a socket set for organelle gene expression. *Trends Plant Sci.* 13, 663–670. doi: 10.1016/j.tplants.2008.10.001
- Shi, Y., Posse, V., Zhu, X., Hyvarinen, A. K., Jacobs, H. T., Falkenberg, M., et al. (2016). Mitochondrial transcription termination factor 1 directs polar replication fork pausing. *Nucleic Acids Res.* 44, 5732–5742. doi: 10.1093/nar/gkw302
- Shkolnik-Inbar, D., Adler, G., and Bar-Zvi, D. (2013). ABI4 downregulates expression of the sodium transporter HKT1;1 in Arabidopsis roots and affects salt tolerance. *Plant J.* 73, 993–1005. doi: 10.1111/tpj.12091
- Stern, D. B., Goldschmidt-Clermont, M., and Hanson, M. R. (2010). Chloroplast RNA metabolism. *Annu. Rev. Plant Biol.* 61, 125–155. doi: 10.1146/annurev-arplant-042809-112242
- Terzioğlu, M., Ruzzenente, B., Harmel, J., Mourier, A., Jemt, E., Lopez, M. D., et al. (2013). MTERF1 binds mtDNA to prevent transcriptional interference at the light-strand promoter but is dispensable for rRNA gene transcription regulation. *Cell Metab.* 17, 618–626. doi: 10.1016/j.cmet.2013.03.006
- Tiller, N., and Bock, R. (2014). The translational apparatus of plastids and its role in plant development. *Mol. Plant* 7, 1105–1120. doi: 10.1093/mp/ssu022
- Ulker, B., Peiter, E., Dixon, D. P., Moffat, C., Capper, R., Bouche, N., et al. (2008). Getting the most out of publicly available T-DNA insertion lines. *Plant J.* 56, 665–677. doi: 10.1111/j.1365-3113X.2008.03608.x
- Voigt, C., Oster, U., Bornke, F., Jahns, P., Dietz, K. J., Leister, D., et al. (2010). In-depth analysis of the distinctive effects of norflurazon implies that tetrapyrrole biosynthesis, organellar gene expression and ABA cooperate in the GUN-type of plastid signalling. *Physiol. Plant.* 138, 503–519. doi: 10.1111/j.1399-3054.2009.01343.x
- Wang, Y., Zhang, W. Z., Song, L. F., Zou, J. J., Su, Z., and Wu, W. H. (2008). Transcriptome analyses show changes in gene expression to accompany pollen germination and tube growth in Arabidopsis. *Plant Physiol.* 148, 1201–1211. doi: 10.1104/pp.108.126375
- Wenz, T., Luca, C., Torraco, A., and Moraes, C. T. (2009). mTERF2 regulates oxidative phosphorylation by modulating mtDNA transcription. *Cell Metab.* 9, 499–511. doi: 10.1016/j.cmet.2009.04.010
- Winter, D., Vinegar, B., Nahal, H., Ammar, R., Wilson, G. V., and Provart, N. J. (2007). An “Electronic Fluorescent Pictograph” browser for exploring and analyzing large-scale biological data sets. *PLoS ONE* 2:e718. doi: 10.1371/journal.pone.0000718
- Wredenberg, A., Lagouge, M., Bratic, A., Metodiev, M. D., Spahr, H., Mourier, A., et al. (2013). MTERF3 regulates mitochondrial ribosome biogenesis in invertebrates and mammals. *PLoS Genet.* 9:e1003178. doi: 10.1371/journal.pgen.1003178
- Zhao, Y., Cai, M., Zhang, X., Li, Y., Zhang, J., Zhao, H., et al. (2014). Genome-wide identification, evolution and expression analysis of mTERF gene family in maize. *PLoS ONE* 9:e94126. doi: 10.1371/journal.pone.0094126
- Zhou, B., Zhang, L., Ullah, A., Jin, X., Yang, X., and Zhang, X. (2016). Identification of multiple stress responsive genes by sequencing a normalized cDNA library from sea-land cotton (*Gossypium barbadense* L.). *PLoS ONE* 11:e0152927. doi: 10.1371/journal.pone.0152927

Conflict of Interest Statement: The authors declare that the research was conducted in the absence of any commercial or financial relationships that could be construed as a potential conflict of interest.

Copyright © 2017 Xu, Leister and Kleine. This is an open-access article distributed under the terms of the Creative Commons Attribution License (CC BY). The use, distribution or reproduction in other forums is permitted, provided the original author(s) or licensor are credited and that the original publication in this journal is cited, in accordance with accepted academic practice. No use, distribution or reproduction is permitted which does not comply with these terms.

3.4 Chapter 4

Cellulose defects in the Arabidopsis secondary cell wall promote early chloroplast development

Cellulose defects in the Arabidopsis secondary cell wall promote early chloroplast development

Duorong Xu¹ , Ravi Dhiman¹, Adriana Garibay², Hans-Peter Mock², Dario Leister¹ and Tatjana Kleine^{1,*} 

¹Plant Molecular Biology, Faculty of Biology, Ludwig-Maximilians University of Munich, Großhaderner Str. 2, 82152, Planegg-Martinsried, Germany, and

²Department of Physiology and Cell Biology, Leibniz Institute of Plant Genetics and Crop Plant Research (IPK-Gatersleben), Corrensstraße 3, 06466, Stadt Seeland, OT Gatersleben, Germany

Received 15 May 2019; revised 12 August 2019; accepted 28 August 2019; published online 9 September 2019.

*For correspondence (e-mail tatjana.kleine@lmu.de).

SUMMARY

Lincomycin (LIN)-mediated inhibition of protein synthesis in chloroplasts prevents the greening of seedlings, represses the activity of photosynthesis-related genes in the nucleus, including *LHCB1.2*, and induces the phenylpropanoid pathway, resulting in the production of anthocyanins. In *genomes uncoupled* (*gun*) mutants, *LHCB1.2* expression is maintained in the presence of LIN or other inhibitors of early chloroplast development. In a screen using concentrations of LIN lower than those employed to isolate *gun* mutants, we have identified *happy on lincomycin* (*holi*) mutants. Several *holi* mutants show an increased tolerance to LIN, exhibiting de-repressed *LHCB1.2* expression and chlorophyll synthesis in seedlings. The mutations responsible were identified by whole-genome single-nucleotide polymorphism (SNP) mapping, and most were found to affect the phenylpropanoid pathway; however, *LHCB1.2* expression does not appear to be directly regulated by phenylpropanoids, as indicated by the metabolic profiling of mutants. The most potent *holi* mutant is defective in a subunit of cellulose synthase encoded by *IRREGULAR XYLEM 3*, and comparative analysis of this and other cell-wall mutants establishes a link between secondary cell-wall integrity and early chloroplast development, possibly involving altered ABA metabolism or sensing.

Keywords: chloroplast, lincomycin, retrograde signaling, cell wall, phenylpropanoids.

INTRODUCTION

The vast majority of the several thousand proteins found in plastids are encoded by nuclear genes (Timmis *et al.*, 2004). As endosymbiotic descendants of cyanobacteria, however, plastids still contain 80–230 genes, most of which are involved in essential plastid functions like energy production and plastid gene expression (PGE) (Ponce-Toledo *et al.*, 2017). As a result, plastid multiprotein complexes (including the photosystems and ribosomes) consist of subunits encoded by both the nuclear and plastid genomes. This in turn accounts for the need for coordination of PGE and nuclear gene expression (NGE). Thus, the nucleus influences activity in the plastids, including PGE, via ‘anterograde control/signaling’ (Stern *et al.*, 2010), whereas plastids communicate their developmental and metabolic status to the nucleus via ‘retrograde signaling’, allowing the nucleus to adjust NGE appropriately (Kleine *et al.*, 2009; Chi *et al.*, 2013; Terry and Smith, 2013; Chan *et al.*, 2016; Kleine and Leister, 2016). Plastid-derived retrograde

signals can be divided into two classes: signals related to the operation of the plastid under changing environmental conditions (operational control) and signals triggered by changes in plastid and photosystem biogenesis (biogenic control) (Chan *et al.*, 2016).

Forward-genetic screens have permitted the identification of components involved in retrograde signaling pathways (Kleine and Leister, 2016). They have exploited the fact that the expression of nuclear genes for plastid proteins like *LHCB1.2* (a major light-harvesting chlorophyll *a/b*-binding protein) is reduced in seedlings exposed to inhibitors of PGE (e.g. lincomycin, LIN) or carotenoid biosynthesis (e.g. norflurazon, NF) (Oelmüller and Mohr, 1986; Oelmüller *et al.*, 1986). The first mutant screen specifically designed to characterize components of biogenic plastid signaling was performed with *Arabidopsis thaliana* seedlings grown on NF (Susek *et al.*, 1993), and identified mutant seedlings that continued to accumulate *LHCB1.2* transcripts. Five different *genomes uncoupled* (*gun*)

mutants were initially isolated (Susek *et al.*, 1993; Mochizuki *et al.*, 2001). *GUN1* codes for a nucleic-acid-binding chloroplast protein (Koussevitzky *et al.*, 2007), whereas *GUN2–GUN5* encode enzymes of the tetrapyrrole biosynthesis pathway (Mochizuki *et al.*, 2001; Larkin *et al.*, 2003). Subsequent investigations of the *gun* mutants led to contradictory conclusions as to a putative plastid signaling function of the tetrapyrrole pathway intermediate Mg-protoporphyrin IX (Strand *et al.*, 2003; Mochizuki *et al.*, 2008; Moulin *et al.*, 2008). To resolve these discrepancies, a gain-of-function screen based on activation tagging was conducted in the reporter line that was used in the original *gun* mutant screen (Woodson *et al.*, 2011). This screen identified the *gun6-1D* mutant, which overexpresses ferrochelatase 1 (FC1), and prompted the proposal that the tetrapyrrole heme – specifically the fraction produced by FC1 – might function as a biogenic retrograde signal (Woodson *et al.*, 2011; Terry and Smith, 2013). With the intention of identifying additional mutants with more subtle *gun* phenotypes than those detected in the original screen (Susek *et al.*, 1993), a transgenic line in which the *LHCB1.1* promoter was fused to the more sensitive reporter luciferase was used in a further screen (Ruckle *et al.*, 2007), and mutants that exhibited a *gun* phenotype on NF were also tested on LIN-containing medium. As a result, four *cryptochrome 1* (*cry1*) alleles and *long hypocotyl 5* (*hy5*) were identified (Ruckle *et al.*, 2007). More recently, overexpressors of GLK1 or GLK2 have been shown to behave like strong *gun* mutants when challenged with NF or LIN (Leister and Kleine, 2016; Martin *et al.*, 2016).

Inhibitors like NF and LIN have numerous secondary effects, however: for example, the massive accumulation of anthocyanins (Cottage *et al.*, 2010; Voigt *et al.*, 2010). A modified version of the *gun* mutant screen was therefore designed, which used less NF and a lower light intensity, and resulted in fewer side effects, primarily by avoiding anthocyanin accumulation (Saini *et al.*, 2011). Unlike the original *gun* mutants and wild-type (WT) plants, the *happy on norflurazon* (*hon*) mutants recovered in this screen remained green in the presence of (lower doses of) NF. The *hon* mutations were mapped to ClpR4, a nucleus-encoded subunit of the plastid-localized Clp protease complex, and to a putative chloroplast translation elongation factor, and thus are likely to interfere with PGE and plastid protein homeostasis (Saini *et al.*, 2011).

Lincomycin and NF have similar effects on *gun1*, *hy5* and *cry1* (Ruckle *et al.*, 2007) mutants, as well as on the GLK overexpressors (Leister and Kleine, 2016; Martin *et al.*, 2016), but *gun2*, *gun4* and *gun5* mutants differ in their responses to these agents (Gray *et al.*, 2003). This distinction suggests that NF and LIN trigger at least partially different signaling pathways.

In an effort to isolate additional *gun* mutants specifically for the LIN pathway(s), we screened an ethyl

methanesulfonate (EMS)-mutagenized *A. thaliana* Col-0 population grown in the presence of a greater than fourfold lower dose of LIN than that used in the earlier screens. In this way, *happy on lincomycin* (*holi*) mutants that are able to green in the presence of LIN were identified. In a second screen with a fivefold lower NF concentration relative to that used in the original screens, we identified additional *hon* mutants. Characterization of these mutants suggested that: (i) there is no correlation between *gun* signaling and anthocyanin biosynthesis; and (ii) early chloroplast development is linked to cell-wall integrity.

RESULTS

Isolation of *happy on lincomycin* (*holi*) mutants

Seedlings grown on LIN experience severe photo-oxidative damage, plastid biogenesis is arrested at a proplastid-like stage, even under normal light conditions (Oelmüller and Mohr, 1986), and the expression of nuclear genes encoding chloroplast proteins is altered (Oelmüller *et al.*, 1986). In screens intended to isolate mutants displaying the *gun* phenotype on LIN, a concentration of 220 $\mu\text{g ml}^{-1}$ LIN (high LIN) and light intensities of 100–125 $\mu\text{mol photons m}^{-2} \text{sec}^{-1}$ were used (Koussevitzky *et al.*, 2007; Ruckle *et al.*, 2007). Under such conditions, 5-day-old

A. thaliana Col-0 seedlings were retarded in growth, failed to green and accumulated appreciable concentrations of anthocyanins (Figure 1a). Using the same light intensity as in previous screens, we gradually reduced the LIN concentration until the coloration of the seedling population turned from purple (as a result of anthocyanin production) to greenish or white. Although some seedlings turned light green with a concentration of 25 $\mu\text{g ml}^{-1}$ LIN, growth on 50 $\mu\text{g ml}^{-1}$ LIN (low LIN) produced uniformly purple-colored seedlings (Figure 1a). The latter concentration was still sufficient to reduce the accumulation of the nucleus-encoded transcripts encoding the chloroplast proteins *Lhcb1.2* and *CA1* to 8.0% (high LIN, 1.5%) and 6% (high LIN, 1.0%), respectively, of the levels seen in MS-grown seedlings (Figure 1b). Thus, this low LIN dose still activates retrograde signaling. The *gun1-1* mutant used as a control accumulated fewer anthocyanins than the WT when grown on high LIN, confirming a previous finding (Cottage *et al.*, 2010). Approximately half of the *gun1-1* seedlings grown on low LIN displayed whitish cotyledons, which were larger than those of the WT (Figure 1a).

Based on these observations, a screen was set up to identify mutants with an altered, visually discernible phenotype on low LIN. To this end, Col-0 seeds were mutagenized with EMS. The M₁ plants were grown to maturity to produce M₂ seeds, and ~20 000 4- to 5-day-old M₂ seedlings were grown on low LIN and screened for alterations in the color or size of cotyledons. This led to the isolation of six *holi* mutants (Figure 2). The mutants *holi1* and *holi3*

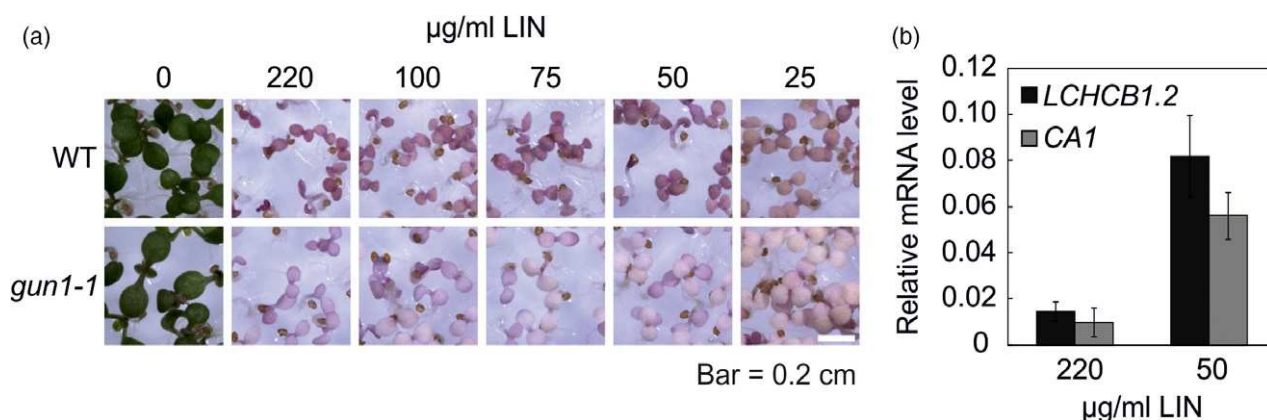


Figure 1. Effects of different lincomycin (LIN) doses on seedling development and nuclear transcript levels. (a) Pictures of wild-type (WT) and *gun1-1* seedlings grown for 5 days on MS supplemented with the indicated concentrations of LIN. (b) Quantitative reverse-transcriptase PCR was used to determine *LHCB1.2* and *CA1* mRNA levels in WT seedlings grown under continuous light ($100 \mu\text{mol photons m}^{-2} \text{sec}^{-1}$) on MS plates without inhibitor or supplemented with either $50 \mu\text{g ml}^{-1}$ LIN or $220 \mu\text{g ml}^{-1}$ LIN. The levels of *LHCB1.2* and *CA1* mRNA are expressed relative to those in the WT control (grown in the absence of inhibitor), which was set to 1. The results were normalized to the expression level of *AT4G36800*. Mean values were derived from two independent experiments, each with three technical replicates. Error bars indicate standard deviations.

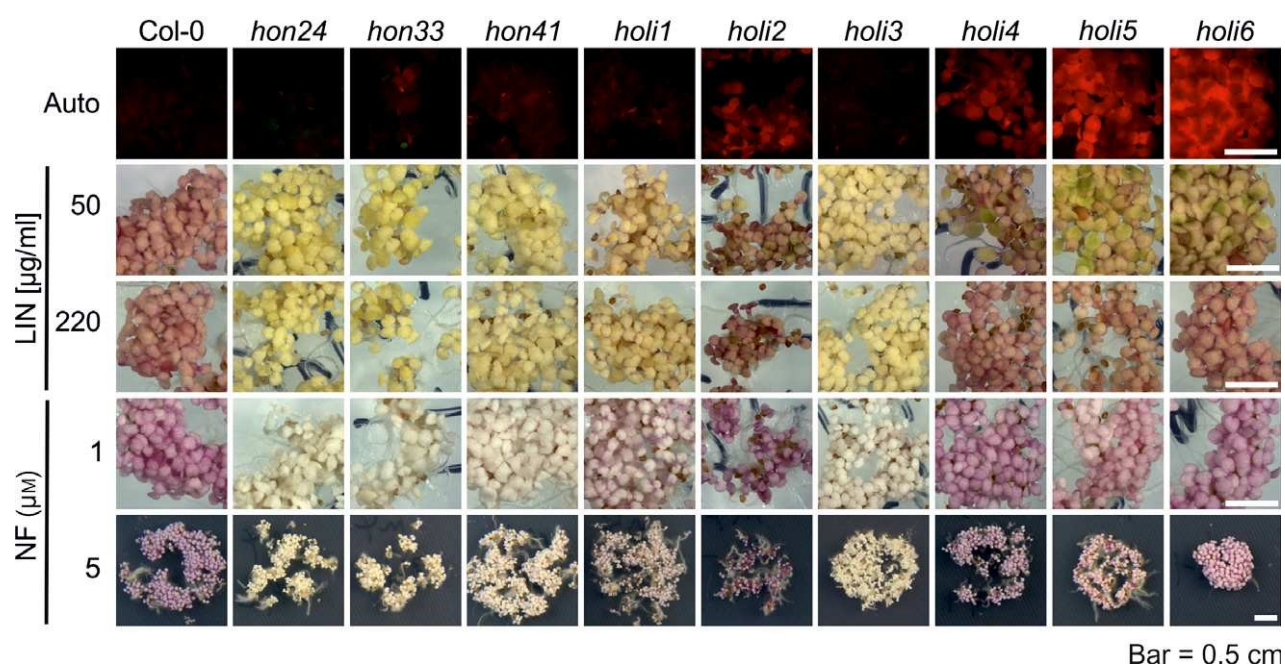


Figure 2. Phenotypes of identified *holi* and *hon* mutants grown in the presence of lincomycin (LIN) or norflurazon (NF). Wild-type (WT), *holi* and *hon* mutant seedlings were grown for 5 days under continuous light ($100 \mu\text{mol photons m}^{-2} \text{sec}^{-1}$) on MS plates supplemented with either LIN (50 or $220 \mu\text{g ml}^{-1}$) or NF (1 or $5 \mu\text{M}$). Autofluorescence after UV excitation was monitored in seedlings grown on MS plates supplemented with $50 \mu\text{g ml}^{-1}$ LIN. The red autofluorescence was used as an indicator for chlorophyll accumulation.

had yellowish cotyledons and did not accumulate anthocyanins. Cotyledons of the other mutants turned light green and accumulated anthocyanins to various levels. When grown on high levels of LIN, *holi2* displayed smaller cotyledons and hyperaccumulation of anthocyanins compared with all other mutants and the WT (Figure 2). A similar screen in which low LIN was replaced by low NF ($1 \mu\text{M}$, instead of the $5 \mu\text{M}$ NF used in the original *gun* mutant

screen; Susek *et al.*, 1993) aimed to identify new *hon* mutants. This screen yielded *hon* mutants (*hon24*, *hon33* and *hon41*) with completely white cotyledons. On low LIN, the cotyledons of these *hon* mutants also appeared yellow-greenish, like those of the *holi* mutants (Figure 2). To confirm that the greenish color was caused by chlorophyll accumulation, autofluorescence was monitored after UV excitation of seedlings grown on low LIN (Figure 2). Col-0,

holi3 and *hon24* seedlings displayed no autofluorescence, as expected when chlorophyll is absent; however, four mutants (*holi2*, *holi4*, *holi5* and *holi6*) displayed marked levels of autofluorescence, whereas three others (*holi1*, *hon33* and *hon41*) displayed weaker autofluorescence. Notably, none of the *hon* or *holi* mutants appeared greener on either high or low NF (Figure 2), in agreement with the absence of chlorophyll autofluorescence observed under these conditions.

Several *holi* mutants display a *gun* phenotype on low LIN

The chlorophyll-autofluorescence phenotype of some of the *hon* and *holi* mutants prompted us to test whether their continued plastid development despite growth on LIN was associated with altered signaling to the nucleus. To this end, RNA was prepared from 5-day-old Col-0, *gun1-1*, and the various *hon* and *holi* mutant seedlings grown on low LIN, and subjected to Northern analysis to determine the steady-state levels of *LHCB1.2* mRNA. Following exposure to the low LIN concentration, the *gun1-1* mutant showed, as expected, higher *LHCB1.2* mRNA expression than the WT (Figure 3). Remarkably, *LHCB1.2* mRNA levels in the *holi2*, *holi4*, *holi5* and *holi6* mutants were comparable with, or even higher than, that of the *gun1-1* mutant. Under control conditions (without inhibitor treatment), however, *LHCB1.2* mRNA levels were already slightly elevated in the *holi2*, *holi3*, *holi5* and *holi6* mutants, which means that the *gun* phenotype on low LIN was relativized by around 1.7-fold (Figure 3). Grown on low NF, some of the *holi* mutants also displayed very weak *gun* phenotypes. But none of the identified *hon* and *holi* mutants behaved like a *gun* mutant when grown on high NF or high LIN (Figure 3).

The majority of *HOLI* and *HON* loci encode proteins involved in the flavonoid pathway

In order to explain the ability of some of the identified mutants to accumulate chlorophyll and maintain *LHCB1.2* transcript accumulation in the presence of low LIN, the M₄ generation of the mutant plants was back-crossed to their parent Col-0, and seedlings displaying recessive and semi-dominant (in the case of *holi2*) mutant phenotypes were identified in the F₂ generation. The underlying mutations were localized by next-generation sequencing (see Experimental procedures) and confirmed by Sanger sequencing.

The *holi1* and *hon41* mutations turned out to be allelic, and both were mapped to the gene for the transcription factor MYB DOMAIN PROTEIN 75 (MYB75; PRODUCTION OF ANTHOCYANIN PIGMENT 1, PAP1). The C@T substitution at nucleotide (nt) 902 (relative to the start codon, as also in the following) in *holi1* results in the replacement of an Arg by an Lys residue and permits some anthocyanin accumulation, whereas in *hon41* a C@T substitution at nt 39 introduces a stop codon in the first exon (Figure 4), completely blocking anthocyanin accumulation (Figure 2).

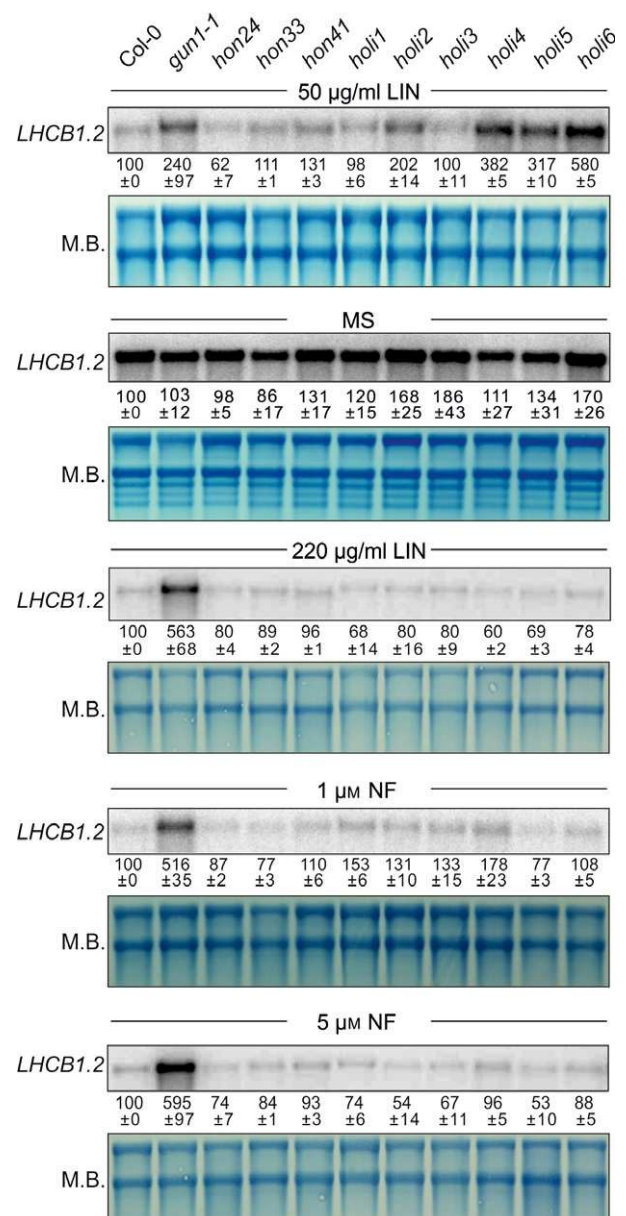


Figure 3. *LHCB1.2* transcript levels found in WT, *gun1-1*, *holi* and *hon* mutant seedlings grown without inhibitor or in the presence of lincomycin (LIN) or norflurazon (NF). Seedlings were grown for 5 days under continuous light (100 µmol photons m⁻² sec⁻¹) on MS plates without inhibitor or supplemented with either LIN (50 or 220 µg ml⁻¹) or NF (1 or 5 µM). *LHCB1.2* mRNA levels were determined by Northern blot analyses. The methylene blue-stained blots served as loading controls (M.B.).

Moreover, in *holi3* a Trp codon is replaced by a stop in the gene for the transcription factor TRANSPARENT TESTA GLABRA 1 (TTG1, required for purple anthocyanin accumulation). The G@A substitution at nt 10 in *hon24* and the C@T substitution at nt 987 in *hon33* caused non-sense mutations in DIHYDROFLAVONOL 4-REDUCTASE (DFR; TRANSPARENT TESTA 3, TT3) and ANTHOCYANIDIN

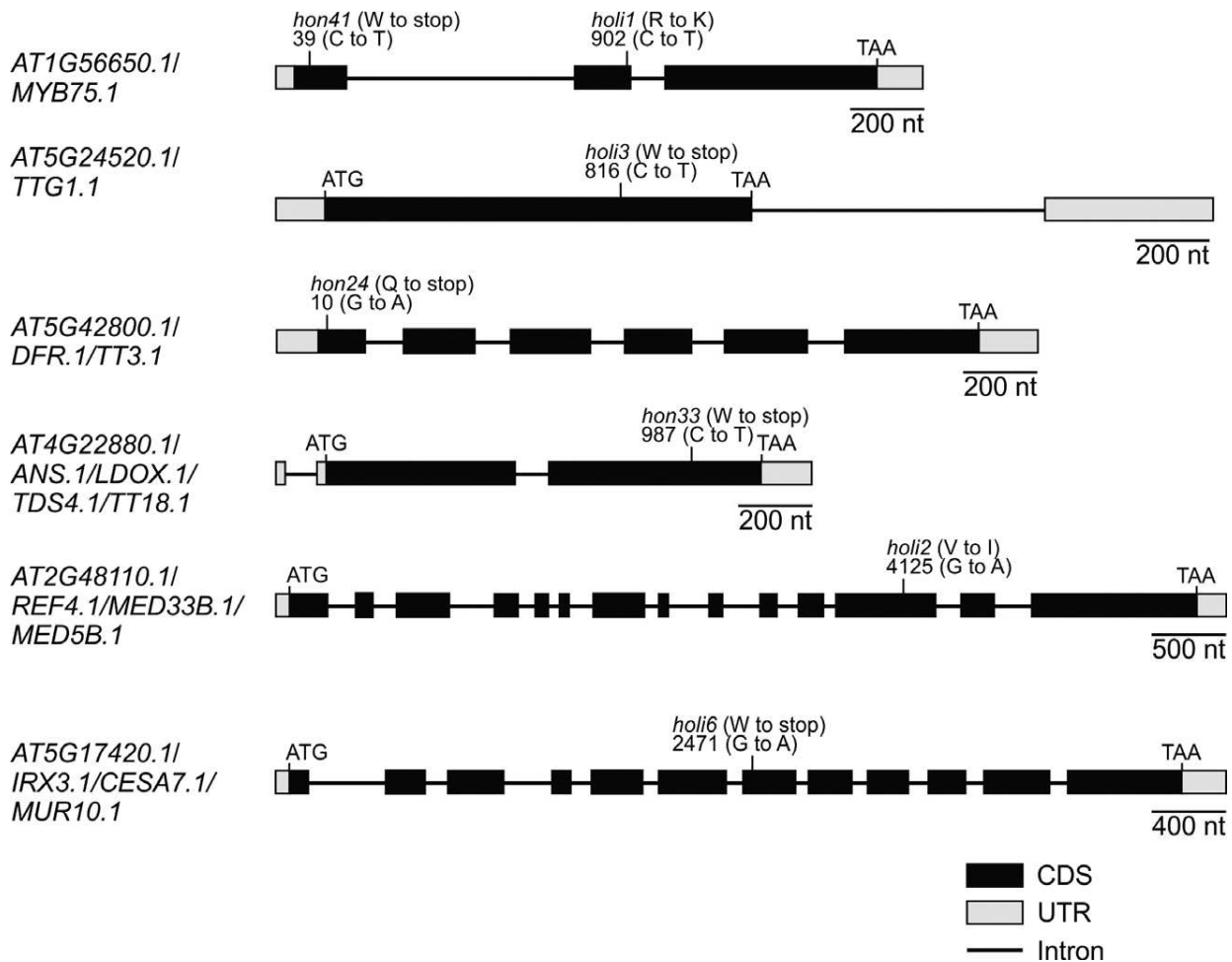


Figure 4. Schematic representation of the positions of identified *HOLI* and *HON* mutation sites. Exons (black boxes), introns (black lines), and the 5' and 3' untranslated regions (UTRs; grey boxes) are shown. Numbers are given relative to the start codon ATG.

SYNTHASE (ANS; LEUCOANTHOCYANIDIN DIOXYGENASE, LDOX; TANNIN DEFICIENT SEED 4, TDS4; TT18), respectively. The mutation that most probably causes the *holi2* mutant phenotype is located at nt 4125, and replaces a Val by an ile residue in *REDUCED EPIDERMAL FLUORESCENCE 4* (*REF4*; *MEDIATOR COMPLEX MED5B*, *MED5B*; *MED33B*). The G→A substitution in *holi6* introduces a premature stop in exon 7 of *IRREGULAR XYLEM 3* (*IRX3*; *CELLULOSE SYNTHASE 7*, *CESA7*; *MURUS 10*, *MUR10*). The mutations responsible for the *holi4* and *holi5* phenotypes could not be identified. With the exception of *IRX3*, all affected proteins have previously been shown to be involved in phenylpropanoid metabolism (Figure S1; Stout *et al.*, 2008; Appelhagen *et al.*, 2014). *MYB75* and *TTG1* are transcription factors, and *DFR* and *ANS* are enzymes that convert dihydroquercetin to leucocyanidin (*DFR*) and leucocyanidin to cyanidin, respectively (Figure S1). *REF4* is required for phenylpropanoid homeostasis and has been shown to interact directly with the conserved transcriptional coregulatory complex Mediator (Bonawitz

et al., 2012).

Disturbances in the phenylpropanoid pathway do not confer a *gun* phenotype

Anthocyanins are produced via the flavonoid pathway, which is a branch of the general phenylpropanoid biosynthetic pathway (Tohge *et al.*, 2005; Appelhagen *et al.*, 2014). The *gun1-1* mutant clearly accumulates less anthocyanin than the WT when grown on both low and high LIN concentrations (Figure 1a), and it was noted previously that *gun2*, *gun4* and *gun5* mutants accumulate less anthocyanin than WT plants when grown on high NF (Voigt *et al.*, 2010). Therefore, the growth of 5-day-old *gun1*, *gun4* and *gun5* mutant seedlings was also tested under our reduced inhibitor conditions (Figure S2). In the WT, *gun1-1* and *gun1-102* seedlings, anthocyanin accumulation was clearly discernible in seedlings grown on low and high NF in continuous white light; however, on high NF, the

stronger *gun1* allele (*gun1-102*) displayed slightly less anthocyanin accumulation than the weaker allele (*gun1-1*) (Figure S2). In contrast, *gun4-1* and *gun5-1* accumulated less anthocyanin on both NF concentrations, whereas they accumulated WT levels of anthocyanins on high LIN. It has previously been speculated that plastid signals that require GUN2–GUN5 might stimulate anthocyanin biosynthesis, although anthocyanin content and *LHCB1.2* mRNA accumulation in *gun* mutants are not strictly correlated (Voigt *et al.*, 2010). As these authors considered only the accumulation of visible anthocyanins, reverse-phase ultra-performance liquid chromatography (UPLC) was used to profile the accumulation of phenylpropanoids in 5-day-old Col-0, *gun1-1*, *gun2-1*, *gun4-1* and *gun5-1* seedlings grown on MS in the absence or presence of high NF or high LIN. In the WT, high NF and high LIN caused approximately 2.0- and 1.5-fold increases in the total phenylpropanoid content, respectively (Figure S3; Table S1). Total phenylpropanoids were similarly boosted in the *gun2-1*, *gun4-1* and *gun5-1* mutants, but in *gun1-1* they were approximately 1.5-fold induced after NF treatment and not induced at all by treatment with high LIN. A closer look at the accumulation of specific phenylpropanoid components revealed that the difference between *gun1-1* and the WT is mainly attributable to a lack of induction of kaempferol derivatives in *gun1-1* (Figure S3; Table S1). In particular, kaempferol 3-O-[6"-O-(rhamnosyl) glucoside] 7-O-rhamnoside (k3; see also Figure S1) was less effectively induced in all investigated *gun* mutants after NF treatment, as well as in *gun1-1* after LIN treatment; none of the other detected compounds showed any consistent alteration in the *gun* mutants relative to the WT (Figure S3; Table S1). Levels of k3 are also reduced in the UDP-glucosyl transferase *ugt78d1 ugt78d2* mutant (Yin *et al.*, 2014). To definitively clarify whether disturbances in the phenylpropanoid pathway are linked to chloroplast development and/or a *gun* phenotype in the presence of inhibitors, 5-day-old *ugt78d1 ugt78d2* mutants, together with mutants impaired in enzymatic steps of the general phenylpropanoid pathway (Figure S1), or regulatory factors of flavonoid biosynthesis and transporters involved in proanthocyanidin accumulation (Appelhaugen *et al.*, 2014), were first tested for chlorophyll autofluorescence on low LIN (Figure 5). Because *cry1* mutants were previously identified as weak *gun* mutants on high LIN (Ruckle *et al.*, 2007), the mutants *cry1-304* and *cry1-304 cry2-1*, and the constitutive photomorphogenesis mutant *cop1-4*, were included as controls together with *gun1-1*. Chlorophyll autofluorescence could be detected in *gun1-1*, *cry1-304*, *cry1-304 cry2-1*, as well as in the *cop1-4* mutant (Figure 5). All transport-related and regulation mutants showed some chlorophyll fluorescence, although this was restricted to the hypocotyl in *ttg1-22*, *ttg2-5* and *tt8-6* mutants. The biosynthesis mutants

tt4-15, *tt5-2*, *tt7-7*, *tt3-1* and *tds4-2* showed the greenish fluorescence typical of kaempferol derivatives (Appelhaugen *et al.*, 2014) and only very weak or no chlorophyll autofluorescence (Figure 5). These mutants are defective in steps in the main pathway leading from chalcone synthase (*tt4-15*) to the conversion of leucocyanidin to cyanidin (*tds4-2*), which is the branch point for the production of anthocyanins and oxidized tannins (Figure S1). Thus, these mutants do not accumulate anthocyanins. The *ban-5*, *tt15-4*, *tt6-2* and *fls1-3* mutants displayed similar levels of chlorophyll fluorescence to the *gun1-1* and *cry1-304* mutants and the transport-related *aha10-6* mutant. The *tt10-8* mutant showed the strongest chlorophyll autofluorescence, which was reflected in a light greenish cotyledon phenotype, with some cotyledons even exhibiting a brighter green color (Figure 5).

When grown in the presence of low LIN or high NF, *gun1-1*, *cry1-304* and *cry1-304 cry2-1* seedlings accumulated *LHCB1.2* in the presence of the inhibitors but, in accordance with Ruckle *et al.* (2007), the *cop1-4* mutant did not (Figure 6a). It is noteworthy here that *cry1* and *cry1 cry2* seedlings grown on low LIN accumulated even higher levels of *LHCB1.2* mRNA than *gun1-1*. The *ugt78d1 ugt78d2* mutant (in which k3 is diminished) and the other phenylpropanoid mutants did not accumulate *LHCB1.2* mRNA, with the sole exception of the *tt10-8* mutant, which continued to express *LHCB1.2* in the presence of low LIN but not in the presence of high NF (Figure 6b). TT10/LAC15 is similar to laccase-like polyphenol oxidases and is involved in lignin biosynthesis (Liang *et al.*, 2006).

Taken together, these data imply that there is no direct link between phenylpropanoid accumulation and *gun* signaling.

A defect in the secondary cell wall promotes seedling greening

The *holi6* mutant was among the identified mutants that displayed the strongest chlorophyll autofluorescence when grown on MS plates supplemented with low LIN (Figure 2). To confirm that the premature stop in *IRX3* (*CESA7*) found in *holi6* was responsible for this phenotype, two additional *irx3* mutant alleles, *irx3-2* (confirmation of the T-DNA insertion and a lack of the full-length transcript is shown in Figure S4) and *irx3-4* (Brown *et al.*, 2005), were grown on low LIN. Indeed, the cotyledons of *irx3-2* and *irx3-4* were visibly greener and displayed higher autofluorescence than the cotyledons of the WT (Figure 7a), which is reflective of a higher chlorophyll content (Figure 7b). Moreover, although attempts to determine the maximum quantum yield of photosystem II (F_v/F_m) with an Imaging PAM fluorometer were unsuccessful in WT grown on low LIN, this parameter could be measured in *holi6*, and *irx3-2* and *irx3-4* displayed even higher F_v/F_m values (Figure 7a).

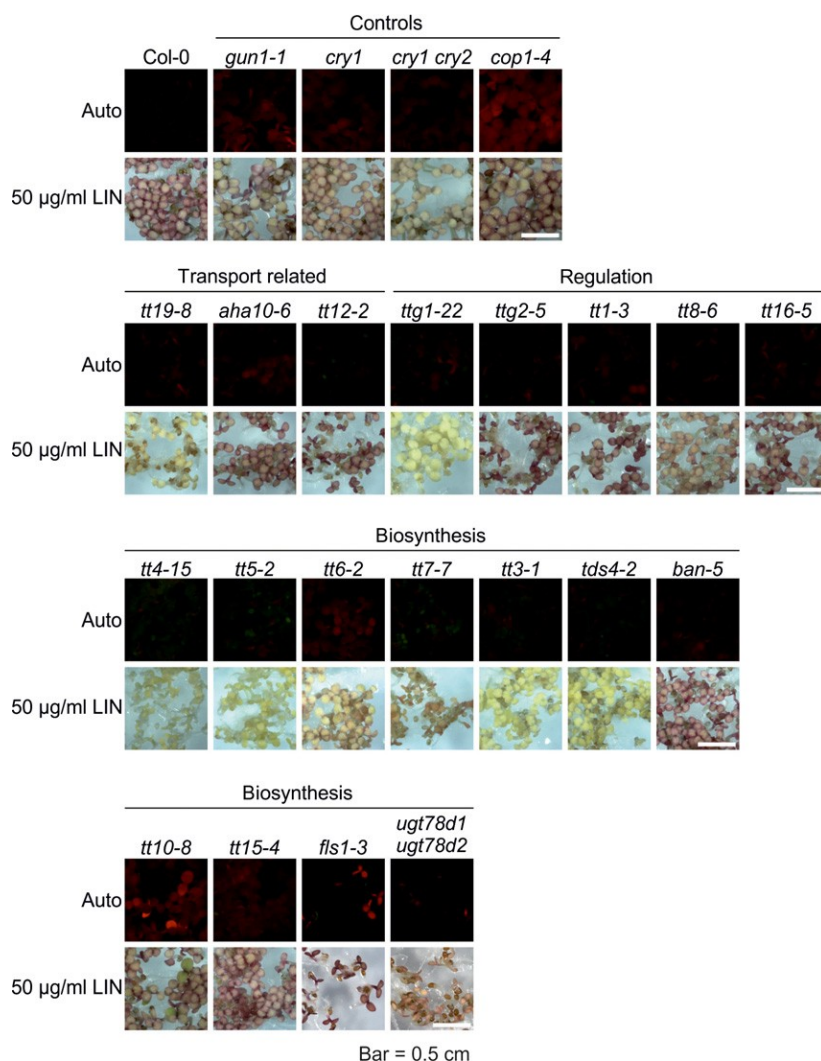


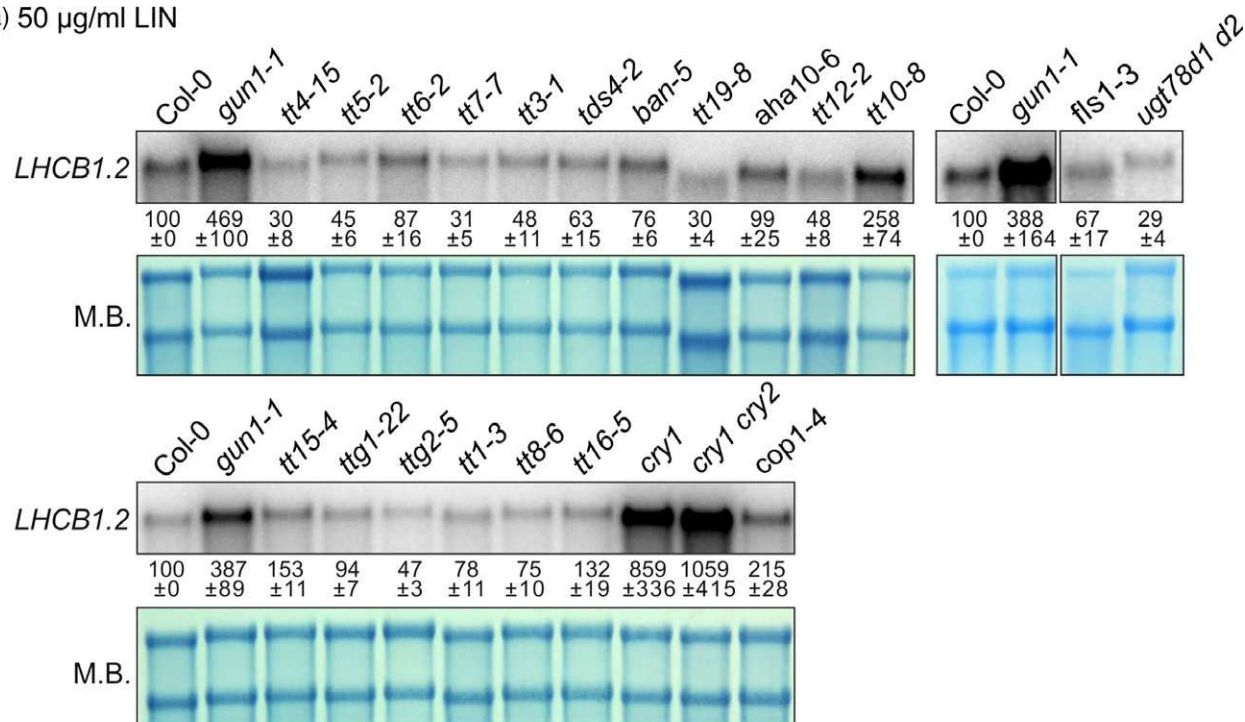
Figure 5. Phenotypes of the wild type (WT), *gun1*, *cry1*, *cry1 cry2*, *cop1-4* and mutants associated with phenylpropanoid biosynthesis grown on low lincomycin (LIN). WT, *gun1-1* and mutant seedlings with defects in the photomorphogenesis pathway (*cry1*, *cry1 cry2* and *cop1-4*), the biosynthesis pathway (*tt4-15*, *tt5-2*, *tt6-2*, *tt7-7*, *tt3-1*, *tds4-2*, *ban-5*, *tt10-8* and *tt15-4*), transport (*aha10-6*, *tt12-2* and *tt19-8*) and regulation (*ttg1-22*, *ttg2-5*, *tt1-3*, *tt8-6* and *tt16-5*) of various phenylpropanoids were grown for 5 days under continuous light (100 $\mu\text{mol photons m}^{-2} \text{sec}^{-1}$) on MS plates supplemented with 50 $\mu\text{g ml}^{-1}$ LIN. Autofluorescence after UV excitation was monitored. The red fluorescence served as an indicator for chlorophyll accumulation.

IRX3/CESA7 is a member of the cellulose synthase (CESA) family. The CESA complexes required for the synthesis of primary and secondary cell walls differ in composition: IRX3, together with IRX1/CESA8 and IRX5/CESA4, is needed specifically for the synthesis of cellulose in the secondary cell wall, which also contains lignin (Meents *et al.*, 2018; Polko and Kieber, 2019). CESA1/RADIALLY SWOLLEN 1 (RSW1), CESA3 and CESA6-like proteins (CESA2, CESA5, CESA6 and CESA9) are involved in primary cell-wall synthesis (Meents *et al.*, 2018; Polko and Kieber, 2019).

These findings raise the question of whether the *holi* phenotype might be caused by: (i) a general reduction in cellulose content in the secondary cell wall; (ii) reduced cellulose content in the primary cell wall; or (iii) a lack of hemicelluloses in the secondary cell wall. To clarify this issue, mutants with reduced cellulose content in the secondary cell wall (*irx1-2*, *irx1-3* and *irx5-4*), together with a mutant with reduced cellulose content in the primary cell wall (*rsw1-1*; Williamson *et al.*, 2001) and a mutant with reduced content

of the hemicellulose xylan in the secondary cell wall (*irx9-2*; Bauer *et al.*, 2006), were germinated on low LIN medium. The *irx1* seedlings displayed comparably high autofluorescence to *holi6* seedlings, whereas *irx5-4* displayed weaker autofluorescence, and *rsw1-1* and *irx9-2* behaved like the WT (Figure 7c). Moreover, F_v/F_m could not be detected in the additionally investigated mutants. Reduced cellulose production can affect growth and morphogenesis in various plant parts, as exemplified by the swollen roots of *rsw1* mutants grown at 31°C (Arioli *et al.*, 1998; Williamson *et al.*, 2001). To test for any temperature dependency of the F_v/F_m phenotype, *rsw1-1* together with the other cell wall mutants was germinated at 31°C on control MS plates and on MS plates supplemented with low LIN. Cotyledons of the *rsw1-1* mutant were smaller under both conditions, confirming the heat growth phenotype observed previously (Williamson *et al.*, 2001), but, as in all other tested mutants, F_v/F_m was WT-like (Figure S5a). Interestingly, both the greening and the elevated F_v/F_m phenotypes were barely detectable under low LIN

(a) 50 $\mu\text{g/ml}$ LIN



(b) 5 μM NF

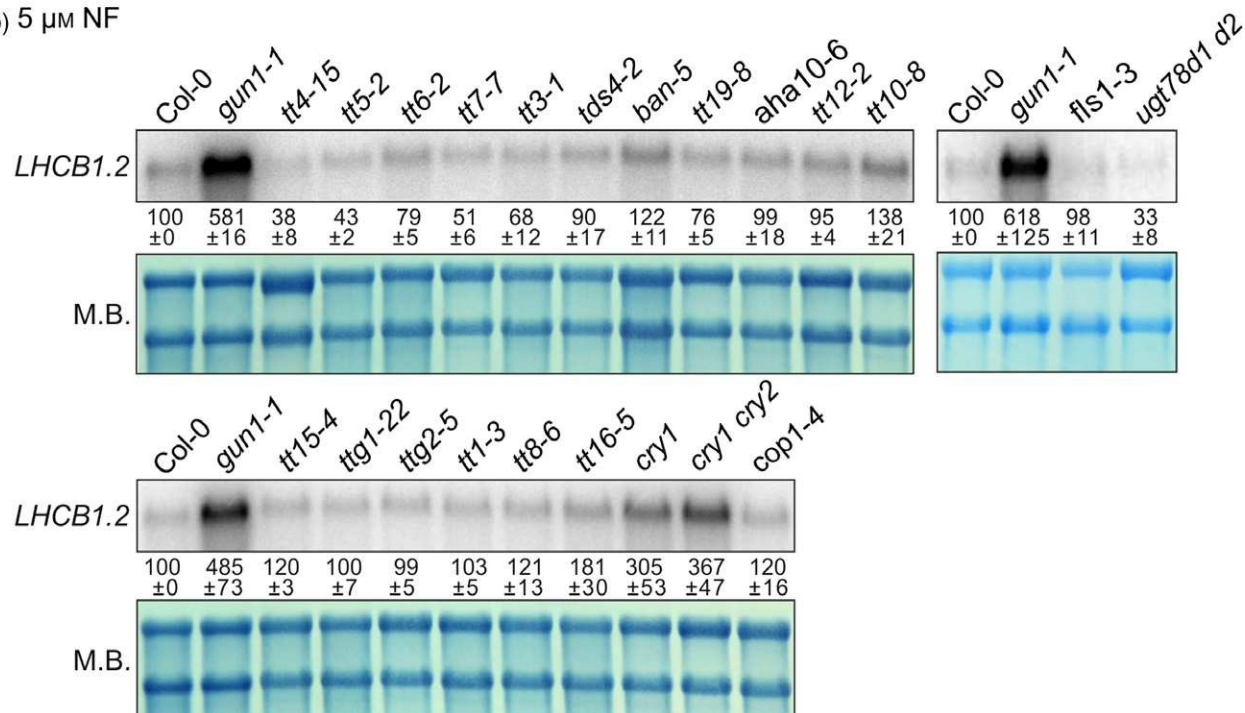


Figure 6. Analysis of *LHCb1.2* transcript levels of the wild type (WT), *gun1*, *cry1*, *cry1 cry2*, *cop1-4* and mutants associated with phenylpropanoid biosynthesis grown in the presence of inhibitors. WT and the mutants described in the legend to Figure 6 were grown for 5 days under continuous light ($100 \mu\text{mol photons m}^{-2} \text{sec}^{-1}$) on MS plates supplemented with (a) $50 \mu\text{g ml}^{-1}$ lincomycin (LIN) or (b) $5 \mu\text{M}$ norflurazon (NF). *LHCb1.2* mRNA levels were determined by Northern blot analyses. The methylene blue-stained blots served as loading controls (M.B.).

conditions in *holi6/irx3* and *irx1* seedlings (Figure S5b), implying that the high temperature overrides the capability of secondary cell wall mutants to green on LIN. Moreover,

the potential greening capacity of *rsw1-1* seedlings on LIN might be masked by the temperature sensitivity of this mutant.

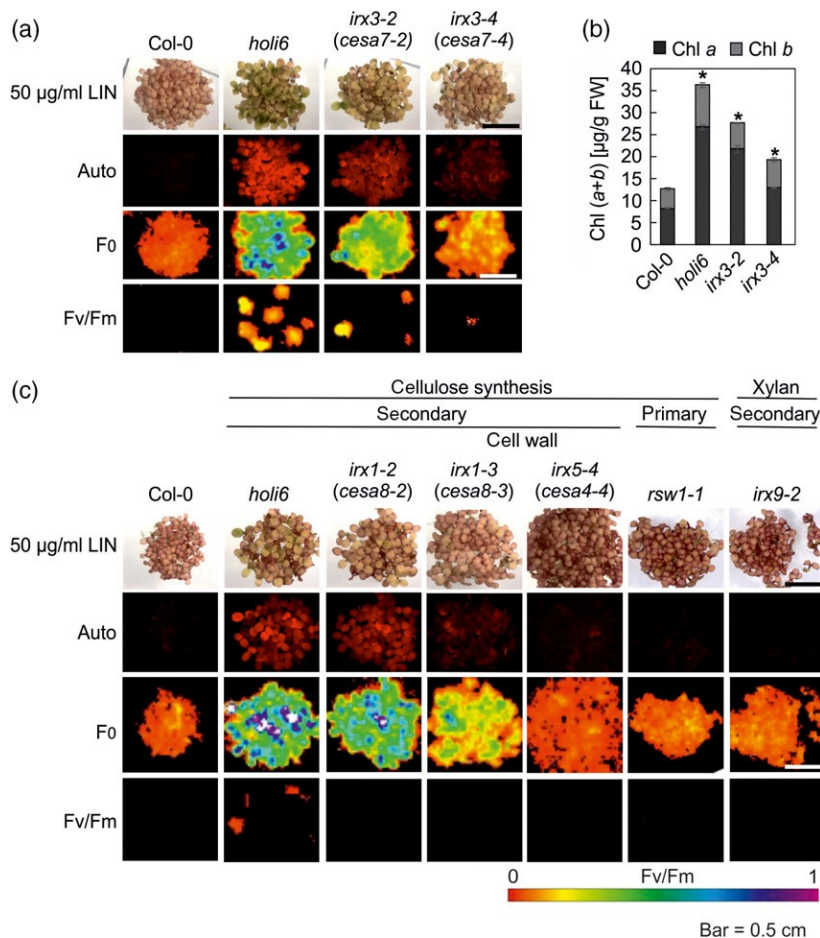


Figure 7. Phenotypes of the wild type (WT), *holi6* and mutants associated with cell-wall synthesis grown on low lincomycin (LIN). (a) WT, *holi6*, *irx3-2* and *irx3-4* mutants were grown for 5 days under continuous light (100 µmol photons m⁻² sec⁻¹) on MS plates supplemented with low LIN (50 µg ml⁻¹). Autofluorescence after UV excitation was monitored. The red fluorescence served as an indicator for chlorophyll accumulation. The maximum quantum yield of photosystem II (F_v/F_m) was measured with an imaging Chl fluorometer (Imaging PAM). (b) Determination of the total chlorophyll (Chl a + b) content of 5-day-old seedlings. Pigments were acetone-extracted, measured spectrophotometrically and concentrations were determined as described by Porra et al. (1989). Data are shown as mean values \pm SDs from three biological replicates. Each replicate pool contained more than 20 seedlings. Significant differences were identified by Tukey's test ($P < 0.05$). (c) WT, *holi6*, *irx1-2*, *irx1-3*, *irx5-4*, *irx9-2* and *rsw1-1* mutants were grown for 5 days under continuous light (100 µmol photons m⁻² sec⁻¹) on MS plates supplemented with low LIN (50 µg ml⁻¹). Autofluorescence after UV excitation was monitored. The red fluorescence served as an indicator for chlorophyll accumulation. The initial Chl a fluorescence (F_0) and the maximum quantum yield of photosystem II (F_v/F_m) were measured with an imaging Chl fluorometer (Imaging PAM).

In sum, it can be concluded that cellulose defects specifically in the secondary cell wall promote seedling greening, and that deactivation of IRX3 results in the strongest greening phenotype.

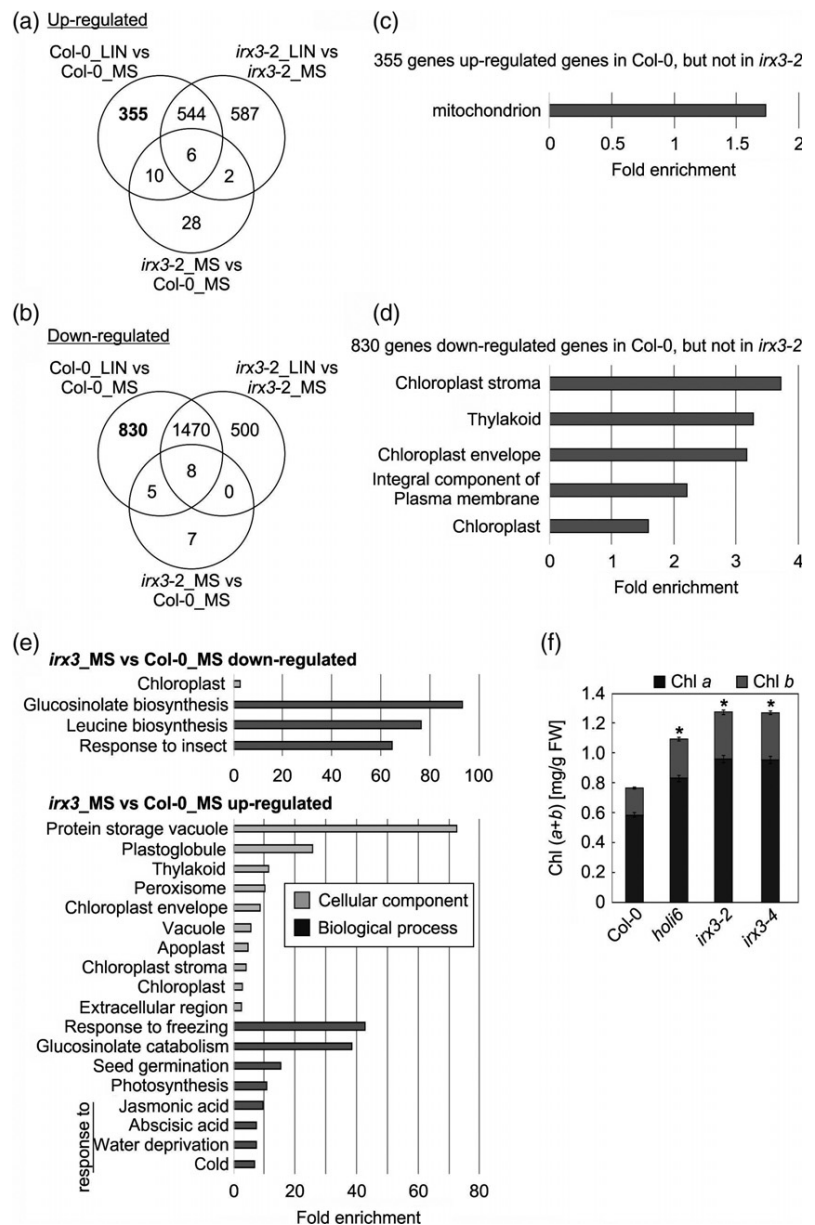
The *irx3* mutant behaves like a *gun* mutant on low LIN

A defect in IRX1 or IRX5, both of which are specific for the secondary cell wall CESA complex, results in the upregulation of ABA-responsive genes (Hernandez-Blanco et al., 2007). Moreover, *LHCB1.2* mRNA expression is higher when the *holi6* mutant is grown on low LIN, as well as in control conditions (Figure 3). To investigate the behavior of ABA-responsive genes and nuclear genes for chloroplast proteins on a transcriptome-wide level in *irx3* mutants, RNA-Seq analysis was performed on RNA isolated from 5-day-old WT and *irx3-2* seedlings grown in the absence of LIN (control) or on low LIN. Low LIN elicited substantial (more than twofold) changes in gene expression in the WT (915 up; 2313 down) and *irx3-2* (1139 up; 1978 down) seedlings (Figure 8a,b; Table S2). Of the genes up- and down-regulated in WT seedlings upon LIN treatment, 39 and 36%, respectively, were dependent on the presence of functional IRX3, namely those that were not more than

twofold differentially expressed in *irx3-2*. Gene ontology (GO) analysis (Huang et al., 2009) of these IRX3-dependent genes identified an enrichment for the cellular component category 'mitochondria' among the 39% upregulated genes (Figure 8c), and in the categories 'chloroplast stroma', 'thylakoid', 'chloroplast envelope', 'integral component of plasma membrane' and 'chloroplast' among the 36% downregulated genes (Figure 8d). This showed that, in addition to *LHCB1.2*, other photosynthesis-related genes were derepressed in *irx3* seedlings.

When grown under control conditions (without LIN), the transcriptome of the *irx3-2* mutant showed only moderate changes relative to the WT: the mRNA levels of 20 (41) or 46 (70) genes were significantly reduced or elevated (by more than 2.0- and 1.5-fold, respectively) (Figure 8a,b; Table S2). Analyses of the 1.5-fold changes revealed that in the downregulated gene set, only 'chloroplast' was significantly enriched in the cellular component category (CC), whereas the biological process (BP) categories 'glucosinolate biosynthesis', 'leucine biosynthesis' and 'response to insect' were more than 60-fold enriched (Figure 8e). In the upregulated gene set, the CC category 'protein storage vacuole' and several chloroplast-associated categories like

Figure 8. RNA-Seq analysis of 5-day-old WT and *irx3-2* seedlings. Seedlings were grown for 5 days on MS or on MS plates supplemented with 50 $\mu\text{g ml}^{-1}$ LIN (LIN). Venn diagrams depict the degree of overlap between the sets of genes whose expression levels were down- (a) or up-regulated (b) by at least twofold in the indicated comparisons. Gene ontology (GO) analysis of genes whose expression was down- (c) or upregulated (d) in the indicated comparisons. GO annotations for the cellular component category were extracted from DAVID (Huang *et al.*, 2009). GO terms for genes with a >1.5-fold change and a Benjamini corrected value of <0.05 are shown. (e) Gene ontology (GO) analysis of genes whose expression was down- or upregulated in *irx3* seedlings grown on MS (without LIN) compared to WT. GO annotations for the cellular component and biological process categories were extracted from DAVID (Huang *et al.*, 2009). GO terms with a Benjamini corrected value of <0.05 are shown. (f) Determination of the total chlorophyll (Chl *a* + *b*) content of 5-day-old seedlings. Pigments were acetone-extracted, measured spectrophotometrically, and concentrations were determined as described (Porra *et al.*, 1989). Data are shown as mean values \pm SD from three biological replicates. Each replicate pool contained more than 20 seedlings. Significant differences were identified by Tukey's test ($P < 0.05$).



'plastoglobule', 'thylakoid', 'envelope' and 'stroma' were enriched, and in the BP category 'response to freezing' and 'glucosinolate catabolism' were enriched approximately 40-fold, and 'seed germination', 'photosynthesis', 'response to jasmonic acid' and 'response to abscisic acid' were enriched approximately 10-fold, respectively (Figure 8e; Table 1). Among the abscisic acid (ABA)-responsive genes were the genes for the chloroplast-localized proteins COLD-REGULATED 15a (COR15a) and COR15b. Of note is also the slight (approximately 1.4-fold) but significant induction of genes encoding several Lhcb proteins and subunits of photosystems I and II (Figure 3; Tables S2 and S3), which was reflected in an approximately 1.5-fold

higher chlorophyll content in 5-day-old holi6 and *irx3* mutant seedlings (Figure 8f).

Taken together, these results suggest a role for the secondary cell wall in seedling greening, even under normal growth conditions. Moreover, a defect in IRX3 results in a weak *gun* phenotype on low LIN and leads to altered ABA metabolism or sensitivity.

DISCUSSION

Norflurazon is an inhibitor of phytoene desaturase and blocks carotenoid biosynthesis, whereas LIN binds to the 50S subunit of the plastid ribosome, thus inhibiting protein synthesis in the organelle. Treatment of seedling plants

Table 1 Differential expression of ABA-responsive genes, and genes involved in chloroplast biogenesis and light reactions in 5-day-old *irx3-2* mutant seedlings, compared with Col-0

Locus identifier	Fold change	Description	Gene symbol
Chloroplast			
AT2G20570	1.47	GOLDEN2-LIKE 1	GLK1
AT1G61520	1.33	PSI CHLOROPHYLL A/B BINDING PROTEIN 3	LHCA3
AT3G47470	1.39	PSI CHLOROPHYLL A/B BINDING PROTEIN A4	LHCA4
AT1G29910	1.36	PSII CHLOROPHYLL A/B BINDING PROTEIN 3	LHCB1.2
AT2G34430	1.41	PSII CHLOROPHYLL A/B BINDING PROTEIN B1	LHCB1.4
AT2G05100	1.51	PSII CHLOROPHYLL A/B BINDING PROTEIN 2.1	LHCB2.1
AT2G05070	1.63	PSII CHLOROPHYLL A/B BINDING PROTEIN 2.2	LHCB2.2
AT3G27690	1.53	PSII CHLOROPHYLL A/B BINDING PROTEIN 2.3	LHCB2.3
AT5G54270	1.47	PSII CHLOROPHYLL A/B BINDING PROTEIN 3	LHCB3.1
AT4G10340	1.33	PSII CHLOROPHYLL A/B BINDING PROTEIN 5	LHCB5
AT4G27440	1.32	PROTOCHLOROPHYLLIDE OXIDOREDUCTASE B	PORB
AT4G28750	1.46	PSI SUBUNIT E-1	PSAE-1
AT1G52230	1.40	PSI SUBUNIT H2	PSAH2
AT1G08380	1.40	PSI SUBUNIT O	PSAO
ATCG00220	1.40	PSII SUBUNIT M	PSBM
AT4G05180	1.36	PSII SUBUNIT Q-2	PSBQ-2
AT2G30570	1.33	PSII SUBUNIT W	PSBW
AT1G67740	1.35	PSII SUBUNIT Y	PSBY
ABA-responsive			
AT2G42540	3.44	COLD-REGULATED 15A	COR15A
AT2G42530	3.17	COLD REGULATED 15B	COR15B
AT1G29395	2.83	COLD REGULATED 314 INNER MEMBRANE 1	COR413IM1
AT5G15970	1.98	Stress-induced protein KIN2/COLD-REGULATED 6.6	KIN2
AT1G52400	2.19	BETA GLUCOSIDASE 18	BGLU18
AT4G04020	1.61	FIBRILLIN	FBN1A
AT4G23600	2.74	CORONATINE INDUCED 1	COR13
AT4G28520	4.52	CRUCIFERIN 3	CRU3
AT5G25980	3.52	GLUCOSIDE GLUCOHYDROLASE 2	TGG2
AT5G44120	4.67	CRUCIFERINA	CRA1

Seedlings were grown on MS without supplementation of LIN. Differential expression was determined with RNA-Seq analysis (Tables S2 and S3) and fold changes are represented. PS, photosystem.

with NF or LIN prevents greening, promotes anthocyanin accumulation and suppresses the light induced transcription of nuclear genes for photosynthesis, such as *LHCB1.2*. In all known *gun* mutants, *LHCB1.2* expression is partly derepressed in the presence of NF, but only a subset of *gun* mutants display this phenotype in the presence of

LIN (Koussevitzky et al., 2007; Ruckle et al., 2007). We attempted to isolate further mutants that can better cope with LIN. High concentrations of LIN (220 $\mu\text{g ml}^{-1}$) were used in previous studies (Koussevitzky et al., 2007; Ruckle et al., 2007; Choy et al., 2008; Cottage et al., 2010; Sun et al., 2016), and we found that a greater than fourfold lower concentration (50 $\mu\text{g ml}^{-1}$) of LIN still repressed nucleus-encoded photosynthesis genes (Figure 1b). Moreover, the use of low LIN uncovered a clear phenotypical difference between *gun1-1* and WT seedlings, as cotyledons were larger and anthocyanin accumulation was less pronounced in the *gun1-1* mutant (Figure 1a). With the exception of the *hon* mutant screen, in which lower NF and light dosages were used (Saini et al., 2011), all previous *gun* mutant screens used reporter genes to identify mutants with de-repressed *LHCB* expression (Kleine and Leister, 2016). In contrast, we attempted to isolate mutants based on visually discernible differences from the WT when grown on low LIN. Although the earlier *hon* mutant screen identified mutants that are affected in chloroplast protein homeostasis, our low-LIN screen led to the identification of '*holi*' and additional '*hon*' mutants for proteins involved in: (i) the flavonoid pathway; and (ii) secondary cell wall formation (Figure 4).

We used 5-day-old seedlings grown on MS supplemented with sucrose to investigate phenylpropanoid accumulation and parameters associated with chloroplast development, i.e. the maximum quantum yield of photosystem II, *LHCB1.2* expression levels and greening. In 1992, it was found that several transcripts for enzymes of the flavonoid biosynthetic pathway reached a maximum in 3-day-old Arabidopsis seedlings grown in continuous light. The authors concluded that the peak anthocyanin content appeared to coincide with the maturation of chloroplasts, and the associated switch to photoautotrophic growth (Kubasek et al., 1992). Subsequent work showed that, in the presence of 2% sucrose, and in the absence of inhibitors, anthocyanin accumulation reaches a maximum in 5-day-old seedlings (Cottage et al., 2010). In addition to the presence of disaccharides, the induction of anthocyanins depends on a functional photosynthetic electron transport chain and on light (Jeong et al., 2010). Thus, the light-signaling mutants *cry1* and *hy5* exhibit significant inhibition of anthocyanin accumulation (Ahmad et al., 1995; Jeong et al., 2010). Notably, *cry1* and *hy5* mutants have been identified as *gun* mutants (Ruckle et al., 2007), and lower levels of anthocyanins were noted in the original set (*gun1–gun5*) in this present study and in other studies (Cottage et al., 2010; Voigt et al., 2010). The idea that changes in anthocyanin accumulation might trigger de-repression of *LHCB1.2* in *gun* mutants has previously been rejected (Voigt et al., 2010); however, the consistent observation of lowered anthocyanin accumulation in mutants showing the *gun* phenotype prompted us to re-evaluate

this putative link. Because anthocyanins represent the only visibly perceptible products of the phenylpropanoid pathway, we performed reverse-phase UPLC to profile the accumulation of phenylpropanoids that absorb in the UV region (280 nm) of the spectrum (Figure S3; Table S1) and found that the kaempferol derivative k3 is less abundant in *gun* mutants after inhibitor treatment. A second approach using various mutants blocked at different steps in the phenylpropanoid pathway (Figures 6 and 7) strongly suggests that neither the abundance of k3 nor that of any other intermediate of the phenylpropanoid pathway is correlated with *LHCB1.2* expression, however. Therefore, our data suggest that changes in phenylpropanoid levels cannot account for *LHCB1.2* de-repression in inhibitor-treated *gun* mutants.

Of all the mutants identified here, *holi6* displayed the strongest chlorophyll autofluorescence when grown in the presence of low LIN (Figures 2 and 8). *HOLI6* encodes the cellulose synthase subunit CESA7, also named IRX3, because in *irx* mutants the xylem collapses (Brown *et al.*, 2005). Further results indicated that perturbation of cellulose formation specifically in the secondary cell wall leads to a happy-on-lincomycin phenotype (Figure 7). This may seem counterintuitive, but the weakening of the cell wall caused by defects in IRX1, IRX3 or IRX5 also confers enhanced resistance to some pathogens (Hernandez-Blanco *et al.*, 2007; Miedes *et al.*, 2014). In analogy to our findings that the *rsw1-1* mutant with a defect in the primary cell wall is not able to green on LIN (Figure 7), susceptibility to these pathogens was not altered in mutants that affect the primary cell wall, like the *cesa3* and *rsw1* mutants (Hernandez-Blanco *et al.*, 2007), although *cesa3* mutants can be more resistant to other pathogens (Ellis *et al.*, 2002). Could this mean that a weakened secondary cell wall might confer resistance to lincomycin? Presumably not, because the chlorophyll content of *irx3* mutants is already higher than that of the WT under normal growth conditions (Figure 8). Moreover, the disease resistance phenotype of *irx1*, *irx3* and *irx5* mutants has been attributed in part to the constitutive activation of plant immune responses rather than to alterations in the passive wall barrier. In *irx1-6* and *irx5-5* plants a large number of ABA-regulated genes are constitutively upregulated (Hernandez-Blanco *et al.*, 2007), which is in agreement with an increased accumulation of ABA in the *irx1-6* mutant (Chen *et al.*, 2005). Accordingly, we found that, in the *irx3-2* mutant, ABA-responsive genes are upregulated under normal growth conditions (Figure 8). ABA has previously been shown to have an impact on *LHCB1.2*, plastid-encoded gene expression (Koussevitzky *et al.*, 2007; Voigt *et al.*, 2010; Yamburenko *et al.*, 2013) and plastid differentiation (Rohde *et al.*, 2000; Penfield *et al.*, 2006; Kim *et al.*, 2009). ABA seems to affect plastid differentiation in opposing ways. High concentrations suppress the expression of certain nucleus-encoded chloroplast proteins as well as plastid formation in etiolated and light-grown seedlings, and in

seedlings grown in the presence of NF (Penfield *et al.*, 2006; Koussevitzky *et al.*, 2007), whereas lower concentrations stimulate these processes (Voigt *et al.*, 2010; Kim *et al.*, 2012). The tetrapyrrole biosynthesis proteins GUN4 and GUN5 (Voigt *et al.*, 2010), the PPR protein GUN1 (Cottage *et al.*, 2010) and GREENING AFTER EXTENDED DARKNESS 1 (GED1) (Choy *et al.*, 2008) all enhance seedling development in the presence of ABA. Interestingly, the *ged1* mutant was identified in a further attempt to isolate *gun1*-like mutants (Gray *et al.*, 2003; Choy *et al.*, 2008); however, like *holi6*, *ged1* is not a true *gun* mutant, because *RBCS* and *LHCB1* mRNA levels are already elevated in the absence of inhibitors, and *ged1* shows only a very subtle *gun* phenotype upon treatment with NF or LIN (Choy *et al.*, 2008).

The phenomenon of signaling from an altered cell wall to influence seedling photomorphogenesis in the dark has been recognized in the case of sugar- (Li *et al.*, 2007) and zinc-responsive (Sinclair *et al.*, 2017) growth and development. Our results suggest that defects in secondary cell walls also generate signals that modify nuclear gene expression and promote seedling greening, possibly via altered ABA metabolism or sensing.

EXPERIMENTAL PROCEDURES

Plant material and growth conditions

The mutant lines used in this study are listed in Table S4. The *irx3-2* mutant was genotyped with the following primers: SAIL_885_D10_LP, 5'-AAGGTTGGATCATGCAAGATG-3', SAIL_885_D10_RP, 5'-CCAGCTGCAATTCGAGATAC-3', and LB, 5'-ATTTGCCGATTTCGGAAC-3'. Surface-sterilized seeds were sown on Murashige and Skoog plates containing 0.8% (w/v) agar (pH 5.8), and stratified for at least 2 days at 4°C. The growth medium contained 1% (w/v) sucrose, unless indicated otherwise. Seedlings were grown at 22°C under continuous illumination (100 $\mu\text{mol photons m}^{-2} \text{sec}^{-1}$) provided by white fluorescent lamps or at 31°C under continuous illumination (80 $\mu\text{mol photons m}^{-2} \text{sec}^{-1}$ provided by LEDs, which corresponds to 100 $\mu\text{mol photons m}^{-2} \text{sec}^{-1}$ provided by white fluorescent lamps). For inhibitor experiments, MS medium was supplemented with the indicated concentration of lincomycin (Sigma-Aldrich, <https://www.sigmaaldrich.com/united-kingdom.html>) or norflurazon (Sigma-Aldrich).

EMS mutagenesis and whole-genome resequencing

Col-0 seeds were mutagenized using 0.2% (v/v) EMS (Sigma-Aldrich). The mutagenized M₁ plants were grown in pools of 500 to produce the M₂ generation of seeds. M₂ plants were screened for *holi* or *hon* phenotypes. Segregating F₂ populations were generated by backcrossing *holi* or *hon* mutants with the parental Col-0 line. To identify the causative mutations, positive pools of 50 plants each were selected based on their *holi* or *hon* mutant phenotype. DNA was extracted with the DNeasy Plant Mini kit (QIAGEN, <https://www.qiagen.com>). Preparation of 350-bp insert DNA libraries and 150-bp paired-end sequencing was carried out at Novogene Biotech (<https://en.novogene.com>) on an Illumina HiSeq 2500 system (Illumina, <https://www.illumina.com>) with standard Illumina protocols. The sequencing depth was at least 7 G of raw data per sample, which corresponds to a more than 50-fold

coverage of the *A. thaliana* genome. After grooming FASTQ files, adaptors were removed with `TRIMMOMATIC` (Bolger *et al.*, 2014), reads were mapped with `BWA` (Li and Durbin, 2009), with parameters 'mem -t 4 -k 32 -M' to the TAIR10 annotation, and duplicates were removed by `SAMTOOLS` (Li *et al.*, 2009) with the `RMDUP` tool. Single-nucleotide polymorphisms (SNPs) were identified using `SAMTOOLS` (Li *et al.*, 2009) with the parameter 'mpileup -m 2 -F 0.002 -d 1000'. Only SNPs that were supported by more than four reads with a mapping quality of > 20 were retained. To identify the SNPs specific for the *holi* and *hon* mutants, the SNPs between each of the *holi* and *hon* mutants were compared with the SNPs of our Col-0 strain. The resulting *holi*- and *hon*-specific SNP lists were subjected to the web application CandiSNP (Etherington *et al.*, 2014), which generates SNP density plots. The output list of CandiSNP was screened for non-synonymous amino acid changes and for the G/C@A/T transitions that were likely to be caused by EMS, with a special focus on the chromosome with the highest SNP density with an allele frequency of > 0.75.

Detection of chlorophyll autofluorescence

Chlorophyll autofluorescence of cotyledons was recorded with a Lumar V12 microscope equipped with the filter set Lumar 09 (no. 485009) connected to an AxioCam digital camera (Zeiss, <https://www.zeiss.com>).

Chlorophyll fluorescence measurements

Chlorophyll fluorescence was detected using an imaging Chl fluorometer (Imaging PAM, M-Series; Walz, <https://www.walz.com>) equipped with the computer-operated PAM control unit `IMAGE*MAXI`, as described previously (Xu *et al.*, 2019).

Chlorophyll concentration measurements

For chlorophyll extraction, the cotyledons were blotted with filter paper to remove excess water, and hypocotyls were removed to ensure that only chlorophyll from the cotyledons was extracted. Briefly, 50-mg (fresh weight) cotyledon samples were ground and chlorophyll was extracted by adding 4 ml of 80% (v/v) acetone to each sample. The extract was centrifuged at 17 900 g for 10 min and the pigments were quantified as described previously (Porra *et al.*, 1989).

Determination of phenylpropanoid levels

Extraction, detection and analysis of phenylpropanoid contents was done as described in Appendix S1.

cDNA synthesis and quantitative RT-PCR analysis

Total RNA was extracted with the RNeasy Plant Mini kit (QIAGEN) according to the manufacturer's protocol, and 2 lg of the RNA was employed to synthesize cDNA using the iScript cDNA Synthesis Kit (Bio-Rad, <https://www.bio-rad.com>). RT-qPCR analysis was performed on a Bio-Rad iQ5 real-time PCR instrument with the iQ SYBR Green Supermix (Bio-Rad). Each sample was quantified in triplicate and normalized using *AT4G36800*, which codes for a RUB1 conjugating enzyme (*RCE1*), as an internal control. The following primers were used: *RCE1*-RT-F, 5'-CTGTTACGGAACCAATTC-3'; *RCE1*-RT-R, 5'-GGAAAAGGTCTGACCGACA-3'; *LHCB1*.2-RT-F, 5'-CCGTGAGCTAGAAGTTATCC-3'; *LHCB1*.2-RT-R, 5'-GTTTC CCAAGTAATCGAGTCC-3'; *CA1*-RT-F, 5'-GAGAAATACGAAACCAACCT-3'; *CA1*-RT-R, 5'-ACATAAGCCCTTTGATCCCA-3'; *IRX3*-exon1-2-RT-F, 5'-AACATGAAGAGCCAAAGCC-3'; *IRX3*-exon1-2-RT-R, 5'-TCGTACTCATAGCAAGGTCTACAC-3'; *IRX3*-exon11-12-RT-F, 5'-ATC

ATGCCACCGATAAGCAC-3; and *IRX3*-exon11-12-RT-R, 5'-GAGGGA TCAGCAGTGTGTGTC-3.

RNA gel-blot analysis

Total RNA was purified using the TRIzol reagent (Invitrogen, now ThermoFisher Scientific, <https://www.thermofisher.com>). To eliminate contaminating genomic DNA, RNA was treated with DNase I (New England BioLabs, <https://www.neb.com>). Total RNA (5 µg) was fractionated on a denaturing agarose gel, blotted onto a nylon membrane (Hybond-XL; GE Healthcare, <https://www.gehealthcare.com>) and subsequently cross-linked by UV light. Hybridizations were performed at 65°C according to standard protocols. Details of these probes have been described previously (Kacprzak *et al.*, 2019).

RNA sequencing (RNA-Seq) and data analysis

Total RNA from plants was isolated using Trizol (Invitrogen, now ThermoFisher Scientific) and purified using Direct-zolTM RNA MiniPrep Plus columns (Zymo Research, <https://www.zymoresearch.com>) according to the manufacturer's instructions. RNA integrity and quality were assessed with an Agilent 2100 Bioanalyzer (Agilent, <https://www.agilent.com>). Ribosomal RNA depletion, the generation of RNA-Seq libraries and 150-bp paired-end sequencing on an Illumina HiSeq 2500 system (Illumina) were conducted at Novogene Biotech with standard Illumina protocols. Three independent biological replicates were used per genotype.

RNA-Seq reads were analyzed on the Galaxy platform (Afgan *et al.*, 2016), as described by Xu *et al.* (2019). Sequencing data have been deposited in the National Center for Biotechnology Information (NCBI) Gene Expression Omnibus (GEO) (Edgar *et al.*, 2002) and are accessible through the GEO series accession number GSE130337.

Data analysis and statistical tests

One-way analysis of variance (ANOVA) was performed to determine statistical significances between genotypes ($P < 0.05$), followed by Tukey's test for differences of group means at a 95% confidence interval using `SPSS STATISTICS 17.0`.

ACKNOWLEDGEMENTS

We thank Bernd Weisshaar and Anton Schöffner for providing seeds of the phenylpropanoid biosynthesis mutants. We thank Paul Hardy and Bernd Weisshaar for their critical reading of the article and Elisabeth Gerick for excellent technical assistance.

CONFLICT OF INTEREST

The authors declare no competing or financial interests.

AUTHOR CONTRIBUTIONS

Conceptualization: TK, DX Experiments: DX, RD, AG, H-P M, and TK Writing original draft: TK Writing review and editing: DL, DX, RD, AG, H-PM, and TK Supervision: TK Funding acquisition: TK and DL.

FUNDING

This work was supported by the Deutsche Forschungsgemeinschaft (KL 2362/1-1 and TRR175, project C01, to T.K.;

TRR175, project C05, to D.L.). D.X. was supported by the China Scholarship Council fellowship.

DATA AVAILABILITY STATEMENT

RNA sequencing data have been deposited in the NCBI GEO (Edgar *et al.*, 2002) and are accessible through the GEO series accession number GSE130337.

SUPPORTING INFORMATION

Additional Supporting Information may be found in the online version of this article.

Figure S1. Illustration of the phenylpropanoid and flavonoid pathways in Arabidopsis.

Figure S2. Phenotypes of *gun* mutants grown in the presence of lincomycin (LIN) or norflurazon (NF).

Figure S3. Determination of phenylpropanoid contents of 5-day-old WT and *gun* mutant seedlings.

Figure S4. Confirmation of the *irx3-2* T-DNA insertion mutant.

Figure S5. Phenotypes of WT, *holi6* and mutants associated with cell-wall synthesis grown at 31°C on MS without or with low lincomycin (LIN).

Table S1. Detection of major phenylpropanoids in methanolic extracts from 5-day-old seedlings grown on MS plates without supplementation or supplemented with either 5 µM NF or 220 µg ml⁻¹ LIN.

Table S2. Genes with transcript levels that differed significantly from Col-0 in 5-day-old *irx3-2* seedlings grown on MS plates without supplementation or supplemented with 50 µg ml⁻¹ LIN.

Table S3. Genes with transcript levels that differed significantly from Col-0 in 5-day-old *irx3-2* seedlings grown on MS plates were sorted into different categories.

Table S4. *Arabidopsis thaliana* mutants used in this study.

Appendix S1. Supplemental materials and methods.

REFERENCES

- Afgan, E., Baker, D., van den Beek, M. *et al.* (2016) The Galaxy platform for accessible, reproducible and collaborative biomedical analyses: 2016 update. *Nucleic Acids Res.* 44, W3–W10.
- Ahmad, M., Lin, C. and Cashmore, A.R. (1995) Mutations throughout an Arabidopsis blue-light photoreceptor impair blue-light-responsive anthocyanin accumulation and inhibition of hypocotyl elongation. *Plant J.* 8, 653–658.
- Appelhaugen, I., Thiedig, K., Nordholt, N., Schmidt, N., Huep, G., Sagasser, M. and Weisshaar, B. (2014) Update on transparent testa mutants from Arabidopsis thaliana: characterisation of new alleles from an isogenic collection. *Planta*, 240, 955–970.
- Arioli, T., Peng, L., Betzner, A.S. *et al.* (1998) Molecular analysis of cellulose biosynthesis in Arabidopsis. *Science*, 279, 717–720.
- Bauer, S., Vasu, P., Persson, S., Mort, A.J. and Somerville, C.R. (2006) Development and application of a suite of polysaccharide-degrading enzymes for analyzing plant cell walls. *Proc. Natl Acad. Sci. USA*, 103, 11417–11422.
- Bolger, A.M., Lohse, M. and Usadel, B. (2014) Trimmomatic: a flexible trimmer for Illumina sequence data. *Bioinformatics*, 30, 2114–2120.
- Bonawitz, N.D., Soltan, W.L., Blatchley, M.R., Powers, B.L., Hurlock, A.K., Seals, L.A., Weng, J.K., Stout, J. and Chapple, C. (2012) REF4 and RFR1, subunits of the transcriptional coregulatory complex mediator, are required for phenylpropanoid homeostasis in Arabidopsis. *J. Biol. Chem.* 287, 5434–5445.
- Brown, D.M., Zeef, L.A., Ellis, J., Goodacre, R. and Turner, S.R. (2005) Identification of novel genes in Arabidopsis involved in secondary cell wall formation using expression profiling and reverse genetics. *Plant Cell*, 17, 2281–2295.
- Chan, K.X., Phua, S.Y., Crisp, P., McQuinn, R. and Pogson, B.J. (2016) Learning the languages of the chloroplast: retrograde signaling and beyond. *Annu. Rev. Plant Biol.* 67, 25–53.
- Chen, Z., Hong, X., Zhang, H., Wang, Y., Li, X., Zhu, J.K. and Gong, Z. (2005) Disruption of the cellulose synthase gene, AtCesA8/IRX1, enhances drought and osmotic stress tolerance in Arabidopsis. *Plant J.* 43, 273–283.
- Chi, W., Sun, X. and Zhang, L. (2013) Intracellular signaling from plastid to nucleus. *Annu. Rev. Plant Biol.* 64, 559–582.
- Choy, M.K., Sullivan, J.A., Theobald, J.C., Davies, W.J. and Gray, J.C. (2008) An Arabidopsis mutant able to green after extended dark periods shows decreased transcripts of seed protein genes and altered sensitivity to abscisic acid. *J. Exp. Bot.* 59, 3869–3884.
- Cottage, A., Mott, E.K., Kempster, J.A. and Gray, J.C. (2010) The Arabidopsis plastid-signalling mutant gun1 (genomes uncoupled1) shows altered sensitivity to sucrose and abscisic acid and alterations in early seedling development. *J. Exp. Bot.* 61, 3773–3786.
- Edgar, R., Domrachev, M. and Lash, A.E. (2002) Gene expression omnibus: NCBI gene expression and hybridization array data repository. *Nucleic Acids Res.* 30, 207–210.
- Ellis, C., Karafyllidis, I., Wasternack, C. and Turner, J.G. (2002) The Arabidopsis mutant cev1 links cell wall signaling to jasmonate and ethylene responses. *Plant Cell*, 14, 1557–1566.
- Etherington, G.J., Monaghan, J., Zipfel, C. and MacLean, D. (2014) Mapping mutations in plant genomes with the user-friendly web application CanDiSNP. *Plant Methods*, 10, 41.
- Gray, J.C., Sullivan, J.A., Wang, J.H., Jerome, C.A. and MacLean, D. (2003) Coordination of plastid and nuclear gene expression. *Philos. Trans. R. Soc. Lond. B Biol. Sci.*, 358, 135–145; discussion 144–135.
- Hernandez-Blanco, C., Feng, D.X., Hu, J. *et al.* (2007) Impairment of cellulose synthases required for Arabidopsis secondary cell wall formation enhances disease resistance. *Plant Cell*, 19, 890–903.
- Huang, D.W., Sherman, B.T. and Lempicki, R.A. (2009) Systematic and integrative analysis of large gene lists using DAVID Bioinformatics Resources. *Nature Protoc.* 4, 44–57.
- Jeong, S.W., Das, P.K., Jeoung, S.C. *et al.* (2010) Ethylene suppression of sugar-induced anthocyanin pigmentation in Arabidopsis. *Plant Physiol.* 154, 1514–1531.
- Kacprzak, S.M., Mochizuki, N., Naranjo, B., Xu, D., Leister, D., Kleine, T., Okamoto, H. and Terry, M.J. (2019) Plastid-to-nucleus retrograde signalling during chloroplast biogenesis does not require ABI4. *Plant Physiol.* 179, 18–23.
- Kim, C., Lee, K.P., Baruah, A., Nater, M., Gobel, C., Feussner, I. and Apel, K. (2009) (1)O₂-mediated retrograde signaling during late embryogenesis predetermines plastid differentiation in seedlings by recruiting abscisic acid. *Proc. Natl Acad. Sci. USA*, 106, 9920–9924.
- Kim, M., Lee, U., Small, I., des Francs-Small, C.C. and Vierling, E. (2012) Mutations in an Arabidopsis mitochondrial transcription termination factor-related protein enhance thermotolerance in the absence of the major molecular chaperone HSP101. *Plant Cell*, 24, 3349–3365.
- Kleine, T. and Leister, D. (2016) Retrograde signaling: organelles go networking. *Biochim. Biophys. Acta*, 1857, 1313–1325.
- Kleine, T., Voigt, C. and Leister, D. (2009) Plastid signalling to the nucleus: messengers still lost in the mists? *Trends Genet.* 25, 185–192.
- Koussevitzky, S., Nott, A., Mockler, T.C., Hong, F., Sachetto-Martins, G., Surpin, M., Lim, J., Mittler, R. and Chory, J. (2007) Signals from chloroplasts converge to regulate nuclear gene expression. *Science*, 316, 715–719.
- Kubasek, W.L., Shirley, B.W., McKillop, A., Goodman, H.M., Briggs, W. and Ausubel, F.M. (1992) Regulation of flavonoid biosynthetic genes in germinating Arabidopsis seedlings. *Plant Cell*, 4, 1229–1236.
- Larkin, R.M., Alonso, J.M., Ecker, J.R. and Chory, J. (2003) GUN4, a regulator of chlorophyll synthesis and intracellular signaling. *Science*, 299, 902–906.
- Leister, D. and Kleine, T. (2016) Definition of a core module for the nuclear retrograde response to altered organellar gene expression identifies GLK overexpressors as gun mutants. *Physiol. Plant*, 157, 297–309.
- Li, H. and Durbin, R. (2009) Fast and accurate short read alignment with Burrows-Wheeler transform. *Bioinformatics*, 25, 1754–1760.
- Li, Y., Smith, C., Corke, F., Zheng, L., Merali, Z., Ryden, P., Derbyshire, P., Waldron, K. and Bevan, M.W. (2007) Signaling from an altered cell wall to the nucleus mediates sugar-responsive growth and development in Arabidopsis thaliana. *Plant Cell*, 19, 2500–2515.

- Li, H., Handsaker, B., Wysoker, A., Fennell, T., Ruan, J., Homer, N., Marth, G., Abecasis, G., Durbin, R. and 1000 Genome Project Data Processing Subgroup. (2009) The sequence alignment/map format and SAMtools. *Bioinformatics*, 25, 2078–2079.
- Liang, M., Davis, E., Gardner, D., Cai, X. and Wu, Y. (2006) Involvement of AtLAC15 in lignin synthesis in seeds and in root elongation of Arabidopsis. *Planta*, 224, 1185–1196.
- Martin, G., Leivar, P., Ludevid, D., Tepperman, J.M., Quail, P.H. and Monte, E. (2016) Phytochrome and retrograde signalling pathways converge to antagonistically regulate a light-induced transcriptional network. *Nat. Commun.* 7, 11431.
- Meents, M.J., Watanabe, Y. and Samuels, A.L. (2018) The cell biology of secondary cell wall biosynthesis. *Ann. Bot.* 121, 1107–1125.
- Miedes, E., Vanholme, R., Boerjan, W. and Molina, A. (2014) The role of the secondary cell wall in plant resistance to pathogens. *Front. Plant Sci.* 5, 358.
- Mochizuki, N., Brusslan, J.A., Larkin, R., Nagatani, A. and Chory, J. (2001) Arabidopsis genomes uncoupled 5 (GUN5) mutant reveals the involvement of Mg-chelatase H subunit in plastid-to-nucleus signal transduction. *Proc. Natl Acad. Sci. USA*, 98, 2053–2058.
- Mochizuki, N., Tanaka, R., Tanaka, A., Masuda, T. and Nagatani, A. (2008) The steady-state level of Mg-protoporphyrin IX is not a determinant of plastid-to-nucleus signaling in Arabidopsis. *Proc. Natl Acad. Sci. USA*, 105, 15178–15183.
- Moulin, M., McCormac, A.C., Terry, M.J. and Smith, A.G. (2008) Tetrapyrrole profiling in Arabidopsis seedlings reveals that retrograde plastid nuclear signaling is not due to Mg-protoporphyrin IX accumulation. *Proc. Natl Acad. Sci. USA*, 105, 15178–15183.
- Oelmüller, R. and Mohr, H. (1986) Photooxidative destruction of chloroplasts and its consequences for expression of nuclear genes. *Planta*, 167, 106–113.
- Oelmüller, R., Levitan, I., Bergfeld, R., Rajasekhar, V.K. and Mohr, H. (1986) Expression of nuclear genes as affected by treatments acting on the plastids. *Planta*, 168, 482–492.
- Penfield, S., Li, Y., Gilday, A.D., Graham, S. and Graham, I.A. (2006) Arabidopsis ABA INSENSITIVE4 regulates lipid mobilization in the embryo and reveals repression of seed germination by the endosperm. *Plant Cell*, 18, 1887–1899.
- Polko, J. and Kieber, J.J. (2019) The regulation of cellulose biosynthesis in plants. *Plant Cell*, 31, 282–296.
- Ponce-Toledo, R.I., Deschamps, P., Lopez-Garcia, P., Zivanovic, Y., Benzerara, K. and Moreira, D. (2017) An early-branching freshwater cyanobacterium at the origin of plastids. *Curr. Biol.* 27, 386–391.
- Porra, R.J., Thompson, W.A. and Kriedemann, P.E. (1989) Determination of accurate extinction coefficients and simultaneous equations for assaying Chlorophyll-a and Chlorophyll-b extracted with 4 different solvents - verification of the concentration of chlorophyll standards by atomic-absorption spectroscopy. *Biochem. Biophys. Acta*, 975, 384–394.
- Rohde, A., De Rycke, R., Beeckman, T., Engler, G., Van Montagu, M. and Boerjan, W. (2000) ABI3 affects plastid differentiation in dark-grown Arabidopsis seedlings. *Plant Cell*, 12, 35–52.
- Ruckle, M.E., DeMarco, S.M. and Larkin, R.M. (2007) Plastid signals remodel light signaling networks and are essential for efficient chloroplast biogenesis in Arabidopsis. *Plant Cell*, 19, 3944–3960.
- Saini, G., Meskauskiene, R., Pijacka, W., Roszak, P., Sjogren, L.L., Clarke, A.K., Straus, M. and Apel, K. (2011) 'happy on norflurazon' (hon) mutations implicate perturbation of plastid homeostasis with activating stress acclimatization and changing nuclear gene expression in norflurazon-treated seedlings. *Plant J.* 65, 690–702.
- Sinclair, S.A., Larue, C., Bonk, L. et al. (2017) Etiolated seedling development requires repression of photomorphogenesis by a Small Cell-Wall-Derived Dark Signal. *Curr. Biol.* 27, 3403–3418.e3407.
- Stern, D.B., Goldschmidt-Clermont, M. and Hanson, M.R. (2010) Chloroplast RNA metabolism. *Annu. Rev. Plant Biol.* 61, 125–155.
- Stout, J., Romero-Severson, E., Ruegger, M.O. and Chapple, C. (2008) Semidominant mutations in reduced epidermal fluorescence 4 reduce phenylpropanoid content in Arabidopsis. *Genetics*, 178, 2237–2251.
- Strand, A., Asami, T., Alonso, J., Ecker, J.R. and Chory, J. (2003) Chloroplast to nucleus communication triggered by accumulation of Mg-protoporphyrin IX. *Nature*, 421, 79–83.
- Sun, X., Xu, D., Liu, Z., Kleine, T. and Leister, D. (2016) Functional relationship between mTERF4 and GUN1 in retrograde signaling. *J. Exp. Bot.* 67, 3909–3924.
- Susek, R.E., Ausubel, F.M. and Chory, J. (1993) Signal transduction mutants of Arabidopsis uncouple nuclear CAB and RBCS gene expression from chloroplast development. *Cell*, 74, 787–799.
- Terry, M.J. and Smith, A.G. (2013) A model for tetrapyrrole synthesis as the primary mechanism for plastid-to-nucleus signaling during chloroplast biogenesis. *Front. Plant Sci.* 4, 14.
- Timmis, J.N., Ayliffe, M.A., Huang, C.Y. and Martin, W. (2004) Endosymbiotic gene transfer: organelle genomes forge eukaryotic chromosomes. *Nat. Rev. Genet.* 5, 123–135.
- Tohge, T., Nishiyama, Y., Hirai, M.Y. et al. (2005) Functional genomics by integrated analysis of metabolome and transcriptome of Arabidopsis plants over-expressing an MYB transcription factor. *Plant J.* 42, 218–235.
- Voigt, C., Oster, U., Bornke, F., Jahns, P., Dietz, K.J., Leister, D. and Kleine, T. (2010) In-depth analysis of the distinctive effects of norflurazon implies that tetrapyrrole biosynthesis, organelle gene expression and ABA cooperate in the GUN-type of plastid signalling. *Physiol. Plant*, 138, 503–519.
- Williamson, R.E., Burn, J.E., Birch, R., Baskin, T.I., Arioli, T., Betzner, A.S. and Cork, A. (2001) Morphology of *rsw1*, a cellulose-deficient mutant of Arabidopsis thaliana. *Protoplasma*, 215, 116–127.
- Woodson, J.D., Perez-Ruiz, J.M. and Chory, J. (2011) Heme synthesis by plastid ferrochelatase 1 regulates nuclear gene expression in plants. *Curr. Biol.* 21, 897–903.
- Xu, D., Marino, G., Klingl, A., Enderle, B., Monte, E., Kurth, J., Hiltbrunner, A., Leister, D. and Kleine, T. (2019) Extrachloroplastic PP7L functions in chloroplast development and abiotic stress tolerance. *Plant Physiol.* 180, 323–341.
- Yamburenko, M.V., Zubo, Y.O., Vankova, R., Kusnetsov, V.V., Kulaeva, O.N. and Borner, T. (2013) Absciscic acid represses the transcription of chloroplast genes. *J. Exp. Bot.* 64, 4491–4502.
- Yin, R., Han, K., Heller, W., Albert, A., Dobrev, P.I., Zazimalova, E. and Schaffner, A.R. (2014) Kaempferol 3-O-rhamnoside-7-O-rhamnoside is an endogenous flavonol inhibitor of polar auxin transport in Arabidopsis shoots. *New Phytol.* 201, 466–475.

4. Discussion

4.1 The role of PP7L in chloroplast development

Although numerous studies describe the chloroplast biogenesis and development process, they especially focus on chloroplast-localized proteins, such as proteins involved in protein import and chloroplast transcription/RNA maturation/protein translation, assembly, and signaling. However, only a few photosynthesis-deficient mutants that are affected in non-chloroplastic proteins have been identified (Pogson and Albrecht-Borth, 2014). For example, it has recently been elucidated that the mitochondrion PALE GREEN1 and the peroxisome SNOWY COTYLEDON3 (SCO3) protein in Arabidopsis are involved in chloroplast biogenesis in cotyledons (Albrecht et al., 2010; Hsieh et al., 2017). Therefore, to understand the functions of other cellular compartments on chloroplast biogenesis are necessary. In this thesis, it was found that PP7L is a nuclear/cytosolic protein that is involved in chloroplast ribosomal RNA (rRNA) maturation and mRNA translation. The results show that all identified *pp7l* T-DNA insertion lines exhibited the photosynthesis phenotype, which suggests that PP7L is required for proper chloroplast development within cotyledons and young leaves. Further analysis was necessary on the expression levels of sigma factors in *pp7l*, due to the similar cotyledon phenotype of *pp7l* to that of *sig2* and *sig6* (see Chapter 1, Fig. 3 B and C). Northern blot analysis demonstrated that *SIG2* and *SIG6* transcripts were elevated in 4- and 5-d-old *pp7l-1* seedlings (Chapter 1, Fig. 3D). Meanwhile, lncRNA-seq analysis showed that the expression of *SIG1-6* is either unchanged or slightly increased in 4-d-old *pp7l-1* seedlings compared to the wild-type counterpart. Additionally, we analyzed the gene expression patterns of *pp7l* and *sig6* (Chapter 1, Fig. 3F). These data indicated no overlapping functions of PP7L and SIGs in the chloroplast biosynthesis process of Arabidopsis. The proteomics experiment was performed for the quantitative analysis of the seedling proteomes of *pp7l*. The chloroplast-encoded subunits of the PSI and PSII complexes, the chloroplast ATP synthase, the cytochrome *b₆f* complex, the large subunit of Rubisco, and ribosomal proteins were all found to accumulate at lower levels compared to the wild-type (Chapter 1, Fig. 5A). However, a comparison with transcriptomics data demonstrated that the relative changes in protein amounts do not involve the fact that the corresponding gene expression decreased in the chloroplast (Chapter 1, Fig. 5, A and B; Supplemental Table S2). In addition, based on the analysis of putative cis-elements, several related mutants, such as *csn5a*, *csn5b*, *pifs*, *cop1*, and *phyAphyB*, were investigated. Nevertheless, studies performed on these mutants show an unaffected

photosynthesis phenotype, thus separating the function of PP7L and light signaling in chloroplast biogenesis. Moreover, PP7L was also found to play a role in intense light and salt tolerance, which suggests that its function is not restricted to the regulation of chloroplast development.

4.2 VEN4 participates in regulating dNTP metabolism

Nevertheless, we identified that the nuclear-localized protein VEN4 has an important function in chloroplast biosynthesis. Previous research shows that the reticulate leaf phenotype of *ven4* is caused by chloroplast size and distribution defects in leaf interveinal tissue (Yoshida et al., 2018). This study reveals that *ven4* mutants exhibited reduced photosynthetic performance in young seedlings and older leaves, stunted growth, and altered abiotic stress response. The *bnen* single mutant and two independent *ven4* T-DNA insertion lines exhibited significantly lower F_v/F_m values than did the wild type in 3-day-old seedlings (Chapter 2, Fig. 1A), which implicates that VEN4 is involved in the photosynthetic activity of PSII. Western blot results demonstrate a significant difference in the abundance of PsaD and PsbD (D2) between the wild type and *ven4* mutants, which suggests that photosynthesis defects in *ven4* are due to the perturbation of PSI/PSII subunits. However, transcript levels of *psaD* and *psbD* (encoding D2) were not dramatically changed in *ven4* mutants compared to wild type, thereby indicating that VEN4 mutations did not affect the accumulation of *psaD* and *psbD* transcripts (Chapter 2, Fig. 1A). In addition, *psbA* (encoding D1) and *psaA* transcripts decreased in *ven4-1* and *ven4-2*, which indicates that the absence of VEN4 affected the transcription of a portion of the chloroplast genome. Moreover, in vivo protein labeling revealed a severe reduction in D1 and D2 levels in *ven4* mutants, and thus VEN4 is required for D1 and D2 translation (Chapter 2, Fig. 3). Overall, these results strongly suggest that VEN4 mutations cause abnormal chloroplast protein synthesis by defective translation or transcription. Interestingly, VEN4 is a nuclear-localized protein, rather than a chloroplast targeted protein. This was confirmed using fluorescence microscopy to visualize VEN4-GFP proteins in protoplasts (Chapter 2, Fig. 2A). VEN4 shares homology with SAMHD1, which is a deoxynucleotide triphosphohydrolase controlling dNTP pool size in mammalian cells (Franzolin et al., 2013). Moreover, loss of ribonucleotide reductase (RNR) leads to decreased synthesis of deoxyribonucleotide triphosphates (dNTPs) and defects in chloroplast division in the *crinkled leaves8* mutant (Garton et al., 2007). Thus, we hypothesized that the loss of VEN4 may cause dNTP pool imbalances and consequently delayed chloroplast

biogenesis. To determine whether an imbalanced dNTP pool is responsible for low photosynthetic efficiency in *ven4*, exogenous dNTPs were fed to Col-0, *ven4-1*, and *ven4-2* during the seed germination stage. As expected, the supply of exogenous dNTPs affect the efficiency of photosynthesis in wild-type and *ven4* seedlings. When supplied with additional exogenous 2 mM dNTPs or dCTP, reduced photosynthetic activity of *ven4* mutants was restored but exogenous dATP, dGTP, or dTTP aggravated the phenotype of *ven4* (Chapter 2, Fig. 2B), which implicates that VEN4 deficiency may affect dNTP pools. Interestingly, Col-0 shows normal F_v/F_m in the presence of 2 mM dTTP. In addition, *ven4* mutants exhibit varied phenotypes and are sensitive to low-temperature and salt stressors (Chapter 2, Fig. 4A; Supplemental Fig. S3B). These data suggest that VEN4 is required for growth under stress conditions. Overall, our preliminary data indicate that VEN4 is a positive regulator of chloroplast development, and that its proper function in the nucleus is essential for dNTP homeostasis in cotyledons. Another role of VEN4 is within the regulation of environmental stress tolerance, as *ven4* exhibits a strong physiological response to various abiotic stressors.

4.3 Perturbed OGE lead to altered salt stress responses in plant

As discussed in the introduction, plastid gene expression (PGE) is essential for the proper function of chloroplast and plant development (Leister et al., 2017). Therefore, three mTERF family proteins, mTERF10, mTERF11, and mTERF12, were identified and described in the chloroplast-associated group. Combining the bioinformatics data (Kleine, 2012) with observations from the subcellular location of these proteins, their localization in the nucleoids was confirmed and involved in PGE. Further, this suggests that these three proteins may participate in PGE. Afterwards, mTERF12 RNAi experiments and overexpression of mTERF10, mTERF11, and mTERF12 were conducted to determine the functionality of these lines. However, none of these lines with altered mTERF10, mTERF11, and mTERF12 levels showed a visibly altered phenotype under normal growth conditions (Chapter 3, Fig. 3B). Several reports show that PGE is crucial for acclimation to various environmental stress conditions (Pfannschmidt et al., 2015; Sun and Zerges, 2015; Leister et al., 2017). Moreover, in silico analysis of MTERF10, -11, and -12 expression levels suggests a possible involvement of mTERF10 and mTERF11 in responses to abiotic stressors. This study found that salt stress not only affected germination of *mterf10-1*, *mterf10-2*, and *mterf11-2*, but also depressed the root length of *mterf10* and *mterf11*. In response to salt stress, mTERF10 and mTERF12 may contribute to PGE. In addition, mTERF10

may alter PEG to be mediated by ABA after exposure to salt conditions. This conclusion is supported by our observation that *oe-mTERF10* lines are more tolerant of ABA and salt than wild-type plants, and the altered responsiveness to ABA of *pge* mutants (*gun1* and *pgn*) has been previously noted (Cottage et al., 2010; Laluk et al., 2011). The *mterf12* mutants did not exhibit growth and developmental defects under various environmental stressors. This suggests that mTERF12 is likely involved in a different mechanism. Overall, our results suggest that mTERF10 and mTERF11 serve as important regulatory factors for PGE in response to salt stress.

4.4 Cell wall integrity modulates nuclear gene expression in Arabidopsis seedling

Traditionally, chloroplasts were believed to be organelles that are responsible for signal production (Woodson and Chory, 2012), but the signaling mechanisms that originate in the chloroplast have only recently begun to be understood (Lepistö and Rintamäki, 2012; Hernández-Verdeja and Strand, 2018). Since the chloroplast genome is too small, most chloroplast proteins are encoded in the nuclear genome. Thus, the expression of the genes in the nucleus and chloroplast should be coordinated. The signaling from the chloroplast to the nucleus is termed retrograde signaling. Today, biogenic and operational control retrograde signals are known. GUN1 is strongly associated with PGE (Tadini et al., 2016; Pesaresi and Kim, 2019). Further, *LHCB1.2* expression of *gun1* is partly de-repressed in the presence of lincomycin (Lin), which is a specific inhibitor of chloroplast ribosomal activity in plant. In this study, six *holi* mutants and three *hon* mutants were screened and highlighted from the EMS-Col-0 population. Interestingly, *hon41* (MYB75), *holi1* (MYB75), *holi3* (TTG1), *hon24* (TT3), *hon33* (TT18), and *holi2* (REF4) loci encode proteins that are involved in the flavonoid pathway (Chapter 4, Supplemental Fig. S1). Anthocyanins are synthesized through a branch of the flavonoid biosynthetic pathway that includes the phenylpropanoid biosynthetic pathway (Falcone Ferreyra et al., 2012; Shi and Xie, 2014). Moreover, *gun1* accumulates less anthocyanin under LIN conditions (Cottage et al., 2010), and *gun2*, *gun4*, and *gun5* accumulate less anthocyanin under NF conditions, compared to WT (Voigt et al., 2010). This enables formulating the hypothesis that the mechanism of action of reduced anthocyanin aims to stimulate retrograde signaling. Thus, the accumulation of phenylpropanoids in 5-day-old Col-0, *gun1-1*, *gun2-1*, *gun4-1*, and *gun5-1* seedlings was grown on MS and in the absence or presence of norflurazon (NF) or LIN and phenylpropanoid content was measured by ultra-performance liquid

chromatography (UPLC) (Chapter 4, Supplemental Fig. S3). On the other hand, phenotype seedlings and *LHCB1.2* transcript levels of mutants that lack the phenylpropanoid pathway-related genes were investigated. Combining these two results, our data suggest no correlation between *gun* signaling and anthocyanin biosynthesis. Additionally, the *holi6* mutant shows the most interesting phenotypes and *Holi6* was *CESA7/IRX3*, which encodes a cellulose synthase subunit. Cesa 4, 7, and 8 are required for cellulose synthesis in the secondary cell wall, and the stoichiometry in each rosette is 1:1:1 (Hill et al., 2014). Thus, the *holi* phenotype of *ces4* (*irx5*) and *ces8* (*irx1*) were also investigated. Unsurprisingly, *ces4* and *ces8* exhibited greening and elevated F_v/F_m phenotypes under low LIN conditions (Chapter 4, Fig. 7B). Therefore, the cell wall can monitor the extracellular and internal cellular environment and involves signaling recognition and transduction. In conclusion, our study considers the intriguing possibility that defects in secondary cell walls also generate signals that modify nuclear gene expression and promote seedling greening, potentially via altered ABA metabolism or sensing. As such, our findings also raise the following questions: how does the chloroplast conduct signals to the cell wall? How does the nucleus respond to these signals? Further work must be done to identify the key signaling component in the cytosolic environment and to understand the exact biological role of GUN1. To solve these problems, an improved retrograde signaling screening system can be applied, by which high efficiency and accuracy can be achieved for seeking *gun1* suppressor. Additionally, it would be very interesting to see the effect of retrograde signals on crop yield improvement and plant response to environmental stresses. This knowledge would improve our understanding of the components of retrograde signaling pathways.

References

- Adam, Z., Charuvi, D., Tsabari, O., Knopf, R.R., and Reich, Z.** (2011). Biogenesis of thylakoid networks in angiosperms: knowns and unknowns. *Plant Molecular Biology* **76**, 221-234.
- Albrecht, V., Simkova, K., Carrie, C., Delannoy, E., Giraud, E., Whelan, J., Small, I.D., Apel, K., Badger, M.R., and Pogson, B.J.** (2010). The cytoskeleton and the peroxisomal-targeted snowy cotyledon3 protein are required for chloroplast development in Arabidopsis. *Plant Cell* **22**, 3423-3438.
- Allen, J.F., de Paula, W.B.M., Puthiyaveetil, S., and Nield, J.** (2011). A structural phylogenetic map for chloroplast photosynthesis. *Trends in Plant Science* **16**, 645-655.
- Alt, J., Winter, P., Sebald, W., Moser, J.G., Schedel, R., Westhoff, P., and Herrmann, R.G.** (1983). Localization and nucleotide sequence of the gene for the ATP synthase proteolipid subunit on the spinach plastid chromosome. *Current Genetics* **7**, 129-138.
- Archibald, J.M.** (2015). Genomic perspectives on the birth and spread of plastids. *Proceedings of the National Academy of Sciences* **112**, 10147.
- Belbin, F.E., Noordally, Z.B., Wetherill, S.J., Atkins, K.A., Franklin, K.A., and Dodd, A.N.** (2017). Integration of light and circadian signals that regulate chloroplast transcription by a nuclear-encoded sigma factor. *New Phytologist* **213**, 727-738.
- Berry, E.A., Guergova-Kuras, M., Huang, L.-s., and Crofts, A.R.** (2000). Structure and Function of Cytochrome bc Complexes. *Annual Review of Biochemistry* **69**, 1005-1075.
- Bird, C.R., Koller, B., Auffret, A.D., Huttly, A.K., Howe, C.J., Dyer, T.A., and Gray, J.C.** (1985). The wheat chloroplast gene for CF₀ subunit I of ATP synthase contains a large intron. *The EMBO journal* **4**, 1381-1388.
- Biswal, B., Raval, M.K., Biswal, U.C., and Joshi, P.** (2008). Response of photosynthetic organelles to abiotic stress: modulation by sulfur metabolism. In *sulfur assimilation and abiotic stress in plants*, N.A. Khan, S. Singh, and S. Umar, eds (Berlin, Heidelberg: Springer Berlin Heidelberg), pp. 167-191.
- Biswal, B., Joshi, P.N., Raval, M.K., and Biswal, U.C.** (2011). Photosynthesis, a global sensor of environmental stress in green plants: stress signalling and adaptation. *Current Science* **101**, 47-56.
- Blankenship, R.E.** (1992). Origin and early evolution of photosynthesis. *Photosynthesis Research* **33**, 91-111.
- Blankenship, R.E.** (2002). Origin and evolution of photosynthesis. In *Molecular Mechanisms of Photosynthesis*, pp. 220-257.
- Blankenship, R.E.** (2010). Early evolution of photosynthesis. *Plant Physiol* **154**, 434-438.
- Bradbeer, J.W., Atkinson, Y.E., BÖRner, T., and Hagemann, R.** (1979). Cytoplasmic synthesis of plastid polypeptides may be controlled by plastid-synthesised RNA. *Nature* **279**, 816-817.
- Bryant, D.A., and Frigaard, N.-U.** (2006). Prokaryotic photosynthesis and phototrophy illuminated. *Trends in Microbiology* **14**, 488-496.
- Bryant, D.A., Costas, A.M.G., Maresca, J.A., Chew, A.G.M., Klatt, C.G., Bateson, M.M., Tallon, L.J., Hostetler, J., Nelson, W.C., Heidelberg, J.F., and Ward, D.M.** (2007). *Candidatus chloracidobacterium thermophilum*: an aerobic phototrophic acidobacterium. *Science* **317**, 523-526.

- Buick, R.** (2008). When did oxygenic photosynthesis evolve? *Philosophical Transactions of the Royal Society B: Biological Sciences* **363**, 2731-2743.
- Butterfield, N.J.** (2015). Proterozoic photosynthesis – a critical review. *Palaeontology* **58**, 953-972.
- Cavalier-Smith, T.** (2000). Membrane heredity and early chloroplast evolution. *Trends in Plant Science* **5**, 174-182.
- Cavalier-Smith, T.** (2008). The origins of plastids. *Biological Journal of the Linnean Society* **17**, 289-306.
- Chan, K.X., Phua, S.Y., Crisp, P., McQuinn, R., and Pogson, B.J.** (2016). Learning the languages of the chloroplast: retrograde signaling and beyond. *Annual Review of Plant Biology* **67**, 25-53.
- Chi, W., Sun, X., and Zhang, L.** (2013). Intracellular signaling from plastid to nucleus. *Annual Review of Plant Biology* **64**, 559-582.
- Chi, W., He, B., Mao, J., Jiang, J., and Zhang, L.** (2015). Plastid sigma factors: Their individual functions and regulation in transcription. *Biochimica et Biophysica Acta (BBA) - Bioenergetics* **1847**, 770-778.
- Cooley, J.W., Roberts, A.G., Bowman, M.K., Kramer, D.M., and Daldal, F.** (2004). The raised midpoint potential of the [2Fe2S] cluster of cytochrome *bc_L* is mediated by both the Q_o site occupants and the head domain position of the Fe–S protein subunit. *Biochemistry* **43**, 2217-2227.
- Cottage, A., Mott, E.K., Kempster, J.A., and Gray, J.C.** (2010). The Arabidopsis plastid-signalling mutant *gun1* (*genomes uncoupled1*) shows altered sensitivity to sucrose and abscisic acid and alterations in early seedling development. *J Exp Bot* **61**, 3773-3786.
- Cramer, W.A., Zhang, H., Yan, J., Kurisu, G., and Smith, J.L.** (2004). Evolution of photosynthesis: time-independent structure of the cytochrome *b₆f* complex. *Biochemistry* **43**, 5921-5929.
- Croce, R.** (2012). Chlorophyll-binding proteins of higher plants and cyanobacteria. In *Photosynthesis: Plastid Biology, Energy Conversion and Carbon Assimilation*, J.J. Eaton-Rye, B.C. Tripathy, and T.D. Sharkey, eds (Dordrecht: Springer Netherlands), pp. 127-149.
- Danon, A.** (1997). Translational regulation in the chloroplast. *Plant Physiol* **115**, 1293-1298.
- Delwiche, C.F., and Palmer, J.D.** (1997). The origin of plastids and their spread via secondary symbiosis. In *Origins of Algae and their Plastids*, D. Bhattacharya, ed (Vienna: Springer Vienna), pp. 53-86.
- Douce, R., and Joyard, J.** (1990). Biochemistry and function of the plastid envelope. *Annual Review of Cell Biology* **6**, 173-216.
- Estavillo, G.M., Crisp, P.A., Pornsiriwong, W., Wirtz, M., Collinge, D., Carrie, C., Giraud, E., Whelan, J., David, P., Javot, H., Brearley, C., Hell, R., Marin, E., and Pogson, B.J.** (2011). Evidence for a SAL1-PAP chloroplast retrograde pathway that functions in drought and high light signaling in Arabidopsis. *The Plant Cell* **23**, 3992.
- Facella, P., Carbone, F., Placido, A., and Perrotta, G.** (2017). Cryptochrome 2 extensively regulates transcription of the chloroplast genome in tomato. *FEBS Open Bio* **7**, 456-471.
- Falcone Ferreyra, M.L., Rius, S.P., and Casati, P.** (2012). Flavonoids: biosynthesis, biological functions, and biotechnological applications. *Front Plant Sci* **3**, 222-222.
- Farkas, I., Dombrádi, V., Miskei, M., Szabados, L., and Koncz, C.** (2007). Arabidopsis PPP family of serine/threonine phosphatases. *Trends in Plant Science* **12**, 169-176.

- Fitter, D.W., Martin, D.J., Copley, M.J., Scotland, R.W., and Langdale, J.A.** (2002). GLK gene pairs regulate chloroplast development in diverse plant species. *The Plant Journal* **31**, 713-727.
- Franzolin, E., Pontarin, G., Rampazzo, C., Miazzi, C., Ferraro, P., Palumbo, E., Reichard, P., and Bianchi, V.** (2013). The deoxynucleotide triphosphohydrolase SAMHD1 is a major regulator of DNA precursor pools in mammalian cells. *Proceedings of the National Academy of Sciences* **110**, 14272.
- Garton, S., Knight, H., Warren, G.J., Knight, M.R., and Thorlby, G.J.** (2007). crinkled leaves 8 – A mutation in the large subunit of ribonucleotide reductase – leads to defects in leaf development and chloroplast division in *Arabidopsis thaliana*. *The Plant Journal* **50**, 118-127.
- Gray, J.C.** (1995). Chloroplast control of nuclear gene expression. *Photosynthesis: From Light to Biosphere* **3**, 543-550.
- Gray, M.W.** (1999). Evolution of organellar genomes. *Current Opinion in Genetics & Development* **9**, 678-687.
- Hennig, J., and Herrmann, R.G.** (1986). Chloroplast ATP synthase of spinach contains nine nonidentical subunit species, six of which are encoded by plastid chromosomes in two operons in a phylogenetically conserved arrangement. *Molecular and General Genetics MGG* **203**, 117-128.
- Hernández-Verdeja, T., and Strand, Å.** (2018). Retrograde signals navigate the path to chloroplast development. *Plant Physiology* **176**, 967.
- Hill, J.L., Hammudi, M.B., and Tien, M.** (2014). The *Arabidopsis* cellulose synthase complex: a proposed hexamer of CESA trimers in an equimolar stoichiometry. *The Plant Cell* **26**, 4834.
- Hollenbaugh, J.A., Gee, P., Baker, J., Daly, M.B., Amie, S.M., Tate, J., Kasai, N., Kanemura, Y., Kim, D.-H., Ward, B.M., Koyanagi, Y., and Kim, B.** (2013). Host factor SAMHD1 restricts DNA viruses in non-dividing myeloid cells. *PLOS Pathogens* **9**, e1003481.
- Hsieh, W.-Y., Liao, J.-C., Wang, H.-T., Hung, T.-H., Tseng, C.-C., Chung, T.-Y., and Hsieh, M.-H.** (2017). The *Arabidopsis* thiamin-deficient mutant *pale green1* lacks thiamin monophosphate phosphatase of the vitamin B1 biosynthesis pathway. *The Plant Journal* **91**, 145-157.
- Inoue, K.** (2007). The chloroplast outer envelope membrane: The edge of light and excitement. *Journal of Integrative Plant Biology* **49**, 1100-1111.
- Jensen, P.E., and Leister, D.** (2014). Chloroplast evolution, structure and functions. *F1000Prime Rep* **6**, 40-40.
- Joliot, P., and Joliot, A.** (1994). Mechanism of electron transfer in the cytochrome *b/f* complex of algae: evidence for a semiquinone cycle. *Proc Natl Acad Sci U S A* **91**, 1034-1038.
- Jordan, P., Fromme, P., Witt, H.T., Klukas, O., Saenger, W., and Krauß, N.** (2001). Three-dimensional structure of cyanobacterial photosystem I at 2.5 Å resolution. *Nature* **411**, 909-917.
- Kacprzak, S.M., Mochizuki, N., Naranjo, B., Xu, D., Leister, D., Kleine, T., Okamoto, H., and Terry, M.J.** (2019). Plastid-to-nucleus retrograde signalling during chloroplast biogenesis does not require ABI4. *Plant Physiol* **179**, 18.
- Keeling, P.J.** (2010). The endosymbiotic origin, diversification and fate of plastids. *Philosophical Transactions of the Royal Society B: Biological Sciences* **365**, 729-748.

- Kleine, T.** (2012). Arabidopsis thaliana mTERF proteins: evolution and functional classification. *Frontiers in Plant Science* **3**.
- Kleine, T., and Leister, D.** (2015). Emerging functions of mammalian and plant mTERFs. *Biochimica et Biophysica Acta (BBA) - Bioenergetics* **1847**, 786-797.
- Kleine, T., and Leister, D.** (2016). Retrograde signaling: Organelles go networking. *Biochimica et Biophysica Acta (BBA) - Bioenergetics* **1857**, 1313-1325.
- Kleine, T., Lockhart, P., and Batschauer, A.** (2003). An Arabidopsis protein closely related to Synechocystis cryptochrome is targeted to organelles. *The Plant Journal* **35**, 93-103.
- Kleine, T., Voigt, C., and Leister, D.** (2009a). Plastid signalling to the nucleus: messengers still lost in the mists? *Trends in Genetics* **25**, 185-192.
- Kleine, T., Maier, U.G., and Leister, D.** (2009b). DNA Transfer from Organelles to the Nucleus: The Idiosyncratic Genetics of Endosymbiosis. *Annual Review of Plant Biology* **60**, 115-138.
- Lahouassa, H., Daddacha, W., Hofmann, H., Ayinde, D., Logue, E.C., Dragin, L., Bloch, N., Maudet, C., Bertrand, M., Gramberg, T., Pancino, G., Priet, S., Canard, B., Laguette, N., Benkirane, M., Transy, C., Landau, N.R., Kim, B., and Margottin-Goguet, F.** (2012). SAMHD1 restricts the replication of human immunodeficiency virus type 1 by depleting the intracellular pool of deoxynucleoside triphosphates. *Nat Immunol* **13**, 223-228.
- Laluk, K., AbuQamar, S., and Mengiste, T.** (2011). The Arabidopsis mitochondria-localized pentatricopeptide repeat protein PGN functions in defense against necrotrophic fungi and abiotic stress tolerance. *Plant Physiol* **156**, 2053.
- Lee, J., He, K., Stolc, V., Lee, H., Figueroa, P., Gao, Y., Tongprasit, W., Zhao, H., Lee, I., and Deng, X.W.** (2007). Analysis of transcription factor HY5 genomic binding sites revealed its hierarchical role in light regulation of development. *The Plant Cell* **19**, 731.
- Leister, D.** (2012). Retrograde signaling in plants: from simple to complex scenarios. *Frontiers in Plant Science* **3**.
- Leister, D., and Kleine, T.** (2016). Definition of a core module for the nuclear retrograde response to altered organellar gene expression identifies *GLK* overexpressors as gun mutants. *Physiologia Plantarum* **157**, 297-309.
- Leister, D., Wang, L., and Kleine, T.** (2017). Organellar gene expression and acclimation of plants to environmental stress. *Frontiers in Plant Science* **8**.
- Leivar, P., and Quail, P.H.** (2011). PIFs: pivotal components in a cellular signaling hub. *Trends in Plant Science* **16**, 19-28.
- Leivar, P., and Monte, E.** (2014). PIFs: Systems integrators in plant development. *The Plant Cell* **26**, 56.
- Leivar, P., Monte, E., Oka, Y., Liu, T., Carle, C., Castillon, A., Huq, E., and Quail, P.H.** (2008). Multiple phytochrome-interacting bHLH transcription factors repress premature seedling photomorphogenesis in darkness. *Current Biology* **18**, 1815-1823.
- Lepistö, A., and Rintamäki, E.** (2012). Coordination of plastid and light signaling pathways upon development of Arabidopsis leaves under various photoperiods. *Molecular Plant* **5**, 799-816.
- Li, Z., Wakao, S., Fischer, B.B., and Niyogi, K.K.** (2009). Sensing and responding to excess light. *Annual Review of Plant Biology* **60**, 239-260.

- Liberton, M., Austin, J.R., Berg, R.H., and Pakrasi, H.B.** (2011). Unique thylakoid membrane architecture of a unicellular N₂-Fixing cyanobacterium revealed by electron tomography. *Plant Physiol* **155**, 1656.
- Ling, Q., and Jarvis, P.** (2015). Regulation of chloroplast protein import by the ubiquitin E3 ligase SP1 is important for stress tolerance in plants. *Current Biology* **25**, 2527-2534.
- Lupi, A.C.D., Lira, B.S., Gramegna, G., Trench, B., Alves, F.R.R., Demarco, D., Peres, L.E.P., Purgatto, E., Freschi, L., and Rossi, M.** (2019). *Solanum lycopersicum* GOLDEN 2-LIKE 2 transcription factor affects fruit quality in a light- and auxin-dependent manner. *PLOS ONE* **14**, e0212224.
- Malone, L.A., Qian, P., Mayneord, G.E., Hitchcock, A., Farmer, D.A., Thompson, R.F., Swainsbury, D.J.K., Ranson, N.A., Hunter, C.N., and Johnson, M.P.** (2019). Cryo-EM structure of the spinach cytochrome b6 f complex at 3.6 Å resolution. *Nature* **575**, 535-539.
- Mareš, J., Strunecký, O., Bučinská, L., and Wiedermannová, J.** (2019). Evolutionary patterns of thylakoid architecture in cyanobacteria. *Frontiers in Microbiology* **10**.
- Marino, G., Naranjo, B., Wang, J., Penzler, J.-F., Kleine, T., and Leister, D.** (2019). Relationship of GUN1 to FUG1 in chloroplast protein homeostasis. *The Plant Journal* **99**, 521-535.
- Martin, W., Rujan, T., Richly, E., Hansen, A., Cornelsen, S., Lins, T., Leister, D., Stoebe, B., Hasegawa, M., and Penny, D.** (2002). Evolutionary analysis of Arabidopsis, cyanobacterial, and chloroplast genomes reveals plastid phylogeny and thousands of cyanobacterial genes in the nucleus. *Proceedings of the National Academy of Sciences* **99**, 12246.
- Mazor, Y., Borovikova, A., and Nelson, N.** (2015). The structure of plant photosystem I super-complex at 2.8 Å resolution. *eLife* **4**, e07433.
- Mazor, Y., Borovikova, A., Caspy, I., and Nelson, N.** (2017). Structure of the plant photosystem I supercomplex at 2.6 Å resolution. *Nature Plants* **3**, 17014.
- McFadden, G.I., and van Dooren, G.G.** (2004). Evolution: Red algal genome affirms a common origin of all plastids. *Current Biology* **14**, R514-R516.
- Mereschkowsky, C.** (1905). Über Natur und Ursprung der Chromatophoren im Pflanzenreiche. *Biologisches Centralblatt* **25**, 293-604.
- Meyer, A.** (1883). Das chlorophyllkorn in chemischer, morphologischer und biologischer beziehung: Ein beitrag zur kenntniss des chlorophyllkornes der angiospermen und seiner metamorphosen. (A. Felix).
- Mignolet-Spruyt, L., Xu, E., Idänheimo, N., Hoeberichts, F.A., Mühlenbock, P., Brosché, M., Van Breusegem, F., and Kangasjärvi, J.** (2016). Spreading the news: subcellular and organellar reactive oxygen species production and signalling. *Journal of Experimental Botany* **67**, 3831-3844.
- Miyagishima, S.-y.** (2011). Mechanism of plastid division: From a bacterium to an organelle. *Plant Physiol* **155**, 1533.
- Mochizuki, N., Brusslan, J.A., Larkin, R., Nagatani, A., and Chory, J.** (2001). Arabidopsis genomes *uncoupled 5* (*GUN5*) mutant reveals the involvement of Mg-chelatase H subunit in plastid-to-nucleus signal transduction. *Proceedings of the National Academy of Sciences* **98**, 2053.
- Møller, S.G., Kim, Y.-S., Kunkel, T., and Chua, N.-H.** (2003). PP7 Is a positive regulator of blue light signaling in Arabidopsis. *The Plant Cell* **15**, 1111.

- Nakamura, H., Muramatsu, M., Hakata, M., Ueno, O., Nagamura, Y., Hirochika, H., Takano, M., and Ichikawa, H.** (2009). Ectopic overexpression of the transcription factor OsGLK1 induces chloroplast development in non-green rice cells. *Plant and Cell Physiology* **50**, 1933-1949.
- Nelson, N., and Yocum, C.F.** (2006). STRUCTURE AND FUNCTION OF PHOTOSYSTEMS I AND II. *Annual Review of Plant Biology* **57**, 521-565.
- Nelson, N., and Junge, W.** (2015). Structure and energy transfer in photosystems of oxygenic photosynthesis. *Annual Review of Biochemistry* **84**, 659-683.
- Neuhaus, H.E., and Wagner, R.** (2000). Solute pores, ion channels, and metabolite transporters in the outer and inner envelope membranes of higher plant plastids. *Biochimica et Biophysica Acta (BBA) - Biomembranes* **1465**, 307-323.
- Núñez-Delegido, E., Robles, P., Ferrández-Ayela, A., and Quesada, V.** (2019). Functional analysis of mTERF5 and mTERF9 contribution to salt tolerance, plastid gene expression and retrograde signalling in *Arabidopsis thaliana*. *Plant Biology* **n/a**.
- Ochoa de Alda, J.A.G., Esteban, R., Diago, M.L., and Houmard, J.** (2014). The plastid ancestor originated among one of the major cyanobacterial lineages. *Nature Communications* **5**, 4937.
- Page, M.T., Kacprzak, S.M., Mochizuki, N., Okamoto, H., Smith, A.G., and Terry, M.J.** (2017). Seedlings lacking the PTM protein do not show a *genomes uncoupled (gun)* mutant phenotype. *Plant Physiol* **174**, 21.
- Palmer, J.D.** (2000). A single birth of all plastids? *Nature* **405**, 32-33.
- Pedersen, P.L., and Amzel, L.M.** (1993). ATP synthases. Structure, reaction center, mechanism, and regulation of one of nature's most unique machines. *Journal of Biological Chemistry* **268**, 9937-9940.
- Pedersen, P.L., Ko, Y.H., and Hong, S.** (2000). ATP Synthases in the year 2000: Evolving views about the structures of these remarkable enzyme complexes. *Journal of Bioenergetics and Biomembranes* **32**, 325-332.
- Pesaresi, P., and Kim, C.** (2019). Current understanding of GUN1: a key mediator involved in biogenic retrograde signaling. *Plant Cell Reports* **38**, 819-823.
- Pesaresi, P., Masiero, S., Eubel, H., Braun, H.-P., Bhushan, S., Glaser, E., Salamini, F., and Leister, D.** (2006). Nuclear photosynthetic gene expression is synergistically modulated by rates of protein synthesis in chloroplasts and mitochondria. *The Plant Cell* **18**, 970.
- Pfannschmidt, T., Blanvillain, R., Merendino, L., Courtois, F., Chevalier, F., Liebers, M., Grüber, B., Hommel, E., and Lerbs-Mache, S.** (2015). Plastid RNA polymerases: orchestration of enzymes with different evolutionary origins controls chloroplast biogenesis during the plant life cycle. *J Exp Bot* **66**, 6957-6973.
- Pogson, B.J., and Albrecht, V.** (2011). Genetic dissection of chloroplast biogenesis and development: An overview. *Plant Physiol* **155**, 1545.
- Pogson, B.J., and Albrecht-Borth, V.** (2014). An overview of chloroplast biogenesis and development. In *Plastid Biology*, S.M. Theg and F.-A. Wollman, eds (New York, NY: Springer New York), pp. 115-128.
- Pogson, B.J., Ganguly, D., and Albrecht-Borth, V.** (2015). Insights into chloroplast biogenesis and development. *Biochimica et Biophysica Acta (BBA) - Bioenergetics* **1847**, 1017-1024.

- Pribil, M., Labs, M., and Leister, D.** (2014). Structure and dynamics of thylakoids in land plants. *Journal of Experimental Botany* **65**, 1955-1972.
- Price, D.C., Chan, C.X., Yoon, H.S., Yang, E.C., Qiu, H., Weber, A.P.M., Schwacke, R., Gross, J., Blouin, N.A., Lane, C., Reyes-Prieto, A., Durnford, D.G., Neilson, J.A.D., Lang, B.F., Burger, G., Steiner, J.M., Löffelhardt, W., Meuser, J.E., Posewitz, M.C., Ball, S., Arias, M.C., Henrissat, B., Coutinho, P.M., Rensing, S.A., Symeonidi, A., Doddapaneni, H., Green, B.R., Rajah, V.D., Boore, J., and Bhattacharya, D.** (2012). Cyanophora paradoxa genome elucidates origin of photosynthesis in algae and plants. *Science* **335**, 843.
- Qin, X., Suga, M., Kuang, T., and Shen, J.-R.** (2015). Structural basis for energy transfer pathways in the plant PSI-LHCI supercomplex. *Science* **348**, 989.
- Quail, P.H.** (2002). Phytochrome photosensory signalling networks. *Nature Reviews Molecular Cell Biology* **3**, 85-93.
- Quesada, V.** (2016). The roles of mitochondrial transcription termination factors (MTERFs) in plants. *Physiologia Plantarum* **157**, 389-399.
- Ramel, F., Birtic, S., Ginies, C., Soubigou-Taconnat, L., Triantaphylidès, C., and Havaux, M.** (2012). Carotenoid oxidation products are stress signals that mediate gene responses to singlet oxygen in plants. *Proceedings of the National Academy of Sciences* **109**, 5535.
- Reumann, S., Inoue, K., and Keegstra, K.** (2005). Evolution of the general protein import pathway of plastids (Review). *Molecular Membrane Biology* **22**, 73-86.
- Rich, P.R.** (1984). Electron and proton transfers through quinones and cytochrome bc complexes. *Biochimica et Biophysica Acta (BBA) - Reviews on Bioenergetics* **768**, 53-79.
- Robles, P., and Quesada, V.** (2019). Transcriptional and post-transcriptional regulation of organellar gene expression (OGE) and its roles in plant salt tolerance. *Int J Mol Sci* **20**, 1056.
- Robles, P., Micol, J.L., and Quesada, V.** (2012). Arabidopsis MDA1, a nuclear-encoded protein, functions in chloroplast development and abiotic stress responses. *PLOS ONE* **7**, e42924.
- Robles, P., Micol, J.L., and Quesada, V.** (2015). Mutations in the plant-conserved MTERF9 alter chloroplast gene expression, development and tolerance to abiotic stress in *Arabidopsis thaliana*. *Physiologia Plantarum* **154**, 297-313.
- Robles, P., Navarro-Cartagena, S., Ferrández-Ayela, A., Núñez-Delegido, E., and Quesada, V.** (2018). The characterization of Arabidopsis mterf6 mutants reveals a new role for mTERF6 in tolerance to abiotic stress. *Int J Mol Sci* **19**.
- Rokka, A., Suorsa, M., Saleem, A., Battchikova, N., and Aro, E.-M.** (2005). Synthesis and assembly of thylakoid protein complexes: multiple assembly steps of photosystem II. *Biochemical Journal* **388**, 159-168.
- Rubinson, E.H., and Eichman, B.F.** (2012). Nucleic acid recognition by tandem helical repeats. *Current Opinion in Structural Biology* **22**, 101-109.
- Ruckle, M.E., DeMarco, S.M., and Larkin, R.M.** (2007). Plastid signals remodel light signaling networks and are essential for efficient chloroplast biogenesis in Arabidopsis. *The Plant Cell* **19**, 3944.
- Rühle, T., and Leister, D.** (2015). Assembly of F1F0-ATP synthases. *Biochimica et Biophysica Acta (BBA) - Bioenergetics* **1847**, 849-860.

- Sakamoto, W., Miyagishima, S.-y., and Jarvis, P.** (2008). Chloroplast Biogenesis: control of plastid development, protein import, division and inheritance. *The Arabidopsis Book* **2008**.
- Sato, N.** (2002). Comparative Analysis of the Genomes of Cyanobacteria and Plants. *Genome Informatics* **13**, 173-182.
- Schimper, A.F.W.** (1883). Über die Entwicklung der Chlorophyllkörner und Farbkörper. *Bot Zeit* **41**, 105-112.
- Schirrmeister, B.E., de Vos, J.M., Antonelli, A., and Bagheri, H.C.** (2013). Evolution of multicellularity coincided with increased diversification of cyanobacteria and the Great Oxidation Event. *Proceedings of the National Academy of Sciences* **110**, 1791.
- Shi, L.-X., and Schröder, W.P.** (2004). The low molecular mass subunits of the photosynthetic supracomplex, photosystem II. *Biochimica et Biophysica Acta (BBA) - Bioenergetics* **1608**, 75-96.
- Shi, M.-Z., and Xie, D.-Y.** (2014). Biosynthesis and metabolic engineering of anthocyanins in *Arabidopsis thaliana*. *Recent Pat Biotechnol* **8**, 47-60.
- Shimizu, T., Kacprzak, S.M., Mochizuki, N., Nagatani, A., Watanabe, S., Shimada, T., Tanaka, K., Hayashi, Y., Arai, M., Leister, D., Okamoto, H., Terry, M.J., and Masuda, T.** (2019). The retrograde signaling protein GUN1 regulates tetrapyrrole biosynthesis. *Proceedings of the National Academy of Sciences* **116**, 24900.
- Shin, J., Kim, K., Kang, H., Zulfugarov, I.S., Bae, G., Lee, C.-H., Lee, D., and Choi, G.** (2009). Phytochromes promote seedling light responses by inhibiting four negatively-acting phytochrome-interacting factors. *Proceedings of the National Academy of Sciences* **106**, 7660.
- Solymosi, K., and Schoefs, B.** (2010). Etioplast and etio-chloroplast formation under natural conditions: the dark side of chlorophyll biosynthesis in angiosperms. *Photosynthesis Research* **105**, 143-166.
- Suga, M., Qin, X., Kuang, T., and Shen, J.-R.** (2016). Structure and energy transfer pathways of the plant photosystem I-LHCI supercomplex. *Current Opinion in Structural Biology* **39**, 46-53.
- Sun, A.-Z., and Guo, F.-Q.** (2016). Chloroplast retrograde regulation of heat stress responses in plants. *Frontiers in Plant Science* **7**.
- Sun, X., Xu, D., Liu, Z., Kleine, T., and Leister, D.** (2015). Functional relationship between mTERF4 and GUN1 in retrograde signaling. *Journal of Experimental Botany* **67**, 3909-3924.
- Sun, X., Feng, P., Xu, X., Guo, H., Ma, J., Chi, W., Lin, R., Lu, C., and Zhang, L.** (2011). A chloroplast envelope-bound PHD transcription factor mediates chloroplast signals to the nucleus. *Nature Communications* **2**, 477.
- Sun, Y., and Zerges, W.** (2015). Translational regulation in chloroplasts for development and homeostasis. *Biochimica et Biophysica Acta (BBA) - Bioenergetics* **1847**, 809-820.
- Surpin, M., Larkin, R.M., and Chory, J.** (2002). Signal transduction between the chloroplast and the nucleus. *The Plant cell* **14 Suppl**, S327-S338.
- Tadini, L., Peracchio, C., Trotta, A., Colombo, M., Mancini, I., Jeran, N., Costa, A., Faoro, F., Marsoni, M., Vannini, C., Aro, E.-M., and Pesaresi, P.** (2019). GUN1 influences the accumulation of NEP-dependent transcripts and chloroplast protein import in *Arabidopsis* cotyledons upon perturbation of chloroplast protein homeostasis. *The Plant Journal* **n/a**.

- Tadini, L., Pesaresi, P., Kleine, T., Rossi, F., Guljamow, A., Sommer, F., Mühlhaus, T., Schroda, M., Masiero, S., Pribil, M., Rothbart, M., Hedtke, B., Grimm, B., and Leister, D.** (2016). GUN1 controls accumulation of the plastid ribosomal protein S1 at the protein level and interacts with proteins involved in plastid protein homeostasis. *Plant Physiol* **170**, 1817.
- Thum, K.E., Kim, M., Christopher, D.A., and Mullet, J.E.** (2001). Cryptochrome 1, Cryptochrome 2, and phytochrome a co-activate the chloroplast psbD blue light-responsive promoter. *The Plant Cell* **13**, 2747.
- Tice, M.M., and Lowe, D.R.** (2004). Photosynthetic microbial mats in the 3,416-Myr-old ocean. *Nature* **431**, 549-552.
- Tice, M.M., and Lowe, D.R.** (2006). The origin of carbonaceous matter in pre-3.0 Ga greenstone terrains: A review and new evidence from the 3.42 Ga Buck Reef Chert. *Earth-Science Reviews* **76**, 259-300.
- Vinti, G., Hills, A., Campbell, S., Bowyer, J.R., Mochizuki, N., Chory, J., and López-Juez, E.** (2000). Interactions between *hy1* and *gun* mutants of *Arabidopsis*, and their implications for plastid/nuclear signalling. *The Plant Journal* **24**, 883-894.
- Voigt, C., Oster, U., Börnke, F., Jahns, P., Dietz, K.-J., Leister, D., and Kleine, T.** (2010). In-depth analysis of the distinctive effects of norflurazon implies that tetrapyrrole biosynthesis, organellar gene expression and ABA cooperate in the GUN-type of plastid signalling. *Physiologia Plantarum* **138**, 503-519.
- von Arnim, A.G., and Deng, X.-W.** (1994). Light inactivation of *Arabidopsis* photomorphogenic repressor COP1 involves a cell-specific regulation of its nucleocytoplasmic partitioning. *Cell* **79**, 1035-1045.
- Vothknecht, U.C., and Soll, J.** (2005). Chloroplast membrane transport: Interplay of prokaryotic and eukaryotic traits. *Gene* **354**, 99-109.
- Wagner, D., Przybyla, D., op den Camp, R., Kim, C., Landgraf, F., Lee, K.P., Würsch, M., Laloi, C., Nater, M., Hideg, E., and Apel, K.** (2004). The genetic basis of singlet oxygen-induced stress responses of *Arabidopsis thaliana*. *Science* **306**, 1183.
- Waters, M.T., and Langdale, J.A.** (2009). The making of a chloroplast. *The EMBO Journal* **28**, 2861-2873.
- Watson, S.J., Sowden, R.G., and Jarvis, P.** (2018). Abiotic stress-induced chloroplast proteome remodelling: a mechanistic overview. *Journal of Experimental Botany* **69**, 2773-2781.
- Weeden, N.F.** (1981). Genetic and biochemical implications of the endosymbiotic origin of the chloroplast. *Journal of Molecular Evolution* **17**, 133-139.
- Westhoff, P., Alt, J., Nelson, N., and Herrmann, R.G.** (1985). Genes and transcripts for the ATP synthase CF₀ subunits I and II from spinach thylakoid membranes. *Molecular and General Genetics MGG* **199**, 290-299.
- Westphal, S., Soll, J., and Vothknecht, U.C.** (2003). Evolution of chloroplast vesicle transport. *Plant and Cell Physiology* **44**, 217-222.
- Wicke, S., Schneeweiss, G.M., dePamphilis, C.W., Müller, K.F., and Quandt, D.** (2011). The evolution of the plastid chromosome in land plants: gene content, gene order, gene function. *Plant Molecular Biology* **76**, 273-297.

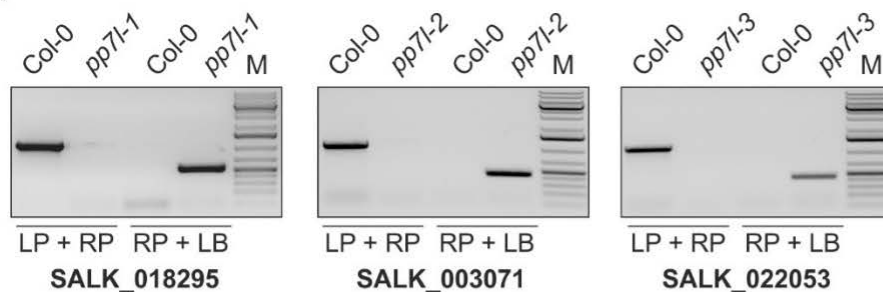
- Woodson, J.D., and Chory, J.** (2008). Coordination of gene expression between organellar and nuclear genomes. *Nature Reviews Genetics* **9**, 383-395.
- Woodson, Jesse D., and Chory, J.** (2012). Organelle signaling: how stressed chloroplasts communicate with the nucleus. *Current Biology* **22**, R690-R692.
- Woodson, Jesse D., Perez-Ruiz, Juan M., and Chory, J.** (2011). Heme synthesis by plastid ferrochelatase I regulates nuclear gene expression in plants. *Current Biology* **21**, 897-903.
- Wostrikoff, K., Girard-Bascou, J., Wollman, F.-A., and Choquet, Y.** (2004). Biogenesis of PSI involves a cascade of translational autoregulation in the chloroplast of *Chlamydomonas*. *The EMBO Journal* **23**, 2696-2705.
- Wu, G.-Z., Meyer, E.H., Richter, A.S., Schuster, M., Ling, Q., Schöttler, M.A., Walther, D., Zoschke, R., Grimm, B., Jarvis, R.P., and Bock, R.** (2019). Control of retrograde signalling by protein import and cytosolic folding stress. *Nature Plants* **5**, 525-538.
- Xiao, Y., Savchenko, T., Baidoo, Edward E.K., Chehab, Wassim E., Hayden, Daniel M., Tolstikov, V., Corwin, Jason A., Kliebenstein, Daniel J., Keasling, Jay D., and Dehesh, K.** (2012). Retrograde signaling by the plastidial metabolite MEcPP regulates expression of nuclear stress-response genes. *Cell* **149**, 1525-1535.
- Xiong, J., and Bauer, C.E.** (2002). COMPLEX EVOLUTION OF PHOTOSYNTHESIS. *Annual Review of Plant Biology* **53**, 503-521.
- Yoo, C.Y., Pasoreck, E.K., Wang, H., Cao, J., Blaha, G.M., Weigel, D., and Chen, M.** (2019). Phytochrome activates the plastid-encoded RNA polymerase for chloroplast biogenesis via nucleus-to-plastid signaling. *Nature Communications* **10**, 2629.
- Yoshida, Y., Sarmiento-Mañús, R., Yamori, W., Ponce, M.R., Micol, J.L., and Tsukaya, H.** (2018). The *Arabidopsis* phyB-9 mutant has a second-site mutation in the *VENOSA4* gene that alters chloroplast size, photosynthetic traits, and leaf growth. *Plant Physiology* **178**, 3.
- Zhao, X., Huang, J., and Chory, J.** (2019). GUN1 interacts with MORF2 to regulate plastid RNA editing during retrograde signaling. *Proceedings of the National Academy of Sciences* **116**, 10162.
- Zhu, J.-K.** (2016). Abiotic Stress Signaling and Responses in Plants. *Cell* **167**, 313-324.

Supplemental information

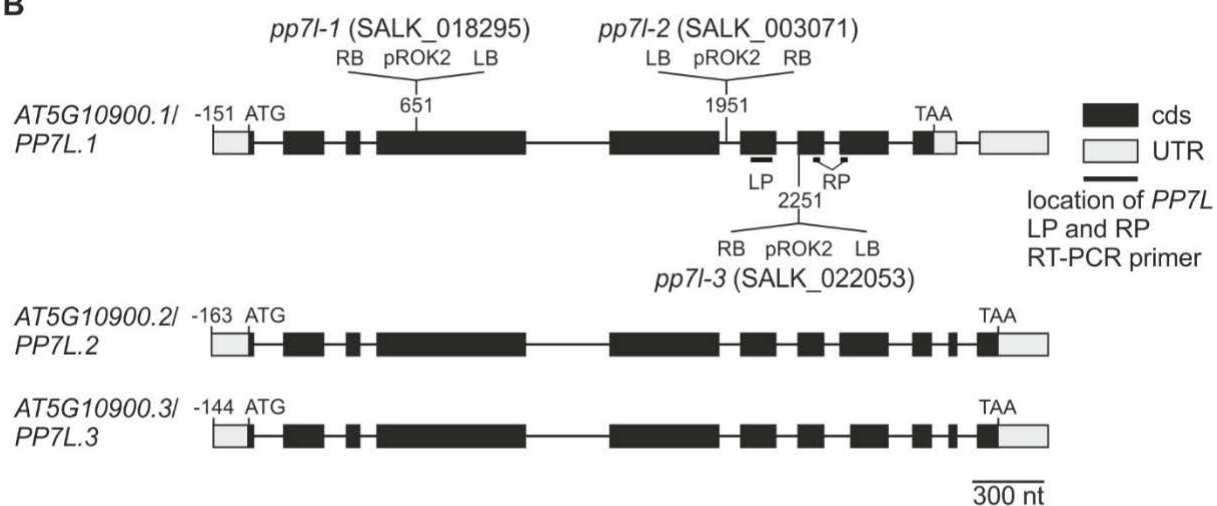
Supplemental information – Chapter 1

SUPPLEMENTAL DATA

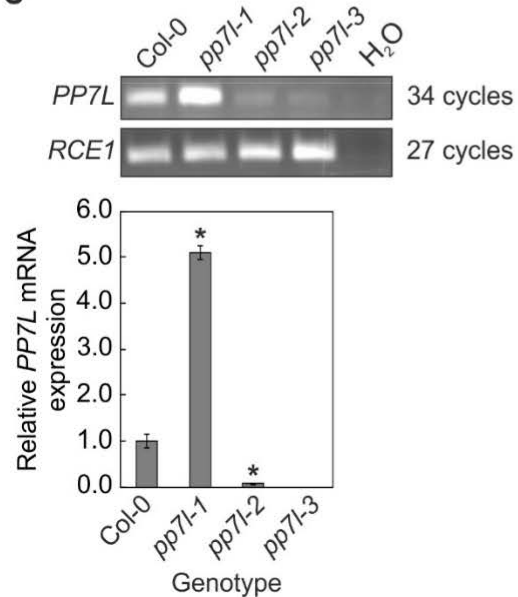
A



B



C



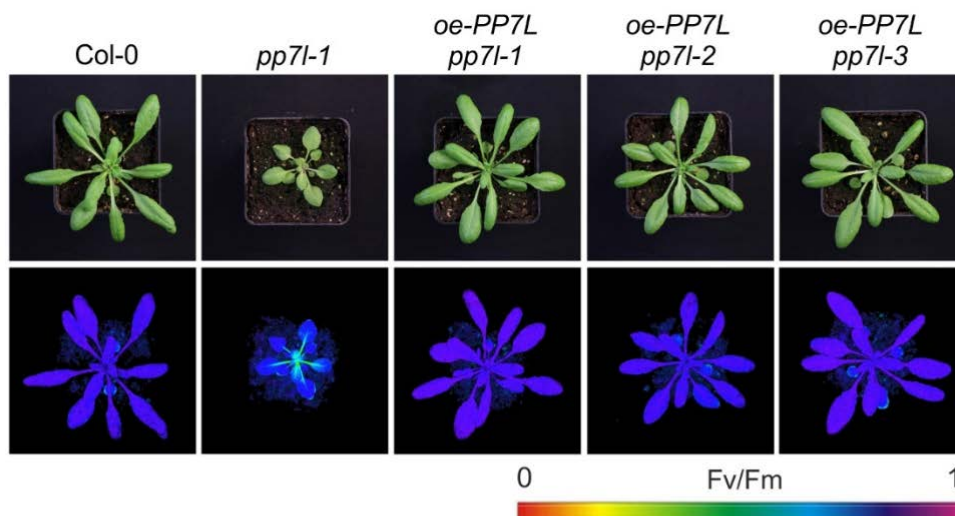
Supplemental Figure S1
 Xu et al., 2019

Supplemental Figure S1. Identification of *pp7l* T-DNA insertion mutants.

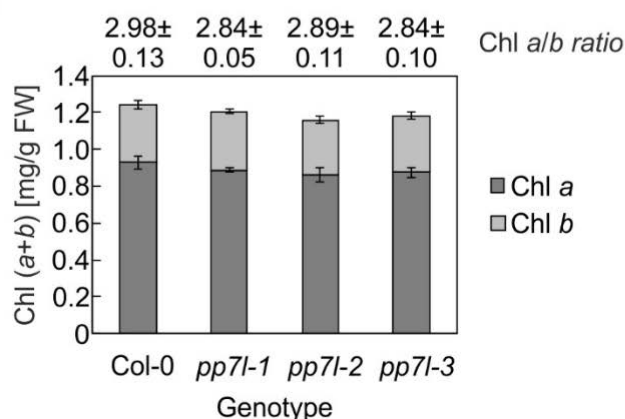
(A) Confirmation and identification of homozygous T-DNA insertions in the different *pp7l* mutant lines. The gene-specific left and right primers (LP and RP) were used for amplification of sequences around the T-DNA insertion, and RP was used together with the T-DNA left border primer (LB) for verification of the T-DNA insertion.

(B) Schematic representation and T-DNA tagging of the *PP7L* (*AT5G10900*) locus. Exons (black boxes), introns (black lines) and the 5' and 3' UTRs (grey boxes) are shown. Numbers are given relative to the start codon ATG. Locations and orientation of T-DNA insertions are indicated, as deduced from RP + LB PCR products shown in (A), which were subsequently sequenced. Note that the insertions are not drawn to scale. Furthermore, the locations of the primers used in the RT-qPCR analysis of *PP7L* expression shown in panel (C) are indicated as thick black lines. The LP primer is an exon-exon primer spanning intron 7 of *PP7L*, which avoids amplification of genomic DNA. RT-qPCR of wild-type (Col-0) and *pp7l* mutant plants. (C) RT-qPCR was performed with primers specific for *PP7L* (locations of the primer annealing sites are indicated in panel (B)) and *AT4G36800*, encoding a RUB1-conjugating enzyme (*RCE1*), which serves as a control. Expression values are reported relative to the corresponding transcript levels in Col-0. The results were normalized with respect to the expression level of *RCE1*. Note that, in the *pp7l-1* allele, the T-DNA of the pROK2 vector is integrated in the 5'RB-T-DNA-LB3' direction and that the 35S promoter in this vector is located on the LB side, and can potentially the 35S promoter activate transcription of flanking downstream genomic sequences. Bars indicate standard deviations. Statistically significant differences (Tukey's test; $p < 0.05$) between wild-type and mutant samples are indicated by an asterisk.

A



B

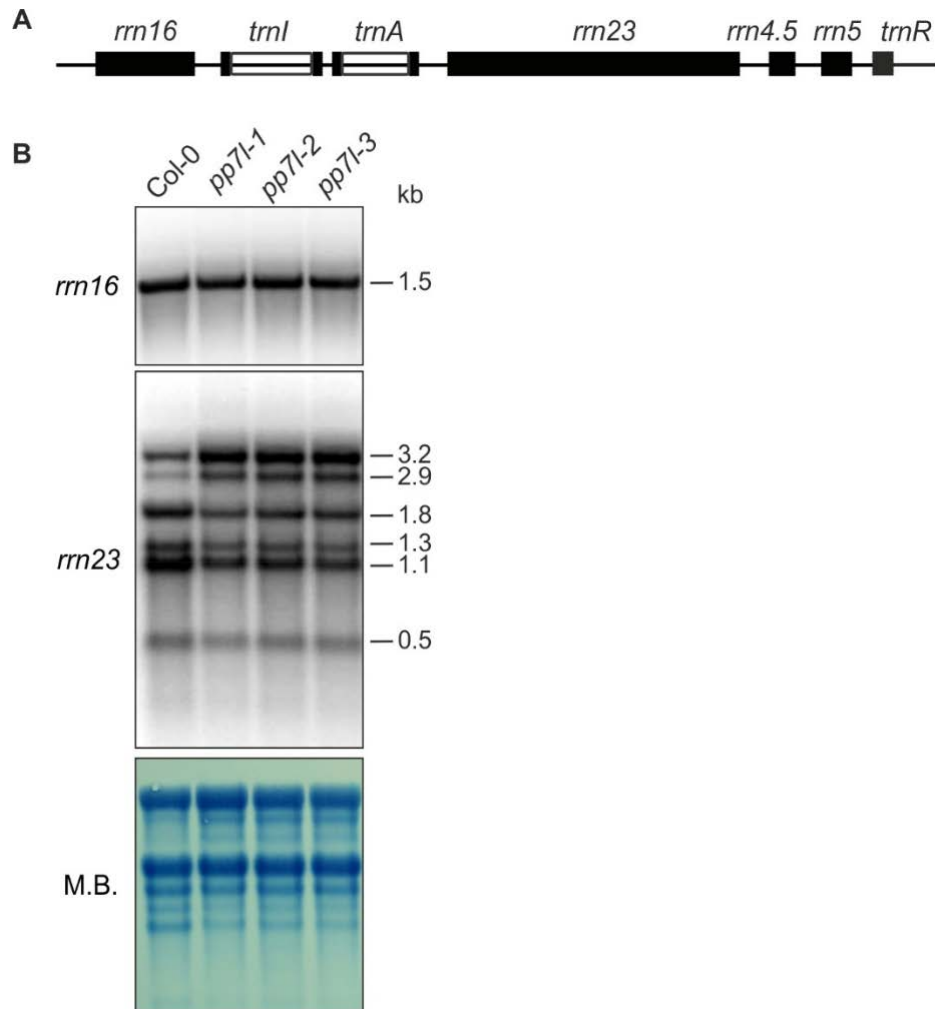


Supplemental Figure S2
Xu et al., 2019

Supplemental Figure S2. Chlorophyll content and complementation of *pp7l* T-DNA insertion mutants.

(A) Phenotypes of 4-week-old Col-0 and complementation of the three *pp7l* mutants with the coding sequence of the *AT5G10900* gene (*oe-PP7L pp7l-1* to -3).

(B) Determination of total chlorophyll (Chl *a* + *b*) and the Chl *a/b* ratio (indicated above the histogram) of 4-week-old plants. Pigments were acetone-extracted, measured spectrophotometrically, and concentrations were determined as described in Jeffrey and Humphrey (1975). Data are shown as mean values \pm SD from three different plant pools. Each pool contained more than 20 plants. No significant differences were identified (Tukey's test).

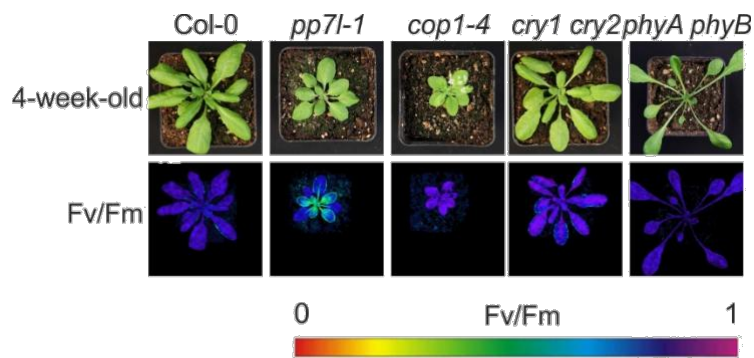


Xu et al., 2019
Supplemental Figure S3

Supplemental Figure S3. Ribosomal RNA maturation in 4-day-old Col-0 and *pp7l* mutant seedlings.

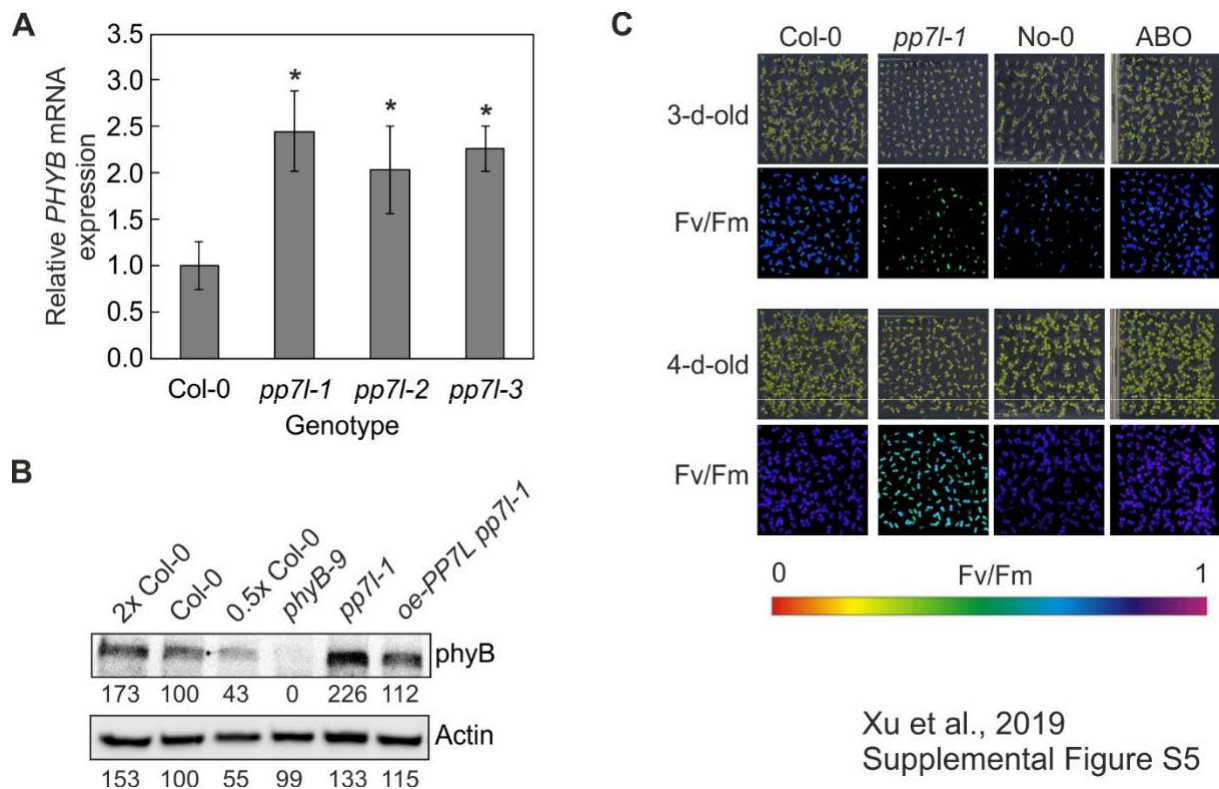
(A) Schematic representation of the chloroplast *rrn* operon. Black and white boxes represent exons and introns, respectively.

(B) Total RNA was isolated, fractionated on a denaturing gel, transferred onto a nitrocellulose membrane, and probed with [α - 32 P]dCTP-labeled cDNA fragments specific for *rrn16* and *rrn23*. rRNA was visualized by staining the membrane with methylene blue (M. B.) which served as a loading control.



Xu et al., 2019
Supplemental Figure S4

Supplemental Figure S4. Phenotypes of 4-week-old Col-0, *pp7l-1*, *cop1-4* and the different photoreceptor (*cry1-304* *cry2-1*, *phyA-211* *phyB-9*) mutant plants. In the lower row Imaging PAM pictures depict the maximum quantum yields of PSII (Fv/Fm).



Xu et al., 2019
Supplemental Figure S5

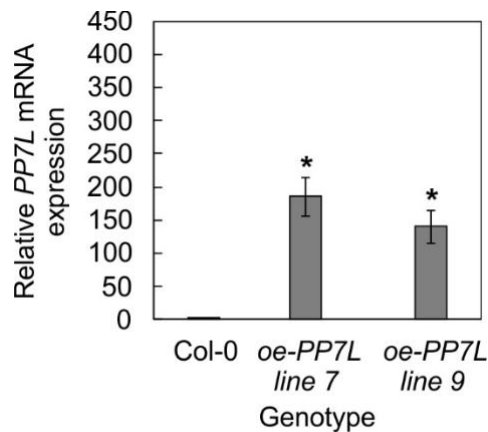
Supplemental Figure S5. PhyB levels are elevated in *pp7l* mutants, but overexpression of phyB does not result in a *pp7l* phenotype.

(A) RT-qPCR of 4-day-old wild-type (Col-0) and *pp7l* mutant plants. RT-qPCR was performed with primers specific for *PHYB* and *AT4G36800* (which codes for a RUB1-conjugating enzyme (*RCE1*)) as a control. Expression values are reported relative to the corresponding transcript levels in Col-0. The results were normalized with respect to the expression level of *RCE1*. Bars indicate standard deviations of three independent experiments. In each experiment at least 50 seedlings per genotype were pooled. Statistically significant differences (Tukey's test; $P < 0.05$) between wild-type and mutant samples are indicated by an asterisk.

(B) Immunoblot analysis of phyB. Total protein extracts from 4-day-old wild-type (Col-0), *pp7l-1* and complemented *pp7l-1* (*oe-PP7L pp7l-1*), and Col-0 overexpressing PP7L-GFP (*oe-PP7L*) were fractionated by SDS-PAGE, and blots were probed with antibodies raised against phyB. Decreasing

levels of wild- type proteins were loaded in the lanes marked 2x Col-0, Col-0 and 0.5x Col-0. (1x Col-0 = 10 µg). Actin served as the loading control.

(C) Phenotypes of 3- and 4-day-old Col-0 *pp7l-1*, No-0 and No-0-overexpressing phyB (ABO) plants together with Imaging PAM pictures depicting the corresponding maximum quantum yields of PSII (Fv/Fm).



Supplemental Figure S6
Xu et al., 2019

Supplemental Figure S6. Overexpression of *PP7L* in Col-0. RT-qPCR of 4-day-old wild-type (Col-0) and Col-0 plants overexpressing *PP7L* (*oe-PP7L*). RT-qPCR PCR was performed with primers specific for *PP7L* and *AT4G36800*, encoding a RUB1-conjugating enzyme (*RCE1*) as a control. Expression values are reported relative to the corresponding transcript levels in Col-0. The results were normalized with respect to the expression level of *RCE1*. Bars indicate standard deviations of three independent experiments performed with individual plants. Statistically significant differences (*t*-test; $p < 0.05$) between wild-type and mutant samples are indicated by an asterisk.

Supplemental Table S1. Standard deviations of the Fv/Fm values measured in the different *pp7l* mutant seedlings presented in Figure 3A.

Supplemental Table S2. Genes whose transcript levels differed by more than 2-fold relative to Col-0 in 4-day-old LD-grown *pp7l-1* seedlings.

Supplemental Table S3. Relative protein accumulation in the *pp7l-1* mutant compared to Col-0 grown for 4 days in LD conditions as determined by shotgun proteomics.

Supplemental Table S4. Primers used in this study.

Atg number	Description	Primer sequence (from 5' to 3')
Genotyping		
AT5G10900	pam46-SALK_018295 LP	ATGCCGTCAACTTCAACAATC
	pam46-SALK_018295 RP	CATTCTTGAAGCTAAGTGCGG
AT5G10900	pam46-SALK_022053 LP	CCAATGTAGCTTTCGTCTTCG
	pam46-SALK_022053 RP	TTACAAGGGACTTCTTTGGGG
AT5G10900	pam46-SALK_003071 RP	ATTGTTGAAGTTGACGGCATC
	pam46-SALK_003071 LP	CCAGTTTCTTACCCTTGGGAC
	SALK LB	GTCCGCAATGTGTTATTAAGTTGTC
	Detection of <i>phyB-9</i> mutation	CAATGTAGCTAGTGGAAGAAGCTCGA TGTGG ACATAACAGTGTCTGCGTTCTCAAAAC GC

AT5G40270	Detection of <i>ven4</i> mutation	TGTAATGTACGTGCTTAACTTTCTCT TCAAGGAATGTGCAAACATACCACTG
Amplification of <i>PP7L.1</i> and complementation		
AT5G10900.1	For complementation	GGGGACAAGTTTGTACAAAAAAGCAG GCTATGCCGCCTC GGGGACCACTTTGTACAAGAAAGCTG GGTGGAGCGAAGA
RNA gel blot analysis		
ATCG00020	<i>psbA</i>	GTGCCATTATTCCTACTTCTG AGAGATTCCTAGAGGCATACC
ATCG00680	<i>psbB</i>	CGGGTCTTTGGAGTTACGAA TCCAGCAACAACAAAAGCTG
AT1G44575	<i>PSBS</i>	GACAGGGATACCGATTACGA ACAATGGACCTTGTTCTTTGAG
ATCG00350	<i>psaA</i>	AACCAATTTCTAAACGCTGG TGATGATGTGCTATATCGGT
AT3G54890	<i>LHCA1</i>	GTCAAGCCACTTACTTGGA GGGATAACAATATCGCCAATG
AT1G64860	<i>SIG2</i>	CTTCTGCTGCTGGAGTCGAT AACGTCTTCATTCTCCCATCCT
AT2G36990	<i>SIG6</i>	GAAAAGTGTAGAAAAATTCAAAC GTAAACAGAGATCGTTATCGGAA
ATCG00270	<i>psbD</i>	ATGACTGGCTAAGGAGAGACCG AAGTCCAGTTATGAAAGCCTTG
ATCG00490	<i>rbcl</i>	CGTTGGAGAGACCGTTTCTT CAAAGCCCCAAAGTTGACTCC
AT5G10900	<i>PP7L</i>	AGTCTTCAGTGCTTCAATGTTCTC AGATTCAAACAAGGGT
ATCG00920	<i>rrn16S</i>	AGTCATCATGCCCTTATGC CAGTCACTAGCCCTGCCTTC
ATCG01180	<i>rrn23S</i>	GTTCGAGTACCAGGCGCTAC CGGAGACCTGTGTTTTTGGT
RT-qPCR		
AT5G10900	<i>PP7L</i>	AGTCTTCAGTGCTTCAATGTTCTC GATTTGATGTTGTAACCTTGGGAC
AT2G18790	<i>PHYB</i>	ATTGAAGACGGTTCATTTGTGC GAGCTGTTGAATCCTTATCTGG

Supplemental information – Chapter 2

Plant material and growth conditions

All *Arabidopsis thaliana* plants used in this study are in the Col-0 ecotype background. The T-DNA insertion lines SALK_023714 (*ven4-1*) and SALK_077401 (*ven4-2*) were obtained from the Nottingham Arabidopsis Stock Centre (<http://arabidopsis.info/>); *phyB-9* (*phyB-9^{OG}*) and *pp7l-1* have been already described (Yoshida et al., 2018; Xu et al., 2019). Seeds of *P35S:PHYB-YFP phyB-9^{OG}* were kindly provided by Ferenc Nagy (Medzihradsky et al., 2013). To obtain *pp7l-1 bnen*, *pp7l-1* was crossed with *P35S:PHYB-YFP phyB-9^{OG}*. *phyB-9^{OG}* was crossed with Col-0 to obtain *phyB-9^{BC}* and *bnen*. Primer sequences are listed in Supplemental Table S1.

Unless specifically noted, wild-type and mutant seeds were sterilized with 20% (v/v) bleach and 0.01% (v/v) Triton X-100 and sown on 1/2 MS medium, pH 5.8, containing 0.8% (w/v) agar (Sigma-Aldrich, Darmstadt, Germany) and 1% (w/v) sucrose, and placed in the dark at 4°C for 2 d to ensure synchronized germination. Plates were then placed under 100 $\mu\text{mol photons m}^{-2} \text{sec}^{-1}$ and a 16/8-h day/night cycle at 22°C. For salt treatment, the surface sterile WT and mutant seeds were sown on 1/2 MS medium as described containing different NaCl concentrations (0, 100, and 150 mM) in lots of 80-100 seeds. For dNTP supplementation experiments, WT and mutant seeds were sown on 1/2 MS medium as described containing 2 mM of each dNTP as indicated in Figure 2B. For cold stress experiments, seeds were germinated and grown on 1/2 MS plates for 6 weeks in a 4°C chamber (Percival Scientific LED 41HL2) equipped with white and red LEDs set at 18% intensity (equivalent to 100 $\mu\text{mol photons m}^{-2} \text{s}^{-1}$). Soil-grown plants were raised on potting soil (Stender, Schermbeck, Germany) under controlled greenhouse conditions (daylight supplemented with illumination from HQI Powerstar 400W/D, providing a total fluence of $\sim 120 \mu\text{mol photons m}^{-2} \text{s}^{-1}$ on leaf surfaces; 16-h light/8-h dark cycle).

Chlorophyll fluorescence analysis

To measure chlorophyll fluorescence emission, the Imaging PAM (M-Series; Walz, Effeltrich, Germany) was used according to the instructions provided by the manufacturer. Samples were dark adapted for 30 min prior to determination of PSII quantum efficiency (F_v/F_m) at room temperature. For cold tolerance experiments, dark acclimation was carried out at 4°C. The maximum yield of chlorophyll fluorescence in the dark-adapted state (F_m) was induced by an 0.8 s pulse of saturating white light ($2700 \mu\text{mol photon m}^{-1} \text{s}^{-1}$). Variable fluorescence F_v , which

is defined as the difference of the maximum fluorescence (F_m) and the minimum fluorescence in the dark-adapted state (F_o), was used to calculate the maximum quantum yield of PSII photochemistry (F_v/F_m). The calculations of the parameters were performed using the ImagingWin software.

Protein extraction and immunoblotting

For immunoblot analysis, 100 mg cotyledon tissues from seedlings at 78 hours after imbibition (HAI) were dissected and homogenized in 400 μ L of sample buffer (0.125 M Tris, 1% (v/v) SDS, 10% (v/v) glycerol, 0.05 M sodium metabisulfite) containing 1 mM PMSF and protease inhibitor cocktail (Sigma-Aldrich, Darmstadt, Germany). The samples were cleared of insoluble debris by centrifugation at 16,000 g for 20 min at room temperature, and the supernatant was boiled with 5x loading dye [5% (w/v) β -mercaptoethanol, 0.02% (w/v) bromophenol blue, 30% (v/v) glycerol] at 95°C for 5 min. For each lane, equal amounts of total protein were resolved on a 10% (w/v) SDS-PAGE minigel and blotted 30 min onto a PVDF membrane using the trans-blot turbo transfer system (Bio-Rad, Munich, Germany). After incubation with primary and secondary antibodies (Agrisera, Vännäs, Sweden; catalog no. AS09 602), chemiluminescence was generated using the PierceECL Western Blotting Kit (Thermo Scientific, Waltham, MA, USA), and the blots were imaged with the Fusion FX7 system (Vilber Lourmat, Eberhardzell, Germany). Antibodies against PsaD (AS09 461, 1:1000) and PsbD (AS06 146, 1:5000) were purchased from Agrisera (Vännäs, Sweden).

RNA extraction and Northern analysis

RNA extractions from 78-HAI-old seedlings (50–100 mg) using the Trizol RNA reagent (Invitrogen, Carlsbad, USA) and RNA gel blot analyses were performed as described (Xu et al., 2019). RT-PCR amplification products of *PsaD* and *PsbD* were used as probes for Northern analyses. Primer sequences are listed in Supplemental Table S1.

cDNA Synthesis and reverse transcription quantitative PCR analysis

Total RNA was extracted from 78-HAI-old seedlings with the RNeasy Plant Mini Kit (Qiagen, Hilden, Germany). Total RNA (1 μ g) was reverse transcribed with the iScript cDNA Synthesis Kit (Bio-Rad, Munich, Germany). Real-time qPCR was performed using the iQ5 real-time PCR instrument with the iQ SYBR Green Supermix (Bio-Rad, Munich, Germany) with primers listed in Supplemental Table S1.

In vivo translation assay of thylakoid proteins

Chloroplast proteins were labeled in vivo using 78-HAI-old seedlings. In brief, seedlings were vacuum-infiltrated in 1 mL of labeling buffer containing 20 µg/mL cycloheximide, 10 mM Tris-HCl, 5 mM MgCl₂, 20 mM KCl, pH 6.8, and 0.1% (v/v) Tween 20, and incubated for 30 min to block cytosolic translation. [³⁵S]Met (1mCi) was applied to the same solution, and the leaves were vacuum-infiltrated for 10 s. After a 30-min labeling pulse, thylakoid proteins were isolated with cold buffer [300 mM sucrose, 50 mM HEPES-KOH, pH 7.6, 5 mM MgCl₂, 1 mM Na-EDTA, 1.25% BSA (w/v), 22 mM ascorbate, and 10 mM NaF]. Subsequently, thylakoid proteins were fractionated on 15% Tricine-SDS-PAGE gel. The gels were dried using a Geldryer (Bio-Rad, Munich, Germany) and exposed to an autoradiograph film.

Intracellular localization of the VEN4-eGFP fusion

The sequence of VEN4 (*AT5G40270*) without the stop codon was amplified from cDNA with primers listed in Supplemental Table S1. This amplified sequence was introduced into pDONR207 and subsequently into the destination vector pB7FWG2 (35S promoter, eGFP) by the BP and LR clonase reactions (Invitrogen, Carlsbad, CA, USA), respectively, generating 35S:VEN4-eGFP. Subcellular localization analysis of the fused protein was conducted in protoplasts isolated from Col-0 as described (Xu et al., 2019).

Statistical analyses

Statistical analyses were performed with the SPSS 17.0 Statistics software.

Medzihradzsky M, Bindics J, Adam E, Viczian A, Klement E, Lorrain S, Gyula P, Merai Z, Fankhauser C, Medzihradzsky KF, Kunkel T, Schafer E, Nagy F (2013)

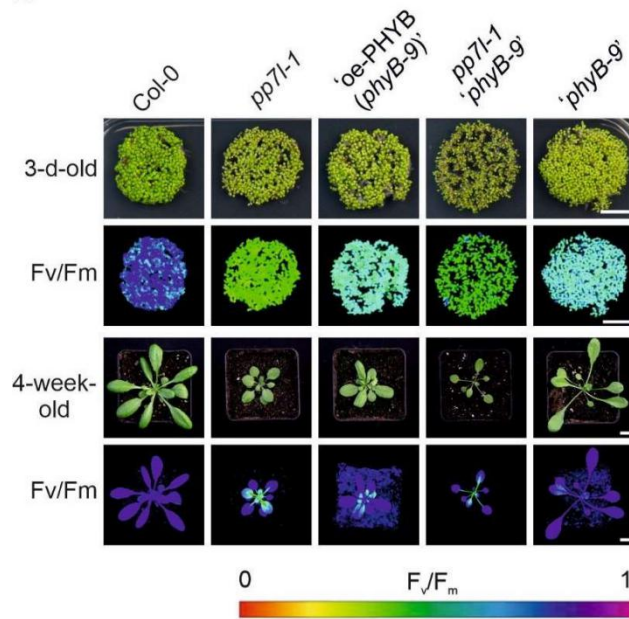
Phosphorylation of phytochrome B inhibits light-induced signaling via accelerated dark reversion in Arabidopsis. *Plant Cell* **25**: 535-544

Xu D, Marino G, Klingl A, Enderle B, Monte E, Kurth J, Hiltbrunner A, Leister D, Kleine T (2019) Extrachloroplastic PP7L Functions in Chloroplast Development and Abiotic Stress Tolerance. *Plant Physiol*

Yoshida Y, Sarmiento-Manus R, Yamori W, Ponce MR, Micol JL, Tsukaya H (2018) The Arabidopsis phyB-9 Mutant Has a Second-Site Mutation in the VENOSA4 Gene That Alters Chloroplast Size, Photosynthetic Traits, and Leaf Growth. *Plant Physiol* **178**: 36

SUPPLEMENTAL FIGURES

A

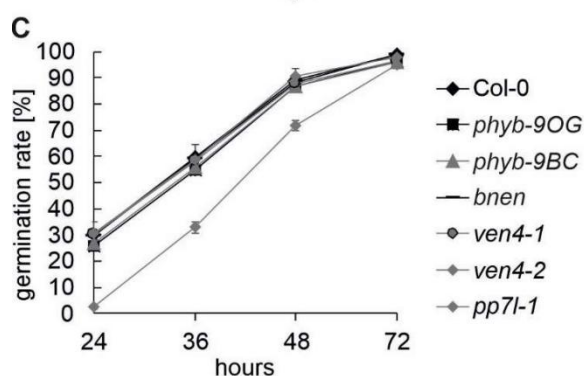
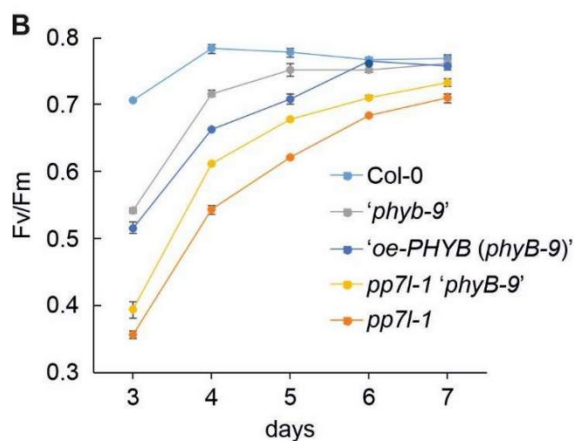


Supplemental Figure S1. Phenotypic characterization of the original *phyB-9* line and the *oe-PHYB (phyB-9)* line.

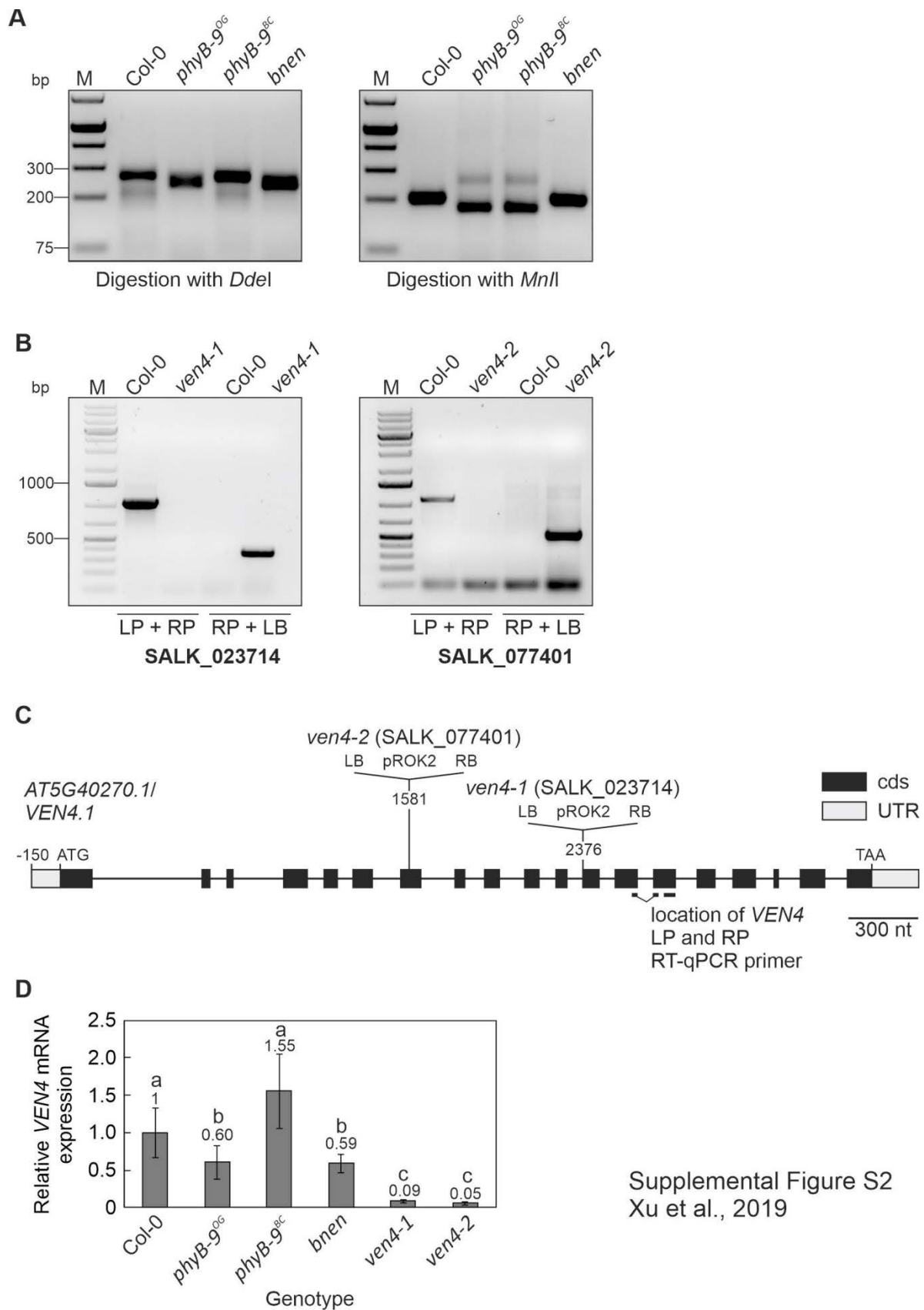
(A) Phenotypes of 3-day-old and 4-week-old wild-type (Col-0) and mutant plants grown under LD (16-h light/8-h dark) conditions. The maximum quantum yield of PSII (Fv/Fm) was measured with an imaging Chl fluorometer (Imaging PAM). The scale bar corresponds to 1 cm. Note that all *phyB-9* descendants of *phyB-9* are named in quotation marks, because they harbor a second-site mutation in the *VEN4* gene.

(B) Graph displaying Fv/Fm values measured for 3- to 7-day-old Col-0 and mutant seedlings.

(C) Graph displaying the germination rates of Col-0, *phyB-9^{OG}*, *phyB-9^{BC}*, *bnen*, *ven4-1*, *ven4-2* and *pp7l-1* seeds on MS medium. The data represent mean values \pm standard deviations of three independent experiments, each performed with 80-100 seeds per treatment and genotype.



Xu et al., 2019
Supplemental Figure S1



Supplemental Figure S2
Xu et al., 2019

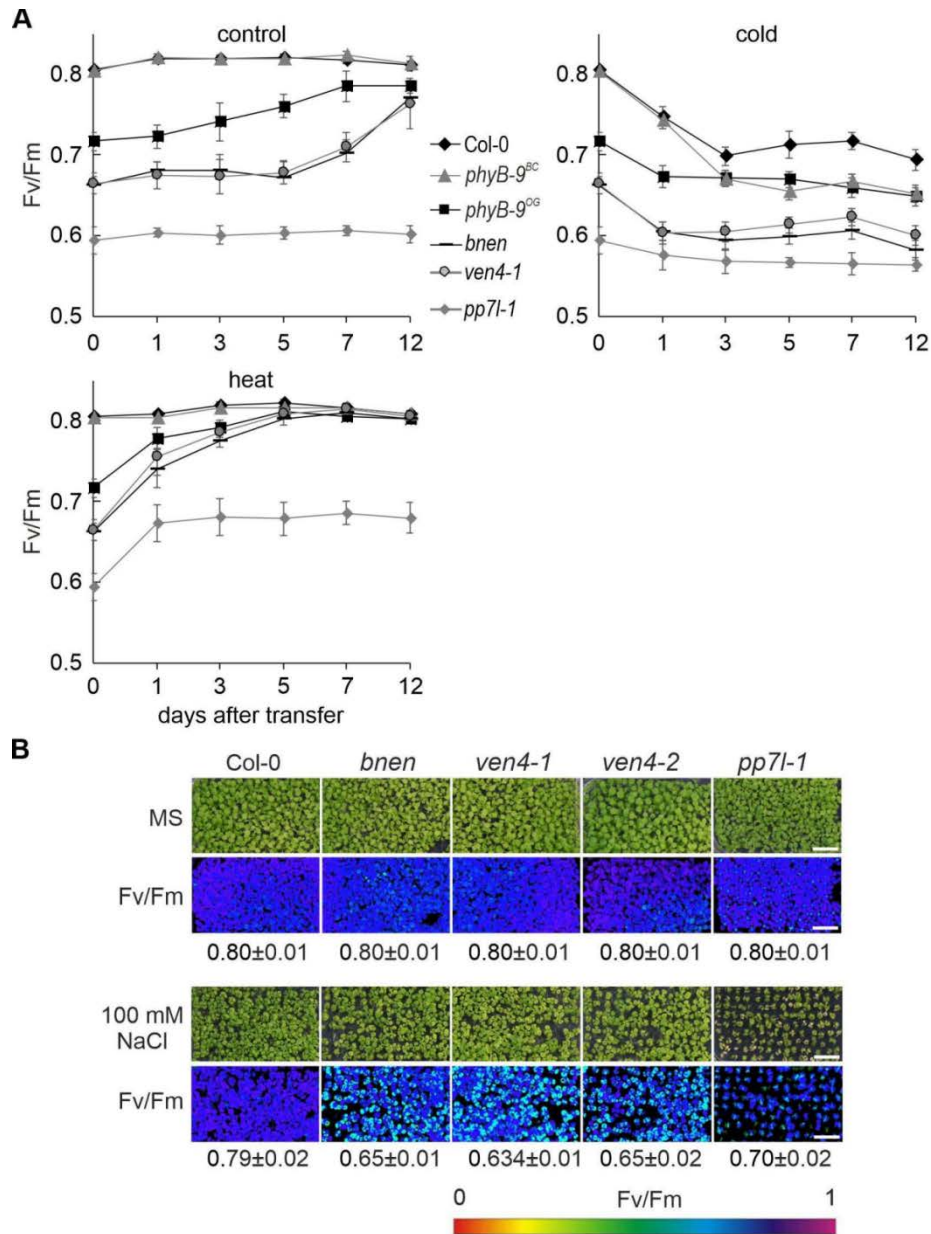
Supplemental Figure S2. Identification of *phyB-9* and *ven4* mutants.

(A) Genotyping of *phyB-9^{OG}*, *phyB-9^{BC}*, and *bnen* lines with dCAPS markers. After PCR amplification, PCR products were digested with *DdeI* or *MnlI* to detect *BNEN* or *PHYB* mutations, respectively.

(B) Confirmation and identification of homozygous T-DNA insertions in the two *ven4* SALK insertion lines. The gene-specific left and right primers (LP and RP) were used for amplification of the sequences surrounding the T-DNA insertion, and RP was used together with the T-DNA left-border primer (LB) for verification of the T-DNA insertion.

(C) Schematic representation and T-DNA tagging of the *VEN4* (*AT5G40270*) locus. Exons (black boxes), introns (black lines) and the 5' and 3' UTRs (grey boxes) are shown. Numbers are given relative to the start codon ATG. Locations and orientation of T-DNA insertions are indicated, as deduced from RP + LB PCR products shown in **(A)**, which were subsequently sequenced. Note that the insertions are not drawn to scale. Furthermore, the locations of the primers used in the RT-qPCR analysis of *VEN4* expression shown in panel **(D)** are indicated as thick black lines. The LP primer is an exon-exon primer spanning intron 7 of *VEN4*, which avoids amplification of genomic DNA.

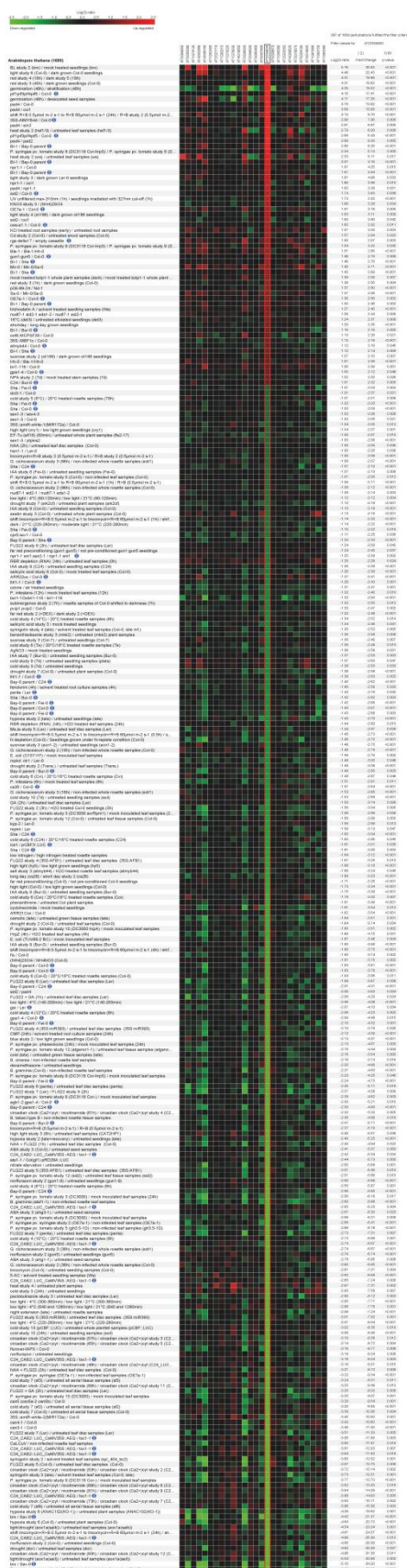
(D) RT-qPCR analysis of wild-type (Col-0), *phyB-9^{OG}*, *phyB-9^{BC}* and *ven4* mutant plants. RT-qPCR was performed with primers specific for *VEN* (locations of the primer annealing sites are indicated in panel **(C)**). Expression values are reported relative to the corresponding transcript levels in Col-0. The results were normalized with respect to the expression level of *RCE1*. Bars indicate standard deviations. Data are shown as mean values \pm SD from three independent experiments. Statistically significant differences (Tukey's HSD test; $P < 0.05$) between samples are indicated by the letters a, b and c, which sort the genotypes into groups. For example, Col-0 and *phyB-9^{BC}* belong to the same group, meaning that *VEN4* mRNA expression does not differ between Col-0 and *phyB-9^{BC}*.



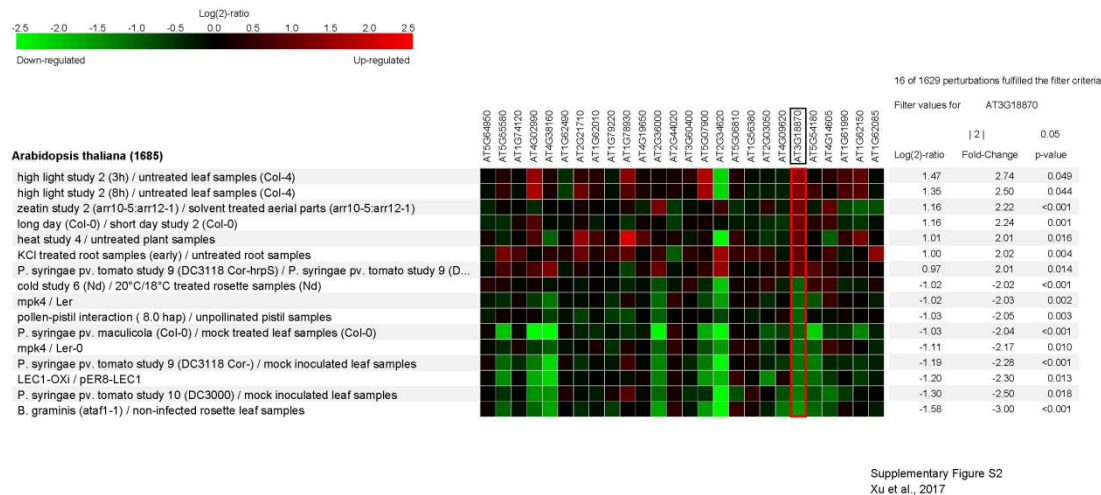
Xu et al., 2019
Supplemental Figure S3

Supplemental Figure S3. VEN4 and PP7L function is required for salt tolerance. **(A)** Graph displaying Fv/Fm values of Col-0, *phyB-9^{BC}*, *phyB-9^{OG}*, *bnen*, *ven4-1* and *pp7l-1* mutants grown for 18 days under long-day conditions (LD; ~120 $\mu\text{mol photons m}^{-2} \text{s}^{-1}$ on leaf surfaces; 16-h light/8-h dark), and were subsequently transferred for 12 days to cold (LD, 4°C and 35 $\mu\text{mol photons}\cdot\text{m}^{-2}\cdot\text{s}^{-1}$) or heat (continuous light, 32°C) conditions, respectively. The data represent mean values \pm standard deviations of three independent experiments. **(B)** Phenotypes of Col-0, *bnen*, *ven4*, and *pp7l-1* seedlings grown for 2 weeks on MS or on MS supplemented with 100 mM NaCl. The Imaging PAM pictures show the maximum quantum yields of PSII (Fv/Fm). Numbers below the pictures depict Fv/Fm values. The scale bar corresponds to 1 cm.

Supplemental information – Chapter 3



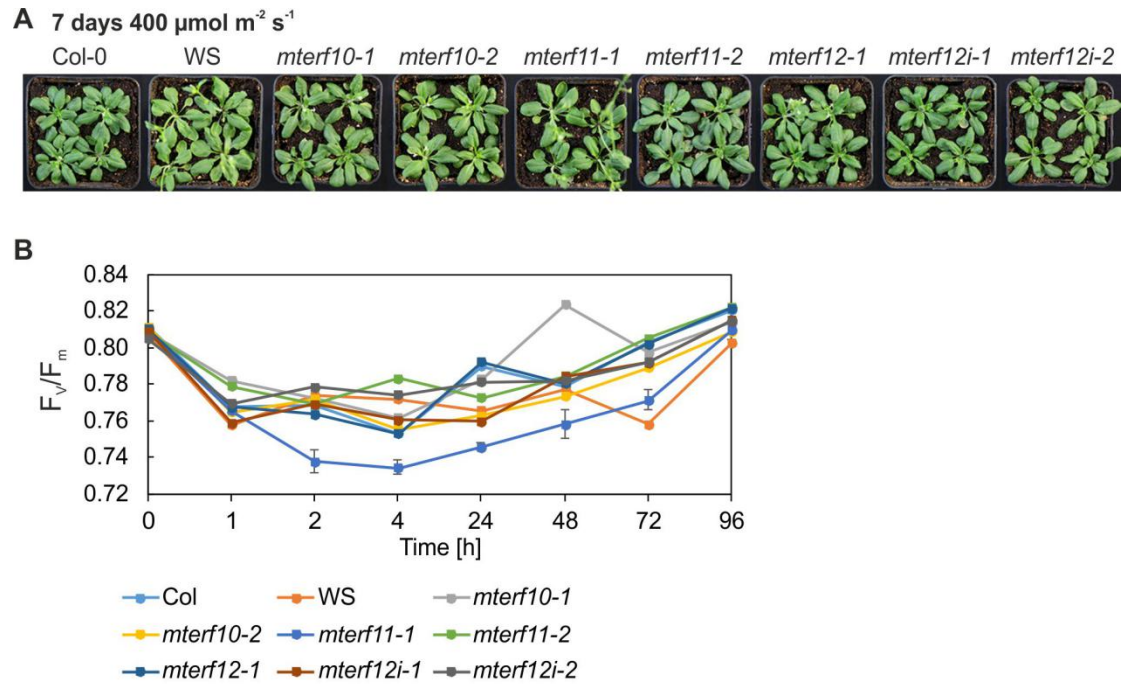
Supplementary Figure S1. Quantification of changes in *MTERF10* mRNA expression in response to perturbations as determined with the Genevestigator Perturbations Tool. The tool was employed on all deposited *A. thaliana* ATH1 arrays together with a 2-fold change filter and a *p*-value of < 0.05.



Supplementary Figure S2. Quantification of changes in *MTERF11* mRNA expression in response to perturbations as determined with the Genevestigator Perturbations Tool. The tool was employed on all deposited *A. thaliana* ATH1 arrays together with a 2-fold change filter and a *p*-value of < 0.05.



Supplementary Figure S3. Quantification of changes in *MTERF12* mRNA expression in response to perturbations as determined with the Genevestigator Perturbations Tool. The tool was employed on all deposited *A. thaliana* ATH1 arrays together with a 2-fold change filter and a *p*-value of < 0.05.



Supplementary Figure S4
 Xu et al., 2017

Supplementary Figure S4. Behavior of wild-type (Col-0) and *mterf10*, -11 and -12 mutant plants under moderate light stress of $400 \mu\text{mol photons m}^{-2} \text{s}^{-1}$. **(A)** To score the phenotypes under moderate heat stress, plants were first grown for 3 weeks under normal growth conditions ($100 \mu\text{mol photons m}^{-2} \text{s}^{-1}$, 22°C) and then exposed to $400 \mu\text{mol photons m}^{-2} \text{s}^{-1}$ for 7 days. **(B)** The maximum quantum yield of PSII (F_v/F_m) of Col-0 and *mterf* mutant plants was determined after the indicated periods of exposure to a fluence of $400 \mu\text{mol photons m}^{-2} \text{s}^{-1}$. The data are shown as mean values \pm SD from 8 to 10 different leaves.

Supplemental information – Chapter 4

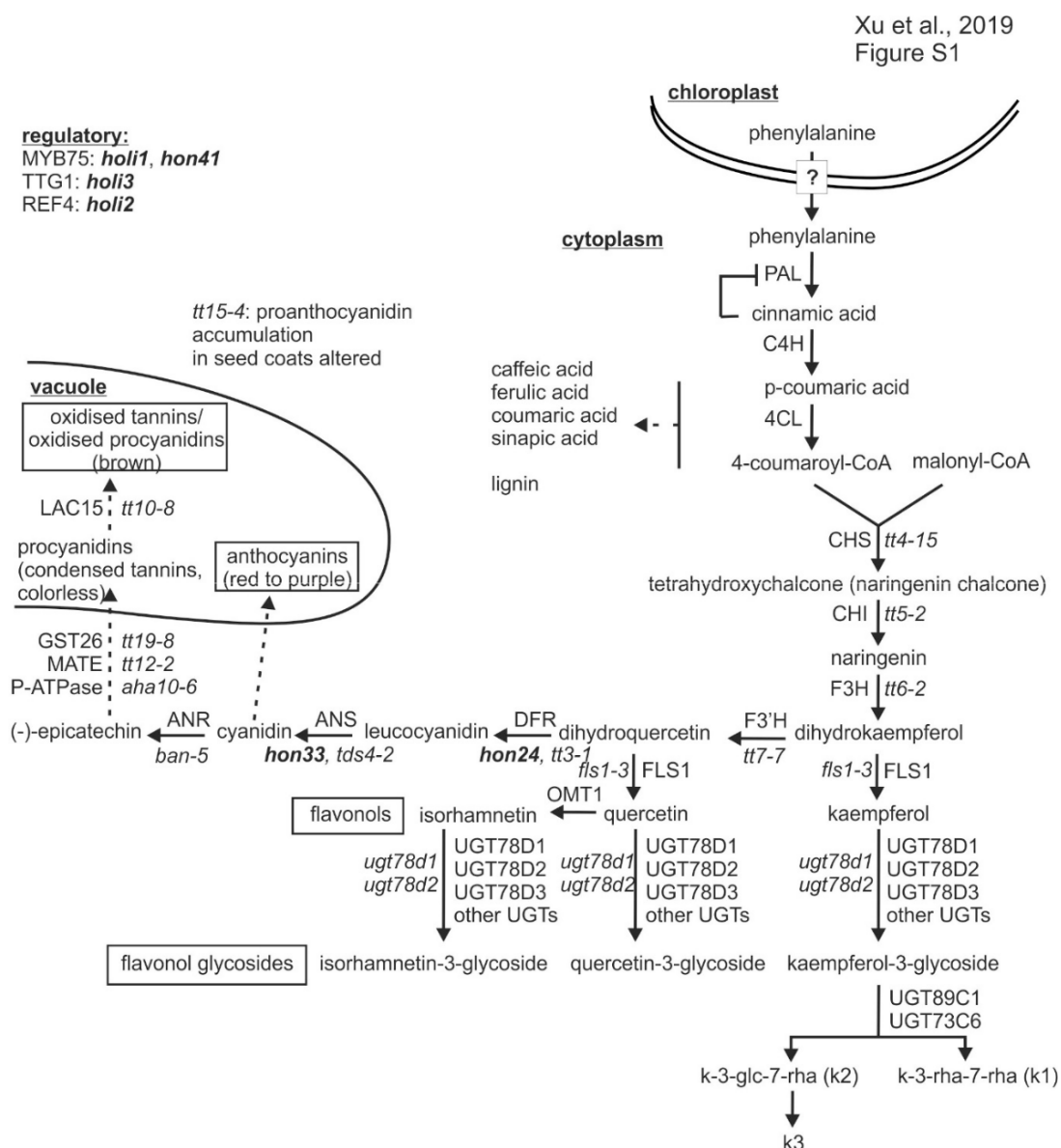


Figure S1. Illustration of the phenylpropanoid and flavonoid pathways in Arabidopsis.

The enzymatic steps leading from the precursor phenylalanine to flavonols, flavonol glycosides, anthocyanins, and oxidised tannins, as well as sinapic acid derivatives and lignin are shown, based on (Tohge et al. 2005; Yin et al. 2012; Appelhagen et al. 2014). Isolated *holi* and *hon* mutants related to the phenylpropanoid pathway (in bold) and further previously investigated mutants (Yin et al. 2012; Appelhagen et al. 2014) are indicated. Regulatory proteins and mutants thereof are also included in this Figure. Dashed arrows indicate multiple steps. Note that most steps take place in the cytoplasm. Complete enzyme names are listed below, in accordance with their positions in the pathway. The main pathway leading to anthocyanins and oxidised tannins comprises: PAL, phenylalanine ammonia-lyase; C4H, cinnamate 4-hydroxylase; 4CL, 4-

coumarate-CoA ligase; CHS, chalcone synthase; CHI, chalcone isomerase; F3H, flavanone 3-hydroxylase; flavonoid 3'-hydroxylase F3'H, dihydroflavonol 4-reductase DFR; ANS, anthocyanidin synthase; ANR, anthocyanidin reductase; P-ATPase, autoinhibited H⁺-ATPase 10 (AHA10); MATE, multidrug and toxic compound extrusion transporter; GST26, glutathione S-transferase 26; LAC15, laccase-like 15. The branched pathway leading to flavonols and flavonol glycosides is made up of: FLS1, flavonol synthase; k3, kaempferol 3-*O*-[6"-*O*-(rhamnosyl) glucoside] 7-*O*-rhamnoside; k3-glc-7-rha, kaempferol 3-*O*-glucoside 7-*O*-rhamnoside; k-3-rha-7-rha, kaempferol 3-*O*-rhamnoside 7-*O*-rhamnoside; OMT1, O-methyltransferase; UGT78D1, flavonol 3-*O*-rhamnosyltransferase; UGT78D2, flavonoid 3-*O*-glucosyltransferase; UGT78D3, flavonol 3-*O*-arabinosyltransferase.

Xu et al., 2019
Figure S2

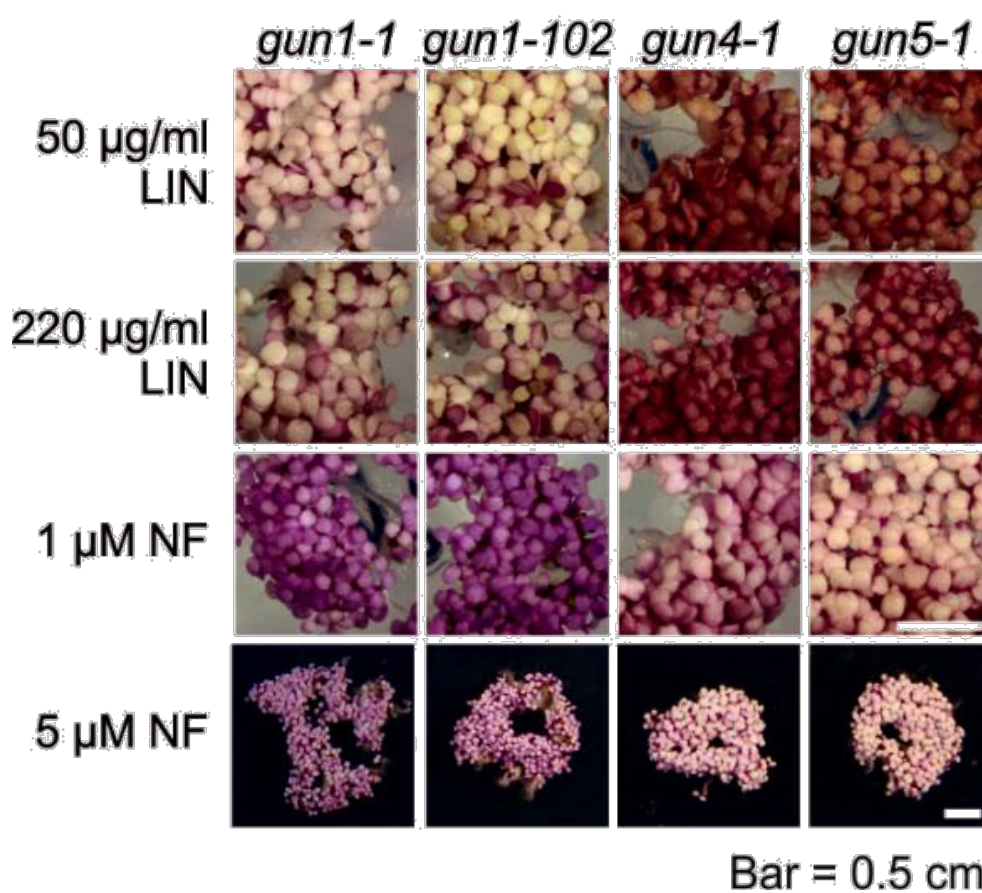


Figure S2. Phenotypes of *gun* mutants grown in the presence of lincomycin (LIN) or norflurazon (NF).

WT and *gun* mutant seedlings were grown for 5 days under continuous light (100 $\mu\text{mol photons m}^{-2} \text{s}^{-1}$) on MS plates supplemented with either LIN (50 $\mu\text{g/ml}$ or 220 $\mu\text{g/ml}$) or NF (1 μM or 5 μM). Autofluorescence after UV excitation was monitored in seedlings grown on MS plates supplemented with 50 $\mu\text{g/ml}$ LIN.

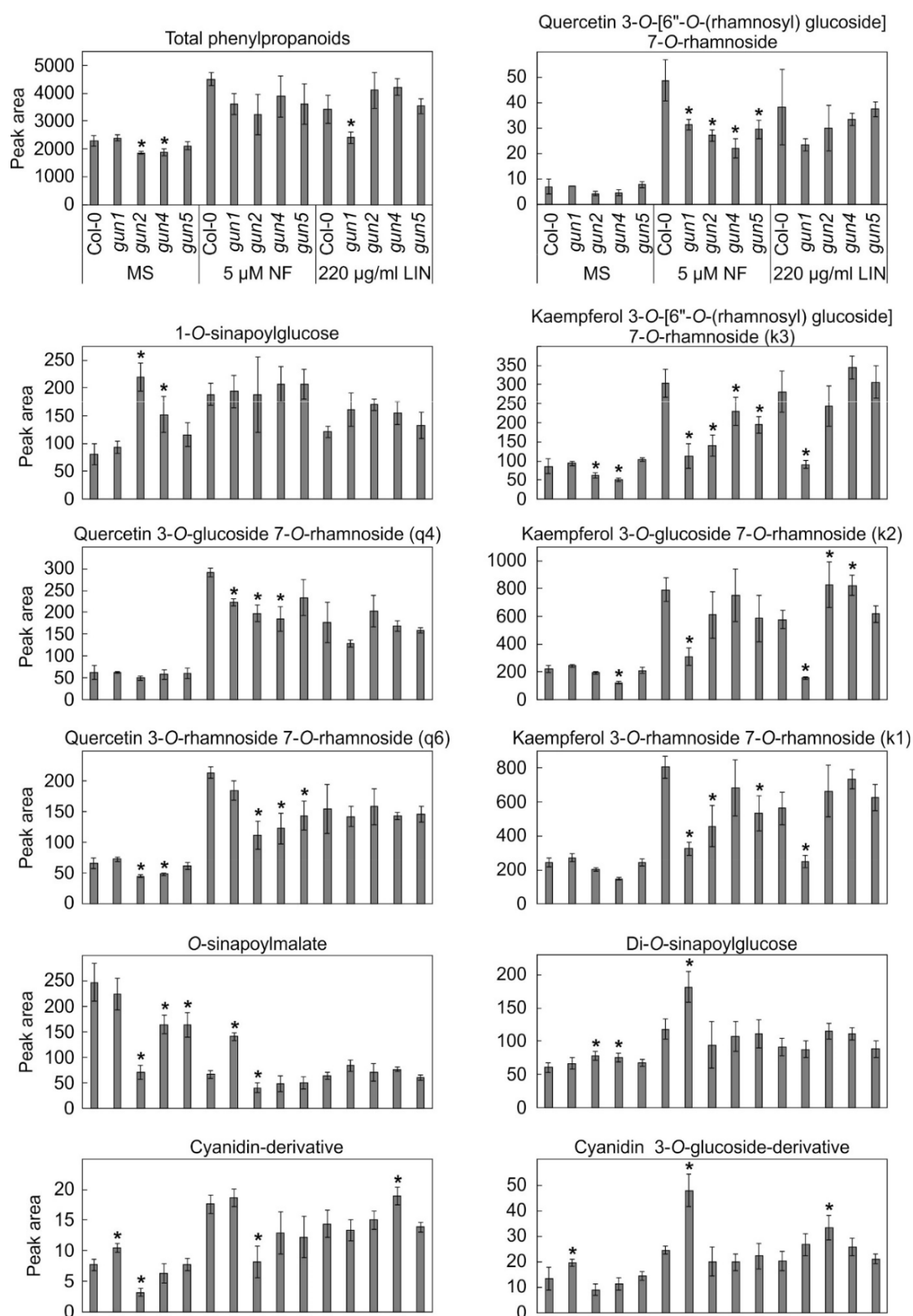


Figure S3. Determination of phenylpropanoid contents of 5-day-old WT and *gun* mutant seedlings.

WT and *gun* mutant seedlings were grown for 5 days under continuous light (100 $\mu\text{mol photons m}^{-2} \text{s}^{-1}$) on MS or on MS plates supplemented with either 5 μM NF or 220 $\mu\text{g/ml}$ LIN. Phenylpropanoid content was measured by reverse-phase UPLC analysis as described in Materials and Methods. Mean values of four independent replicates are shown. Bars indicate standard deviations. Statistically significant differences (Tukey's HSD test; $P < 0.05$) between WT and mutant samples are indicated by an asterisk.

Xu et al., 2019
Figure S4

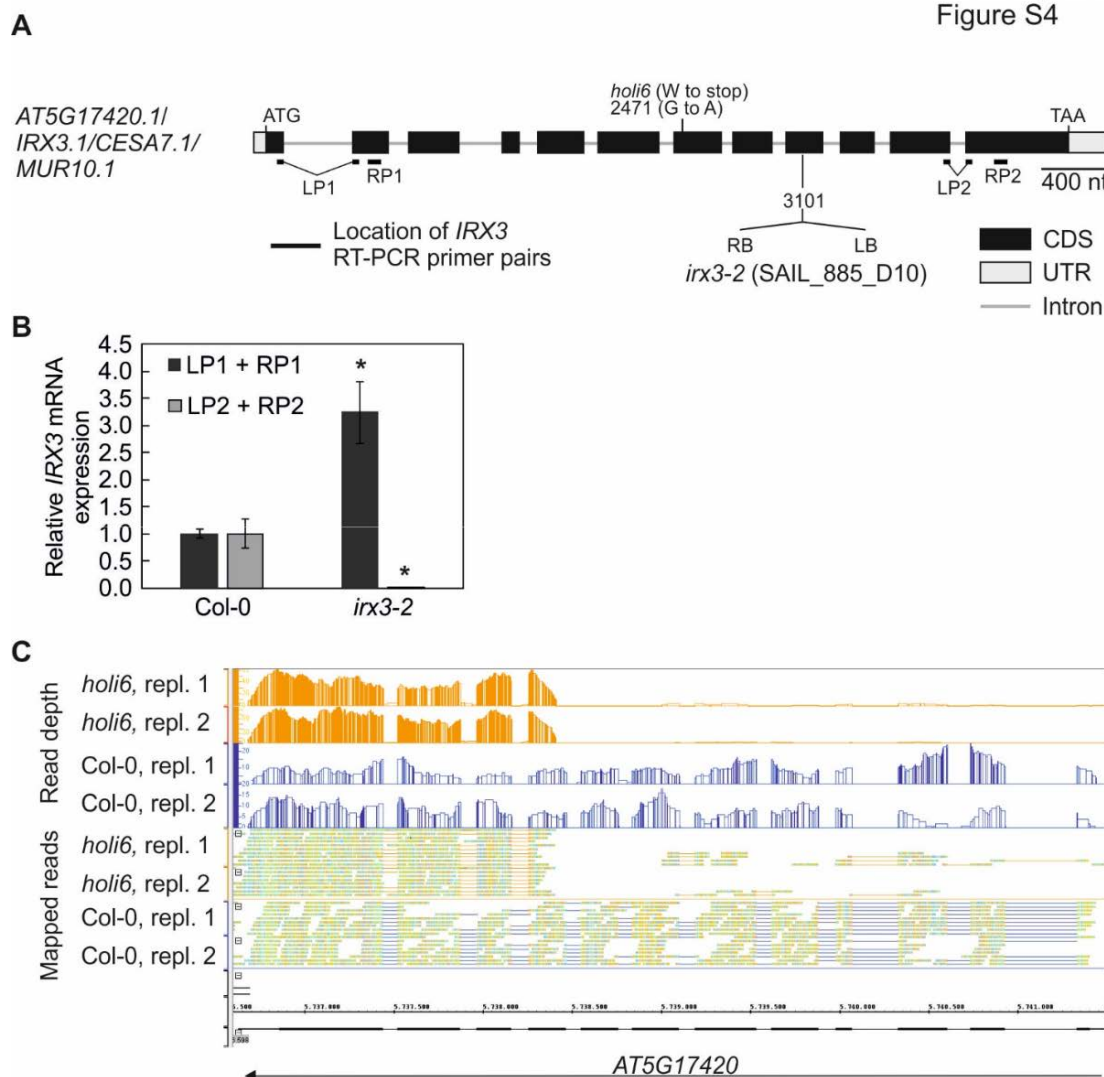


Figure S4. Confirmation of the *irx3-2* T-DNA insertion mutant.

(A) Schematic representation and T-DNA tagging of the *IRX3* (AT5G17420) locus. Exons (black boxes), introns (grey lines) and the 5' and 3' UTRs (grey boxes) are shown. Numbers are given relative to the start of the 5'UTR. Location and orientation of the T-DNA insertion is indicated, as deduced from a PCR product generated with a gene specific plus a left border primer, which was subsequently sequenced. Note that the insertion is not drawn to scale. Furthermore, the locations of the primers used in the real-time PCR analysis of *IRX3* expression shown in panel (B) are indicated as thick black lines. The LP primers are exon-exon primers spanning intron 1 and 11 of *IRX3*,

respectively, which avoids amplification of genomic DNA. Real-time analyses of wild-type (Col-0) and *irx3-2* mutant plants. Real-time PCR was performed with primers specific for *IRX3* (locations of the primer annealing sites are indicated in panel (A)) and *AT4G36800*, encoding a RUB1-conjugating enzyme (*RCE1*), which serves as a control. Expression values are reported relative to the corresponding transcript levels in Col-0. The results were normalized with respect to the expression level of *RCE1*. Note that, in the *irx3-2* allele, the T-DNA is integrated in the 5'RB–T-DNA–LB3' direction. Bars indicate standard deviations. Statistically significant differences ($p < 0.05$) between wild-type and *irx3-6* are indicated by an asterisk. (C) RNA-Seq reads generated from Col-0 and the *irx3-2* mutant were mapped to the TAIR10 annotation and are displayed in the Integrated Genome Browser (<https://bioviz.org/>). The snapshot confirms accumulation of truncated transcripts of *IRX3* in the *irx3-2* mutant.

Acknowledgement

I would like to thank Prof. Dr. Dario Leister for giving me the opportunity of working in his research group.

I am deeply indebted to my supervisor PD Dr. Tatjana Kleine, for her constant guidance throughout my work, her enthusiasm in my project and regular interest in its progress, as well as some wisdom and excellent advice on thesis related issues.

I gratefully acknowledge the funding received towards my PhD from the CSC Scholarship No. 201406180089. I am also grateful to the funding DFG KL 2362/1-1 to accomplish my PhD.

I am thankful to Dr. Xuwu Sun, Dr. Nikolay Manavski and Dr. Luca Tadini for teaching me the molecular biology laboratory skills.

Many thanks also to Elisabeth Gerick for technical assistance. And of course a big thank you to Ravi Dhiman and all collaborators for helping in my research and the papers that we published together.

Many thanks to the members of small group and my colleagues within the lab: Dr. Liangsheng Wang, Dr. Kwanuk Lee, Dr. Chiara Gandini and Dr. Lisa-Marie Schmid, for their experience and help.

Thanks to all gardeners for taking care of my plants.

I am also grateful to my friends Dr. Wenlong Zhang, Dr. Yuehui Tian, Dr. Qiang Liu, Ningning Zhao, and Shan Jia for being a part of my life and sharing so many wonderful memories and experiences during my time in Munich.

Finally, I would like to say a heartfelt thank you to my Mum, Dad, Yufang Wang(王毓芳), and Hengliang Xu(徐亨良) for their love and support. They always believing in me and encouraging me to follow my dreams. Thanks to my sister Jing Xu(徐静), for her constant unconditional support both in my study and my career as well.

To my fiancée Jing Wang(王晶), thank you for supporting me for everything, and especially I can't thank you enough for encouraging me throughout this experience.

Curriculum vitae

Personal details

Name: Duorong Xu 徐多荣

Date of birth: 09 July 1987

Place of birth: Gansu, China

Citizenship: Chinese

Education

10.2015 - Present PhD student in Ludwig-Maximilians-Universität München

09.2014 - 09.2015 CSC-LMU Program student in LMU München

09.2011- 06.2014 M.S. in Cell Biology, Lanzhou University

09.2007-06.2011 B.S. in Biotechnology, Gansu Agricultural University

Publications

- **Duorong Xu**, Dario Leister, Tatjana Kleine (2020) VENOSA4, a human dNTPase SAMHD1 homolog, contributes to chloroplast development and abiotic stress tolerance. *Plant Physiol* **182**: 721–729
- **Duorong Xu**, Ravi Dhiman, Adriana Garibay, Hans-Peter Mock, Dario Leister, Tatjana Kleine (2020) Cellulose defects in the Arabidopsis secondary cell wall promote early chloroplast development. *Plant J* **101**: 156-170
- **Duorong Xu**, Giada Marino, Andreas Klingl, Beatrix Enderle, Elena Monte, Joachim Kurth, Andreas Hiltbrunner, Dario Leister, Tatjana Kleine (2019) Extrachloroplastic PP7L functions in chloroplast development and abiotic stress tolerance. *Plant Physiol* **180**: 323–341
- Sylwia M. Kacprzak, Nobuyoshi Mochizuki, Belén Naranjo, **Duorong Xu**, Dario Leister, Tatjana Kleine, Haruko Okamoto, Matthew J. Terry (2019) Plastid-to-nucleus retrograde signalling during chloroplast biogenesis does not require ABI4. *Plant Physiol* **179**: 18–23
- **Duorong Xu**, Dario Leister and Tatjana Kleine (2017) Arabidopsis thaliana mTERF10 and mTERF11, but Not mTERF12, Are Involved in the Response to Salt Stress. *Front Plant Sci* **8**: 1213.
- Xuwu Sun, **Duorong Xu**, Zhixin Liu, Tatjana Kleine, Dario Leister (2016) Functional relationship between mTERF4 and GUN1 in retrograde signaling. *J Exp Bot* **67**: 3909-3924